VOLUME 76 JULY 6, 1972 NUMBER 14

JPCHAx

THE JOURNAL OF PHYSICAL CHEMISTRY

PUBLISHED BIWEEKLY BY THE AMERICAN CHEMICAL SOCIETY

THE JOURNAL OF

PHYSICAL CHEMISTRY

AMERICAN CHEMICAL SOCIETY, *1155 Sixteenth St., N.W., Washington, D. C. 20036*

Books and Journals Division
JOHN K CRUM, *Director*
JOSEPH H. KUNEY, *Head, Business Operations Department*
RUTH REYNARD, *Assistant to the Director*

 Published biweekly by the American Chemical Society at 20th and Northampton Sts., Easton, Pa. 18042. Second-class postage paid at Washington, D. C., and at additional mailing offices.

All manuscripts should be sent to *The Journal of Physical Chemistry,* Department of Chemistry, University of Minnesota, Minneapolis, Minn. 55455.

Additions and Corrections are published once yearly in the final issue. See Volume 75, Number 26 for the proper form.

Extensive or unusual alterations in an article after it has been set in type are made at the author's expense, and it is understood that by requesting such alterations the author agrees to defray the cost thereof.

The American Chemical Society and the Editor of *The Journal of Physical Chemistry* assume no responsibility for the statements and opinions advanced by contributors.

Correspondence regarding accepted copy, proofs, and reprints should be directed to Editorial Production Office, American Chemical Society, 20th and Northampton Sts., Easton, Pa. 18042. Manager: CHARLES R. BERTSCH. Assistant Editor: EDWARD A. BORGER.

Advertising Office: Centcom, Ltd. (formerly Century Communications Corporation), 142 East Avenue, Norwalk, Conn. 06851.

Business and Subscription Information

Remittances and orders for subscriptions and for single copies, notices of changes of address and new professional connections, and claims for missing numbers should be sent to the Subscription Service Department, American Chemical Society, 1155 Sixteenth St., N.W., Washington, D. C. 20036. Allow 4 weeks for changes of address. Please include an old address label with the notification.

Claims for missing numbers will not be allowed (1) if received more than sixty days from date of issue, (2) if loss was due to failure of notice of change of address to be received before the date specified in the preceding paragraph, or (3) if the reason for the claim is "missing from files."

Subscription rates (1972): members of the American Chemical Society, $20.00 for 1 year; to nonmembers, $60.00 for 1 year. Those interested in becoming members should write to the Admissions Department, American Chemical Society, 1155 Sixteenth St., N.W., Washington, D. C. 20036. Postage to Canada and countries in the Pan-American Union, $5.00; all other countries, $6.00. Single copies for current year: $3.00. Rates for back issues from Volume 56 to date are available from the Special Issues Sales Department, 1155 Sixteenth St., N.W., Washington, D. C. 20036.

This publication and the other ACS periodical publications are now available on microfilm. For information write to: MICROFILM, Special Issues Sales Department, 1155 Sixteenth St., N.W., Washington, D. C. 20036.

Notice to Authors last printed in the issue of June 22, 1972

THE JOURNAL OF

PHYSICAL CHEMISTRY

Volume 76, Number 14 July 6, 1972

JPCHAx 76(14) 1919–2060 (1972)

COMMUNICATIONS TO THE EDITOR

AUTHOR INDEX

In papers with more than one author the name of the author to whom inquiries about the paper should be addressed is marked with an asterisk in the by-line.

THE JOURNAL OF
PHYSICAL CHEMISTRY

VOLUME 76, NUMBER 14 JULY 6, 1972

The Reaction of Hydrogen Peroxide with Nitrogen Dioxide and Nitric Oxide

by David Gray, Eduardo Lissi, and Julian Heicklen*

Department of Chemistry and Ionosphere Research Laboratory, The Pennsylvania State University, University Park, Pennsylvania 16802 *(Received October 6, 1971)*

Publication costs borne completely by The Journal of Physical Chemistry

The reactions of NO and NO_2 with H_2O_2 have been examined at 25°. Reaction mixtures were monitored by continuously bleeding through a pinhole into a monopole mass spectrometer. NO_2 was also monitored by its optical absorption in the visible part of the spectrum. Reaction mixtures containing initially 1.5–2.5 Torr of NO_2 and 0.8–1.4 Torr of H_2O_2 or 1–12 Torr of NO and 0.5–1.5 Torr of H_2O_2 were studied. In the NO_2–H_2O_2 system the overall reaction was $(1 + \alpha)H_2O_2 + 2NO_2 \rightarrow 2HONO_2 + \alpha H_2O + (\alpha/2)O_2$. The reaction was probably heterogeneous and followed the rate law $-d[H_2O_2]/dt = k[NO_2][H_2O_2]^n$, where n was between 0 and 1. Assuming that $n = 1$, an upper limit for the homogeneous rate coefficient is 1×10^{-18} cm³/molecule sec. The H_2O_2–NO reaction was complex. There was an induction period followed by a marked acceleration in reactant removal. The final products of the reaction, NO_2, probably H_2O, and possibly $HONO_2$, were produced mainly after all the H_2O_2 was removed. The overall stoichiometry in the presence of excess NO was $H_2O_2 + NO \rightarrow H_2O + NO_2$. The initial induction period gives an upper limit to the homogeneous gas-phase reaction coefficient of 5×10^{-20} cm³/molecule sec for the reaction $NO + H_2O_2 \rightarrow HONO + HO$. The HO radical presumably is removed *via* $HO + NO \rightarrow HONO$. The HONO intermediate was shown to disproportionate to $NO_2 + NO + H_2O$ in a relatively slow first-order reaction. The acceleration in H_2O_2 removal after the NO–H_2O_2 reaction is started is caused by NO_2 catalysis: $NO_2 + H_2O_2 \rightarrow HONO_2 + HO$ and $HONO_2 + NO \rightarrow HONO + NO_2$. The latter reaction was demonstrated in separate experiments in which NO was added to $HONO_2$ (in the presence of NO_2, O_2, and H_2O). A minor part of the catalysis may also be caused by HONO *via* $HONO^* + H_2O_2 \rightarrow H_2O + NO_2 + HO$, where HONO* must have retained sufficient energy to overcome the 12 kcal/mol endothermicity of the reaction.

Introduction

The reaction of H_2O_2 with NO and NO_2 has been postulated as a possible means of H_2O_2 removal in the upper atmosphere. No direct measurements of the rate coefficients have been reported, though Nicolet[1a] has pointed out that the reactions will be important if their rate coefficients exceed 10^{-14} cm³/sec. Since the same gases are also constituents in polluted urban atmospheres, such reactions could also be occurring there too. Therefore we have studied these systems at 25° and this paper reports our findings.

The only previous work is that of Tyler,[1b] who examined the reaction between NO and H_2O_2 at 297–473° in the presence of excess N_2. Though no quantitative results were obtained, he concluded that the initial reaction produced HO or HO_2 or both, and that these were removed *via*

$$HO + H_2O_2 \longrightarrow H_2O + HO_2$$

$$HO_2 + NO \longrightarrow HO + NO_2$$

$$HO + NO + M \longrightarrow HONO + M$$

Experimental Section

All the experiments were carried out in a 10-cm cylindrical quartz cell having optically flat windows at both ends. The gases to be introduced into this cell were

(1) (a) M. Nicolet, *Aeronomica Acta*, No. 79 (1970) "Aeronomic Reactions of Hydrogen and Ozone"; Ionosphere Research Laboratory Report No. 350; The Pennsylvania State University, 1970; (b) B. J. Tyler, *Nature (London)*, **195**, 280 (1962).

stored in glass bulbs connected to a conventional Hg-free gas handling system. The hydrogen peroxide was stored in a blackened glass finger to prevent any photodecomposition. Pressures of all reactants were measured on a dibutyl phthalate manometer.

The course of the reaction was followed by means of a G. E. 600 monopole mass spectrometer. A very small pinhole, made by drawing out a piece of glass tubing into a fine short capillary, was inserted into the center of the cell through a side arm. This tube terminated at the entrance to the ion chamber of the mass spectrometer. Decomposition of hydrogen peroxide on the stainless steel surfaces of the spectrometer was eliminated in this manner. This pinhole was sufficiently small that the high-pressure differential required for the normal working of the spectrometer was realized. Working with a cell pressure of up to 15 Torr the mass spectrometer chamber was maintained at a pressure of approximately 6×10^{-7} Torr. At these pressures the loss of reactants was less than 2% in 1 hr.

This pinhole bleed system provided continuous sampling of the gas mixture in the cell during the course of the reaction. By scanning the suitable mass range, the peak heights of the reactants and products relative to argon as standard were obtained.

All reactants except H_2O_2 were calibrated using argon as a standard in the following way. A gas was introduced into the cell and its pressure was read on the D.B.P. manometer. The cell stopcock was closed and the whole vacuum line was evacuated to less than 1 μ. The argon was introduced into the whole line to a certain pressure greater than the previously added gas, the cell stopcock was opened, and the final pressure reading on the manometer was measured. The difference of these two readings gave the added pressure of argon. A mass spectrum of the added gas peak and the argon peak was taken and the ratio of the peak heights was obtained. The procedure was repeated for various ratios and a graph of ratio of added gas pressure to argon pressure against ratio of peak heights was plotted.

H_2O_2 could not be calibrated in this way since some H_2O was always present. Therefore calibrations were done in two other ways utilizing the stoichiometry of chemical reactions. In one method H_2O_2 was photolyzed with 2139-Å radiation to completion as determined by the disappearance of the mass spectral peak at m/e 34. The O_2 produced was measured and was presumed equal to one half the initial H_2O_2 pressure, since the photochemical decay of H_2O_2 follows the stoichiometry:[2] $H_2O_2 + h\nu \rightarrow H_2O + {}^1/_2O_2$. Scattered results were obtained by this method. A more reproducible method was to allow a large excess of NO_2 to react with H_2O_2 ($[NO_2]/[H_2O_2] > 3$), which produced $HONO_2$ as the sole product. The stoichiometric equation presumably is $H_2O_2 + 2NO_2 \rightarrow 2HONO_2$. From the NO_2 consumed both the H_2O_2 and $HONO_2$ were calibrated. The calibrations for H_2O_2 from the two methods agreed, but since the latter method was more reproducible, it was used.

Introduction of the gas mixtures into the cell for an experiment was conducted in a similar manner. First, the hydrogen peroxide–water mixture was thoroughly degassed and then allowed to expand into the cell. A measured pressure of argon was then introduced into the cell containing the hydrogen peroxide–water mixture. After a mass spectrum of the mixture was taken to determine the initial concentration of H_2O_2, a certain known amount of either NO or NO_2 was added to the cell in a similar manner. Then mass spectra of the mixture were determined at frequent intervals to determine the concentration of reactants during the course of the reaction.

The concentration of NO_2 was also monitored using its absorption of light above 3600 Å. The light source was a mercury resonance lamp in combination with a Corning 5-60 filter to eliminate wavelengths below 3500 Å. The light was monitored with an RCA 935 phototube and a 1-mV recorder to measure the voltage drop across a known variable resistor. To avoid any photolysis effects a very small beam of light was used. The same results were obtained by chopping this beam or allowing continuous illumination proving that any photolysis is negligible.

Materials. The hydrogen peroxide was a pure 90% solution obtained by the courtesy of E. I. DuPont de Nemours Ltd. Apart from constant outgassing this solution was used unpurified.

NO_2 was prepared *in situ* on the vacuum line from pure NO and O_2. It was repurified before every use by additional oxygen. It contained no measurable N_2O or NO impurity.

NO was obtained from the Matheson Co. The NO was distilled from liquid argon. It contained no measurable impurity.

Argon was obtained from Air Products Ltd.

Reaction of H_2O_2 with NO_2

Several runs were done in the presence of 2.5–3.0 Torr of Ar with initial reactant pressures of 1.5–2.5 Torr of NO_2 and 0.8–1.4 Torr of H_2O_2, and $[NO_2]/[H_2O_2]$ ratios of 1.2–2.7. The reaction was extremely rapid and one of the reactants was at least 90% consumed in 1–3 min. Higher pressures of H_2O_2 could not be used because its vapor pressure at room temperature is about 1.5 Torr. Higher pressures of NO_2 were not used because the reaction became too rapid to follow. Lower initial pressures of reactants were not used since then the reaction could not be followed to a significant extent because of limits in detectability.

(2) D. H. Volman, *Advan. Photochem.*, 1, 43 (1963).

The major product of the reaction was $HONO_2$, as determined from the growth of the mass spectral peaks at m/e 46 and 63. The peak at m/e 63 was very small and barely detectable. However, the peak at m/e 46 first decayed and then grew during the reaction even though NO_2 (parent m/e 46) was being consumed. Small amounts of O_2 were also produced in runs for low $[NO_2]/[H_2O_2]$ ratios as determined from the growth of the mass spectral peak at m/e 32. There was no evidence for the production of H_2O or NO, though both would have been difficult to detect, and they could have been produced as minor products.

During each run H_2O_2 and $HONO_2$ were monitored by their mass spectral peaks at m/e 34 and 46, respectively. In order to monitor $HONO_2$, the fraction of the 46 peak due to NO_2 had to be taken into account. Thus values early in a run could not be obtained because of the large correction required. The NO_2 was monitored optically. In each run the NO_2 and H_2O_2 were consumed in a ratio of about 2 to 1. The $HONO_2$ produced was proportional to the NO_2 consumed. From mass balance considerations, we assume that the constant of proportionality is one, since absolute calibrations were not made for $HONO_2$. The overall reaction can be represented as

$$(1 + \alpha)H_2O_2 + 2NO_2 \longrightarrow 2HONO_2 + \alpha H_2O + (\alpha/2)O_2 \quad (1)$$

where $\alpha < 1$.

The pressures in a typical run are plotted *vs.* reaction time in Figure 1. The NO_2 and H_2O_2 decay rapidly, the H_2O_2 being consumed essentially at 4 min reaction time. Paralleling the reactant decay is the growth of O_2. However, the $HONO_2$ growth showed a noticeable lag compared to reactant removal. Since the reaction was so rapid and there is evidence that the reaction proceeds on the vessel surface (see below) the $HONO_2$ lag might be partly attributed to the strong adsorption of $HONO_2$ to the reaction vessel. After about 15 min, the gas pressures were stabilized and the stoichiometry in eq 1 was satisfied ($-\Delta[H_2O_2] = 1.3$ Torr, $-\Delta[NO_2] = 1.55$ Torr, $\Delta[O_2] = 0.25$ Torr, and $\Delta[HONO_2] = 1.50$ Torr) with $\alpha \sim 0.4$.

A kinetic analysis was made from the curves of growth of several runs both by using integral rate expressions and rates measured from the slopes of the curves at different reactant pressures. Figure 2 shows plots of the slopes of the reactant decay curves at fixed H_2O_2 pressures *vs.* NO_2 pressure at the same time. The rates are first order in $[NO_2]$ within the scatter of the data. The results are essentially the same at 0.5 and 0.8 Torr of H_2O_2. The slopes of the two curves give first-order rate coefficients of 1.57 and 0.71 min^{-1} for the NO_2 and H_2O_2 decay, respectively. The ratio of these coefficients is 2.2. From eq 1, the expected ratio is $2/(1 + \alpha)$, which is approximately 2 since $\alpha \ll 1$

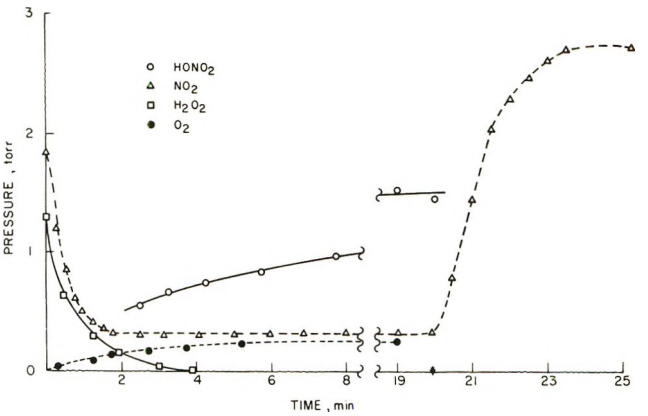

Figure 1. Plots of pressures *vs.* time in the reaction of NO_2 with H_2O_2 at 25°: $[NO_2]_0 = 1.85$ Torr; $[H_2O_2]_0 = 1.3$ Torr; [Ar] = 2.8 Torr. The NO_2 was monitored optically; the O_2, H_2O_2, and $HONO_2$, by their mass spectral peaks at m/e 32, 34, and 46, respectively. For $HONO_2$, corrections due to the NO_2 contribution were made. After 20 min 2.0 Torr of NO was added. Note break in abscissa between 8 and 18 min.

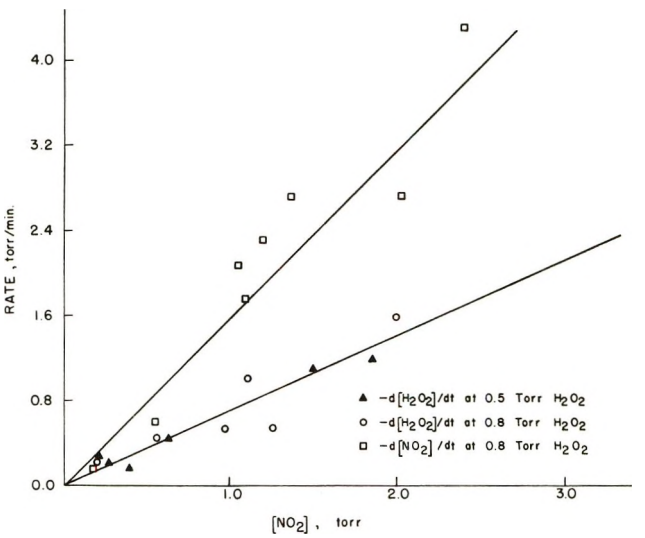

Figure 2. Plots of the slopes of reactant decay curves *vs.* the NO_2 pressure in the reaction of NO_2 with H_2O_2 at 25° during the course of several runs when the H_2O_2 pressure was 0.5 or 0.8 Torr.

for most runs. (The run in Figure 1 had a large α because it had one of the lowest initial ratios for $[NO_2]_0/[H_2O_2]_0$. Also the slopes cannot be used too near the beginning or end of any run, because the experimental errors are large.). The discrepancy between the measured and expected ratios of slopes is within the experimental uncertainty.

Similar plots were made for the decay rates *vs.* H_2O_2 pressure. The data were badly scattered, but both plots indicated zero-order dependence on $[H_2O_2]$ at high H_2O_2 pressures (>0.5 Torr). At lower H_2O_2 pressures, both reactant decays were dependent on $[H_2O_2]$. The dependence seemed to approach first order at low enough H_2O_2 pressures.

The mechanism for reaction can be represented as

$$NO_2 + H_2O_2 \longrightarrow HO + HONO_2 \quad (2)$$

$$HO + NO_2 \longrightarrow HONO_2 \quad (3)$$

$$HO + H_2O_2 \longrightarrow H_2O + HO_2 \quad (4)$$

$$2HO_2 \longrightarrow H_2O_2 + O_2 \quad (5)$$

The HO_2 radical might also be removed *via*

$$HO_2 + NO_2 \longrightarrow O_2 + HONO \quad (6)$$

The HONO would ultimately revert to H_2O and NO_2, possibly *via*

$$HONO + HONO_2 \longrightarrow H_2O + 2NO_2 \quad (7)$$

even though this reaction is ~9 kcal/mol endothermic. There is good evidence for HONO as an intermediate, since there is an induction period in $HONO_2$ production and since the NO_2 reached its ultimate value before all the H_2O_2 was consumed. (See Figure 1.) The latter observation can be attributed to the fact that near the end of the run, NO_2 is being produced from HONO as fast as it is being removed by H_2O_2. In fact in some runs, $[NO_2]$ increased after the H_2O_2 was completely consumed.

Other reactions can also participate. For example, reaction 2 might be accompanied by the endothermic (~13 kcal/mol) reaction, $H_2O_2 + NO_2 \rightarrow HO_2 + HONO$. However, this reaction followed by reaction 5 is equivalent to reaction 6, and need not be considered separately. Another possible reaction is $HO + HONO_2 \rightarrow H_2O + NO_3$. This reaction probably occurs to some extent near the end of the reaction when $[HONO_2]$ is relatively large; the NO_3 would either react with NO_2 to produce N_2O_5 or with itself to produce $2NO_2 + O_2$. For simplicity we shall ignore the reaction between HO and $HONO_2$.

Reaction 3 has been reported previously and is rapid.[3] The ratio k_3/k_4 can be estimated from the expression

$$\frac{-\beta d[H_2O_2]/dt}{d[O_2]/dt} = 2 + k_3[NO_2]/k_4[H_2O_2] \quad (I)$$

where β is $^1/_2$ if reaction 6 is negligible, 1 if reaction 5 is negligible, or otherwise, between $^1/_2$ and 1. The ratio k_3/k_4 is estimated from the rates in Figure 1 to be between 2 and 8, though this may be the ratio of rate coefficients on the wall rather than in the gas phase. Since k_4 is 8.0×10^{-13} cm^3/molecule sec at 25°,[4] k_3 exceeds 10^{-13} cm^3/molecule sec.

Reaction 2 is rate controlling and is first order in $[NO_2]$. Since it is less than first order in $[H_2O_2]$, it presumably occurs on the wall, the reaction involving gas-phase NO_2 and adsorbed H_2O_2 following the Langmuir adsorption isotherm

$$[H_2O_2]_{ads} = \frac{a[H_2O_2]}{1 + a[H_2O_2]} \quad (8)$$

where a is some constant.

The rate law would then be first order in $[H_2O_2]$ if $1 \gg a[H_2O_2]$, zero order in $[H_2O_2]$ if $1 \ll a[H_2O_2]$, and appear to have an intermediate order at intermediate H_2O_2 pressures, *viz.*

$$-d[H_2O_2]/dt = k[NO_2][H_2O_2]^n \quad (9)$$

The rate coefficient k was found to be between 1 and 2 Torr^{-1} min^{-1} assuming $n = 1$ or 0.71 min^{-1} assuming $n = 0$. The former rate constant, which is an upper limit to the gas-phase reaction, becomes (0.5–1) $\times$ 10^{-18} cm^3/molecule sec.

Reaction of NO with $HONO_2$

The reaction of NO with $HONO_2$ has been reported by Smith[5] who found the stoichiometry to be

$$2HONO_2 + NO \longrightarrow 3NO_2 + H_2O \quad (10)$$

though the rate law was exceedingly complex. We have reexamined this reaction by adding NO to the $HONO_2$ produced in the reaction of H_2O_2 and excess NO_2. In each case the H_2O_2 was consumed prior to the addition of NO, but NO_2, O_2, and H_2O were present. The results of such an experiment are shown in Figure 1, where 2.0 Torr of NO was added after 20 min. The 1.5 Torr of $HONO_2$ was converted to 2.4 Torr of NO_2 and the above stoichiometry was confirmed. The most reasonable reaction sequence is

$$HONO_2 + NO \longrightarrow HONO + NO_2 \quad (11)$$

$$HONO_2 + HONO \longrightarrow H_2O + 2NO_2 \quad (7)$$

It is interesting that reaction 11 proceeds so readily since it is thermal neutral. Perhaps this reaction is more complex than indicated, especially since Smith found the rate to be at least partly heterogeneous and to be catalyzed by NO_2. Of course the fact that one of the products of reaction 11 (HONO) is removed by further reaction shifts the equilibrium far to the right.

Reaction of H_2O_2 with NO

The reaction of H_2O_2 with NO is slower than with NO_2, but is considerably more complex. Reactions were run in the presence of 1–2 Torr of Ar with initial NO pressures, $[NO]_0$, from 1 to 12 Torr; initial H_2O_2 pressures, $[H_2O_2]_0$, from 0.5 to 1.5 Torr; and $[NO]_0/[H_2O_2]_0$ ratios of 1–10. A typical reaction time history is shown in Figure 3. There is an induction period followed by a more rapid reaction. The products are NO_2 and probably $HONO_2$, both of which appear after considerable induction periods. In fact, the H_2O_2 was almost entirely consumed before NO_2 was observed, either optically or by mass spectral analysis. There was no evidence for O_2 production, though it may

(3) M. F. R. Mulcahy and R. H. Smith, *J. Chem. Phys.*, **54**, 5215 (1971).

(4) D. L. Baulch, D. D. Drysdale, and A. C. Lloyd, "High Temperature Reaction Rate Data," No. 3, Leeds University, April 1969.

(5) J. H. Smith, *J. Amer. Chem. Soc.*, **69**, 1741 (1947).

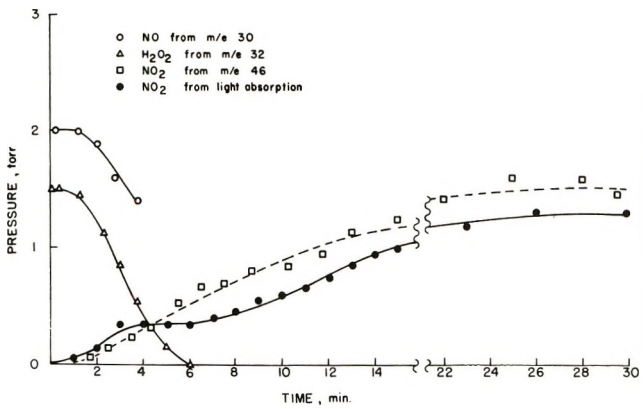

Figure 3. Plots of pressure *vs.* reaction time in the reaction of H_2O_2 with NO at 25°: $[NO]_0 = 2.0$ Torr; $[H_2O_2]_0 = 1.5$ Torr; [Ar] = 2.7 Torr. The excess NO_2 from the mass spectral determination reflects the presence of $HONO_2$. The NO pressure could not be monitored after measurable amounts of NO_2 were produced because the NO_2 mass spectral peak at *m/e* 30 interfered. Note break in abscissa between 15 and 22 min.

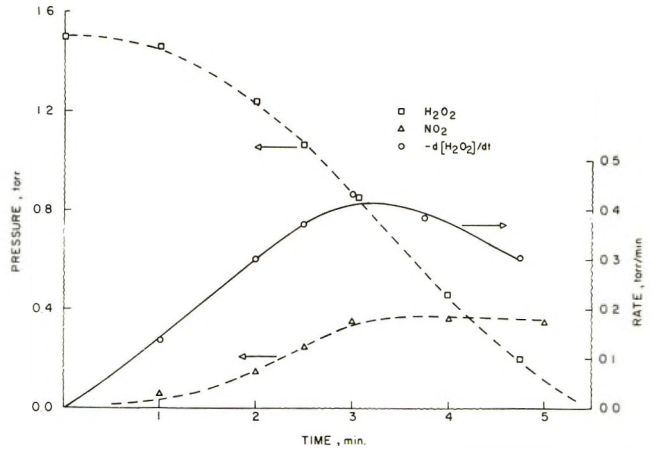

Figure 4. Early time history for H_2O_2 decay and NO_2 growth in run depicted in Figure 3. Also plotted is the slope of the H_2O_2 decay curve.

have been produced in small amounts. H_2O was probably also produced, though it was difficult to detect because of the large background peak in the mass spectrometer. No serious effort was made to look for this presumed product. When the reaction was completed the NO_2 produced equalled the H_2O_2 consumed in each run as determined from optical measurements. In Figure 3, where the final values have not quite been reached, the NO_2 is also shown as computed from the mass spectral peak at *m/e* 46, assuming that all the 46 peak can be attributed to NO_2. Clearly in the later stages of the runs, an additional compound, $HONO_2$, must also be present. Since the sensitivities of the peak at *m/e* 46 for both NO_2 and $HONO_2$ are similar, the difference ($\sim$0.3 Torr) can be considered to be $HONO_2$. Another interesting feature in the optical NO_2 curve is the plateau observed at about 4 min in the optical measurement. This occurred in all runs and apparently is not an artifact. The discrepancy with the mass spectral peak (which did not occur in every run) is due to the inaccuracy of the mass spectral analysis at low NO_2 pressures. Neglecting the $HONO_2$ production, the overall stoichiometry for the reaction is

$$H_2O_2 + NO \longrightarrow H_2O + NO_2 \qquad (12)$$

It is clear from the long time lag in NO_2 production that some intermediate must be produced as a precursor to NO_2 formation. Undoubtedly, this precursor is HONO, which probably would not be detected in our system. The nitrites and nitrates have almost no mass spectral parent or parent-minus-one peaks. For $HONO_2$, the parent peak (*m/e* 63) is $<1\%$ of the 46 peak, and no 62 peak was observed at all. Therefore in HONO, the peaks at *m/e* 46 and 47 are also probably undetectably small. The major expected peak at *m/e* 30 of course corresponds to NO, one of the reactants.

The initial slow decay of H_2O_2 corresponds to the attack of NO on H_2O_2

$$NO + H_2O_2 \longrightarrow HONO + HO \qquad (13)$$

Assuming that this reaction occurs entirely in the gas phase, which may not be so, gives an upper limit to the gas-phase rate constant of 0.10 $Torr^{-1}$ min^{-1} or 5.2×10^{-20} cm^3/molecule sec.

The acceleration in the rate must be due to catalysis by either HONO or NO_2, or both. Of course, NO_2 reacts more rapidly than NO with H_2O_2, so that reaction 2 would occur if any NO_2 were present. The resulting $HONO_2$ would react with NO to regenerate the NO_2, and $HONO_2$ would be only a minor product of the reaction. The NO_2 reaction sequence would be

$$NO_2 + H_2O_2 \longrightarrow HO + HONO_2 \qquad (2)$$

$$HONO_2 + NO \longrightarrow NO_2 + HONO \qquad (11)$$

$$HO + H_2O_2 \longrightarrow HO_2 + H_2O \qquad (4)$$

$$HO + NO \longrightarrow HONO \qquad (14)$$

$$HO_2 + NO \longrightarrow HO + NO_2 \qquad (15)$$

Figure 4 shows the early time portion of Figure 3 for the H_2O_2 decay and NO_2 growth. Also plotted are the decay rates of H_2O_2 as a function of reaction time. As the NO_2 accumulates, $-d[H_2O_2]/dt$ increases, reaching a maximum at the plateau in the $[NO_2]$ curve. Then both $-d[H_2O_2]/dt$ and $[H_2O_2]$ drop as the reaction between NO_2 and H_2O_2 passes out of the regime zero order in $[H_2O_2]$.

About 70% of the acceleration in the H_2O_2 decay can be accounted for by the NO_2–H_2O_2 reaction, as estimated from our results discussed earlier. Perhaps within the uncertainty of our measurements, all the enhancement is due to NO_2. However, if not, then some

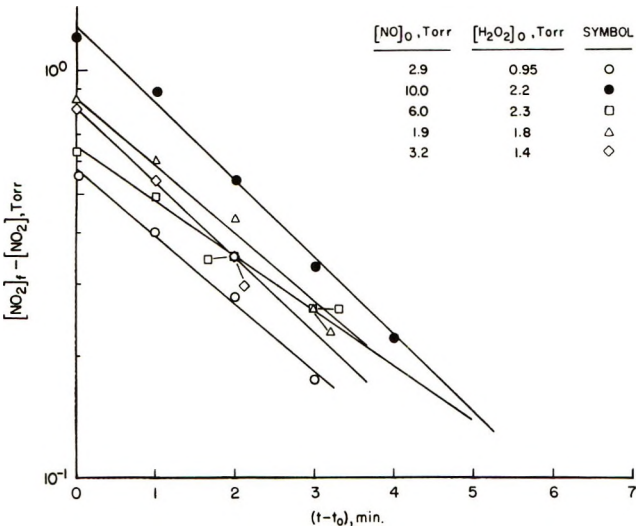

Figure 5. Semilog plots of $[NO_2]_f - [NO_2]$ *vs.* $t - t_0$ in the reaction of NO with H_2O_2 at 25° for several runs. $[NO_2]_f$ is the final $[NO_2]$ concentration and t_0 is a time after the H_2O_2 has been consumed.

of the acceleration may also be due to catalysis by HONO. A possible reaction step is

$$HONO^* + H_2O_2 \longrightarrow H_2O + NO_2 + HO \quad (16)$$

where HONO* is excited HONO. Reaction 16 is 12 kcal/mol endothermic and could only occur if the HONO retained some of the excess energy of formation in reaction 14.

HONO is known to disproportionate to H_2O, NO, and NO_2. After the H_2O_2 is completely removed this reaction should have no complications and obey a simple rate law. All of the runs were analyzed for that portion where the H_2O_2 was already completely consumed. None fitted a second-order law, and all gave satisfactory first-order plots, as shown in Figure 5. Thus HONO removal must occur on the wall

$$HONO \xrightarrow{\text{wall}} HONO_{ads} \quad (17)$$

$$HONO_{ads} + HONO \longrightarrow H_2O + NO + NO_2 \quad (18)$$

with reaction 17 rate determining. The slopes in Figure 5 give $k_{17} = 0.30$–$0.45\ min^{-1}$.

Conclusion

The reaction scheme in the H_2O_2–NO–NO_2 system has been elucidated and is at least partly heterogeneous. The homogeneous reactions of NO and NO_2 with H_2O_2 are too slow to be of importance in the upper atmosphere. However, in polluted urban atmospheres where H_2O_2 concentrations can reach ~0.2 ppm,[6] the heterogeneous reactions may be of considerable importance in the conversion of NO to NO_2 especially in the presence of particulates which could act as surfaces on which the reactions proceed.

Acknowledgment. The authors wish to thank Drs. H. A. Wiebe and R. Simonaitis for their help. This work was supported by NASA Grant NGL-009-003 and NSF Grant No. GP-5611 for which we are grateful.

(6) J. Bufalini, private communication, 1971.

Disulfur and the Lower Oxides of Sulfur in Hydrogen Sulfide Flames

by Earl L. Merryman and Arthur Levy*

Battelle Columbus Laboratories, Columbus, Ohio 43201 *(Received December 28, 1971)*

Publication costs assisted by Battelle Columbus Laboratories

The probing of H_2S flames at pressures of 0.1 and 0.05 atm under molecular-flow sampling conditions has provided conclusive evidence on the type of transient species existing in these flames. The mass spectrometric analyses indicate the species to be S_2, S_2O, and SO and also provide evidence that the species appear in the sequence shown. The appearance of S_2O prior to SO formation, as implied from the flame data, suggests that additional steps are involved in the oxidation of H_2S which have not yet been considered in the oxidation process. This information is of importance in developing the mechanism involved in the oxidation of sulfur in flames and may lead to some additions and changes in the proposed H_2S oxidation mechanism presented in previous papers. The appearance of a species at m/e 34 which is more easily ionized in the mass spectrometer than H_2S has resulted in speculation on the formation of H_2O_2 in these H_2S flames. To the authors' knowledge this molecule has not been postulated in previous H_2S oxidation mechanisms. Estimates have been made of the mass spectrometric sensitivities to the intermediate species, and mole fractions of the species were determined from these estimated values. The results indicate that each species is present in concentrations up to several thousand parts per million. Several elementary reactions have been suggested to account for the formation of sulfur-containing intermediates in the H_2S flame.

Introduction

Studies of the oxidation of sulfur-bearing compounds under various experimental conditions have been a subject of interest to numerous investigators over the past several decades. Two review articles, one by Cohen and Heicklen[1] and the other by the authors,[2] have been published recently; much of the available literature on the subject matter has been presented therein. The results from these past studies clearly show that many of the steps involved in the oxidation of these sulfur compounds are not yet well understood. This is especially true with respect to the type of sulfur oxide intermediates present during the oxidation of the sulfur compounds.

In nonflame systems, Norrish and Zeelenberg[3] and Emanuel[4] have presented evidence for the existence of sulfur monoxide, SO, as an intermediate in their hydrogen sulfide oxidation studies. Marsden[5] and Meschi and Myers[6] have indicated, in more recent work, that the SO observed by these earlier investigators is probably a mixture of the oxides S_2O and SO_2. On the other hand, Schenk and Steudel[7] reported that SO is observed in their studies and that is it quite reactive, disproportionating very rapidly to S_2O and SO_2

$$2SO \longrightarrow (SO)_2$$

$$SO + (SO)_2 = S_2O + SO_2$$

Furthermore, they suggested that the presence of S_2O in a system indicates prior existence of SO. However, in this paper and other recent work by the authors in flame systems,[8] the data indicate that S_2O can form prior to SO. Also, results from the work of Halstead and Thrush[9] imply that SO is a relatively unreactive molecule except toward oxygen atoms. Thus, studies on sulfur oxide intermediates are not conclusive at this time.

In the present study, the authors present new information on the above intermediates as obtained from the oxidation of hydrogen sulfide in low-pressure flames. Data are presented which confirm the existence of S_2, S_2O, and SO as intermediates in the oxidation of H_2S in flames. The conditions under which the intermediates are produced as well as their role in the sequence of flame reactions are discussed.

Experimental Procedure

Data on the intermediates discussed in this study have been obtained from the probing of low-pressure (0.1–0.05-atm) hydrogen sulfide flames. The experimental procedure for the probing of low-pressure flames has been described in previous papers.[10,11] The overall

(1) N. Cohen and J. Heicklen, *Compr. Chem. Kinet.*, **6**, 1 (1970).

(2) A. Levy, E. L. Merryman, and W. T. Reid, *Environ. Sci. Technol.*, **4**, 653 (1970).

(3) R. G. W. Norrish and A. P. Zeelenberg, *Proc. Roy. Soc., Ser. A*, **240**, 293 (1957).

(4) N. M. Emanuel, *Acta Physicochim., U.R.S.S.*, **19**, 360 (1944).

(5) D. G. H. Marsden, *Can. J. Chem.*, **41**, 2607 (1963).

(6) D. M. Meschi and R. J. Myers, *J. Amer. Chem. Soc.*, **78**, 6220 (1956).

(7) P. W. Schenk and R. Steudel, *Angew. Chem., Int. Ed. Engl.*, **4**, 402 (1965).

(8) E. L. Merryman and A. Levy, paper presented at the Second International Air Pollution Conference of the International Union of Air Pollution Prevention Association, Washington, D. C., Dec 6–11, 1970.

(9) C. J. Halstead and B. A. Thrush, *Proc. Roy. Soc., Ser. A*, **295**, 363 (1966).

(10) A. Levy and E. L. Merryman, *Combust. Flame*, **9**, 229 (1965).

(11) E. L. Merryman and A. Levy, *J. Air Pollut. Contr. Ass.*, **17**, 800 (1967).

apparatus remains essentially the same in these studies; however, an important modification has been made in the sampling procedure. This modification allows the samples to be removed from the flame system under molecular flow conditions. As a result, the highly active intermediates survive the short path to the analyzer section of the mass spectrometer, thus allowing direct detection of these species.

A Finnigan 1015 quadrupole mass spectrometer was modified for use in these flame probings. The instrument has fast-scanning features, has unit resolution to 750 amu, and can detect most species in the low-ppm range. A 2.25-in. diameter flat-flame burner attaches directly to the analyzing unit of the mass spectrometer producing a short unrestricted straight path from the sampling probe tip to the analyzer section (Figure 1).

The sampling probe is made of quartz tubing drawn to a fine tip at one end. In the tip of the probe is a 50–75-μ orifice through which the flame samples pass and are immediately quenched, at pressures from 10^{-3} to 10^{-4} mm. For temperature profiles, the quartz probe is replaced with a temperature probe consisting of a 25-μ Pt—Pt–10% Rh thermocouple coated with silicon dioxide.

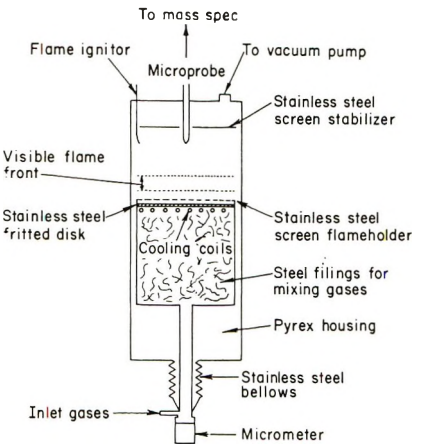

Figure 1. Low-pressure flat-flame burner.

Results

Composition Profiles. Stable Species. Although concentration profiles were obtained for all of the stable species in each of the hydrogen sulfide flames probed in this study, only a representative set of profiles is shown here since we are presently concerned mainly with the active intermediates in the H_2S flame and not with final products. Other papers present detailed profiles of stable reactants and products.[10,11]

Figure 2 shows the profiles from a stoichiometric H_2S flame probed at 0.05 atm. The profiles are typical of those encountered under normal mass spectrometric operating conditions, *i.e.*, 70-V electron-accelerating potential and 150–300-μA electron current. As seen in Figure 2, the sulfur in the H_2S molecule is rapidly oxidized to SO_2 while the hydrogen is less rapidly oxidized to H_2O. A corresponding depletion of O_2 consistent with the stoichiometric reaction $H_2S + {}^3/_2O_2 = H_2O + SO_2$, is observed in the combustion process. Hydrogen is produced as a transient species and serves as an additional source of H_2O in the flames. As seen later, the shapes of the H_2S and SO_2 curves change noticeably when the electron-accelerating voltage is reduced in the appearance potential studies. This change in profiles is taken as evidence for the existence of intermediates in the H_2S flames.

Transient Sulfur Compounds in H_2S Oxidation. Transient sulfur compounds have been identified in recent H_2S oxidation studies. Under the revised molecular-flow sampling conditions at normal operating potential, three sulfur-bearing intermediates have been observed in the mass spectrometric data. These intermediates have been assigned the molecular composition S_2, S_2O, and SO.

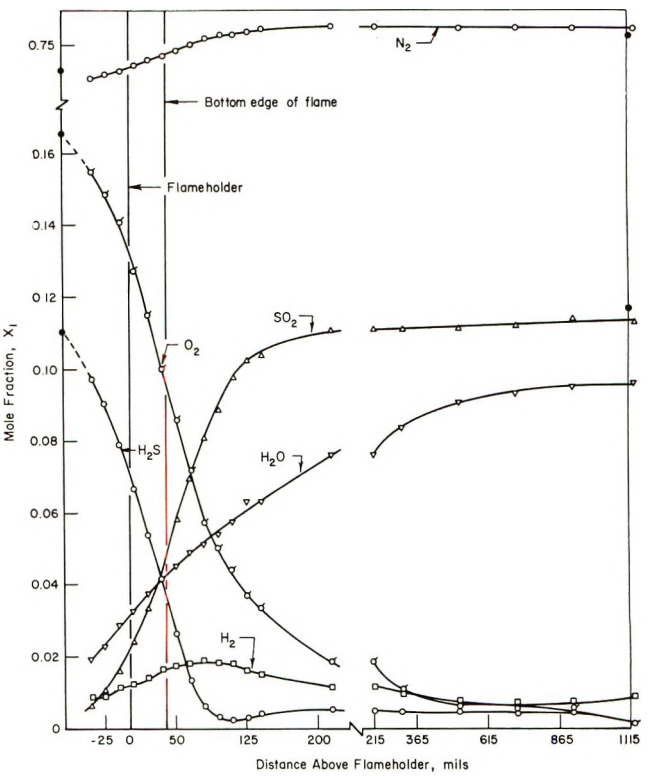

Figure 2. Composition profiles of stable reactants and products in H_2S flame, pressure 0.05 atm.

S_2O is observed directly in the mass spectrometric flame sampling data. However, S_2 and SO require more elaborate techniques for direct detection. The difficulty in detecting S_2 and SO arises from two facts: one, not only are S_2 and SO very reactive intermediates, but, two, in a heated system containing sulfur and oxygen, there is usually a relatively large amount of SO_2 present. The SO_2 fragmentation pattern interferes with the mass spectrometric patterns for S_2 and SO but not with that for S_2O. Both SO_2 and S_2 have molecular weights of 64 and both produce major peaks

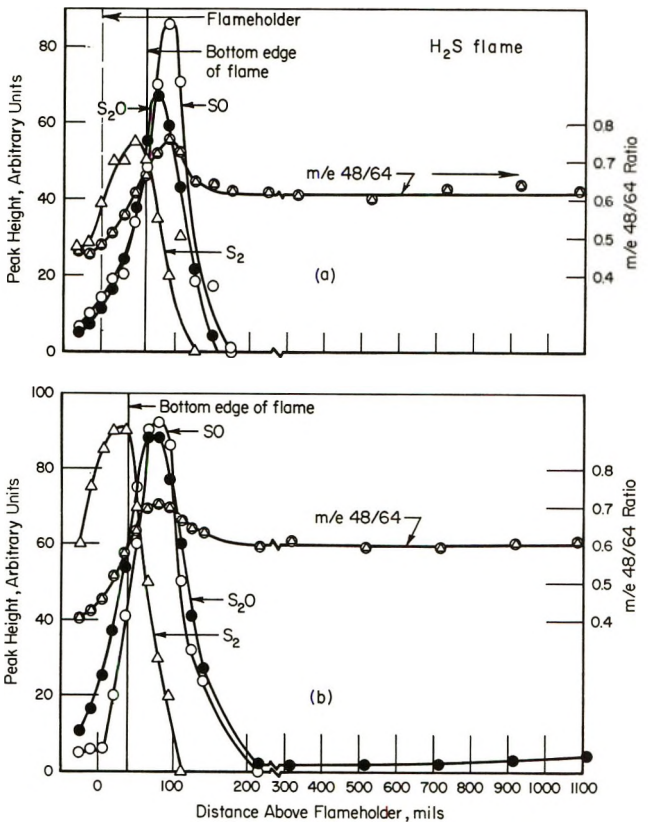

Figure 3. Intermediates in H_2S flames, 70-V ion-accelerating potential, pressure 0.05 atm: (a) oxygen-rich flame; (b) stoichiometric flame.

which appear at mass to charge ratio (m/e) of 64. In addition, SO_2 fragments to produce a large m/e 48 peak which interferes with the small peak from the SO intermediate. Therefore, in determining the presence of S_2 and SO in these systems, it is necessary to correct for the large SO_2 contribution to m/e 64 and 48, or one may also use appearance potential techniques to reduce greatly or eliminate the contributions to m/e 64 and 48 from SO_2 while still allowing detection of the m/e 64 and 48 from the more active S_2 and SO intermediates, respectively.

SO_2-Correction Technique. Figures 3a and 3b show typical profiles of each of the species S_2, S_2O, and SO derived from the flame data after appropriate corrections for SO_2 contribution to the m/e 64 and 48 peaks determined from the constant m/e 48/64 ratio observed in the postflame region. Profiles in Figure 3a represent O_2-rich flames, while those in Figure 3b represent stoichiometric flames. Total flame pressure was 0.05 atm and ionization potential was 70 V in each case.

S_2O. The S_2O peak shown in Figures 3a and 3b was taken from the mass spectrometric data and represents the total m/e 80 peak height. Although SO_3 is present in the O_2-rich flames and also has a major m/e 80 peak, it is not detected in the mass spectrometer even at levels of 200–300 ppm or more. That there is essentially no contribution from SO_3 to the m/e 80 peak here is confirmed by the following observations: (1) a wet-chemical analysis for SO_3 showed that the SO_3 profile reaches a maximum ahead of the recorded S_2O peak maximum, (2) in the O_2-rich flames (Figure 3a) the SO_3 concentration is not zero in the postflame region whereas the m/e 80 peak height is zero beyond 200 mils in these flames, (3) in stoichiometric flames the SO_3 concentration is essentially zero in the postflame region whereas in Figure 3b the m/e 80 peak is not zero, and (4) the observed m/e 82 peak which arises in the fragmentation pattern from the ^{34}S isotope (4.2% abundance) is about 9% of the m/e 80 peak in these flame probings which is consistent with two sulfur atoms in the sulfur oxide molecule S_2O. If, on the other hand, only SO_3 were present, m/e 82 would be about 4.5% of m/e 80, indicative of one sulfur atom. (Possibly the SO_3 unites with water vapor to form H_2SO_4 prior to analysis.) From these considerations, the peak heights shown in Figures 3a and 3b for S_2O are attributed solely to this species.

SO. S_2O, like SO_2, yields a m/e 48 peak in its fragmentation pattern. Both S_2O and SO_2, therefore, must be considered in the analysis of SO, which has a major peak at m/e 48. Meschi and Myers[6] have shown in their data, however, that S_2O has a major peak at m/e 80 and indicated that S_2O contributes only about 7% to the m/e 48 peak. This contribution is sufficiently small to present no problem in the analysis of SO in the flames. Therefore, in developing the final SO profiles shown in Figure 3, the main contribution to the m/e 48 peak is from SO_2.

The profiles developed from the flame data, using the ratio of m/e 48/64, indicate the appearance of SO. It is quite evident in the plots in Figures 3a and 3b that the m/e 48/64 peak ratio is constant in the postflame region where only SO_2 is present. As one approaches the visible-flame zone the 48/64 ratio varies. An increase would occur in the 48/64 ratio if SO were forming in the flame since SO contributes to the 48 peak but not the 64 peak. This behavior has been observed and substantiates the presence of SO in the flames. Ozone is not considered a contributor to the m/e 48 peak based on the appearance of a m/e 50 peak from $^{34}S^{16}O$ and on the approximately constant m/e 50/48 ratio. Ozone does not contribute noticeably to the m/e 50 peak since the abundance of ^{18}O is only 0.2% compared to 4.2% for ^{34}S.

The profiles indicate that SO first appears in the cooler regions below the bottom edge of the visible-flame zone and is completely consumed in the hotter flame regions within 175–250 mils above the flameholder in either the O_2-rich or the stoichiometric flame. This is contrasted to the apparent survival of S_2O into the postregion of the stoichiometric flame, Figure 3b. The SO profiles as determined here are further confirmed in the appearance potential studies discussed shortly.

The data in Figure 3 indicate the sequence S_2, S_2O,

and SO for the formation of the intermediates in the flames. The separation of the S_2O and SO maxima, however, is very small, amounting to only 5 or 10 mils. In oxygen-rich systems (Figure 3a) the S_2O and SO curves actually coincide below the visible flame. In stoichiometric flames, the earlier appearance of S_2O is noted below the visible flame (Figure 3b). The S_2O curve generally peaks before the SO curve in each case, thus providing additional evidence for the formation of S_2O prior to SO.[12]

S_2. In the preflame region the *m/e* 48/64 ratio is considerably less than that observed in the postflame region. This is attributed to the presence of S_2 in the system which contributes significantly to *m/e* 64 in this region. Since S_2 does not contribute to the *m/e* 48 peak, a decrease in the *m/e* 48/64 ratio would result from the presence of S_2 providing that the SO concentration is constant or decreasing. The latter situation is observed here. Further verification of the presence of S_2 was made by observing that the *m/e* 66 peak, while normally less than 5% of *m/e* 64 from SO_2 in the postflame region, increased to over 6.5% of the *m/e* 64 in the preflame region. The data are presented in Table I for an O_2-rich H_2S flame at 0.05 atm. This increase would occur if S_2 were present since *m/e* 66 (from ^{32}S-^{34}S) is about 9% of *m/e* 64 from S_2 and would thus add to the overall *m/e* 66/64 ratio. The 9% value is not attained here since a considerable amount of SO_2 is also present with the S_2.

Table I: Change in *m/e* 66/64 Peak Ratio from 0.05-Atm O_2-Rich H_2S Flame

Distance above flameholder, mils	Peak height		Percentage *m/e* 66/64 × 100
	m/e 64	*m/e* 66	
1100	590	29	4.9
700	570	28	4.9
300	600	29	4.8
150	605	30	5.0
110	520	27	5.2[a]
80	400	21	5.3
65	290	16.5	5.7
50	205	12	5.8[b]
35	140	8	5.7
20	86	5.5	6.4
5	52	3.5	6.7

[a] Top edge of flame at 95 mils. [b] Bottom edge of flame at 45 mils.

The data thus far present convincing evidence for the existence of all three transient species S_2, S_2O, and SO in the flame system. However, to confirm these findings further, H_2S flames of identical compositions were examined in separate probings using appearance potential techniques to identify the intermediates.

Appearance Potential Technique. The appearance potential studies were carried out at electron-accelerating voltages of 12.0 and 13.8 V. Typical data from two of the flame probings are presented in Figures 4 and 5.

Figure 4 shows the H_2S, SO_2, S_2O, and SO data obtained from a stoichiometric H_2S flame probed at 0.05 atm using an appearance potential of 13.8 V. At this voltage, the SO_2 contribution to *m/e* 48 vanishes (note *m/e* 48 in postflame region). It is apparent from these flame probings that a *m/e* 48 peak makes its initial appearance in the same general region as designated for SO at the higher accelerating potential (Figure 3b). However, at this lower potential, the formation of a *m/e* 48 peak must be due solely to SO, since there is essentially no contribution from SO_2 or S_2O. That S_2O is contributing very little to the *m/e* 48 peak at the low electron voltages can be seen from the low preflame values of the ratio *m/e* 48/80, as shown in Figure 3 or 4. Also, since S_2O has a parent peak at *m/e* 80, the contribution to *m/e* 48 from S_2O at 13.8-V accelerating potential can be expected to be much less in total peak height than that observed by Meschi and Myers at higher electron voltage (discussed earlier). Thus, direct detection of SO is attained at the operating potential of 13.8 V. Furthermore, the data also confirm the formation of S_2O prior to SO in these flames.

The trends in the H_2S, SO_2, S_2O, and SO curves in Figure 4 at 13.8 V are essentially the same as those observed at the higher electron voltages in Figures 2 and 3; *i.e.*, the H_2S (*m/e* 34) and O_2 (*m/e* 32) decrease while the SO_2 (*m/e* 64) increases in the region from 0 to 150 mils. Upon further reduction of the accelerating potential to 12.0 V, the *m/e* 64 and 34 peaks from SO_2 and H_2S, respectively, were still present but significant changes were observed in the shape of the curves for these stable molecules. On the other hand, the profiles of the active intermediates S_2O and SO remained essentially the same.

The data from a stoichiometric H_2S flame are plotted in Figure 5. The change in the SO_2 profile can be seen in following the *m/e* 64 curve from the postflame region to the flameholder. At the lower potential of 12.0 V, the *m/e* 64 curve actually increases in the visible flame region of the stoichiometric flame. The normal trend at the higher electron voltages is for the *m/e* 64 to de-

(12) Comment added in review: One reviewer rightfully questioned the justifiability for the argument that S_2O precedes SO in these flame systems. It is quite true that the quantitative treatment for SO cannot be very good in the cases where the contribution to *m/e* 48 from SO_2 has to be considered (Figures 3a and 3b). However, in the appearance potential studies (Figures 4 and 5), there is no contribution, within detection limits, to *m/e* 48 from SO_2. Therefore, the *m/e* 48 peak is principally due to SO in these studies. Since the data of Figures 4 and 5 show an *m/e* 80 peak, *i.e.*, S_2O, present in the preflame region at the point where the *m/e* 48 peak is zero and since the S_2O maxima are generally at least 5 mils upstream of the SO maxima (on an expanded scale the S_2O maximum in Figure 4 is about 5 mils upstream of the SO maximum), we have concluded that S_2O formation can precede SO formation in the flame.

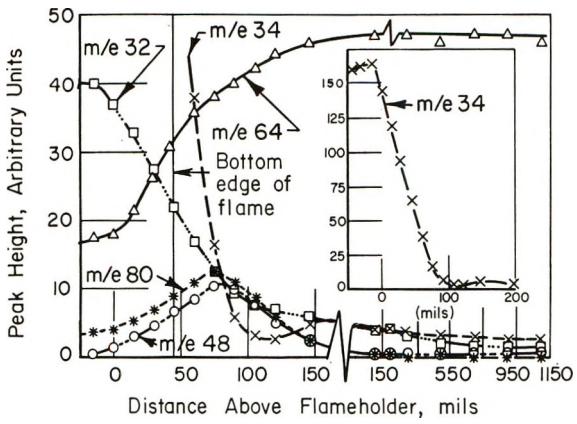

Figure 4. Profiles of the intermediates S_2O (m/e 80), SO (m/e 48), SO_2 (m/e 64), H_2S (m/e 34), and O_2 and/or S (m/e 32) in stoichiometric H_2S flame at 0.05 atm and 13.8-V ion-accelerating potential.

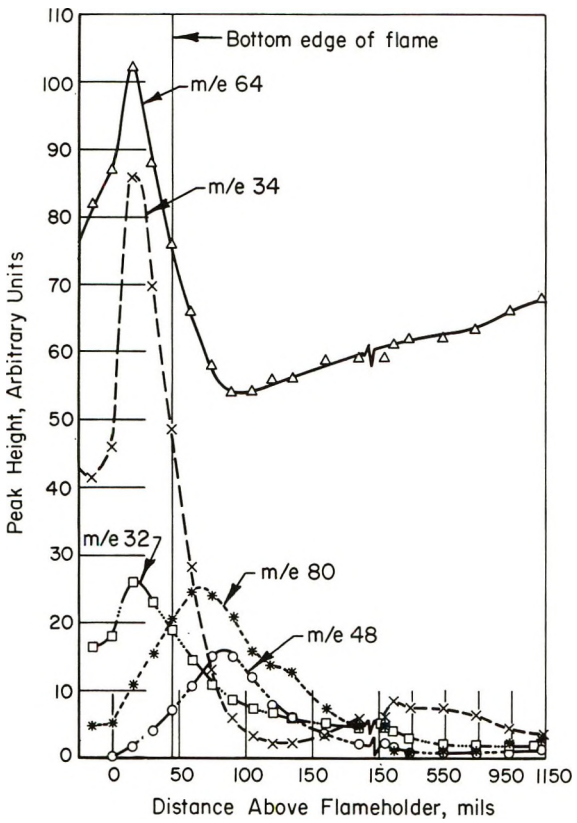

Figure 5. Repeat profiles of Figure 4 at 12.0-V ion-accelerating potential.

crease in the 150–0-mil region as seen in Figure 4 (m/e 64 = SO_2). The abnormal behavior (the increase) at this lower accelerating potential is taken as evidence for the presence of S_2. The 12.0-V ionizing potential is sufficient to ionize S_2 readily but is considerably less effective in ionizing SO_2. The result is an increase in the m/e 64 peak height in the region where S_2 is being produced. Hagemann[13] has reported an ionization potential of 9.7 ± 0.1 eV for S_2 while that reported for SO_2 is higher at 12.5 ± 0.2 eV.

A further interesting observation is seen in the m/e 34 peak curve. Since the normal profiles of H_2S curves in flames (Figure 2) show the H_2S to start at a given level and decrease continuously to zero as the flame is approached from the flameholder, it might be expected that the H_2S curve at 12.0 V would be similar to that at 13.8 V. Instead, we see an initial rise in the H_2S curve starting near 0 mil, reaching a maximum value below the bottom edge of the flame, and then decreasing to a minimum at 125 mils (Figure 5). There appear to be a second smaller rise in the m/e 34 curve beyond 150 mils. As in the case of the m/e 64 curve, the large rise observed in the m/e 34 curve below the flame is attributed to the presence of an intermediate which has an ionization potential below that for H_2S. However, no sulfur-bearing species with a value of m/e 34 is readily apparent, other than H_2S. The same effect is also reflected in the m/e 32 peak curve, but this could be due to the S_2 molecule fragmentation pattern or to S atom ionization.

A species that comes to mind which satisfies the m/e 34 requirement is H_2O_2. This molecule has not been postulated in any of our H_2S oxidation steps. However, other investigators have reported the formation of H_2O_2 in various H_2–O_2 oxidation studies.[14,15] Indications are that the hydrogen peroxide forms from the reaction of HO_2 radicals with H_2. This being the case, H_2O_2 could also likely form in the H_2S oxidation process since H_2 is present as an intermediate in this flame and the HO_2 radical is postulated to form in one of the early H_2S flame reactions.[11] The increase in m/e 34 observed in the preflame region is therefore tentatively attributed to H_2O_2. The slight rise in m/e 34 in the postflame region may be due to re-formation of H_2S under the near-stoichiometric flame conditions.

Concentration of Transient Species. Although standards are not available for S_2, S_2O, and SO calibrations in the mass spectrometer, attempts have been made to approximate the concentrations of one of these transient species. From the analyses of earlier flame samples,[11] the SO concentration was determined by oxidizing the SO in 3% hydrogen peroxide solutions. Results from this method indicate that the maximum concentration of SO is about 10,000 ppm, ~0.01 mole fraction. By estimating the mass spectrometric sensitivity for SO near that for O_2 a mole fraction of approximately 0.01 is also obtained for SO from the present data. Although the two sensitivities are not likely the same (SO being more easily ionized than O_2), they probably do not differ greatly. Both the wet analysis and mass spectrometer methods substantiate the relatively high concentration of SO in these H_2S flames.

(13) R. Hagemann, *C. R. Acad. Sci.*, **255**, 1102 (1962).
(14) C. Kourilsky and H. James, *Bull. Soc. Chim. Fr.*, 410 (1965).
(15) G. J. Minkoff and C. F. H. Tipper, "Chemistry of Combustion Reactions," Butterworths, London, 1962, pp 34–55.

S_2 and S_2O concentrations can only be estimated at present by assigning mass spectrometric sensitivities to these molecules comparable to those observed for stable species of similar molecular structure. The data indicate that the maximum concentrations of the species S_2 and S_2O are several thousand parts per million, each, *i.e.*, comparable to the SO concentrations, depending on such flame conditions as the amount of excess oxygen available and total flame pressure.

Mechanism. Due to the steep concentration gradients and the resulting strong diffusion currents encountered in flames, it is likely that several reactions can contribute to the formation of an intermediate during an oxidation process. A number of reactions which may contribute to S_2, S_2O, and SO formation are presented in the following paragraphs. The relative importance of each reaction is discussed in terms of the energy requirements, nature of the reactions, and appropriate interpretation of the available flame data.

SO Formation. A detailed mechanism has been presented for the oxidation of H_2S flames.[11] Of the three intermediates, S_2, S_2O, and SO, only the formation of SO has been accounted for in this mechanism

$$SH + O_2 = SO + OH + 22.3 \text{ kcal} \quad (1)$$

and is presented as a major source of SO in H_2S flames. Other reactions such as

$$S + O_2 = SO + O + 5.5 \text{ kcal} \quad (2)$$

$$S_2O + O = 2SO + 35.3 \text{ kcal}[16] \quad (3)$$

$$SH + O = SO + H + 38.7 \text{ kcal} \quad (4)$$

were not included in the earlier mechanism but could also contribute to SO formation. Since SO can readily be produced in the absence of hydrogen-containing species as brought out in recent COS flame probings,[17] reactions 2 and 3 are likely to be important sources of SO in flames.

All four reactions are thermodynamically favorable. The fact that O_2 is present in the preflame region in much larger quantities than O atoms makes reactions 1 and 2 more favorable than reactions 3 and 4. However, the latter two reactions no doubt have lower energy requirements than the others and are, therefore, favored from this point of view. The relative rates of reactions at the prevailing temperatures would, of course, determine the importance of each in contributing to SO formation.

S_2 Formation. Mention has been made of reactions of the types

$$SH + SH = H_2S + S + 3.4 \text{ kcal} \quad (5)$$

and

$$SH + SH = H_2 + S_2 + 32.9 \text{ kcal} \quad (6)$$

resulting in sulfur formation.[11] These could be important sources of elemental sulfur early in the flame reaction. Other reactions such as

$$SO + SH = S_2 + OH - 7.6 \text{ kcal} \quad (7)$$

$$S_2O + H = S_2 + OH + 19.7 \text{ kcal} \quad (8)$$

may also contribute to sulfur formation by diffusion processes in the cooler preflame regions. However, reaction 8 might be replaced by a seemingly more favorable reaction

$$S_2O + H = SH + S \quad (8a)$$

which could then produce S_2 by reactions 5, 6, or 7. All of the reactions, except reaction 7, are thermodynamically favorable. Three of the four reactions involve SH radicals indicating it is a major source of sulfur in the flames.

S_2O Formation. The diffusion process could also account for some of the S_2O formation *via* SO disproportionation

$$SO + SO = S_2O + O - 35.3 \text{ kcal}[18] \quad (9)$$

and

$$3SO = S_2O + SO_2 + 94.6 \text{ kcal} \quad (10)$$

and also

$$SO + S_n = S_2O + S_{n-1} \quad (11)$$

Reaction 9 is highly endothermic and not likely to occur to any large extent in the flames. Reaction 10, on the other hand, is highly exothermic and may be thermodynamically favorable but would be of less importance as a source of S_2O due to the three-body nature of the reaction in the sequence

$$2SO \longrightarrow S_2O_2 \xrightarrow{SO} S_2O + SO_2$$

involving SO—a species of relatively low concentration compared to the stable species present. Reaction 11 may be an important source of S_2O. However, since the flame probings indicate some S_2O formation prior to SO formation, other steps must also be involved in S_2O production. These most likely involve elemental sulfur already formed in the preflame region (see eq 5–8a). Reaction 12 would require a relatively high

$$S_2 + O_2 = S_2O + O - 36.3 \text{ kcal} \quad (12)$$

$$S_2 + O + M = S_2O + M + 81.7 \text{ kcal} \quad (13)$$

$$S_n + O = S_2O + S_{n-2} \quad (n \geq 3) \quad (14)$$

$$S_2 + OH = S_2O + H - 19.6 \text{ kcal} \quad (15)$$

activation energy and would, therefore, probably be

(16) Calculated at 0°K based on $\Delta H^\circ = -22.7$ kcal/mol for S_2O.[7] Other heats of reaction calculated at 1000°K.

(17) A. Levy and E. L. Merryman, *Environ. Sci. Technol.*, **3**, 63 (1969).

(18) ΔH's for reactions 8–15 were calculated at 0°K.

less likely to occur than some of the others. The same is true to a lesser extent for reaction 15. Reactions 13 and 14 appear most favorable for S_2O formation.

Conclusion

Obviously, a number of reactions exist which could be important in the formation of the intermediates S_2, S_2O, and SO. Many of the reactions involve radicals and atoms essential to flame propagation. The three sulfur-bearing intermediates from H_2S oxidation are, therefore, likely to form generally in any flame oxidation process.

From the air pollution point of view, the removal of any one of the three intermediates in a combustion process would, of course, reduce SO_2 formation in the system. However, since the formation of SO_2 is believed to occur predominantly through the reaction

$$SO + O_2 = SO_2 + O \quad (16)$$

it is apparent that removing SO would greatly reduce SO_2 formation and, therefore, its emission to the atmosphere. There are obvious problems involved in any attempt to remove any of the intermediates—problems such as finding reactants which will react rapidly and specifically with S_2, S_2O, or SO and which will form compounds with the intermediates that will withstand the high temperatures encountered in flame processes. Nevertheless, the possibility of removing the sulfur-bearing intermediates to control sulfur oxide emission should not be ignored.

Acknowledgment. The authors wish to acknowledge the assistance of the Research Grants Branch, Environmental Protection Agency, under Grants AP 00464-04 and -05.

The Reaction of Cyanogen Radicals with Ammonia[1]

by G. E. Bullock, R. Cooper,*

Chemistry Department, University of Melbourne, Parkville, Victoria 3052, Australia

S. Gordon, and W. A. Mulac

Chemistry Division, Argonne National Laboratory, Argonne, Illinois 60439 *(Received January 10, 1972)*

Publication costs assisted by Argonne National Laboratory

The pulse radiolysis of dilute C_2N_2–NH_3 mixtures in argon has been used to study the reaction of CN radicals with NH_3 at 300 and 375°K. An increase in the rate constant for CN radical disappearance was observed for radicals with higher vibrational excitation than the ground state. Removal of the ground and fourth vibrational states showed a negative temperature dependence. ("These results are discussed with respect to the possible roles played by chemical reaction and by vibrational relaxation.")

Introduction

Cyanogen (CN) radicals have received a great deal of attention in spectroscopic[2] and thermodynamic[3] studies but fewer data are available on the kinetics of reactions of this reactive radical. Bimolecular rate constants of varying reliability have been determined for reaction with oxygen,[4,5] ammonia,[5] methane,[5] water,[4a] nitric oxide[4b,5] and the dimer cyanogen (C_2N_2).[4a,5] Some measurements have included estimates of activation energies.[4a,5,6]

The results of work done at this laboratory on the rates of reaction with saturated and unsaturated hydrocarbons are to appear shortly.[7] In this paper we wish to report kinetic parameters for the reaction of CN radicals with gaseous ammonia at 303 and 375°K. CN radicals, produced by pulse radiolysis of dilute solutions of C_2N_2 in argon, have been monitored spectrophoto-

(1) Based on work performed under the auspices of the U. S. Atomic Energy Commission.

(2) (a) G. Herzberg, "Molecular Spectra and Molecular Structure, Vol. I. Spectra of Diatomic Molecules," 2nd ed, Van Nostrand, Princeton, N. J., 1950, and references therein; (b) N. Basco, J. E. Nicholas, R. G. W. Norrish, and W. H. J. Vickers, *Proc. Roy. Soc., Ser. A*, **272**, 147 (1963).

(3) (a) D. D. Davies and H. Okabe, *J. Chem. Phys.*, **49**, 5526 (1968); (b) T. L. Cottrell, "The Strengths of Chemical Bonds," Butterworths, London, 1954.

(4) (a) D. E. Paul and F. W. Dalby, *J. Chem. Phys.*, **37**, 592 (1962); (b) N. Basco and R. G. W. Norrish, *Proc. Roy. Soc., Ser. A*, **283**, 291 (1965); N. Basco, *ibid.*, **283**, 302 (1965).

(5) J. C. Boden and B. A. Thrush, *ibid.*, **305**, 107 (1968).

(6) C. A. Goy, D. H. Shaw, and H. O. Pritchard, *J. Phys. Chem.*, **69**, 1504 (1965).

metrically in the ground, second, and fourth vibrational levels of the ground electronic state ($X^2\Sigma$). An attempt was also made to follow the appearance of the product NH_2 radical.[8]

Experimental Section

The pulse radiolysis equipment has been described in detail previously.[8] The radiolysis cell used in this work, while of the same design, was modified in several ways to allow controlled elevated temperatures to be obtained. "Viton" O-rings were replaced by gold and the adjustable mirror controls were changed to a temperature-insensitive type using a metal bellows rather than O-rings. A thermocouple (Pt—10% Rh–90% Pt) was included to monitor the gas temperature. The cell was completely enclosed in a thermostated oven which permitted accurate temperature control ($\pm\sim1.5$°K) up to ~425°K.

The optics and kinetic spectroscopic arrangements were unchanged from the earlier publications.[7,8] The Hilger-Engis Model 600/1000 was used as a monochromator and with 100-μ entry and exit slits gave a band pass of ~0.8 Å. This meant the vibrational bands of the CN $X^2\Sigma \rightarrow B^2\Sigma$ electronic transition could be separately monitored *via* the $\Delta v = 0$ sequence at ~3880 Å. These wavelengths were arbitrarily chosen but were ~1.5 Å below the band heads. The absorptions did not obey Beer's law and the modified form, $OD = \epsilon'(cl)^n$, was used.[7-9] The n values were determined by varying either path length or dose[7] and were effectively constant at 0.75 ± 0.05 for the three bands. For the NH_2 radical an n value of 0.77 was used.[8]

The cyanogen was Matheson Co. CP grade and was purified as described previously.[7] Ammonia was stored over metallic sodium and purified by conventional trap-to-trap distillations. Argon was Matheson Ultra-Pure and was subject to freeze–thaw–pump cycles in the vacuum system prior to use.

The cell was typically filled with 15 Torr of C_2N_2, 0–3 Torr of NH_3, and 700 Torr of argon. The ammonia pressure was either measured directly or *via* an ammonia–argon mixture which gave higher and therefore more accurately measurable pressures. The differences here were insignificant.

Results

The removal of CN radicals in the absence of scavengers other than the parent C_2N_2 occurred relatively slowly. The observed first-order rate constants with 15 Torr of C_2N_2 and 700 Torr of argon were $<2 \times 10^4$ sec^{-1} and $<6 \times 10^4$ sec^{-1} for the 0,0 and 4,4 bands, respectively. Further work on this "natural" decay of the CN radical absorptions will be reported in a later paper. Addition of ammonia at pressures of 0.3–3 Torr resulted in much greater CN removal rates. Plots of the observed first-order rate constants for this removal against NH_3 concentration therefore had very small intercepts. Figure 1 shows the results for the ground vibrational state reaction at 300°K. Similar plots for the second and fourth vibrational states at 300°K and the zero and fourth states at 375°K are shown in Figures 2 and 3, respectively.

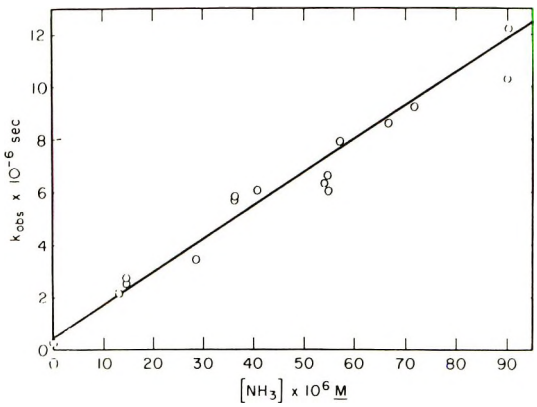

Figure 1. Reaction of vibrationally unexcited CN radicals with NH_3: variation of observed first-order rate constant with NH_3 concentration at 300°K.

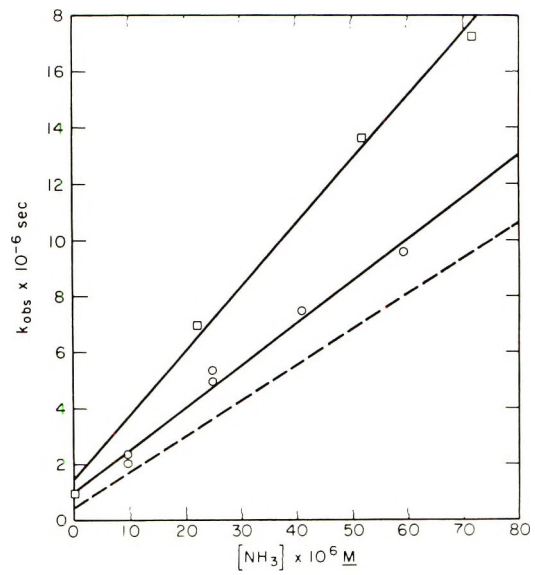

Figure 2. Dependence of first-order rate constant for CN(2,2) and -(4,4) band decay on NH_3 concentration at 300°K: O, 2,2 band; □, 4,4 band. Dashed line corresponds to Figure 1.

The product NH_2 radical was monitored at 5976 Å *via* the vibrational ground state of the $^2A_1$–$^2B_1$ transition. At this wavelength the response of the detection arrangement was much poorer, resulting in oscilloscope traces with a low signal to noise ratio and hence reduced accuracy. The results are presented in Figure 4. The bimolecular rate constants are collected in Table I.

(7) G. E. Bullock and R. Cooper, *Trans. Faraday Soc.*, in press.

(8) S. Gordon, W. A. Mulac, and P. Nangia, *J. Phys. Chem.*, **75**, 2087 (1971).

(9) (a) A. B. Callear and W. J. Tyerman, *Trans. Faraday Soc.*, **64**, 677 (1968); (b) P. Fowler, M. deSorgo, A. J. Yarwood, O. P. Stowersy, and H. E. Gunning, *J. Amer. Chem. Soc.*, **89**, 1352 (1967).

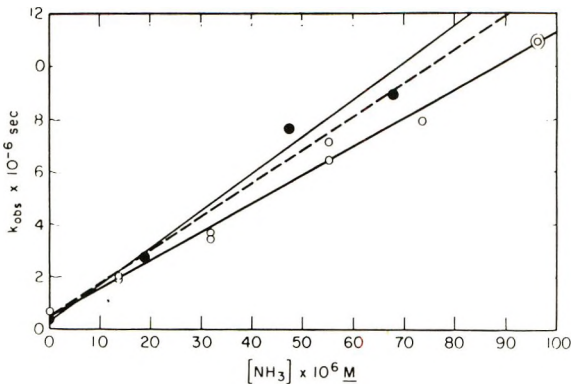

Figure 3. Reaction of CN radicals with NH_3 at 375°K. Ground (○) and fourth (●) vibrational states of CN. Dashed line corresponds to Figure 1.

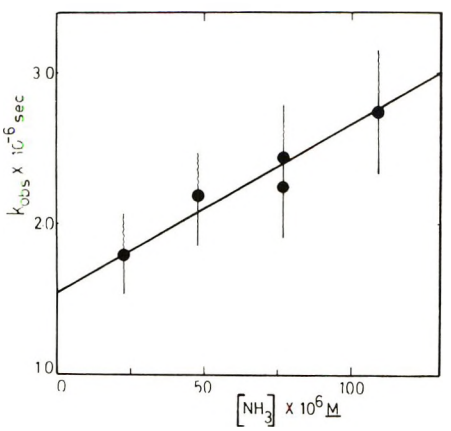

Figure 4. Dependence of first-order rate constant for NH_2 radical appearance on NH_3 concentration.

Table I: Summary of Bimolecular Rate Constants

Species observed	Temp, °K	Rate constant, l. mol^{-1} sec^{-1}
CN(0,0) removal	300	1.26×10^{10}
CN(2,2) removal	300	1.50×10^{10}
CN(4,4) removal	300	2.27×10^{10}
NH_2(0,0,0) appearance	300	1.15×10^{10}
CN(0,0) removal	375	1.08×10^{10}
CN(4,4) removal	375	1.4×10^{10}

The only previous data on this reaction consisted of a determination of the rate constant at 687°K by Thrush and Boden.[5] They obtained a bimolecular rate constant of 5.3 (± 3) × 10^9 l. mol^{-1} sec^{-1} for both the ground vibrational state and the overall $\Delta v = 0$ sequence.

Discussion

The relevant reactions occurring in this system are

$$CN + C_2N_2 \xrightarrow{k_1} C_3N_3 \quad (1)$$

$$CN\ (v = n) + C_2N_2 \longrightarrow CN\ (v = n - 1) + C_2N_2 \quad (2)$$

$$CN + NH_3 \xrightarrow{k_3} HCN + NH_2 \quad (3)$$

$$CN\ (v = n) + NH_3 \xrightarrow{k_4} CN\ (v = n - 1) + NH_3 \quad (4)$$

Reaction 1 was postulated by Paul and Dalby[4a] as the prinicpal means of CN radical removal in the absence of other scavengers. It is believed to lead to the formation of polymeric paracyanogen which was observed as a brown deposit in the cell after many weeks of use. Reaction 2 is an inefficient vibration–translation transfer process as mentioned in the Experimental Section. Since the concentration of C_2N_2 was constant for a given series of NH_3 concentrations, this relaxation has a small effect on the intercept of plots such as in Figures 2 and 3.

Reaction 3 is likely to be the main reaction of vibrationally unexcited radicals with NH_3. It is some 18 kcal/mol exothermic according to bond strength data of Cottrell[3b] and Davies and Okabe.[3a] The final products would include NH_4CN and N_2H_4,[10] but no detailed product analysis was attempted.

Effect of Vibrational Excitation

The bimolecular rate constants show a definite increase with degree of vibrational excitation of the CN bond. This can be interpreted either as a vibrational relaxation process or as a genuine influence of molecular vibration on the reaction rate.

(*i*) *Vibrational Relaxation.* If relaxation is occurring, the quoted rate constants for the second and fourth levels will be composites of reaction and relaxation, *i.e.*, reactions 3 and 4. Since both processes are pseudo-first order under these conditions, no deviations from first-order kinetics would be expected and none was observed. The stepwise increase with increasing excitation is also in accord both with the theory of vibrational relaxation and with results from other systems.[11] Relaxation from the first excited level to the ground state could result in the bimolecular rate constant for CN(0,0) reaction being slightly low. The excited states were all present in lower yields than the ground state, however, and the rate difference between the ground and second levels was ~20%. The effect of relaxation in "feeding" the second and fourth levels from the next higher level may be more serious but does not invalidate the subsequent discussion. The efficiency of the relaxation in the presence of small amounts of ammonia requires that the mechanism is vibration → vibration rather than vibration → translation transfer. Since the fundamental frequencies of NH_3 are not close to that of CN (ν_4 for NH_3 is 1627 cm^{-1}; *cf.*

(10) C. Willis, A. W. Boyd, and O. A. Miller, *Can. J. Chem.*, **47**, 3007 (1969).

(11) A. B. Callear in "Photochemistry and Reaction Kinetics," P. G. Ashmore, F. S. Dainton, and T. M. Sugden, Ed., Cambridge University Press, New York, N. Y. 1967, Chapter 7.

2042 cm^{-1} for CN $X^2\Sigma$), excess energy must be dissipated in rotational or translational excitation. Cottrell and Matheson[12] have suggested that molecules with low moments of inertia are better able to interact with vibration because of their high peripheral speeds of rotation. This implies that molecules such as CH_4 and NH_3 would cause relaxation *via* V → V + R processes.

Millikan[13] studied the relaxation of CO ($v = 1$) by CH_4 and found a lifetime (at 1 atm of CH_4) of 3.89 × 10^{-6} atm sec. Similarly, lifetimes can be calculated for CN radicals in the second and fourth levels by assuming that the increment observed is due to vibrational relaxation by transfer to NH_3. The values obtained are ~1 × 10^{-8} and ~3 × 10^{-9} atm sec, respectively. These are anomalous compared to Millikan's result. In our related paper,[7] we observed a 10% increment in the apparent rate of reaction of CN radicals with CH_4 on going from the zero to the fourth vibrational level of CN. This leads to a relaxation time of ~5 × 10^{-7} atm sec and since the first level would relax more slowly it is in satisfactory agreement with Millikan's data for CO and CH_4. These observations indicate that if the increments are a relaxation phenomenon, NH_3 is >50 times more efficient than CH_4 as a vibrational energy scavenger in these systems. Further, the relaxation of the fourth level of CN by NH_3 must be occurring on approximately every twentieth collision, an efficiency beyond the upper limit suggested by Lambert[14] for a nonresonant process.

Callear and Williams[15] observed fast relaxation of NO by a number of triatomic hydrides and suggested[11,15] that the anomalous efficiency may be due to hydrogen bonding in the collision complex (see later).

(*ii*) *Influence of Vibrational Energy on Reaction Rates.* Considerations of vibrational energy in chemical kinetics have in the past concentrated on two cases: the accumulation of energy in unimolecular reactions and the production of vibrationally excited species as a result of reaction. Despite the absence of any precedent,[16] it remains possible that internal energy in the form of vibration of one of the reactants may be able to contribute to the overall energetics of reactions. Transition state theory predicts that variations in vibrational partition functions on forming a transition state can cause a rate enhancement. Unfortunately, such predictions are doubtful when the activation energy is negligibly small and it appears that this is the case in this reaction (see later).

The NH_2 appearance was followed in an attempt to determine the overall reaction rate constant. As shown (Figure 4 and Table I), the rate constant, ~1.15 × 10^{10} l. mol^{-1} sec^{-1}, is in good agreement with the value for CN(0,0) removal. Apart from the larger errors in these data, the high intercept in Figure 4 causes some doubts about the validity of the rate constant obtained from the slope. It implies that there is a rapid production of NH_2 which does not come from reaction 3.

Temperature Effects

For the high-temperature work (Figure 3), the concentrations of NH_3 were calculated at the temperature measured by the thermocouple in the gas itself. Any effect of nonequilibration should thus be eliminated. It seems that the lower rate constant at higher temperatures is real and we conclude that there is a small negative activation energy of <500 cal/mol. Thrush and Boden[5] found a rate constant for reaction 3 of 5.3 ± 3 × 10^9 l. mol^{-1} sec^{-1} at 687°K. Using the negative activation energy we calculate a value of 8 × 10^9 l. mol^{-1} sec^{-1} at 687°K, and the two results are essentially in agreement with each other.

The fourth vibrational level was also removed more slowly at the higher temperature but the effect was much more marked. Negative *activation energies* for vibrational relaxation have been observed in other systems where the relaxation efficiency is very high.[17] If a particular orientation of two molecules results in a significant potential minimum and is favorable for energy transfer, the exchange of energy will be more likely at lower temperatures and a negative activation energy follows.[18] Thus where strong interactions related to hydrogen bonding or incipient reaction occur, the vibrational transfer may be very efficient and have a negative temperature dependence. For nitric oxide self-relaxation it has been proposed that the transfer is strongly orientation dependent, explaining the observed negative temperature effect below 700°K. It should be emphasized, however, that the dimer $(NO)_2$ is known and the interaction between two NO molecules at the lower temperatures will be much stronger than between such molecules as CO and CH_4, for example. A negative temperature dependence was also found in the relaxation of CO_2 by H_2O,[17] another case where hydrogen bonding or an analogous interaction is possible.

Thrush and Boden[5] found no difference in rate constants (within their rather large error limits) when they observed the removal of the CN(0,0 band), compared to the whole of the $\Delta v = 0$ sequence which was isolated by bandpass filters. The absence of any effect of vibrational excitation in their system at 687°K is in

(12) T. L. Cottrell and A. J. Matheson, *Trans. Faraday Soc.*, **58**, 2336 (1962).

(13) R. C. Millikan, *J. Chem. Phys.*, **43**, 1439 (1965).

(14) J. D. Lambert, *Quart. Rev., Chem. Soc.*, **21**, 67 (1967).

(15) A. B. Callear and G. J. Williams, *Trans. Faraday Soc.*, **62**, 2030 (1966).

(16) H. O. Pritchard in "Transfer and Storage of Energy by Molecules," Vol. 2, G. M. Burnett and A. M. North, Ed., Wiley–Interscience, London, Chapter 5.

(17) T. L. Cottrell and J. C. McCoubrey, "Molecular Energy Transfer in Gases," Butterworths, London, 1961, p 162.

(18) A. B. Callear and J. D. Lambert in "Comprehensive Chemical Kinetics, Vol. 3. The Formation and Decay of Excited Species," C. H. Bamford and C. F. H. Tipper, Ed., Elsevier, Amsterdam, 1969, Chapter 4.

agreement with the negative temperature dependence observed in this work.

Conclusions

It is of interest that vibrational effects can be superimposed on a fast reaction. We conclude that the reaction of CN radicals with NH_3 involves the formation of a transition state which has a small potential minimum corresponding to an interaction similar to hydrogen bonding. This results in an anomalous vibrational transfer efficiency and in negative temperature dependences for both the ground state and vibrationally excited radicals.

Acknowledgments. R. Cooper and G. E. Bullock wish gratefully to acknowledge the Australian Research Grants Commission (A.R.G.C.) for a grant to aid this project. We are also indebted to the Argonne National Laboratory Center for Educational Affairs for sponsorship in the A.N.L. summer research program. G. E. B. also wishes to acknowledge the receipt of a Commonwealth Post-Graduate Award.

Energy Transfer in Thermal Methyl Isocyanide Isomerization. Relative Efficiency of Mercury Atoms[1]

by Fa-Mei Wang, T. Fujimoto, and B. S. Rabinovitch*

Department of Chemistry, University of Washington, Seattle, Washington 98195 *(Received January 3, 1972)*

Publication costs assisted by the National Science Foundation

The low-pressure thermal isomerization of methyl isocyanide has been studied at 280.5° with mercury as the bath gas. The relative efficiency is $\beta_0(\infty) = 0.34$. Comparison with earlier studies reinforces a previous grouping of bath gases into three classes with respect to efficiency for vibrational energy transfer: monatomic, diatomic–linear, and polyatomic–nonlinear colliders. The present result provides some insight into an assumption used in ref 4a that statistical redistribution of energy occurs between the internal modes of the hot molecule (CH_3NC) moiety of a collision complex (CH_3NC–M) and the newly formed transitional modes of the complex.

Introduction

We recently published a study of collisional transfer of vibrational energy in the low-pressure methyl isocyanide isomerization.[2] A large variety of bath gases were examined. It was suggested[3,4] that relative collisional efficiency, $\beta_0(\infty)$, calculated on a collision-per-collision basis, increases with the number of transitional modes formed in the collision complex and that conservation of angular momentum places severe restrictions on a quasi-statistical accommodation of energy between the vibrational modes of the hot molecule and the transition modes of the collision complex. Three classes of bath molecules—monatomic, linear, and nonlinear—were distinguished.

To our knowledge, the collision efficiency of mercury as an inert bath molecule has not yet been measured in a thermal unimolecular system. It seemed useful to measure the efficiency of monatomic mercury bath species and to compare it with earlier noble gas data. Because of a lapse of time, and because our previous work was done at higher pressures than are accessible for mercury, a concurrent reinvestigation of xenon efficiency was made so that the efficiency of mercury could be determined by comparison with xenon used as a standard.

Experimental Section

The experimental method, especially for xenon, has been described previously.[3,5] A static method was employed. A 12-l. Pyrex flask was maintained at 280.5°. Mercury was weighed in a capillary tube, introduced into a heated side arm, degassed, and then expanded into the reactor with a known amount of

(1) This work was supported by the National Science Foundation.

(2) F. W. Schneider and B. S. Rabinovitch, *J. Amer. Chem. Soc.*, **84**, 4015 (1962).

(3) S. C. Chan, J. T. Bryant, and B. S. Rabinovitch, *J. Phys. Chem.*, **74**, 2058 (1970).

(4) (a) Y. N. Lin and B. S. Rabinovitch, *ibid.*, **74**, 3151 (1970); (b) S. C. Chan, B. S. Rabinovitch, J. T. Bryant, L. D. Spicer, T. Fujimoto, Y. N. Lin, and S. P. Pavlou, *ibid.*, **74**, 3160 (1970); (c) S. P. Pavlou and B. S. Rabinovitch, *ibid.*, **75**, 1366, 2164 (1971).

(5) F. J. Fletcher, B. S. Rabinovitch, K. W. Watkins, and D. J. Locker, *ibid.*, **70**, 2803 (1966).

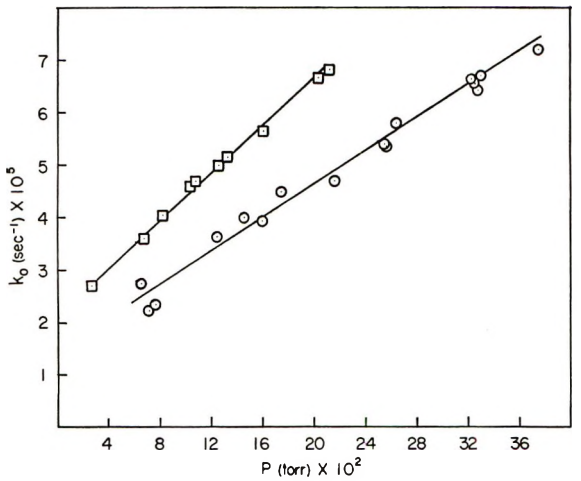

Figure 1. Low-pressure methyl isocyanide isomerization at 280.5°; plots of k_0 *vs.* pressure of added bath gas: □, Hg; ○, Xe.

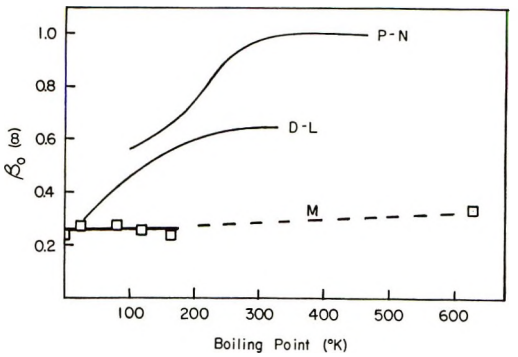

Figure 2. Plot of $\beta_0(\infty)$ *vs.* boiling point, taken from Figure 7 of ref 4b with the data point for mercury added: M, monatomic bath gases; the five squares below 200°K are values from ref 4b for the rare gases; D–L and P–N, diatomic–linear and polyatomic–nonlinear bath gases, respectively. The solid curves summarize the position of approximately one hundred bath gases shown in detail in Figure 7 of ref 4b.

purified methyl isocyanide (A). Approximately 4.0 × 10^{-6} mol of A, containing 7% propionitrile which served as an internal standard, was used (~0.012 Torr). Reaction was carried to 7–26% conversion. Dilution ratios of inert gases varied from 2- to 32-fold excess over the parent substrate.

Products were analyzed by gas chromatography on 15 ft of 3% tricresyl phosphate on Chromosorb W. Calibrations were made regularly.

Results and Discussion

Corrections[2-4] to the data were made for temperature variation (0.2°), for dead space (0.5%), and for the time to introduce the mercury into the reactor (less than 3% of the reaction time). Plots of the low-pressure rate constants k_0 are given in Figure 1. Least-squares straight line fits were made. For mercury, the intercept is 2.23 × 10^{-5} sec^{-1} and slope 21.8 × 10^{-5} sec^{-1} Torr^{-1}; for Xe, the values are 1.5 × 10^{-5} sec^{-1} and 15.4 × 10^{-5} sec^{-1} Torr^{-1}. As discussed previously,[4,6] the intercepts are a little greater than the base rate $k_A{}^a C_A{}^0$ due, in part, to a small dilution effect. The measured collisional efficiencies, on a pressure-per-pressure basis, $\beta_p(D)$, correspond to finite dilution and must be corrected to infinite dilution for comparison with the earlier measurements.[4b] The theoretical curves given by TR[7] were used. They defined a dimensionless parameter $E' = \langle \Delta E \rangle / \langle E^+ \rangle$, where $\langle \Delta E \rangle_{down}$ is the average energy down-step size and $\langle E^+ \rangle$ is the average energy of excited species above the critical reaction threshold E_0 for a Boltzmann distribution. TR calculated universal curves of $\beta_0(D)$ as a function of D, for a range of E' values and for different collisional transition probability distribution functions.

The average correction proved to be very minor for the present work. Thus, for xenon at a mean dilution D = 15 (with use of the value,[4a] E' = 0.89) the average decrease between $\beta_p(15)$ and $\beta_p(\infty)$ was only 1–2%, so D = 15 approximates infinite dilution. For mercury, the correction of $\beta_p(D)$ to $\beta_p(\infty)$ proceeded from values of E' evaluated by successive approximation. Mercury is a more efficient bath gas than xenon, so that the mean correction (at D = 8) was also only a few per cent. Thus, the ratio of the Hg/Xe rate constant slopes at finite dilution gives the relative values of $\beta_p(\infty)$ for the two gases, so that $\beta_p(\infty)(\mathrm{Hg})/\beta_p(\infty)(\mathrm{Xe})$ = 1.42. The value for xenon was reported as[4b] 0.119, so that $\beta_p(\infty)(\mathrm{Hg})$ = 0.168. The ratio $\beta_p(\infty)$ was brought to a collision-per-collision basis: $\beta_0(\infty)(\mathrm{Hg})/\beta_0(\infty)(\mathrm{Xe}) = \beta_p(\mathrm{Hg})/\beta_p(\mathrm{Xe})(\mu_{A,Hg}/\mu_{A,Xe})^{1/2}(s_{A,Xe}/s_{A,Hg})^2$; where[8] $s^2 = \sigma^2\Omega^{(2,2)*}(T^*)$, with use of the Lennard-Jones force constants employed previously.[4b] The values are summarized in Table I.

Values of E' and $\langle \Delta E \rangle_{down}$ for mercury have been estimated from $\beta_0(\infty)$ and the theoretical curves of TR; for a stepladder (SL) model of collisional transitions, $\langle \Delta E \rangle_{down}$ is 1.6 kcal mol^{-1} and it is 2.3 kcal mol^{-1} for an

Table I: Collisional Efficiency Quantities for Mercury and Xenon

	Bp, °K	$\beta_p(\infty)$	$\beta_0(\infty)^a$	E' SL	E' Exp	$\langle \Delta E \rangle_{down}$, kcal mol^{-1} SL	$\langle \Delta E \rangle_{down}$, kcal mol^{-1} Exp
Hg	630	0.168	0.34[b]	1.15	1.70	1.6	2.3
Xe	166	0.119	0.23		0.90		1.2

[a] Lennard-Jones force constants for CH_3NC and xenon as previously used in ref 4b. [b] σ = 2.90 Å and ϵ/kT = 851°K; it transpires that $s_{A,Hg}/s_{A,Xe}$ = 1.00.

(6) Y. N. Lin and B. S. Rabinovitch, *J. Phys. Chem.*, **72**, 1926 (1968).

(7) (a) D. C. Tardy and B. S. Rabinovitch, *J. Chem. Phys.*, **45**, 3720 (1966); (b) D. C. Tardy and B. S. Rabinovitch, *ibid.*, **48**, 1282 (1968).

(8) J. O. Hirschfelder, C. F. Curtiss, and R. B. Bird, "Molecular Theory of Gases and Liquids," Wiley, New York, N. Y., 1954.

exponential (exp) distribution. The true model is probably intermediate in nature.

We examine now the relation between $\beta_0(\infty)$ and some parameters which earlier were found to correlate well. With the value of the polarizability,[9] $\alpha = 5.13$ Å^3, for mercury, the departure of monatomic gases from the general correlation given by a plot of $\beta_0(\infty)$ *vs.* α_M (not shown; see Figure 3 in ref 4b) is emphasized. Even more dramatic is the delineation of the subclassification of inert bath gases as revealed in Figure 2. The separation of the monatomic subclass from the diatomic–linear and polyatomic–nonlinear groups is strengthened.

A simple theoretical interpretation was given earlier.[4a] The classification into three groups suggested the importance of conservation of angular momentum restrictions as a feature of the general level of efficiency. Subject to this restriction, the energy of the hot substrate entity within the collision complex was assumed to undergo statistical redistribution with the newly formed "transition" modes (three for monatomics, and five and six, respectively, for the two other groups) of the collision complex. An increase of $\beta_0(\infty)$ with boiling point within the D–L and P–N subclasses was interpreted as suggesting that some internal modes of the bath gas entities might play an increasingly important role in the relaxation process. However, since monatomics have no internal degrees of freedom, this rationale is not applicable to mercury. Thus, the moderate increase in $\beta_0(\infty)$ for mercury in Figure 2, assumed real, could indicate some modest failure, for the noble gases, of the limiting assumption of statistical accommodation. The assumption should have enhanced validity for mercury, with its increased attractive interaction and longer life of the AHg collision complex; the collision dynamics for mercury do not differ significantly in other respects from xenon with A. It would then follow that the observed general increase of $\beta_0(\infty)$ with boiling point is not solely due to increasing participation of internal modes of the bath molecules but to an increased efficiency, also, of their transition modes.

(9) Landolt-Bornstein, "Physikalisch-Chemische Tabellen," Vol. 1, Part 3, Springer-Verlag, Berlin, 1951.

The Ligand Field Photochemistry of Halopentaamminerhodium(III) Complexes[1]

by Timm L. Kelly and John F. Endicott*

Department of Chemistry, Wayne State University, Detroit, Michigan 48202 *(Received February 7, 1972)*

Publication costs assisted by The National Science Foundation

The irradiation of ligand field absorption bands of halopentaamminerhodium(III) complexes results in high yields of aquated products. Two different and apparently uncoupled photoaquation processes are observed: (1) halide aquation (most important for $Rh(NH_3)_5Cl^{2+}$) and (2) *trans*-ammonia aquation (most important for $Rh(NH_3)_5I^{2+}$). The products and yields are the same for the direct and the biacetyl-sensitized excitations. Since the rhodium(III) complexes quench the biacetyl phosphorescence, the photochemical products are attributed to reactions characteristic of ligand field excited states of triplet spin multiplicity. It is proposed that the combination of halide and *trans*-ammonia aquation obtained from ligand field excitation of $Rh(NH_3)_5Br^{2+}$ results from the competitive population, decomposition, and deactivation of two different triplet states. It is further proposed that the nonradiative deactivation of these complexes involves a strong coupling mechanism and metal–ligand vibrational states.

Introduction

Despite much recent interest, careful mechanistic thinking about the photochemically reactive ligand field excited states of transition metal complexes has been restricted mostly to d^3 systems.[2-13] This is so largely because the ligand field excited states of chromium(III) complexes are photochemically active[2-13] in fluid solutions and are spectroscopically well characterized in rigid media at low temperatures.[2,14-16] By way of contrast, few cobalt(III) (a $3d^6$ metal) complexes are known to emit at any temperature and few cobalt-

(1) (a) Partial support of this research by the National Science Foundation (Grant GP-24053) is gratefully acknowledged. (b) Taken in part from the Ph.D. dissertation of T. L. Kelly, Wayne State University, 1971.

(2) V. Balzani and V. Carassiti, "The Photochemistry of Coordination Compounds," Academic Press, New York, N. Y., 1970.

(3) A. W. Adamson, *J. Phys. Chem.*, **71**, 798 (1967).

(III) complexes have photoactive ligand field absorption bands.[2,16,17-21]

Thomas and Crosby[22] have recently reported on the emission spectroscopy of the $4d^6$ rhodium(III) ammine complexes. These authors conclude that the emission observed for these complexes is phosphorescence, from the lowest energy ligand field triplet excited state (^3T, $^3A_2$, or ^3E) to the $^1A_1$ ground state. Furthermore, Moggi[23] has reported that reasonably high yields of product result from ligand field excitation of $Rh(NH_3)_5Cl^{2+}$. The products in this case (1) contrast strikingly

$$Rh(NH_3)_5Cl^{2+} + h\nu \longrightarrow Rh(NH_3)_5OH_2^{3+} + Cl^- \quad (1)$$

with those which we[24] have observed to result from the ligand field excitation of $Rh(NH_3)_5I^{2+}$ (2).

$$Rh(NH_3)_5I^{2+} + h\nu \longrightarrow trans\text{-}Rh(NH_3)_4OH_2I^{2+} + NH_4^+ \quad (2)$$

These two examples serve to illustrate that the ligand field photochemistry of rhodium(III) complexes is potentially even more varied and instructive than that of the chromium(III) analogs. The present report relates our detailed mechanistic studies of the ligand field photochemistry of halopentaammine complexes of rhodium(III).

Experimental Section

A. Preparation of Materials and Solutions. $[Rh(NH_3)_5Cl]Cl_2$ was purchased from either Alfa Inorganics, Inc., Beverly, Mass. or Matthey-Bishop, Co., Malvern, Pa., converted to the perchlorate salt which was crystallized from dilute $HClO_4$. Standard literature procedures were used to prepare $[Rh(NH_3)_5Br](ClO_4)_2$ from $[Rh(NH_3)_5Cl](ClO_4)_2$.[25] The purity of the complexes after recrystallization was determined by comparison of their absorption spectra with published data.[26,27]

trans-$Rh(NH_3)_4OH_2Br^{2+}$. We were unable to obtain a pure crystalline sample of this complex owing to its considerable solubility (see discussion of attempted isolation of $Rh(NH_3)_4OH_2I^{2+}$ in ref 24a). The presence of *trans*-$Rh(NH_3)_4OH_2Br^{2+}$ in photolyzed solutions was confirmed by a comparison of absorption spectra with *trans*-$Rh(en)_2OH_2Br^{2+}$.[28] Concentrations of *trans*-$Rh(NH_3)_4OH_2Br^{2+}$ were determined by converting this complex to *trans*-$Rh(NH_3)_4Br_2^+$, whose concentration could be determined spectrophotometrically (see Table I).

trans-$[Rh(NH_3)_4Br_2]ClO_4$. A solution of 0.5 g of $[Rh(NH_3)_5Br](ClO_4)_2$ in 75 ml of 0.1 *M* $HClO_4$ was photolyzed at 254 nm for approximately 2 hr. About 2 g of NaBr was added to the photolyzed solution and the volume was reduced to approximately 10 ml on a steam bath. The complex was recrystallized as a bromide salt by cooling the concentrated solution in an ice bath. The complex was collected and converted to the perchlorate salt by the addition of solid $NaClO_4$ to a solution of the bromide salt in a minimum volume of warm water. *Anal.* Calcd for $RhN_4H_{12}O_4ClBr_2$: N, 13.0; H, 2.8; Br, 36.6. Found: N, 13.1, H, 2.8; Br, 36.6.

Preparation of Solutions. Solutions were prepared for photolysis using reagent grade salts and water redistilled from alkaline potassium permanganate. All solutions were deaerated, except as noted, by passing Cr^{2+} scrubbed N_2 or argon through them before and during photolysis.

The sodium perchlorate used to maintain constant ionic strength was prepared by neutralizing reagent grade anhydrous Na_2CO_3 with reagent grade $HClO_4$. The solution was heated to remove the dissolved CO_2. The concentration of the stock solution was determined by passing an aliquot through a cation-exchange resin in the H^+ form and titrating the acid released with standard NaOH.

(4) H. F. Wasgestian and H. L. Schläfer, *Z. Phys. Chem. (Frankfurt am Main)*, **57**, 282 (1968); **62**, 127 (1968).

(5) P. Riccieri and H. L. Schläfer, *Inorg. Chem.*, **9**, 727 (1970).

(6) R. D. Lindholm, E. Zinato, and A. W. Adamson, *J. Phys. Chem.*, **71**, 3713 (1967); E. Zinato, R. D. Lindholm, and A. W. Adamson, *J. Amer. Chem. Soc.*, **91**, 1076 (1969).

(7) M. F. Manfrin, L. Moggi, and V. Balzani, *Inorg. Chem.*, **10**, 207 (1971).

(8) A. D. Kirk, *J. Amer. Chem. Soc.*, **93**, 283 (1971).

(9) V. Balzani, R. Ballardini, M. T. Gandolfi, and L. Moggi, *ibid.*, **93**, 339 (1971).

(10) S. C. Pyke and R. G. Linck, *ibid.*, **93**, 5281 (1971).

(11) G. B. Porter, S. M. Chen, H. L. Schläfer, and H. Gaussmann, *Theoret. Chem. Acta*, **20**, 81 (1971).

(12) E. Zinato, P. Tulli, and P. Riccieri, *J. Phys. Chem.*, **75**, 3504 (1971).

(13) C. Kutal and A. W. Adamson, *J. Amer. Chem. Soc.*, **93**, 5581 (1971).

(14) G. B. Porter and H. L. Schläfer, *Ber. Bunsenges. Phys. Chem.*, **68**, 316 (1964).

(15) L. S. Forster, *Transition Metal Chem.*, **5**, 1 (1969).

(16) P. D. Fleischauer and P. Fleischauer, *Chem. Rev.*, **70**, 199 (1970).

(17) The pentacyancobaltate(III) complexes are exceptions in both regards.[16,18-21]

(18) A. W. Adamson, A. Chiang, and E. Zinato, *J. Amer. Chem. Soc.*, **91**, 5467 (1969).

(19) G. B. Porter, *ibid.*, **91**, 3980 (1969).

(20) M. Wrighton, G. S. Hammond, and H. B. Gray, *ibid.*, **93**, 5254 (1971).

(21) F. Scandola and M. A. Scandola, *ibid.*, **94**, 1805 (1972).

(22) T. R. Thomas and G. A. Crosby, *J. Mol. Spectrosc.*, **38**, 118 (1971).

(23) L. Moggi, *Gazz. Chim. Ital.*, **97**, 1089 (1967).

(24) T. L. Kelly and J. F. Endicott, *J. Amer. Chem. Soc.*, **94**, 1797 (1972).

(25) G. U. Bushnell, G. L. Lalor, and E. A. Moelewyn-Hughes, *J. Chem. Soc., A*, 717 (1966).

(26) C. K. Jorgensen, *Acta Chem. Scand.*, **10**, 500 (1956).

(27) H. H. Schmidtke, *Z. Phys. Chem. (Frankfurt am Main)*, **45**, 305 (1965).

(28) H. L. Bott and A. J. Pöe, *J. Chem. Soc., A*, 205 (1967); (b) *ibid.*, 593 (1965).

Table I: Absorption Spectra of Some Rh(III)N_4XY Complexes

Complex	Absorption maxima[a]	Ref
trans-$Rh(NH_3)_4I_2^+$	470 (333), 340 (1.9×10^4), 270 (3.5×10^4), 222 (1.8×10^4)	24
trans-$Rh(NH_3)_4OH_2I^{2+}$	485 (185),[c] 295 (2050), 226 (3.6×10^4)	24
trans-$Rh(en)_2I_2^+$	462 (260), 340 (1.4×10^4), 269 (3.1×10^4), 222 (2×10^4)	28
trans-$Rh(en)_2OH_2I^{2+}$	465 (95),[c] 300 (1000)	28
trans-$Rh(NH_3)_4Br_2^+$	438 (135), 278 (4025), 235 (4.2×10^4)	*b*
trans-$Rh(NH_3)_4OH_2Br^{2+}$	470 sh (25),[c] 396 (53), 370 sh (48), 235 sh (205)	*b*
trans-$Rh(en)_2Br_2^+$	425 (120), 276 (3000), 231 ($\sim 3 \times 10^4$)	28
trans-$Rh(en)_2OH_2Br^{2+}$	$\sim$465 (20),[c] $\sim$395 (48)	28

[a] Wavelength in nm, ϵ, in M^{-1} cm^{-1}, given in parentheses. [b] This work. [c] Estimated for a sample prepared *in situ* and concentration determined by conversion to dihalo complex.

B. Analytical Procedures. Ammonia was determined by the change in pH method as described elsewhere.[24] Ammonia which was a photolysis product of $Rh(NH_3)_5Br^{2+}$ could also be inferred when the concentration of product *trans*-$Rh(NH_3)_4OH_2Br^{2+}$ was determined as *trans*-$Rh(NH_3)_4Br_2^+$. For quantitative purposes this latter was accomplished by adding an aliquot of photolyte to a 0.1 *M* NaBr solution and heating the solution at 80° for 1 hr.

Halide Determinations. The concentration of any halide ion which was released during photolysis was determined potentiometrically. A method based on one developed by Shriner and Smith was used.[29] Potential differences were measured using an Instrumentation Laboratory Model 145 pH meter. The mV *vs.* ml Ag^+ readings were treated in a first derivative manner.[30]

Separation and Identification of Rhodium(III) Containing Reaction Products. Ion-exchange chromatography was used to separate various cationic reaction products from the unphotolyzed starting material. Before use the column was cleaned by passing 25 ml of 2 *M* $NaClO_4$ through it, then washing with 100 ml of distilled water. An aliquot of photolyte was placed on a cation exchange resin column (Bio-Rad Ag 50W-X2 or X4, 200–400 mesh, Na^+ form) 10 cm long and 1 cm in diameter. After the photolyte was absorbed onto the resin, the column was washed with 25 ml of distilled water. Slow elution with 0.1 *M* $NaClO_4$ was continued until the original band of absorbed material had separated into two or more distinct bands. The first product was removed by using 0.5 *M* $NaClO_4$ as the eluent. Elution was continued with 25 ml of 0.5 *M* $NaClO_4$, followed by 50 ml of 1 *M* $NaClO_4$ and finally 25 ml of 2 *M* $NaClO_4$. The effluent was collected in 10-ml portions for spectral measurements. The charge type of all the products was determined by comparing their elution characteristics to those of other rhodium(III) ammine complexes of known charge type. The rhodium(III) complexes in the various ion-exchange fractions were identified by comparing their uv-visible absorption spectra with those of known rhodium(III) ammine or ethylenediamine complexes.

C. Continuous Photolysis; Apparatus and Procedures. Photolyses were performed using a Xenon Corp., Medford, Mass., Model 727 Spectralirradiator in the monochromator mode. The desired wavelength region was selected using a Bausch and Lomb high-intensity monochromator in combination with a RDR-F2 thermophile from Charles M. Reeder and Co., Detroit, Mich., and a Keithley Model 155 microvoltmeter. The monochromator–thermopile–microvoltmeter combination was also used to determine the half width of the irradiating bands. Half widths of all bands were found to be approximately 20 nm. Photolysis was performed on 3 ml of solution which was pipetted into a rectangular quartz spectrophotometer cell and Cr^{2+} scrubbed N_2 was passed through the solution during irradiation. The solution was irradiated for a preset time period, then analyzed for products. An average rate of product formation was calculated by using product concentration and irradiation time. This average rate together with I_a was used to calculate a quantum yield. Various irradiation times were used to ensure that the average rate was not a function of irradiation time. A dark sample was analyzed to check for thermal reactions for each set of photolyzed samples. The constancy of the light flux both during the course of a series of irradiations and from day to day was monitored with the RDR-F2 thermophile. The light path in the spectra irradiator was continuously flushed with N_2 to prevent the buildup of O_3 due to uv photolysis of air.

Many of the 254-nm irradiations were performed using an immersion type low-pressure mercury lamp in a thermostated apparatus as described elsewhere.[31] In these determinations quantum yields were determined using the usual[31] photokinetic procedure: samples were irradiated for timed periods and syringes were

(29) V. J. Shriner, Jr., and M. L. Smith, *Anal. Chem.*, **28**, 1043 (1958).

(30) A. I. Vogler, "Quantitative Inorganic Analysis," 3rd ed, Wiley, New York, N. Y., 1961.

(31) (a) J. F. Endicott and M. Z. Hoffman, *J. Amer. Chem. Soc.*, **87**, 3348 (1965); (b) J. F. Endicott, M. Z. Hoffman, and L. S. Beres, *J. Phys. Chem.*, **74**, 1021 (1970).

used to withdraw samples for analysis through a Teflon needle. In each kinetic determination the product yield was plotted as a function of irradiation time and the initial slope was compared with that of an actinometer solution of the same absorbance which had been irradiated for similar intervals.

For runs at temperatures other than room temperature the reaction cell was thermostated by use of a Cary 14 constant-temperature 1-cm cell holder. In order to correct for thermal reactions a dark experiment was performed with the solution maintained at the photolysis temperature for the same length of time as the irradiated sample.

D. Actinometry. The light intensity was determined by ferrioxalate actinometry.[32] Owing to the high sensitivity of ferrioxalate solutions to light with $\lambda < 500$ nm, all work with this actinometer was performed in a room where the only lights used were photographic red safety lamps. By observing these precautions the results obtained with the ferrioxalate actinometer were very reproducible.

E. Flash Photolysis. The flash apparatus (Xenon Corp., Medford, Mass., Model 720) has been described elsewhere.[33] It was operated in the kinetic-spectrophotometric mode.[33] The flash lamps dissipated 250 J at 10 kV with a rise time of 5 μsec, a half-peak duration of 20 μsec, and a total duration of about 50 μsec.

F. Photolysis of Perdeuterated Complexes. Deuterated samples of $Rh(NH_3)_5X^{2+}$ ($X^- = Br, Cl$) were prepared by recrystallizing the protonated salts four times from hot D_2O solutions. The resultant products were dried at 100° under vacuum and stored in a vacuum desiccator over $CaSO_4$. The extent of deuteration was checked by the absence of N–H stretch in the ir spectra of the complexes. The ir spectra were run in Nujol mulls with NaCl salt plates on a Perkin–Elmer IR 135 infrared spectrophotometer. The exact isotopic purity of the complexes was determined using a pmr method. A weighed sample of the deuterated complex was dissolved in 5 ml of D_2O which was 0.1 *M* in OD^-. The resulting solutions were heated in closed flasks at 80° for about 1 hr to equilibrate any protons in the complex with the solvent. The integrated intensity of the H–O–D signal for the solvent was subtracted from the intensity for the equilibrated solutions. A calibration was performed by adding enough H_2O to a sample of D_2O–OD^- to increase [H] by 0.1 *M*. The increase in intensity for the equilibrated sample and the increase in intensity for the calibration sample were used to calculate the number of protons present in the weighed sample of the complex. The $Rh(ND_3)_5Br^{2+}$ was found to be 99.4 atom % D (0.06 H per complex ion), while the $Rh(ND_3)_5Cl^{2+}$ was found to be 93.7 mole % D (0.9 H per complex ion).

Solutions of these perdeuterated complexes in D_2O (99.9 mole % D, Merck Sharpe and Dohme) and $DClO_4$ (98 mole % D, Alfa Inorganic) were photolyzed at various wavelengths as described previously. The N_2 used to deaerate and stir the solutions was dried by passing it through two $CaSO_4$ drying towers and then saturated with D_2O to avoid concentrating the solution by evaporation. Halide aquation was followed in the usual way, and conversion of the tetraammines to the *trans*-dihalo ions was used to determine the amount of NH_3 aquation.

G. Biacetyl Energy Transfer. The Aldrich Chemical Co. biacetyl used in these experiments was redistilled under a nitrogen atmosphere. The solutions to be photolyzed were prepared 0.4 *M* in biacetyl and 0.01 or 0.001 *M* in $HClO_4$. The concentration of rhodium(III) substrate was kept low enough (5% of total absorbance) so that direct photolysis of the complex would not be a problem. Since quenching of biacetyl triplets by O_2 is quite efficient,[34] all solutions were deaerated for the same amount of time by passing Cr^{2+} scrubbed argon through them. The low-energy singlet absorption of biacetyl was irradiated at 400 nm. Some solutions were photolyzed with air bubbling instead of argon. Quantum yields for the various aquation processes as a function of substrate concentration were determined from the rates of product formation and the amount of light absorbed by the biacetyl. The efficiency of the quenching of biacetyl phosphorescence for carefully deaerated solutions, 0.2 *M* in biacetyl, was determined using an Aminco-Bowman spectrofluorimeter. For the measurements solutions were deaerated by passing scrubbed argon through them for 1 hr. The deaerated solutions were then transferred to deaerated fluorescence cells which had been sealed with serum caps, using syringes and Pt hypodermic needles. The ratio of phosphorescence to fluorescence for solutions of biacetyl deareated in this manner and containing no substrate was 5.9:1, in good agreement with the value of 6:1 determined by Okabe and Noyes.[35]

Results

Each of the complexes discussed in this paper has been flash photolyzed, using appropriate cutoff filters,[24,36] in its ligand field absorption bands. Such irradiation does not give rise to X_2^- radical transients, indicating that there is no complication from photoredox processes at these wavelengths. It is also the case for each of the complexes irradiated that the product yields are insensitive to the presence of O_2.

(32) G. G. Hatchard and C. A. Parker, *Proc. Roy. Soc., Ser. A*, **235**, 518 (1956).

(33) G. Caspari, R. G. Hughes, J. F. Endicott, and M. Z. Hoffman, *J. Amer. Chem. Soc.*, **92**, 6801 (1970).

(34) H. L. J. Bäckström and K. Sandros, *Acta Chem. Scand.*, **12**, 823 (1958).

(35) H. Okabe and W. A. Noyes, Jr., *J. Amer. Chem. Soc.*, **79**, 801 (1957).

(36) W. L. Wells and J. F. Endicott, *J. Phys. Chem.*, **75**, 3075 (1971).

Table II: Ligand Field Photochemistry of Halopentaammine-Rhodium(III) Complexes

Complex	Irradiation wavelength, nm[a]	Absorption band irradiated[b]	$10^4 I_a$, einsteins $l.^{-1}$ min^{-1}	Product yields ϕ_x[c]	Product yields ϕ_{NH_3}[d]
$Rh(NH_3)_5Cl^{2+}$	254	$^1T_2 \leftarrow {}^1A_1$		0.11 ± 0.01[e]	$\leq 10^{-3}$ [d]
	280	$^1T_2 \leftarrow {}^1A_1$	1.8	0.12 ± 0.01 (16)	$\leq 10^{-3}$
	350	$^1T_1 \leftarrow {}^1A_1$	5.5	0.16 ± 0.01 (6)	$< 10^{-3}$
	380	$^1T_1 \leftarrow {}^1A_1$		0.14 ± 0.01[e]	$< 10^{-3}$ [d]
$Rh(NH_3)_5Br^{2+}$	360	$^1A_2 \leftarrow {}^1A_1$	6.1	0.019 ± 0.001 (5)	0.18 ± 0.02 (6)
	420	$^1E \leftarrow {}^1A_1$	4.0	0.019 ± 0.001 (3)	0.17 ± 0.02 (6)
$Rh(NH_3)_5I^{2+}$	385	$^1A_2 \leftarrow {}^1A_1$	7.7	0.01[f]	0.82 ± 0.08[f]
	420	$^1E \leftarrow {}^1A_1$	8.5	0.01[f]	0.87 ± 0.07[f]
	470	$^1E \leftarrow {}^1A_1$	5.6	[g]	0.85 ± 0.05[f]
trans-$Rh(NH_3)_4I_2^+$	470	$^1T_1 \leftarrow {}^1A_1$	5.4	0.48 ± 0.01[f]	

[a] Bandwidth ±20 nm except as indicated. [b] Band assignments as in ref 22 or 40. [b] 25°, μ = 0.1 ($NaClO_4$), pH 2 ($HClO_4$). Number of determinations in parentheses. [d] 25°, μ = 0.1 ($NaClO_4$), pH 2 ($HClO_4$). Number of determinations in parentheses. [e] Reference 23. [f] Reference 24. [g] Not determined.

Table III: Quantum Yields for the Photolysis of $RH^{III}(NH_3)_5X$ (X = Cl, Br, I) at 75°

Complex	Irradiating wavelength, nm[a]	$10^4 I_a$, einsteins $l.^{-1}$ min^{-1}	Quantum yield[b] X[c]	Quantum yield[b] NH_3[d]
$Rh(NH_3)_6Cl^{2+}$	350	3.3	0.18 ± 0.01	10^{-3}
$Rh(NH_3)_6Br^{2+}$	360	3.3	0.021 ± 0.001 (3)	0.34 ± 0.03 (4)
$Rh(NH_3)_6I^{2+}$	385	4.0	[e]	0.83 ± 0.04 (4)

[a] For type of absorption bands see Table II. [b] Mean and average deviation for (n) determinations. [c] μ = 0.1 ($NaClO_4$), pH 2 ($HClO_4$). [d] μ = 0.1 ($NaClO_4$), pH 3 ($HClO_4$). [e] Not determined.

Irradiation of $Rh(NH_3)_5Br^{2+}$. This complex has been irradiated in the ligand field absorption bands at 360 and 420 nm.[22,37] The net photolysis products observed were NH_4^+, *trans*-$Rh(NH_3)_4OH_2Br^{2+}$, and Br^- independent of the wavelength of irradiation (Table II). The quantum yield for Br aquation was independent of irradiation time up to at least 25% decomposition of $Rh(NH_3)_5Br^{2+}$. This indicates that it was a result of the photolysis of $Rh(NH_3)_5Br^{2+}$ and not a result of secondary photolysis. Ion-exchange chromatography was used to separate *trans*-$Rh(NH_3)_4OH_2Br^{2+}$ from other rhodium(III) containing products and unphotolyzed starting material.

Irradiation of $Rh(NH_3)_5Cl^{2+}$. The quantum yields for the photochemical aquation of $Rh(NH_3)_5Cl^{2+}$ are summarized in Table II. Our results for ligand field irradiation[26,37] (254–380 nm) of this complex, where Cl^- was the only detectable aquation product, were in good agreement, within experimental error, with Moggi's[23] report. Attempts to detect NH_3 aquation by measuring changes in pH showed that $\phi_{NH_3} < 10^{-3}$.

Temperature Dependence of Photoaquation Reactions of $Rh(NH_3)_5X^{2+}$ (X = Cl, Br, I). The effect of temperature on the photochemical reactions of the $Rh(NH_3)_5X^{2+}$ complexes was investigated by irradiating solutions of the complexes thermostated at 75°. The results are summarized in Table III. Although the increased temperature had virtually no effect on the products or quantum yields from the photolysis of either $Rh(NH_3)_5I^{2+}$ or $Rh(NH_3)_5Cl^{2+}$, the quantum yield for ammonia aquation from $Rh(NH_3)_5Br^{2+}$ nearly doubled while bromide aquation was not significantly changed. There was considerable thermal I^- aquation from $Rh(NH_3)_5I^{2+}$. The I^- thus liberated rapidly anated the *trans*-$Rh(NH_3)_4(OH_2)I^{2+}$ produced in the photochemical reaction, making it impossible to use the rate of appearance of *trans*-$Rh(NH_3)_4I_2^+$ as an accurate measure of photochemical aquation of I^-.[24] No NH_3 aquation was detected from $Rh(NH_3)_5Cl^{2+}$, by measuring the change in pH ($\phi_{NH_3} < 10^{-3}$).

Irradiation of $Rh(ND_3)_5X^{2+}$ in D_2O–$DClO_4$. The perdeuterated complexes were irradiated in D_2O–$DClO_4$ solutions and their photochemical reaction products were determined. The quantum yields are summarized in Table IV. No evidence for ND_3 aquation from $Rh(ND_3)_5Cl^{2+}$ was found ($\phi_{ND_3} < 10^{-3}$).

Biacetyl Energy Transfer. When solutions 0.4 M in biacetyl, 0.002 M in $HClO_4$, and containing relatively nonabsorbing quantities of rhodium(III) complexes, were irradiated at 400 nm, a biacetyl singlet absorbtion, photochemical reactions characteristic of the rho-

(37) C. K. Jorgensen, "Orbitals in Atoms and Molecules," Academic Press, New York, N. Y., 1962.

Table IV: Quantum Yields for Photolysis of $Rh^{III}(NH_3)_5X$ (X = Cl, Br) in D_2O

Complex	Irradiating wavelength, nm[a]	$10^4 I_a$, einsteins $l.^{-1}$ min^{-1}	Quantum yield[b]	
			NH_3	X
$Rh(ND_3)_6Cl^{2+}$	280	1.3	$<10^{-3}$	0.16 ± 0.01 (6)
	350	5.5	$<10^{-3}$	0.23 ± 0.01 (11)
$Rh(ND_3)_6Br^{2+}$	360	5.8	0.18 ± 0.01 (6)	0.019 ± 0.001 (6)

[a] For type of irradiation band see Table II. [b] 25°, μ = 0.1 ($DClO_4$). Mean and average derivation of (n) determinations.

Table V: ϕ_{lim} and K_s for Biacetyl-Sensitized Reactions of Rhodium(III) Haloammine Complexes[a]

Complex	Purging gas	Mode of reaction	ϕ_{lim}[b]	K_s, M^{-1} [c]
$Rh(NH_3)_6Cl^{2+}$	N_2[d]	Cl^- aquation	0.16	172
	Air[e]	Cl^- aquation	0.16	122
		NH_3 aquation	$<10^{-3}$	
$Rh(NH_3)_6Br^{2+}$	N_2	NH_3 aquation	0.20	312
	Air	NH_3 aquation	0.20	143
		Br^- aquation	~0.02	
$Rh(NH_3)_5I^{2+}$	N_2	NH_3 aquation	0.90	370
	Air	NH_3 aquation	0.90	250
trans-$Rh(NH_3)_4I_2^+$	N_2	Decomposition to *trans*-$Rh(NH_3)_4OH_2I^{2+}$	0.59	370

[a] 0.4 M biacetyl, 0.002 M $HClO_4$ 25°, 400-nm irradiation, 2×10^{-2} $M \geq$ [Rh(III)] $\geq 2 \times 10^{-4}$ M. [b] ϕ_{lim} obtained from a plot of $1/\phi_{app}$ *vs.* [Rh(III)]. [c] $K_s = 1/(\phi_{lim} \times$ slope); slope from plots of ϕ_{app}^{-1} *vs.* [Rh(III)]$^{-1}$. [d] 15-min deaeration with scrubbed N_2 and N_2 bubbling during irradiation. [e] Air bubbling during irradiation and no deaeration.

dium(III) substrates were observed, concomitant with quenching of the biacetyl phosphorescence. The absorption due to biacetyl did not change during the course of the reaction, indicating that photochemical decomposition of biacetyl was not a complication under these conditions. The concentration of the complexes was kept low so that they never accounted for more than 5% of the total light absorbed by the solutions. None of the rhodium(III) complexes absorbs appreciably at 510 nm, the wavelength of biacetyl emission; therefore one can eliminate any photochemical reactions due to absorption of this radiation, *i.e.*, from the so-called "trivial" sensitization.[2] Limiting quantum yields, of the sensitized photolysis and Stern–Volmer quenching constants, K_s, are summarized in Table V (see Discussion for definition of these terms).

Discussion

The halopentaammine complexes of rhodium(III) exhibit a rich and varied photochemistry. The observation that rhodium(III) complexes quench the biacetyl phosphorescence to result in the same products as produced in the direct excitation of $Rh(NH_3)_5X^{2+}$ (Tables II and V) strongly suggests that the photoreactive states of the rhodium complexes have triplet electronic spin multiplicity.[38] Thus the overall mechanism of energy transfer between the biacetyl donor and rhodium(III) acceptor may be represented.[39]

$$\text{biacetyl}(S_0) + h\nu \longrightarrow \text{biacetyl}(S_1) \quad (3)$$

$$\text{biacetyl}(S_1) \longrightarrow \text{biacetyl}(S_0) + h\nu' \quad (4)$$

$$\text{biacetyl}(S_1) \longrightarrow \text{biacetyl}(T_1) \quad (5)$$

$$\text{biacetyl}(T_1) \longrightarrow \text{biacetyl}(S_0) + h\nu'' \quad (6)$$

$$\text{biacetyl}(T_1) \xrightarrow{O_2} \text{biacetyl}(S_0) \quad (7)$$

$$\text{biacetyl}(T_1) \longrightarrow \text{biacetyl}(S_0) \quad (8)$$

$$\text{biacetyl}(T_1) + Rh(III)(S_0) \longrightarrow \text{biacetyl}(S_0) + Rh(III)(T_1) \quad (9)$$

$$Rh(III)(T_1) \longrightarrow Rh(III)(S_0) \quad (10)$$

$$Rh(III)(T_1) \longrightarrow \text{products} \quad (11)$$

By this mechanism the quantum yield for the photosensitized reaction is

$$\phi = \frac{k_5}{k_4 + k_5} \times \frac{k_9[\text{Rh(III)}]}{k_8 + k_6 + k_7[O_2] + k_9[\text{Rh(III)}]} \frac{k_{11}}{k_{10} + k_{11}} \quad (12)$$

(38) T. L. Kelly and J. F. Endicott, *J. Amer. Chem. Soc.*, **94**, 278 (1972).

(39) The symbols S and T in eq 3–10 only differentiate states of singlet and triplet spin multiplicity. The likely involvement of two photoreactive rhodium(III) triplet states need not complicate the algebraic discussion at this point.

If the limiting quantum yield of the sensitized reaction is taken to be ϕ_{lim} (*i.e.*, in the limit that $k_9[Rh(III)] \gg k_6 + k_8 + k_7[O_2]$), ϕ_{isc}^{D} is taken to be the quantum yield of intersystem crossing in the biacetyl donor (5), and ϕ_R^A is taken to be the quantum yield of products from the rhodium(III) acceptor triplet states (11), then

$$\phi_{lim} = \frac{k_5}{k_4 + k_5} \frac{k_{11}}{k_{10} + k_{10}} = \phi_{isc}^{D}\phi_R^A \qquad (13)$$

After appropriate substitution and rearrangement of (12), one finds

$$\frac{1}{\phi} = \frac{1}{\phi_{lim}}\left\{1 + \frac{1}{K_s[Rh(III)]}\right\} \qquad (14)$$

where $K_s = k_9/(k_6 + k_7[O_2] + k_8)$. We have found plots of $1/\phi$ *vs.* $1/[Rh(III)]$ to be linear with slopes dependent on $[O_2]$ and values of $1/\phi_{lim}$ independent of $[O_2]$ (Table V).

The fluorescence intensity of very carefully deaerated biacetyl solution was not affected by the presence of rhodium(III) substrates while the phosphorescence intensity was found to decrease as rhodium(III) concentration increased. Triplet-to-triplet energy transfer (9) resulting in quenching of the donor triplet at unit efficiency should follow a Stern–Volmer quenching law.[40]

$$I_P^0/I_P = 1 + \tau_0 k_9[Rh(III)]$$

where I_P^0 is the phosphorescence efficiency in the absence of the quencher, I_P is the efficiency with the quencher, τ_0 is the lifetime of the triplet with no quencher, *i.e.*, $\tau_0 = 1/(k_0 + k_8)$ and k_9 is the quenching rate constant (in the absence of O_2). Taking the relative intensity of phosphorescence to be proportional to its efficiency, we find that a plot of $[(I_P^0/I_P) - 1]$ *vs.* $[Rh(NH_3)_5Cl^{2+}]$ gives a straight line with a slope of $\tau_0 k_9 = 1.38 \times 10^4\ M^{-1}$. If the lifetime of the biacetyl triplet is the same in the well degassed water solution as for benzene solutions[34] (1.0 msec), then $k_9 \simeq 1.38 \times 10^7\ M^{-1}\ sec^{-1}$.

It is to be observed that the value of $\tau_0 k_9$ estimated above is about two orders of magnitude larger than the values of K_s listed for $Rh(NH_3)_5Cl^{2+}$ in Table V. This discrepancy no doubt has its source in the relative efficiency of (7) and the inadequacy of the deaeration procedures used in the sensitized photolyses.[41] The deaeration procedures used in the emission quenching studies were necessarily (in order to observe emission) far more scrupulous. Thus the values of the Stern–Volmer constant listed in Table V are not indicative of the efficiency of reaction 9. Oxygen is expected to be very important in the present systems as k_9 appears to be much smaller than k_7.

For $Rh(NH_3)_5Cl^{2+}$ the only observable sensitized reaction is Cl^- aquation. With $Rh(NH_3)_5Br^{2+}$ the principal sensitized reaction was NH_3 aquation, while Br^- aquation occurred with an apparent quantum yield of 0.02. The low yield coupled with the need to keep irradiation times short (<30 min) to avoid complications due to biacetyl photolysis made it impossible to irradiate long enough to obtain a good plot of $1/\phi$ *vs.* $1/[Rh(III)]$ for Br^- aquation. It is apparent, however, that ϕ_{lim} could not be significantly greater than 0.02. Ammonia aquation was the only detectable sensitized reaction for $Rh(NH_3)_5I^{2+}$. The high concentration of biacetyl made it impossible to measure the concentration of any *trans*-$Rh(NH_3)_4I_2^+$ that may have been a product of the sensitized reaction.

From the similarity of values of ϕ_{lim} in Table V and the product yields from direct photolysis (Table II) we infer that the photochemically reactive state is a ligand field excited state of triplet spin multiplicity and that the intersystem crossing between the lowest energy ligand field singlet excited state (^1E or $^1A_2$) and the triplet excited state manifolds occurs with nearly unit efficiency. The latter inference has been drawn also by Thomas and Crosby from the emission spectroscopy of these same complexes at 77°K.[22]

It is to be observed that ligand field excitation of $Rh(NH_3)_5Cl^{2+}$ leads only to Cl^- aquation and that ligand field excitation of $Rh(NH_3)_5I^{2+}$ leads almost exclusively to *trans*-ammonia aquation while $Rh(NH_3)_5Br^{2+}$ exhibits somewhat intermediate behavior. These observations alone suggest that the reaction modes are uncoupled[38] and not to be confused with the energetics of aquation reactions of the respective ground state species.[25] We have pointed out elsewhere[38] that the observation of the two apparently uncoupled processes, reactions 15 and 16 (Tables II and III), suggests that

$$Rh(NH_3)_5X^{2+} + h\nu \xrightarrow[H^+]{H_2O} \begin{cases} \xrightarrow{\phi_X} Rh(NH_3)_5OH_2^{3+} + X^- & (15) \\ \xrightarrow[\phi_{NH_3}]{} trans\text{-}Rh(NH_3)_4OH_2X^{2+} + NH_4^+ & (16) \end{cases}$$

these products are produced from *different* photochemically active excited states[42] (Figure 1). The conclusion that $\phi_{isc} \simeq 1$ requires that the photochemically active states have triplet spin multiplicity. In Figure 1 we have called these states ^3X and ^3Y since the appropriate term symbols for these states are not known at present. In Figure 1 we have indicated intersystem crossing as an isoenergetic tunnelling process[43-47] between the singlet and triplet excited state manifolds,

(40) C. A. Parker, "Photoluminescence of Solutions," Elsevier, Amsterdam, 1968.

(41) Note that any rhodium(III)-dependent quenching process will affect the limiting quantum yield and the apparent Stern–Volmer quenching constant K_s. A rhodium(III)-dependent quenching process which did not lead to photochemical products would lead to an anomalously low value for ϕ_{lim}. Since our values of ϕ_{lim} are identical with the values of ϕ obtained from direct excitation, we infer that only the quenching process in reaction 8 is important.

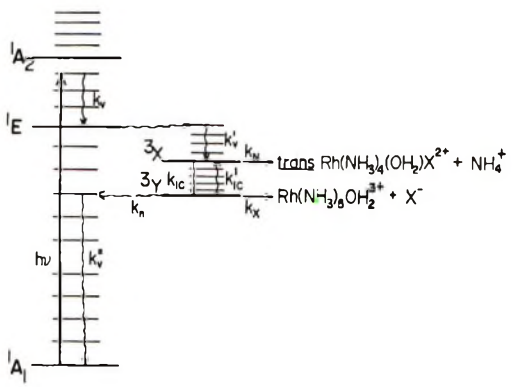

Figure 1. Qualitative energy level scheme for the photochemistry of halopentaamminerhodium(III) complexes. The absorption of radiation is indicated by the vertical straight line; intramolecular nonradiative processes are indicated by wavy lines. First-order rate constants are indicated for vibrational relaxation (k_v, k_v', k_v''), internal conversion (k_{ic}, k_{ic}'), intersystem crossing (k_n) and product formation (k_N and k_x).

followed by rapid thermal equilibration (k_v', k_{ic}, k_{ic}') among vibrational levels of the reactive states. Using the appropriate stationary-state approximations in [^{3}X] and [^{3}Y], we find

$$\phi_{NH_3} = \frac{k_N[^3X]}{I_a} \frac{k_N(k_x + k_{ic}' + k_n)\phi_{isc}}{(k_N + k_{ic})(k_x + k_n) + k_N k_{ic}'} = \frac{k_N(k_x + k_{ic}' + k_n)}{(k_N + k_{ic})(k_x + k_n) + k_N k_{ic}'}$$

$$\phi_x = \frac{k_x[^3Y]}{I_a} = \frac{k_{ic}k_x\phi_{isc}}{(k_N + k_{ic})(k_x + k_n) + k_i k_{ic}'} = \frac{k_{ic}k_x}{(k_N + k_{ic})(k_x + k_n) + k_N k_{ic}'}$$

It is instructive to compare two limiting cases.

1. $k_{ic} \gg k_N$. In this limit

$$\phi_{NH_3} \simeq \frac{k_N}{k_{ic}} \frac{(k_x + k_n + k_{ic}')}{k_x + k_n + (k_N k_{ic}'/k_{ic})}$$

and

$$\phi_x \simeq \frac{k_x}{k_x + k_n + (k_N k_{ic}'/k_{ic})}$$

Noting that

$$\frac{k_{ic}'}{k_{ic}} = e^{-\Delta E/RT}; \quad \Delta E = E(^3X) - E(^3Y)$$

let us further assume that $(k_x + k_n) > (k_N k_{ic}')/k_{ic}$ and that $k_{ic}' > k_x + k_n$; then $\phi_{NH_3} \sim [k_N/(k_x + k_n)]e^{-\Delta E/RT}$ and $\phi_x \sim k_x/(k_x + k_n)$.

Since k_N, k_x, and k_n are not expected to be strongly temperature dependent, this model adequately accounts for our observations with $Rh(NH_3)_5Br^{2+}$. Within the limits imposed by the above approximations $\Delta E \simeq 2.6$ kcal/mol (900 cm^{-1}) for this complex. Our observations for this complex also suggest that $k_{ic} > k_{ic}' > k_N > k_x$. In order for (16) to be unimportant for the $Rh(NH_3)_5Cl^{2+}$ complex, ΔE must be much greater than 10^3 cm^{-1} or k_N must be much less than k_x, or some combination of these conditions. Since $\phi_{NH_3} \sim 1$ for $Rh(NH_3)_5I^{2+}$, one could infer that $k_N > k_n$ for this complex; further, within the context of this limit it seems likely that $E(^3X)$ is less than $E(^3Y)$ for this complex.

2. $k_N > k_{ic}$. In this limit

$$\phi_{NH_3} \sim 1; \quad \phi_x \sim \frac{k_{ic}k_x}{k_n(k_x + k_n + k_{ic}')}$$

This limiting case seems reasonable only for $Rh(NH_3)_5I^{2+}$.

It is clear that the proposed model (that there are two chemically distinct, reactive excited states, ^{3}X and ^{3}Y in Figure 1, involved in the ligand field photochemistry of rhodium(III)) adequately accounts for the observed photochemical behavior of the halopentaammine complexes. This model has the very interesting feature of requiring that antibonding electron density, in the ligand field excited states of triplet spin multiplicity, be localized in definite chemical bonds; *i.e.*, it appears that either the Rh(III)–NH_3 or the Rh(III)–X bond is weakened, but not both.

The model proposed also permits some comparisons of the properties of excited states produced from $Rh(NH_3)_5X^{2+}$. For example, using the values of ϕ_x from Table II and the first limiting case above we find $k_n \sim 5k_x$ for X = Cl while $k_n \sim 50k_x$ for X = Br. Clearly one cannot make a unique comparison of the rates of the individual processes for different complexes. However, it is also clear that one would expect that k_n to be larger for $Rh(NH_3)_5Br^{2+}$ than for $Rh(NH_3)_5Cl^{2+}$ owing to the larger spin–orbit coupling constant for the heavier atom.[48] Thus k_x may actually not vary much from one complex to another. The very high value

(42) In this regard recall that the lowest energy spin allowed ligand field absorption bands have maxima which differ only by 4.2×10^{-3} cm^{-1} and 1.6×10^{-3} cm^{-1} in the cases of $Rh(NH_3)_5Br^{2+}$ and $Rh(NH_3)_5I^{2+}$, respectively.[22,26,27] These bands are the $^1A_2$ and ^1E components of the $^1T_1$ transition in a ligand field of O_h symmetry.[22] The energy gap between the zeroth vibration states of the $^1A_2$ and ^1E states is not known. One would, of course, expect the energy differences between the "$^3A_2$" and "^3E" states to be roughly of the same magnitude and indeed a gap of about 900 cm^{-1} is inferred below. It should be further noted that if the excited-state distortions result in an effective ligand field of symmetry lower than C_{4v} (or D_{4h}) the remaining degeneracies may be removed; in principle there could be as many as six different ligand field triplet excited electronic states.

(43) (a) G. W. Robinson, *J. Mol. Spectrosc.*, **6**, 58 (1961); (b) G. W. Robinson and R. P. Frosch, *J. Chem. Phys.*, **37** (1962); **38**, 1187 (1963).

(44) J. P. Byrne, E. F. McCoy, and I. G. Ross, *Aust. J. Chem.*, 18, 1589 (1965).

(45) J. B. Birks, "Photophysics of Aromatic Molecules," Wiley-Interscience, New York, N. Y., 1970, Chapter 5.

(46) J. Jortner, S. A. Rice, and R. M. Hochstrasser, *Advan. Photochem.*, **7**, 149 (1969).

(47) E. W. Schlag, S. Schneider, and S. F. Fischer, *Annu. Rev. Phys. Chem.*, **22**, 465 (1971).

(48) D. S. McClure, *J. Chem. Phys.*, **17**, 905 (1949).

observed for ϕ_{NH_3} in the case of $Rh(NH_3)_5I^{2+}$ is particularly interesting since spin–orbit contributions to radiationless deactivation should be largest with this complex. For this reason it seems likely that $k_N > k_{ic}$ for this complex. Thus it seems likely that k_N is larger in the case of $Rh(NH_3)_5I^{2+}$ than in the case of $Rh(NH_3)_5Br^{2+}$. On the basis of the product stereochemistry one could call this latter inference evidence for a "photochemical *trans*-effect," with the halide ions as "*trans*-directing" groups.

Although the proposed model is self-consistent and reasonable, it cannot at present be regarded as a unique model of the ligand field photochemistry of rhodium(III). A reasonably attractive alternative would be to attribute the observed products to the generation of a vibrationally hot ground state species in the nonradiative deactivation of the ligand field triplet states.[49] Thus the nonradiative deactivation at room temperature may well involve strong coupling[46,47] of ground-state and excited-state metal–ligand vibrations (see below). In such a case the isoenergetic tunnelling of the system from the excited state manifold to the ground-state manifold would leave the system in the ground electronic state with some metal–ligand vibration very greatly excited. If solvent–ligand exchange can proceed from these very hot vibrational states at a rate competitive with vibrational deexcitation ($k_{vib} \geq 10^{10}$ sec^{-1}) then some ligand aquation should result. Within the context of this second, or hot ground state model, the observation of two different, uncoupled reaction modes among $Rh(NH_3)_5X^{2+}$ complexes would imply that nonradiative deactivation couples only specific vibrational modes. Such a model does have some appealing features and cannot be unequivocally excluded. At present we do not regard the hot ground state model as sufficient to accommodate easily all of our observations. Among the observations which seem difficult to accommodate we note the following: (1) nonradiative deactivation of the charge-transfer-to-metal excited states of $Rh(NH_3)_5I^{2+}$ is accompanied by relatively little aquation;[24] (2) the failure to find *cis*-$Rh^{III}(NH_3)_4OH_2X$ products; (3) the temperature dependence of *trans*-ammonia aquation only in the case of $Rh(NH_3)_5Br^{2+}$; and (4) the relatively small yields of aquation observed to result from ligand field excitation of *trans*-$Rh(NH_3)_4I_2^+$.

In any case it is clear that the mechanisms of nonradiative deactivation of excited-state species are of fundamental importance in understanding photochemical reactivity. According to the widely accepted[45,50] theory of Robinson and Frosch,[43] and further elaborations and treatments,[44,47] nonradiative deactivation of electronic excited states is isoenergetic and couples the zeroth vibrational level of the excited state with a ground-state vibrational level of nearly the same energy. The probability of this transition is thought to decrease with increasing quantum number for the ground state vibrational level populated.[44] In effect this condition restricts deactivation mechanisms to processes which activate R–H (or N–H in ammine complexes) stretching frequencies.[44,45,47,50] Since ν_{N-D} is smaller than ν_{N-H}, deuteration of coordinated ammines in a $Rh(NH_3)_5X^{2+}$ complex should have the effect of increasing the quantum number of the ground vibrational state which couples efficiently to deactivate the excited state; therefore, such deuteration should appreciably decrease k_n (Figure 1). At 77°K this argument is consistent with the observations of Thomas and Crosby[22,51] that the phosphorescence lifetimes ($\tau = 1/(k_p + k_n)$) of $Rh^{III}(ND_3)_5X$ complexes are much longer than the phosphorescence lifetimes of $Rh^{III}(NH_3)_5X$ complexes. Our evidence is that the quantum yields are insensitive to deuteration and forces us to conclude that some other mechanism for nonradiative deactivation of excited-state species must be operative at room temperature in fluid media.

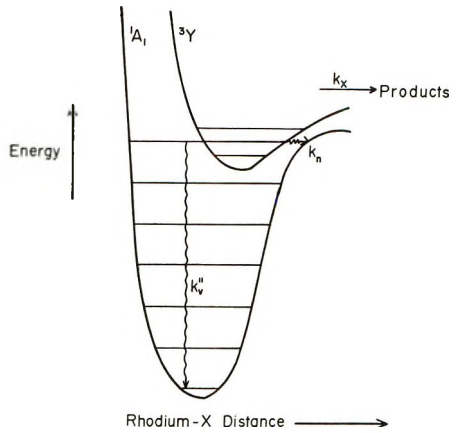

Figure 2. Hypothetical potential energy manifolds for the ground singlet and lowest triplet electronic states; illustration of nonradiative deactivation mechanism. For explanation of symbols see Figure 1.

Any mechanism proposed to account for the nonradiative deactivation of excited-state rhodium(III) species at room temperature should take account of the following facts in addition to the contrasting sensitivities of the 77°K phosphorescence yields and the 300°K photochemical yields to deuteration: (1) at 77°K (in glassy media) no photochemistry is observed, while at 300°K (in fluid media) rhodium(III) complexes are very photosensitive; (2) both the phosphorescence and photochemistry appear to involve ligand field triplet states; and (3) the quantum yields of products in fluid media are, with one exception, temperature independent for temperatures above 298°K.

(49) Another, more viable, alternative would be a combination of these limiting models, *i.e.*, attributing NH_3 aquation to a reaction of a triplet state and X^- aquation to the population of higher M–X vibrational states on nonradiative deactivation. Many of the objections listed can also be raised with regard to this compromise.

(50) G. S. Hammond, *Advan. Photochem.*, **7**, 373 (1969).

(51) T. R. Thomas and G. A. Crosby, private communication.

We believe that a very attractive alternative to nonradiative deactivation through weak coupling of N–H stretching vibrations is a strong coupling mechanism[46,47] involving some metal ligand vibration (or vibrations). The lack of photochemistry at 77°K is consistent with only the first few vibrational levels of the ligand field triplet manifold being bound; at room temperature, provided vibrational levels are closely spaced, dissociation could proceed from the highest bound vibrational state in competition with nonradiative deactivation (Figure 2). It is intuitively appealing to implicate the metal–ligand stretching frequencies in the deactivation mechanism since even in the ground state these are low energy vibrations (100–500 cm^{-1})[52] and would be expected to be even lower in energy in an excited state containing appreciable, localized antibonding electron density. Thus the temperature-insensitive quantum yields could be attributed to the insensitivity of the population of the implicated vibrational level to temperature at the relatively high temperatures of the photochemical studies. Furthermore, excited states with yields as high as we have observed here are consistent with nearly dissociative (in the case of $Rh(NH_3)_5I^{2+}$ perhaps totally dissociative) excited states and therefore with states in which the vibrations are expected to be extremely anharmonic. This feature is again consistent with the strong coupling case.[46,47] Finally, nonradiative deactivation from an excited metal–ligand vibrational level is consistent with the apparent change of deactivation mechanism between 77 and 300°K. Furthermore, this mechanism is consistent with the differences in sensitivity of ϕ_x to deuteration in the cases of $Rh(NH_3)_5Cl^{2+}$ and $Rh(NH_3)_5Br^{2+}$ since in both cases the lowest energy photoreactive excited state appears to involve cleavage of the rhodium–halide bond (Figure 1) and since $\nu_{Rh-Cl} > \nu_{Rh-Br}$; thus the experimental evidence suggests that for $Rh(NH_3)_5Cl^{2+}$ the excited-state vibrational levels are sufficiently far apart in energy that the strong coupling (Rh–X) and weak coupling (N–H) deactivation mechanisms compete at room temperature.

In general in this study we have found evidence that for $Rh^{III}(NH_3)_5X$ complexes, ϕ_{isc} (Figure 1) is about unity. An exception to this may be the case of *trans*-$Rh(NH_3)_4I_2^+$ where the sensitized product yield is about 20% greater than the product yield from direct ligand field excitation. This would suggest that spin–orbit coupling effects may even operate to provide a very efficient mechanism for deexcitation of the singlet excited states to the ground state.

(52) K. Nakamoto, "Infrared Spectra of Inorganic and Coordination Compounds," 2nd ed, Wiley, New York, N. Y., 1970.

Evidence against the Doublet Hypothesis. The Photolysis of Hexacyanochromate(III) in Dimethylformamide

by H. F. Wasgestian

Institut für physikalische Chemie der Universität, D6 Frankfurt am Main, West Germany *(Received January 3, 1972)*

Publication costs borne completely by The Journal of Physical Chemistry

The photolysis of tetrabutylammonium hexacyanochromate(III) dissolved in dimethylformamide (DMF) has been studied. The first reaction product was shown to be $[Cr(CN)_5DMF]^{2-}$, which could be isolated in solution. It is produced with a quantum yield of 0.08 at 25°. Between −60 and 50° the quantum yield shows an apparent activation energy of 2.8 kcal mol^{-1}. Under identical experimental conditions the phosphorescence behavior of hexacyanochromate was also studied. Differences to the photoreaction with respect to temperature dependence and influence of water and oxygen were observed. These differences exclude the possibility that the photoreaction originates from the same excited state as the phosphorescence (^2E_g). According to the present state of the discussion the $^4T_{2g}$ remains the photoactive state.

Introduction

The doublet hypothesis was primarily developed by Schläfer[1] and Plane.[2] It explains the photosensitivity of chromium(III) compounds assuming that the photoreactions originate from the lowest doublet state (^2E_g in octahedral symmetry). The transition from this state to the quartet ground state is spin forbidden. Therefore one can expect that the molecule remains excited sufficiently long for a chemical reaction to occur. Adamson, on the other hand, interpreted the experimental results supposing that excited quartet states were precursors to the photochemical reactions.[3] At the present state of the discussion it is generally accepted that either the lowest doublet or the first excited quartet state must be the photoactive one.[4-7]

To decide experimentally between the two alternatives, hexacyanochromate(III) was selected because this complex has the largest known energy separation of the two states in question. A thermal equilibrium between them seems very improbable. The studies of the photochemistry in aqueous solution have not provided the answer.[8,9] In aqueous solution no luminescence of either of the two states is observed at room temperature. Therefore no independent spectroscopic method was available to follow the fate of the excited states concerned, but a solution of tetrabutylammonium hexacyanochromate(III) in dimethylformamide (DMF) shows a strong phosphorescence from the ^2E_g state at 805 mμ, even at room temperature. Since the complex is also photosensitive in this solvent, a system was found in which the decay of the doublet state could be related to the photochemical reaction under identical experimental conditions.

Experimental Section

Tetrabutylammonium hexacyanochromate(III) was prepared from $K_3[Cr(CN)_6]$ and tetra-*n*-butylammonium bromide.[10] DMF (Merck, Uvasol) was dried over a molecular sieve 4 Å. The phosphorescence was excited with the 366-mμ mercury line (Osram HBO 100) and analyzed by a Zeiss double monochromator MM12 with glass optics. The photomultiplier output (Valvo 150 CVP) was recorded and electronically integrated between 700 and 1000 mμ.

Luminescence decay curves were obtained by excitation with a frequency doubled ruby laser (104A TRG/Control Data Corp.). The oscilloscope tracings (Siemens Oscillar M214) were photographed and graphically analyzed.

The quantum yields of the photoreactions at temperatures $T \geq 20°$ were determined using an apparatus previously described.[11] The light source was a high-pressure mercury lamp (Osram HBO 100). For the determinations at lower temperatures a relative procedure was applied. The number of absorbed quanta was measured using as actinometer the solution of the complex at room temperature. Since at the wave-

(1) H. L. Schläfer, *Z. Phys. Chem.* (*Frankfurt am Main*), 11, 65 (1957); *Acta Chim. Hung.*, 18, 375 (1959); *J. Phys. Chem.*, 69, 2201 (1965).

(2) R. A. Plane and J. P. Hunt, *J. Amer. Chem. Soc.*, 79, 3343 (1957).

(3) A. W. Adamson, *J. Phys. Chem.*, 71, 798 (1967).

(4) H. L. Schläfer, *Z. Chem.*, 10, 9 (1970).

(5) A. W. Adamson, *Pure Appl. Chem.*, 24, 451 (1970).

(6) V. Balzani and V. Carassiti, "Photochemistry of Coordination Compounds," Academic Press, London, 1970.

(7) G. B. Porter, S. N. Chen, H. L. Schläfer, and H. Gausmann, *Theoret. Chim. Acta*, 20, 81 (1971).

(8) A. Chiang and A. W. Adamson, *J. Phys. Chem.*, 72, 3827 (1968).

(9) H. F. Wasgestian, *Z. Phys. Chem.* (*Frankfurt am Main*), 67, 39 (1969).

(10) H. L. Schläfer, H. Wagener, F. Wasgestian, G. Herzog, and A. Ludi, *Ber. Bunsenges. Phys. Chem.*, 75, 878 (1971).

(11) H. F. Wasgestian and H. L. Schläfer, *Z. Phys. Chem.* (*Frankfurt am Main*), 51, 208 (1966).

length of excitation (366 mμ) the optical densities proved to be practically temperature independent, the number of absorbed quanta determined at room temperature also applies at lower temperatures.

Absorption spectra were recorded on a Cary 14 spectrophotometer. The photochemical reaction was followed spectrophotometrically at 444 mμ, using a Zeiss PMQ II spectrophotometer. The difference in extinction coefficients of $[Cr(CN)_5DMF]^{2-}$ and $[Cr(CN)_6]^{3-}$ was 108 l. mol^{-1} cm^{-1} in DMF.

For the low-temperature experiments, the samples were brought into quartz dewars or appropriate styropore housings and cooled with a stream of evaporated nitrogen. Degassing was performed by the freeze–pump technique. Three cycles at 10^{-3} Torr proved to be sufficient.

The photochemical reaction product was separated from the unreacted complex by displacement chromatography; 4.5 ml of a 0.04 *M* solution of $[Bu_4N]_3[Cr(CN)_6]$ in DMF was exposed to the full intensity of the high-pressure mercury lamp for 7 min, and 0.5 ml was diluted 1:10 and used for recording an absorption spectrum. The spectrum showed that only a small part of the hexacyanochromate had reacted. Therefore a further photoreaction of the photolysis product could be neglected. The other 4 ml was passed through the column (acidic Al_2O_3). The first fraction was eluted with 300 ml of 0.02 *M* LiCl in DMF, the second with 50 ml of 0.1 *M* LiCl in DMF. Within both fractions, no change in the absorption spectrum was observed, showing that the fractions were homogeneous. In some samples the chromium content was analytically determined by alkaline oxidation to chromate, detected spectrophotometrically at 366 mμ. A simpler and better reproducible method for the determination of the chromium content was obtained from the optical density at the wavelength of the isosbestic point at 405 mμ (ε 63.9 l. mol^{-1} cm^{-1}).

Results

(*a*) *Qualitative Experiments.* On irradiation into the d–d bands of hexacyanochromate, dissolved in DMF, changes in the absorption spectrum are observed (Figure 1). The long wavelength band at 390 mμ gradually disappears and a new band at 444 mμ arises. ($[Cr(CN)_6]^{3-}$ shows a slight solvatochromic effect. In DMF, compared to water, a shift of 900 cm^{-1} to longer wavelength is observed.) For small conversions two isosbestic points at 405 and 365 mμ are observed. In the region of the short wavelength band, the situation is less clear. Larger experimental errors are obviously caused by the incipient self-absorption of the solvent. The existence of isosbestic points permits the assumption that only one reaction product is formed during the first period of irradiation. The spectral changes were stable after irradiation. This indicated that secondary thermal reactions were slow.

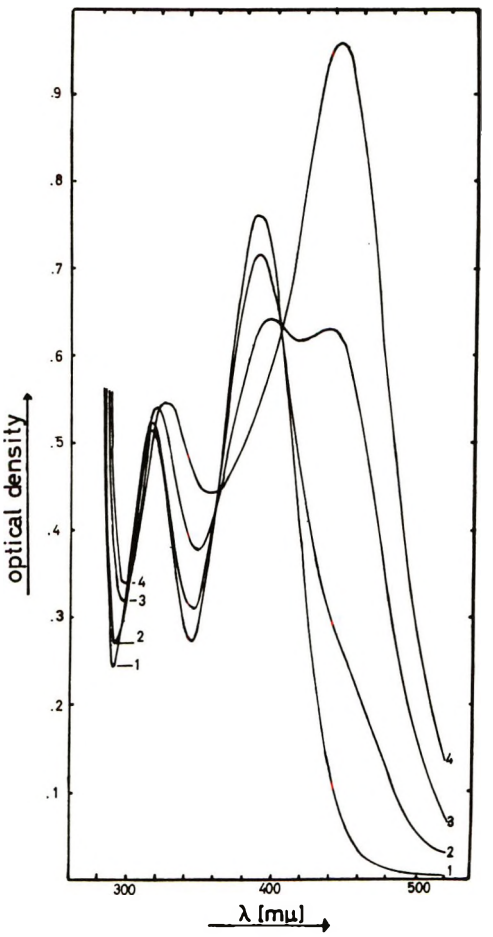

Figure 1. Spectral changes on irradiation of 0.01 *M* $[Bu_4N]_3[Cr(CN)_6]$ in DMF; aerated solution at room temperature; unfiltered mercury light; irradiation times: 1, not exposed; 2, 2 min; 3, 7 min; 4, 16 min.

Therefore, the photochemical reaction product could be separated.

By displacement chromatography on Al_2O_3 two fractions were obtained. The spectrum of the second fraction was identical with that of the unreacted hexacyanochromate. The first fraction absorbed at longer wavelength. Its spectrum is given in Figure 2. In position and the shape of its bands it corresponds to that of the photochemical aquation product of $[Cr(CN)_6]^{3-}$, which was described by Chiang and Adamson.[8] On the grounds of published spectra of various aquocyano complexes,[12,13] Chiang and Adamson assumed that the first detectable reaction product in H_2O was the diaquotetracyanochromate. A recent study of Jeftić and Feldberg,[14] however, proved that the spectrum, previously assigned to the tetracyano complex, is in reality that of $[CrH_2O(CN)_5]^{2-}$. Therefore it seems rather

(12) R. Krishnamurthy, W. B. Schaap, and R. J. Perumareddi, *Inorg. Chem.*, 6, 1338 (1967).

(13) W. B. Schaap, R. Krishnamurthy, D. K. Wakefield, and W. F. Coleman in "Coordination Chemistry," S. Kirschner, Ed., Plenum Press, New York, N. Y., 1969.

(14) L. Jeftić and S. Feldberg, *J. Amer. Chem. Soc.*, 92, 5272 (1970).

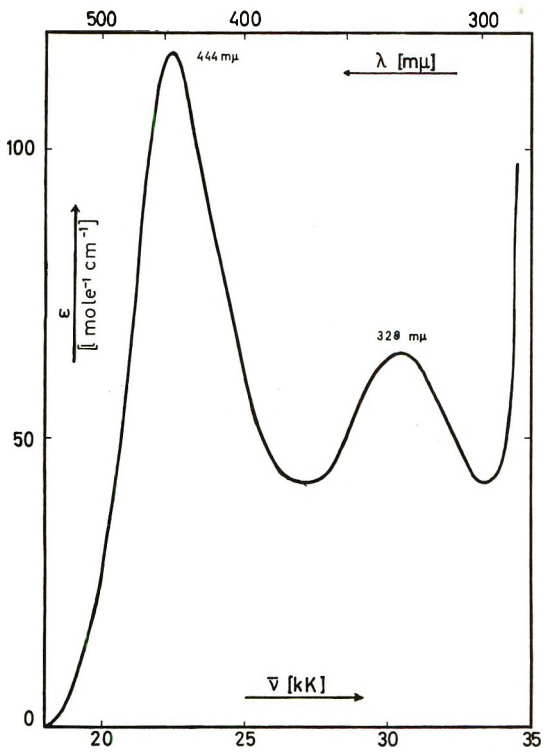

Figure 2. Absorption spectrum of the chromatographically separated reaction product $[CrDMF(CN)_5]^{2-}$.

certain that Chiang and Adamson had obtained the aquopentacyanochromate(III)

Since the spectra of chromium complexes with coordinated DMF are very similar to the corresponding aquo complexes,[15] it is safe to assume that in DMF the photoreaction also leads to the pentacyano complex.

$$[Cr(CN)_6]^{3-} + DMF \xrightarrow{h\nu} [CrDMF(CN)_5]^{2-} + CN^-$$

Some preliminary quantitative experiments support this assumption. Titrations of the photochemically produced cyanide in connection with the spectrophotometrically determined conversion showed that one CN^- only was released per reacted chromium complex.

(*b*) *Phosphorescence and Photochemistry. 1. Influence of Oxygen and Water.* The photochemical quantum yields of air-saturated as well as degassed solutions are shown in Table I. They can be compared to the phosphorescence lifetimes obtained under the same experimental conditions (Table II).

The oxygen dissolved in DMF reduces the lifetime to one-tenth of that of an oxygen-free solution. Water deactivates the doublet state so drastically that at room temperature no phosphorescence is observed, not even in a degassed solution. The photochemical quantum yield, however, is only moderately affected by water and not at all by oxygen.

2. Temperature Dependence. The low freezing point of DMF (−61°) allows the temperature dependence to be determined over a larger range than in water. Within the experimental error the photochemical

Table I: Photochemical Quantum Yields of 0.01 *M* $[Bu_4N]_3[Cr(CN)_6]$ in DMF at 25°; Excitation at 366 mμ

	Vol, ml	Irradiation time, min	Absorbed quanta × 10^6, einsteins	Quantum yield, mol einstein^{-1}
Solution air saturated	2.5	10	16.8	0.080
	3.0	15	20.1	0.097
	2.5	15	10.1	0.069
	2.5	30	20.4	0.072
	3.0	46	62.7	0.088
Solution degassed	3.0	15	20.3	0.096
	2.5	20	13.6	0.077
	2.5	30	19.6	0.077
	2.5	39	26.6	0.084
	3.0	46	60.3	0.091

Table II: Comparison of Photochemical Quantum Yields with Phosphorescence Lifetimes; 0.01 *M* $[Cr(CN)_6]^{3-}$ at 25°

Medium	Photochem. quantum yield, mol einstein^{-1}	Phosphorescence lifetime, sec
DMF air sat.	0.081	0.54×10^{-3}
DMF degassed	0.085	6.5×10^{-3}
H_2O air sat.	0.12[a]	*b*

[a] Reference 9; 20°. [b] No phosphorescence detectable.

quantum yield (Figure 3) shows a linear Arrhenius relationship. However, the phosphorescence lifetime and the relative phosphorescence intensity are quite differently affected (Figure 4).

At lower temperatures only a very small temperature dependence is observed, but warming above room temperature considerably reduces the phosphorescence. In this region an apparent activation energy of 9 kcal mol^{-1} is calculated.

Discussion

Upon comparing the photochemical and the luminescence behavior of $[Cr(CN)_6]^{3-}$ the following differences become apparent. (a) In DMF the doublet state has a long lifetime (τ = 6 msec); nevertheless the complex reacts photochemically. It therefore seems obvious that the photoreaction does not provide an efficient quenching process for the doublet. (b) The phosphorescence is strongly quenched by water, but the photochemical quantum yields differ only slightly in water (ϕ = 0.12) and DMF (ϕ = 0.08). (c) Oxygen has no influence on the photoreaction in DMF. The phosphorescence, however, is quenched to one-tenth in an air-saturated solution compared to a degassed one. (d) The phosphorescence and the photoreaction have different temperature dependences. (e) Binet, Gold-

(15) C. K. Jorgensen, "Oxidation Numbers and Oxidation States," Springer Verlag, Berlin, 1969.

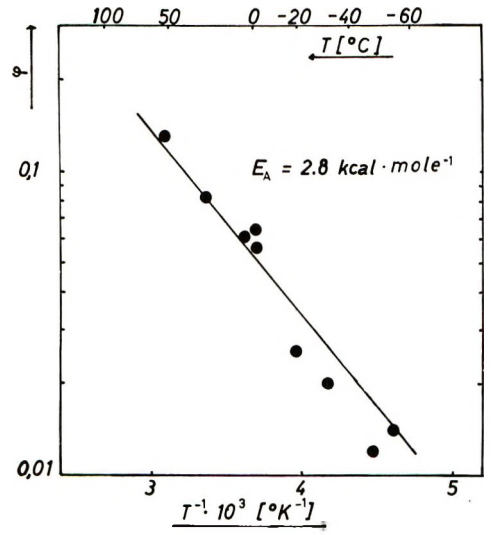

Figure 3. Temperature dependence of the photochemical quantum yield; 0.01 M $[Bu_4N]_3[Cr(CN)_6]$ in DMF; samples degassed.

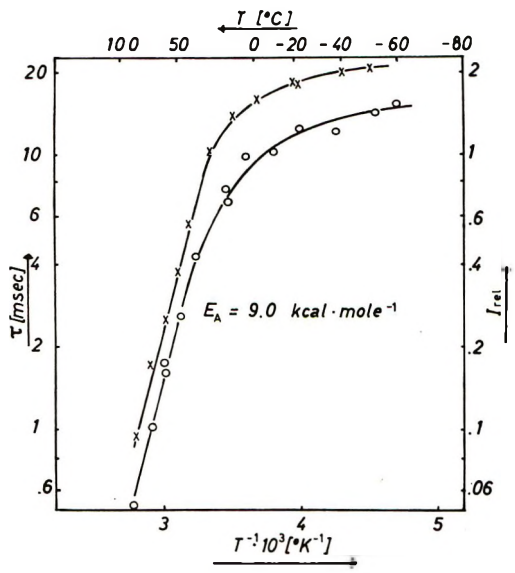

Figure 4. Temperature dependence of the phosphorescence of 0.01 M $[Bu_4N]_3[Cr(CN)_6]$ in DMF; samples degassed; ○, lifetimes; ×, phosphorescence intensities relative to 25°.

berg, and Forster[16] obtained sensitized phosphorescence by energy transfer from triplet states of organic molecules to $[Cr(CN)_6]^{3-}$. These experiments were repeated, however, using anthracene dissolved in DMF. The sensitized phosphorescence was again obtained, but under the same experimental conditions no sensitized photoreaction was observed.[17]

These differences rule out the possibility that the photoreaction and the phosphorescence originate from the same excited level. As the phosphorescence originates from the ^2E_g state, the photoactive state must be the $^4T_{2g}$, since these are the only two that enter into question.[5-7]

The quantum yield of hexacyanochromate(III) does not obey the ligand field dependence observed among other chromium complexes, for which the photochemical quantum yield corresponds to their position in the spectrochemical series. The quartet hypothesis explains this effect as follows. The excitation of a nonbonding t_{2g} electron to an antibonding e_g orbital destabilizes the complex. Thus a larger labilization is expected, the stronger the field of the ligands. According to this idea, hexacyanochromate, which possesses the strongest known ligand field, should have a large photochemical quantum yield, which is not the case. This descrepancy Adamson[8] attributed to the influence of π-bonding effects.

We would prefer another explanation: The photoreaction competes with the other radiationless transitions. The latter are promoted by a small energy separation from the next lower state.[18] If we neglect very low ligand fields (At very low ligand fields an inversion of the levels occurs so that the $^4T_{2g}$ is the lowest excited state. Until now, no complex of such a low ligand field has been photochemically studied.) the $^4T_{2g}-^2E_g$ separation increases with increasing ligand fields (octahedral symmetry assumed). This favors the photoreaction compared to the radiationless deactivation, but the very strong field of the cyano ligands puts another doublet state ($^2T_{2g}$) below the $^4T_{2g}$. In this case the energy gap is reduced, and the radiationless deactivation again becomes more effective.

Of course, the exclusion of the doublet hypothesis is only valid for the photoreaction of hexacyanochromate. Cyano complexes often differ from other transition metal compounds. Unusual coordination numbers, oxidation states, or stabilities are common among this class of compounds. Therefore, it is quite possible that this result may not be generalized.

On the other hand, some effects observed on other chromium complexes permit the assumption that the quartet hypothesis is generally valid. (1) The main argument of the doublet hypothesis is the assumption that the longer natural lifetime of the ^2E_g facilitates the chemical reaction. Provided the nonchemical radiationless deactivations do not depend on the viscosity of the solvent or on temperature, the phosphorescence observed on melting a glassy solution should be caused by the chemical reaction. In this case the photochemical quantum yields in solution should correlate with the solid-state phosphorescence lifetimes. The fact that no correlation is generally found does not mean a proof against the doublet hypotheses, because the abovementioned assumption may be wrong. However, if a correlation had been found, it would have been strong

(16) D. J. Binet, E. L. Goldberg, and L. S. Forster, *J. Phys. Chem.*, 72, 3017 (1968).

(17) Unpublished results of this laboratory.

(18) J. Jortner, S. A. Rice, and R. M. Hochstrasser, *Advan. Photochem.*, 7, 149 (1969).

evidence for this hypothesis. (2) Differences in the temperature dependence of phosphorescence and photoreaction are also observed for $[Cr(en)_3]^{3+}$.[19] (3) Energy transfer experiments, in which excitation of the $^4T_{2g}$ state was possible on energetic grounds, have yielded sensitized photoreactions.[20-23] (4) The photoaquation of $[Cr(NH_3)_5NCS]^{2+}$ has lower quantum yields on irradiation into the doublet band than on irradiation into the spin-allowed quartet bands.[24] (5) Chen and Porter[25,26] have studied the influence of $[Cr(CN)_6]^{3-}$ on the phosphorescence and the photoreaction of $[Cr(NH_3)_2(SCN)_4]^-$. Both processes were quenched, but the photoreaction less than the phosphorescence. The authors concluded that either both states (the quartet and the doublet) were photosensitive or that only the quartet was the photoactive state, while the quenchable part of the photoreaction was due to thermal back population from the doublet state. Therefore, it seems that in the photochemistry of chromium complexes the doublet state only plays a minor role or none at all.

Acknowledgment. Financial support from the Deutsche Forschungsgemeinschaft is gratefully acknowledged.

(19) W. Geis, Thesis, University of Frankfurt am Main, 1971.

(20) A. W. Adamson, J. E. Martin, and F. Diomedi-Camassei, *J. Amer. Chem. Soc.*, **91**, 7530 (1969).

(21) J. E. Martin and A. W. Adamson, *Theoret. Chim. Acta*, **20**, 119 (1971).

(22) E. Zinato, P. Tulli, and P. Riccieri, *J. Phys. Chem.*, **75**, 3504 (1971).

(23) V. Balzani, R. Ballardini, M. T. Gandolfi, and L. Moggi, *J. Amer. Chem. Soc.*, **92**, 3196 (1970).

(24) E. Zinato, R. D. Lindholm, and A. W. Adamson, *J. Amer. Chem. Soc.*, **91**, 1076 (1969).

(25) S. N. Chen and G. B. Porter, *Chem. Phys. Lett.*, **6**, 41 (1970).

(26) S. N. Chen and G. B. Porter, *J. Amer. Chem. Soc.*, **92**, 3196 (1970).

Effect of Charge-Transfer Complex Formation on the Positronium–Iodine Reaction

by B. Lévay[1] and P. Hautojärvi*

Department of Technical Physics, Helsinki University of Technology, SF-02150 Otaniemi, Finland
(Received January 24, 1972)

Publication costs assisted by Helsinki University of Technology

The effect of charge-transfer complex formation on the reaction of positronium and iodine was investigated by performing positron lifetime measurements in cyclohexane solutions with various concentrations of iodine and pyridine. It was found that the pyridine–iodine complex is a weaker quencher of orthopositronium and a stronger inhibitor of the positronium formation than the free iodine molecule. The quenching rate constant was 41.4 ± 0.4 $nsec^{-1}\ M^{-1}$ for iodine and 28.9 ± 0.3 $nsec^{-1}\ M^{-1}$ for the pyridine–iodine complex. The inhibition coefficient of iodine in cyclohexane was estimated to be 21 M^{-1} but the inhibition properties of the pyridine–iodine complex were not proportional to the concentration. It is suggested that the positronium–iodine substitution reaction and positronium–iodine complex formation, both of which are followed by a rapid annihilation, are two parallel reaction ways for the quenching of orthopositronium by iodine. It is also demonstrated that the equilibrium of the charge-transfer complex formation can be studied by positron lifetime measurements.

Introduction

The bound state between a positron and an electron, the positronium atom (Ps), can be formed in a medium when the positron during slowing down captures an outer-shell electron from a molecule. The formation probability and the lifetime of the positronium depend strongly on the properties of the medium. The use of positron annihilation as a tool to investigate various chemical and physical phenomena is described in several books and review articles.[2,3]

(1) On leave from Department of Physical Chemistry and Radiology, L. Eötvös University, Budapest, Hungary.

(2) (a) J. H. Green and J. Lee, "Positronium Chemistry," Academic Press, New York, N. Y., 1964; (b) V. I. Goldanskii, *At. Energy Rev.*, **6**, 3 (1968).

(3) A. T. Stewart and L. O. Roelling, Ed., "Positron Annihilation," Academic Press, New York, N. Y., 1967.

Because of its hydrogen-like structure, the positronium atom can take part in chemical reactions with different kinds of species. A theoretical treatment of the chemical effects on the positronium lifetime has been given by Tao and Green.[4] They considered the effect of different substances on positronium in a mixture to be additive but pointed out that complex formation may alter this simple picture considerably.

Recently Tao has investigated the quenching of long-life orthopositronium by iodine in various organic liquids.[5] He found this reaction to be diffusion controlled, because the reaction rate was inversely proportional to the viscosity of the solvents. The great deviation from this relationship in acetone and diethyl ether solvent was attributed to the charge-transfer complex formation.

In the present work we have investigated the effect of charge-transfer complex formation on the positronium and iodine reaction. The pyridine–iodine complex formation in cyclohexane solvent was chosen as a model because this particular complex formation has been investigated by several authors.[6] In addition, data on the self-diffusion of iodine and the pyridine–iodine complex are available.[7]

Experimental Methods

Positron lifetime spectra were measured with a conventional fast–slow coincidence system,[8] where a commercial Ortec 437 time-to-amplitude converter was used. The time resolution in these measurements was FWHM = 0.32 nsec. The positron source was about 7 μCi of ^{22}NaCl deposited and sandwiched between two thin (0.87 mg/cm^2) "Melinex" polyester foils. The time spent for one spectrum was 10 hr and about 2×10^5 counts were accumulated. All measurements were performed under temperature control at 20°.

All the chemical materials were reagent grade with further purification as described earlier.[7] The samples were carefully deoxygenated by the vacuum freeze–thaw technique.

Two series of measurements with varying iodine concentration from 0.002 to 0.015 M were performed: iodine in pure cyclohexane and iodine in the cyclohexane–0.15 M pyridine system. The equilibrium constant of pyridine–iodine complex formation is about 160 M^{-1} in cyclohexane at 20°.[9] Thus in the latter case about 95% of iodine molecules were in the complex. In the third series the fraction of iodine in the complex was varied by keeping the iodine concentration (0.015 M) constant and changing the pyridine concentration from zero to 0.15 M. In addition, the effect of pyridine on the positronium formation in cyclohexane without any iodine was studied.

Some examples of the effect of iodine and pyridine–iodine complex on the positron lifetime spectrum in cyclohexane can be seen in Figure 1.

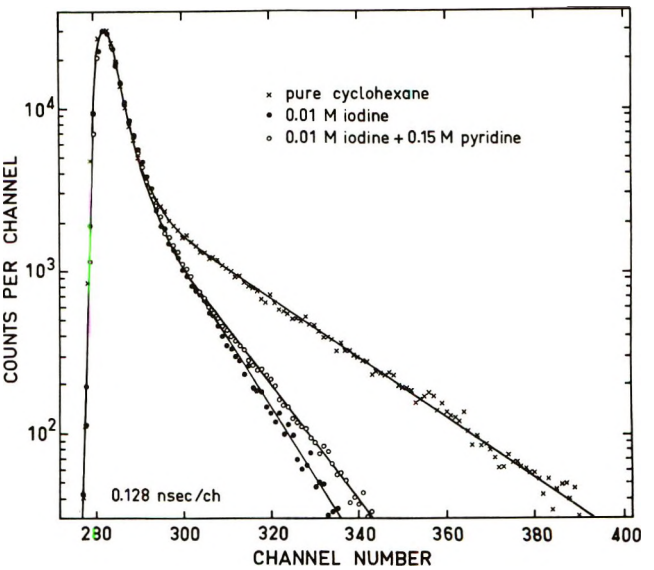

Figure 1. The effect of iodine and the pyridine–iodine complex on the positron lifetime spectrum in cyclohexane solvent. In the presence of 0.15 M pyridine about 95% of iodine molecules have formed the complex with a pyridine molecule.

It was estimated that about 5% of the positrons were annihilated in the foils. After substraction of the foil spectrum, the measured lifetime spectra were analyzed with a two-exponential fit. The results are presented in Tables I–III.

Results and Discussion

A. The Effect of Chemical Quenching on the Lifetime Spectrum. When forming of positronium atoms occurs

Table I: Results of Positron Lifetime Measurements in Iodine Solutions of Cyclohexane[a]

$10^3 C_{I_2}$, M	τ_1, nsec	τ_2, nsec	I_2, %
0[b]	0.376 ± 0.005	2.40 ± 0.03	37.6 ± 1.0
0	0.367 ± 0.005	3.03 ± 0.03	36.8 ± 1.0
2.0	0.379 ± 0.005	2.28 ± 0.03	36.4 ± 1.0
4.0	0.375 ± 0.005	2.05 ± 0.02	37.1 ± 1.0
6.0	0.379 ± 0.004	1.74 ± 0.02	37.3 ± 1.0
8.0	0.384 ± 0.006	1.50 ± 0.02	36.3 ± 1.0
10.0	0.394 ± 0.007	1.27 ± 0.02	35.4 ± 1.0
12.0	0.411 ± 0.008	1.17 ± 0.03	33.7 ± 1.0
15.0	0.425 ± 0.008	1.09 ± 0.03	31.2 ± 1.0

[a] The indicated errors are statistical standard deviations. The accuracy in the time calibration is about 1%. [b] Air saturated.

(4) S. J. Tao and J. H. Green, *J. Chem. Soc. A*, 408 (1968).

(5) S. J. Tao, *J. Chem. Phys.*, 52, 752 (1970).

(6) R. Forster, "Organic Charge-Transfer Complexes," Academic Press, New York, N. Y., 1969.

(7) B. Lévay, *Acta Chim. (Budapest)*, in press.

(8) A. Tamminen and P. Jauho, *Nucl. Instrum. Methods*, 65, 132 (1968).

(9) P. V. Huong, N. Platzer, and M. L. Josien, *J. Amer. Chem. Soc.*, 91, 3669 (1969).

Table II: Results of Positron Lifetime Measurements in Iodine Solutions of Cyclohexane Containing 0.15 *M* Pyridine

$10^3C_{I_2}$, *M*	τ_1, nsec	τ_2, nsec	I_2, %
0	0.349 ± 0.005	2.98 ± 0.03	44.5 ± 1.0
0.5	0.354 ± 0.004	2.77 ± 0.03	40.8 ± 1.0
2.0	0.361 ± 0.004	2.44 ± 0.02	37.8 ± 1.0
4.0	0.375 ± 0.004	2.11 ± 0.02	35.7 ± 1.0
6.0	0.389 ± 0.005	1.91 ± 0.03	34.0 ± 1.0
8.0	0.400 ± 0.004	1.64 ± 0.02	30.3 ± 1.0
10.0	0.411 ± 0.004	1.57 ± 0.02	27.5 ± 1.0
15.0	0.422 ± 0.004	1.30 ± 0.02	24.2 ± 1.0

Table III: Results of Positron Lifetime Measurements in Pyridine Solutions of Cyclohexane Containing 0.015 *M* Iodine

10^3C_{py}, *M*	τ_1, nsec	τ_2, nsec	I_2, %	X_C[a]
0.0	0.425 ± 0.008	1.09 ± 0.03	31.2 ± 1.0	0
4.55	0.424 ± 0.007	1.14 ± 0.03	25.2 ± 1.0	0.20
10.3	0.427 ± 0.007	1.14 ± 0.03	24.1 ± 1.0	0.40
18.3	0.412 ± 0.006	1.16 ± 0.03	24.4 ± 1.0	0.60
43.2	0.434 ± 0.006	1.27 ± 0.04	19.8 ± 1.0	0.83
150	0.422 ± 0.004	1.30 ± 0.02	24.2 ± 1.0	0.95

[a] Fraction of iodine in complex.

in the medium, there are at least three modes of annihilation: (1) self-annihilation of parapositroniums at the rate $\lambda_p \leq 8$ nsec^{-1}, (2) annihilation of the free positrons at a rate λ_f, and (3) the pick-off annihilation of the positrons in orthopositroniums by electrons of the surrounding medium at a rate λ_t.

Because of the finite instrumental time resolution, the first two modes usually cannot be separated and thus they both together form the first lifetime component (I_1, τ_1). The second component (I_2, τ_2) is attributed to the annihilation of orthopositroniums.

When the chemical reaction of positroniums occurs, it usually results in a short-lived positron or a positronium compound with the annihilation rate $\lambda_{CP} \gg \lambda_t$. The longer lifetime τ_2 in the measured spectra decreases, and the increase of the annihilation rate $\lambda_2 = 1/\tau_2$ is of the form

$$\lambda_2 = \lambda_t + \lambda_{ox} \quad (1)$$

where λ_{ox} is the reaction rate of the chemical quenching. In dilute solutions λ_{ox} is proportional to the concentration of the reaction agent

$$\lambda_{ox} = k_q C \quad (2)$$

where k_q is the rate constant of the quenching reaction. In addition, the intensity belonging to the lifetime of the Ps compound formed in the reaction is negative and thus the measured intensity for orthopositronium (I_2) will be spuriously enhanced. The complete analysis of this effect has been given by McGervey.[10]

If there is no ortho–para conversion in positronium atoms, then the relative number of positrons left at time t can be written in the form

$$\frac{N(t)}{N(0)} = \frac{1}{3} I^0_2 e^{-\lambda_p t} + \left(1 - \frac{4}{3} I^0_2\right) e^{-\lambda_f t} - I^0_2 \frac{\lambda_{ox}}{\lambda_{CP} - (\lambda_t + \lambda_{ox})} e^{-\lambda_{CP} t} + I^0_2 \left(1 + \frac{\lambda_{ox}}{\lambda_{CP} - (\lambda_t + \lambda_{ox})}\right) e^{-(\lambda_t + \lambda_{ox})t} \quad (3)$$

where I^0_2 is the initial intensity of the orthopositronium. Because of the possible spin states the intensity of parapositroniums is simply $I^0_2/3$, when no ortho–para conversion exists. The intensity of free positrons is obtained from the normalization condition according to which the sum of intensities is equal to unity. λ_{CP} is of the same order as λ_f and therefore all the first three terms in eq 3 belong to the experimental lifetime component I_1, τ_1.

B. The Effect of Pyridine in Pure Cyclohexane. We found that pyridine has no effect on the orthopositronium lifetime in the concentration range from zero to 0.15 *M*. This means that there is no reaction between pyridine and positronium. However, the increase in I_2 values shows that pyridine enhances the positronium formation in cyclohexane. In the concentration region we have used, the relative increase of I_2 was simply proportional to the pyridine concentration and the proportionality coefficient was estimated to be 1.4 M^{-1}.

In pure pyridine the I_2 value is about 10%.[11,12] The possible explanation for the enhanced positronium formation by pyridine in cyclohexane is in the different position of the Ore gap of these two molecules. The ionization potential of pyridine is about 1.2 eV lower than that of cyclohexane.[13] Thus positrons which have slowed down below the Ore gap of cyclohexane may still form a positronium by capturing an electron from a pyridine molecule.

In conclusion, when studying positronium reactions with the iodine–pyridine complex, the presence of 0.15 *M* pyridine only increases the initial intensity of positroniums but has no effect on the chemical reactions of positronium.

C. Quenching of the Longer Lifetime by Iodine and the Pyridine–Iodine Complex. The annihilation rates (λ_2) as a function of iodine concentration in cyclohexane and cyclohexane–pyridine solvent are shown in Figure 2. The linear relationship of eq 1 and 2 seems to be valid in our concentration range. The reaction

(10) J. McGervey in ref 3, p 143.

(11) P. R. Gray, C. F. Cook, and G. P. Sturm, Jr., *J. Chem. Phys.*, **48**, 1145 (1968).

(12) K. P. Singh, R. M. Singru, and C. N. R. Rao, *Proc. Phys. Soc., London (At. Mol. Phys.)*, **4**, 261 (1971).

(13) A. Hustrulid, P. Kusch, and J. T. Tate, *Phys. Rev.*, **54**, 1037 (1938).

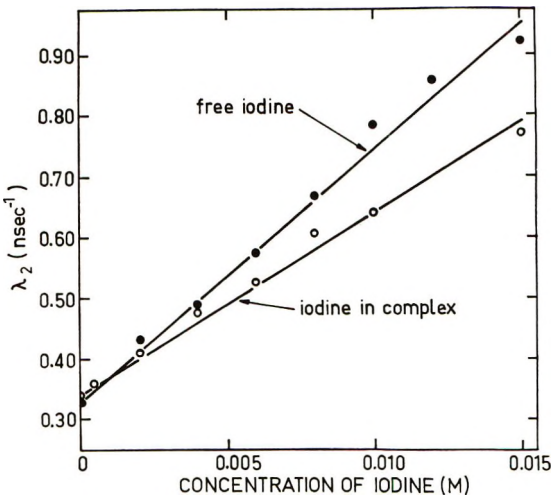

Figure 2. The annihilation rate λ_2 of the orthopositronium as a function of iodine concentration. The black circles describe iodine solutions of cyclohexane. The open circles belong to iodine solutions of cyclohexane containing 0.15 M pyridine, when 95% of iodine is in the complex form.

rate constants were determined from the slope of the least-squares-fit lines and the result was $k_I = 41.4 \pm 0.4$ nsec^{-1} M^{-1} for the free iodine and $k_C = 28.9 \pm 0.3$ nsec^{-1} M^{-1} for iodine, of which 95% is in complex form.

For comparison, from the measurement in air-saturated cyclohexane (Table I) the quenching rate constant of oxygen can be estimated to be 38 nsec^{-1} M^{-1}, when the equilibrium concentration of oxygen in cyclohexane is about 2.3×10^{-3} M^{-1}.[14] Thus we see the well-known relation that oxygen is a very strong quencher.[15]

By assuming that the reactions of positronium with both free iodine and the pyridine–iodine complex are diffusion controlled, the rate constant values can be interpreted on the basis of the theory of fast reactions. The molar rate constant is then of the form[16]

$$k = F(4\pi ND/1000)(r_a + r_b) \qquad (4)$$

where k is expressed in M^{-1}, N is Avogadro's number, and D is the sum of diffusion coefficients of the two species which take part in the reaction. Their effective radii are denoted by r_a and r_b. The factor F expresses the effect of forces interacting between the species. Because of the long wavelength and small concentration of positroniums, orientation and surface concentration effects can be neglected.[5]

By assuming that the diffusion coefficients can be expressed by Stoke's law

$$D = (k_B T/6\pi\eta)(r_a^{-1} + r_b^{-1}) \qquad (5)$$

where k_B is Boltzmann's constant, T is the temperature, and η is the viscosity, we obtain the formula for the diffusion-controlled reaction rate

$$k = F(8k_B NT/3000\eta)\left(\frac{1}{4}\right)\left(2 + \frac{r_a}{r_b} + \frac{r_b}{r_a}\right) \qquad (6)$$

Let us first assume that the factor F is equal for the reactions of positronium with free iodine and with the pyridine–iodine complex. Then the difference in measured reaction rates should be due to different diffusion coefficients or, rather, different radii in eq 6. By following Tao,[5] we take the effective radii for Ps and iodine molecules to be 0.53 and 2.66 Å, respectively. From the preliminary results of similar measurements as in ref 7 concerning the self-diffusion of iodine and the pyridine–iodine complex in cyclohexane, we have estimated the effective radius of the complex to be 4.26 Å. From these data we get for the ratio of rate constants $k_C/k_I = 1.41$, which is significantly longer than the measured value $k_C/k_I = 0.70$.

This means that the F factors are not equal for the iodine and pyridine–iodine complex. In fact, the ratio should be $F_C/F_I = 0.5$. The absolute values calculated from eq 6 are $F_C = 1.8$ and $F_I = 3.6$. Although these figures are based on the simple Stokes law of diffusion their ratio is a real measure of the difference in the interaction of positronium with the iodine molecule and the pyridine–iodine complex.

A greater F factor represents more attractive forces between the interacting molecules. The large decrease in the attractive character of these forces after complex formation indicates the decrease in electron acceptor capacity of the iodine caused by the complex formation. This means that the electron-acceptor capacity plays an important role in the positronium and iodine reaction. The change in the rate of the quenching reaction between positronium and an electron acceptor might be a useful measure for electron-acceptor capacity of a molecule.

Tao[5] has suggested two alternative possibilities for the quenching reaction of orthopositronium by iodine

$$Ps + I_2 \longrightarrow PsI + I \longrightarrow I + I + 2\gamma \qquad (7)$$

or

$$Ps + I_2 \longrightarrow PsI_2 \longrightarrow I_2 + 2\gamma \qquad (8)$$

One can think that the first substitution type reaction is affected only slightly by the complex formation, as the bond strength between pyridine and iodine (about 0.35 eV) is weak as compared to the bonding between the two iodine atoms (1.6 eV).[17] On the other hand, when almost all iodine molecules have already formed complexes with pyridine molecules, reaction 8 is no longer possible because of the unlikeliness of a double complex formation.

(14) H. Landolt and R. Börnstein, "Zahlenwerte und Funktionen," Vol. II, Part 2b, 6th ed, Springer-Verlag, Berlin, 1962, pp 1–74.

(15) J. Lee and G. J. Celitans, *J. Chem. Phys.*, **44**, 2506 (1966).

(16) J. Q. Umberger and V. K. LaMer, *J. Amer. Chem. Soc.*, **67**, 1099 (1945).

(17) C. Reid and R. S. Mulliken, *ibid.*, **76**, 3869 (1954).

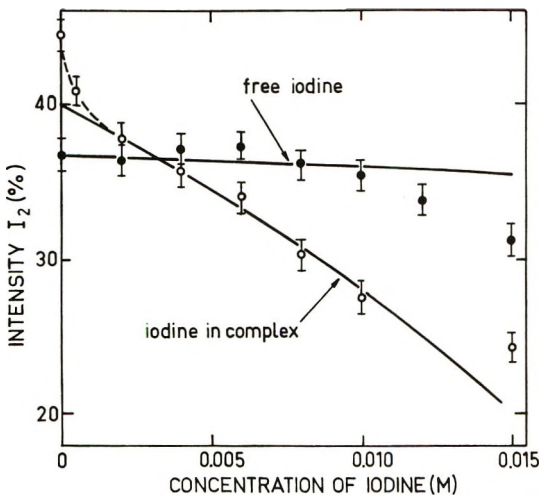

Figure 3. The intensity I_2 of the second lifetime component in iodine solutions of cyclohexane (black circles) and in iodine solutions of cyclohexane containing 0.15 M pyridine (open circles).

Thus to explain the decrease in the quenching rate caused by the complex formation and the existence of the residual high quenching rate of the pyridine–iodine complex, we suggest that eq 7 and 8 represent two possible parallel ways for the reaction between Ps and iodine. After the complex formation, the reaction way 8 is closed, and, for the complex, only reaction 7 is still possible.

D. Inhibition of Positronium Formation. Chuang and Tao[18] have reached the conclusion that iodine is both a strong chemical quencher and a weak inhibitor of positronium formation. We found significant differences between inhibition properties of the iodine molecule and pyridine–iodine complex. The measured I_2 values are plotted against the iodine concentration in Figure 3.

The inhibition of positronium formation manifests itself in the decrease of the intensity of the longer lifetime. In dilute solutions the relative decrease is proportional to the inhibitor concentration.[5] In addition, as we saw in eq 3, the chemical quenching reaction enhances the intensity I_2 in the measured spectrum. By combining both effects the intensity of the orthopositronium lifetime component can be written in the form

$$I_2 = I^0_2(1 - \mu C)\left(1 + \frac{\lambda_{ox}}{\lambda_{CP} - (\lambda_t + \lambda_{ox})}\right) \quad (9)$$

where I^0_2 is the intensity of orthopositroniums in the pure solvent and μ is the inhibition coefficient. The unknown parameters were estimated by fitting formula 9 to the measured intensity values for concentrations not greater than 0.01 M, because at higher concentrations this simple formula was no longer valid. The results, λ_{CP} about 2.5 nsec^{-1} and μ about 21 M^{-1} for iodine in pure cyclohexane, are in good agreement with Tao's results[5] for iodine in other hydrocarbons.

The pyridine–iodine complex is a stronger inhibitor. The form of the decrease of I_2 is quite different than in the case of the free iodine molecule. In fact, the decrease seems to be proportional to $C^{1/2}$ instead of C. The nonlinear behavior of I_2 can be understood if we assume two types of inhibition reaction. The sharp decrease (dashed line in Figure 3) at smaller concentrations would be due to a rapid inhibition reaction, which takes place, for example, in a narrow energy region of positroniums already formed, so that not more than about 10% of positroniums can take part in this process. The other inhibition reaction would be linear to the complex concentration (solid line) and we can apply formula 9 to it. In this model the inhibition coefficient for the complex would be $\mu \approx 40\ M^{-1}$, when $\lambda_{CP} \approx 2.5$ nsec^{-1} again.

A similar sharp decrease of intensity I_2 at small concentrations has been observed by Tao and Green[19] in oxyacid–water systems. The I_2 values extrapolated to zero concentration were always smaller than the intensity of the longer lifetime in pure water.

After complex formation, a great change occurs in the dipole character of molecules in our system. The dipole moment of the pyridine–iodine complex in cyclohexane is 4.44 D, which is almost twice as much as the dipole moment of the pyridine molecule.[17,20] We have assumed that the reason for the increase in the inhibition property of the system after complex formation is due to the charge localization. The reaction between the localized negative charge and positrons competes with the positronium formation. A similar effect of the charge localization has been observed by Hatcher, *et al.*,[21] in *o*-, *m*-, and *p*-xylene, where the increasing delocalization of the negative charge on the benzene ring increases the intensity of the longer lifetime.

The inhibition of positronium formation is also a possible explanation for the increase of the first lifetime (τ_1) in Tables I and II. From eq 3 we saw that the first component (I_1, τ_1) is in fact composed of three annihilation modes and the parapositronium has the largest annihilation rate. Therefore, when positronium formation is inhibited, the intensity of the component with the shortest lifetime decreases and thus the first lifetime (τ_1) in the two-component experimental fit increases.

By taking into account the enhancement of I_2 due to the chemical quenching we can estimate from eq 3 and 9 that the intensity of parapositroniums decreases from 12 to 7% and from 15 to 6% in Tables I and II, respectively. These changes together with the very rapid

(18) S. Y. Chuang and S. J. Tao, *J. Chem. Phys.*, **52**, 749 (1970).
(19) S. J. Tao and J. H. Green, *J. Phys. Chem.*, **73**, 882 (1969).
(20) S. S. Singh and C. P. Saxena, *Indian J. Chem.*, **8**, 1116 (1970).
(21) C. R. Hatcher, W. E. Millet, and L. Brown, *Phys. Rev.*, **111**, 12 (1958).

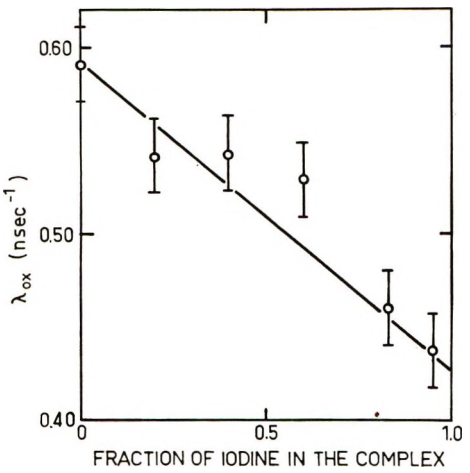

Figure 4. The quenching rate λ_{ox} as a function of the iodine fraction X_C being in the complex.

annihilation rate (λ_p = 8–5 nsec^{-1}) do give an effect which is of the same order of magnitude as the measured increase of τ_1.

E. Investigation of Complex Formation Equilibrium. The difference between the quenching rate of the iodine molecule and that of the pyridine–iodine complex makes it possible to investigate the complex formation equilibrium between pyridine and iodine. The decrease in the annihilation rate measured at a constant concentration of iodine (0.015 M) and at increasing pyridine concentration indicates that the fraction of iodine molecules in complex form increases (Table III).

By assuming that the quenching rate varies linearly with the fraction of iodine in complex form, we get

$$\lambda_{ox} = \lambda_{ox,I} - (\lambda_{ox,I} - \lambda_{ox,C})X_C \qquad (10)$$

where subscripts I and C refer to the quenching rates of iodine and complex, respectively, at the given concentration, and X_C is the fraction of iodine molecules in complex form. The values for X_C, calculated with the equilibrium constant K_C = 160 M^{-1}, are listed in Table III. A plot of λ_{ox} *vs.* X_C is drawn in Figure 4. We see that the points are not too far from the line of eq 10.

Conversely, it is possible to determine the equilibrium constant K_C with the aid of measured quenching rates. In the present case, however, the difference between $\lambda_{ox,I}$ and $\lambda_{ox,C}$ is relatively small as compared to the inaccuracy of the individual points and it is not possible to calculate an accurate K_C value. However, in more favorable conditions positron annihilation can be used as a new tool for the determination of the equilibrium constant of complex formation reactions.

The decrease of I_2 in Table III is mainly caused by the decrease of the chemical quenching rate in eq 9, and therefore τ_1 stays constant in contrast to Tables I and II. The reason for the minimum of I_2 is in the increase of pyridine concentration, which enhances the positronium formation but decreases I_2 by increasing complex concentration.

Conclusion

The quenching of orthopositronium and inhibition of positronium formation by iodine in cyclohexane is strongly affected by the charge-transfer complex formation of iodine with pyridine.

The quenching rate constants of iodine and of the pyridine–iodine complex are 41.4 ± 0.4 and 28.9 ± 0.3 nsec^{-1} M^{-1}, respectively. The value for the complex is 2 times smaller than expected on the theory of diffusion-controlled reactions. The reason for this decrease has been attributed to saturation of the electron-acceptor capacity of iodine molecules by complex formation with pyridine.

The suggested quenching mechanism of iodine is two parallel reactions

$$\mathrm{Ps} + \mathrm{I_2} \begin{cases} \longrightarrow \mathrm{PsI_2} \longrightarrow \mathrm{I_2} + \gamma\ \text{rays} \\ \longrightarrow \mathrm{PsI} + \mathrm{I} \longrightarrow \mathrm{I} + \mathrm{I} + \gamma\ \text{rays} \end{cases}$$

which lead to rapid annihilation at a rate λ_{CP} = 2.5 nsec^{-1} in agreement with Tao.[5] For the pyridine–iodine complex only the second reaction way, the substitution of one iodine atom by positronium, is possible.

The inhibition coefficients were estimated to be 21 and 40 M^{-1} for iodine and the pyridine–iodine complex, respectively. In the latter case, however, the intensity of the orthopositronium component already shows a rapid decrease at very low concentrations. The reason for the stronger inhibition property of the pyridine–iodine complex is assumed to be in the charge localization on the complex molecule.

The variation of the orthopositronium lifetime at constant iodine concentration as a function of pyridine concentration followed the complex formation equilibrium, which was calculated with the aid of the equilibrium constant available in the literature.

Acknowledgments. The authors thank Professor P. Jauho for his interest in this work. We are much indebted to R. Nieminen for his help in computer analysis of the lifetime spectra and to A. Tamminen for taking care of the electronics. B. L. wishes to thank the Department of Technical Physics of Helsinki University of Technology for its hospitality.

Electron Spin Resonance Study of Radicals Produced by the Reactions of Hydrated Electrons with Unsaturated Acids[1]

by P. Neta* and Richard W. Fessenden

Radiation Research Laboratories, Center for Special Studies, and Department of Chemistry, Mellon Institute of Science, Carnegie-Mellon University, Pittsburgh, Pennsylvania 15213
(Received January 24, 1972)

Publication costs assisted by Carnegie-Mellon University and the U. S. Atomic Energy Commission.

A search has been made for the esr spectra of radicals formed as the result of e_{aq}^- addition to a number of unsaturated carboxylate anions in irradiated aqueous solution. The adducts of acrylic and acetylenedicarboxylic acids were found to protonate rapidly on carbon to give the radicals $CH_3\dot{C}HCO_2^-$ and $^-O_2CCH=\dot{C}CO_2^-$, respectively. Stable anion radicals were formed from muconic, chelidonic, maleic, and dihydroxyfumaric acids. The acid–base equilibria of these radicals were followed and protonation was found to occur on the carboxyl groups. In the cases of maleic and dihydroxyfumaric acids strong intramolecular hydrogen bonds were formed which resisted dissociation even in 1 *M* base.

Introduction

Hydrated electrons react with unsaturated aliphatic compounds with rate constants which vary between $<10^6$ and 3×10^{10} M^{-1} sec^{-1}.[2] The rate constant for $RCH{=}CH_2$ strongly depends on the electron withdrawing property of R. For compounds where R is H or OH the rates are very low, but for compounds where R is COOH, COO^-, COOR, $CONH_2$, $CH{=}CH_2$, CN, or C_6H_5 the rate constants are $\sim 10^9$ to 10^{10} M^{-1} sec^{-1}. A quantitative correlation of the electron-withdrawing property of R with the rate constant for $e_{aq}^- + RCH{=}CH_2$ has not been possible because the rates for all the reactive compounds approach rather closely the diffusion-controlled limit.[3] The role of the group R in these reactions could be both the creation of a positive center on C=C which facilitates attack by e_{aq}^- and also the resonance stabilization of the radical formed through conjugation. It is the purpose of the present study to investigate the latter point by electron spin resonance observation of the e_{aq}^- adduct radicals produced in irradiated aqueous solutions.

Few electron adduct radicals from olefinic compounds have been studied by pulse radiolysis.[4-6] The acrylamide anion–radical was observed in alkaline solutions and found to undergo rapid protonation in neutral solutions.[4,5] Rates of electron transfer from this and from the dimethylfumarate[6] anion–radical to ferricyanide ions[4] and to oxygen[4,6] have been measured.

In a recent esr study of irradiated aqueous solutions of fumarate ion the formation of the electron adduct was demonstrated.[7] The radical shows hyperfine splitting by two equivalent hydrogen atoms and its structure can be represented by

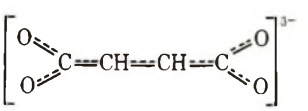

The protonated form of this radical has been produced in acid solution by the reduction of fumaric acid with $\dot{C}O_2^-$ and $\dot{C}O_2H$.[8] The corresponding radical from maleic acid has also been studied[8] and the main difference between the *trans* and the *cis* isomers involves the formation in the latter case of a hydrogen bridge between the two carboxyl groups. In the present study the effects of hydrogen bridging and of conjugation of C=C and C=O bonds on the structure and stability of the electron adducts will be investigated. The compounds studied were acrylic, maleic, dihydroxyfumaric, muconic, β-hydromuconic, hexdienoic, chelidonic, and acetylenedicarboxylic acids. The reactions of e_{aq}^- with these compounds were carried out in irradiated aqueous solutions and studied by the *in situ* radiolysis–esr technique described previously.[9]

Experimental Section

The organic compounds were obtained from Baker

(1) Supported in part by the U. S. Atomic Energy Commission.

(2) M. Anbar and P. Neta, *Int. J. Appl. Radiat. Isotop.*, **18**, 493 (1967).

(3) M. Anbar, *Advan. Phys. Org. Chem.*, **7**, 115 (1969).

(4) K. W. Chambers, E. Collinson, F. S. Dainton, W. A. Seddon, and F. Wilkinson, *Trans. Faraday Soc.*, **63**, 1699 (1967).

(5) K. W. Chambers, E. Collinson, and F. S. Dainton, *ibid.*, **66**, 142 (1970).

(6) G. E. Adams, B. D. Michael, and J. T. Richards, *Nature (London)*, **215**, 1248 (1967).

(7) P. Neta, *J. Phys. Chem.*, **75**, 2570 (1971).

(8) N. H. Anderson, A. J. Dobbs, D. J. Edge, R. O. C. Norman, and P. R. West, *J. Chem. Soc. B*, 1004 (1971).

(9) K. Eiben and R. W. Fessenden, *J. Phys. Chem.*, **75**, 1186 (1971).

Chemical Co. (dihydroxyfumaric and acetylenedicarboxylic acid), Eastman Organic Chemical Co. (maleic and acrylic acid), and Aldrich Chemical Co. (*trans,-trans*-muconic, *trans*-β-hydromuconic, chelidonic, and 2,4-hexadienoic acid). All the inorganic compounds were Baker Analyzed reagents. Water was doubly distilled. The pH was adjusted using potassium hydroxide or perchloric acid. Solutions at pH 4–10 were buffered with sodium phosphates or sodium tetraborate. Oxygen was removed from solutions by bubbling with pure nitrogen. The irradiation of solution with 2.8-MeV electrons was carried out directly in the esr cavity while the solution flowed through a flat silica cell located in the cavity. All the other details of the experiment were as previously described.[9]

Results and Discussion

Several reactions are possible in the radiolysis of aqueous solutions of unsaturated acids. In the absence of other scavengers all three of the primary radicals, e_{aq}^-, H, and OH, potentially can react with the solute-derived radicals. It is necessary, therefore, to identify the primary radical precursor for each radical observed. The usual approach is to add a selective scavenger for one of the primary radicals and to note the decrease in intensity of the esr lines of the corresponding product radical. Although the radical formed by OH reaction is usually readily identified, it is sometimes possible for e_{aq}^- and H to give the same product. In cases where this possibility exists the use of N_2O, which reacts only with e_{aq}^-, should cause a big decrease in signal intensity of the e_{aq}^- reaction product. Once the OH reaction product has been identified it is usually convenient to eliminate the lines of this radical from the spectrum by scavenging OH with *tert*-butyl alcohol or formate (the lines of the resultant radicals $\dot{C}H_2C(CH_3)_2OH$ or $\dot{C}O_2^-$ do not interfere). Most experiments were carried out with one of these OH scavengers present. Because of the high reactivity of $\dot{C}O_2^-$ either by addition or electron transfer it was necessary, when formate was used, to carry out the experiment with N_2O also present. The esr lines of a radical formed exclusively from e_{aq}^- (rather than from e_{aq}^- and/or $\dot{C}O_2^-$) should then be of greatly reduced intensity.

Acrylic Acid. The spectra of two radicals were observed with irradiated aqueous solutions at pH 12. They were identified as

$CH_3\dot{C}HCO_2^-$	$HOCH_2\dot{C}HCO_2^-$
I	II
g = 2.00323	g = 2.00312
a_α^H = 20.33 G	a_α^H = 20.43 G
a_β^H = 25.00 G (quartet)	a_β^H = 27.87 G (triplet)

Radical I has been produced previously by the reaction of e_{aq}^- with α-alanine[10] and the parameters determined in the present study are in very good agreement with the previous values. Second-order corrections[11] of the g factors have been made. Radical II has not been observed previously but its acid form, $HOCH_2\dot{C}HCOOH$, has.[12] This latter form displays hyperfine constants of 20.45 and 27.58 G which are similar to those determined here for the basic form. The spectra of radicals I and II were also observed at pH 13.3. The addition of N_2O which converts e_{aq}^- into OH caused the disappearance of the spectrum of I and a doubling in intensity of the spectrum of II. It is obvious that radical II is formed by addition of OH to acrylate. Radical I can be formed either by addition of an H atom or by addition of e_{aq}^- followed by protonation on the β carbon. Although the first reaction certainly contributes to the yield of I at pH 12, its contribution at pH 13.3 is expected to be much smaller (at the concentration of 1×10^{-3} M acrylic acid used only ~20% of H will add to this compound and the rest will react with OH^- to produce e_{aq}^-). No decrease in yield was found with increase in pH. Moreover, the spectrum of the radical I disappeared with the addition of N_2O which reacts rapidly with e_{aq}^- but not with H. It can be concluded, therefore, that radical I is produced by the reaction of e_{aq}^- with acrylate followed by rapid protonation. This protonation is complete in less than ~1 msec even at pH 13.3 and must involve a molecule of water and not H^+.

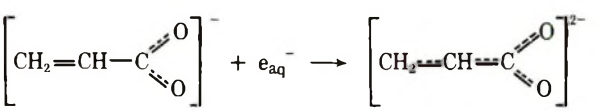

$$[CH_2CHCO_2]^{2-} + H_2O \longrightarrow CH_3CHCO_2^- + OH^-$$

Muconic Acid (2,4-Hexadienedioic Acid. The spectrum recorded with an irradiated aqueous solution of muconic acid at pH 12.3 consisted of lines of three different radicals. The radical formed by reaction of e_{aq}^- contains a fully conjugated system similar to that produced from fumarate[7] but with an additional H H —C=C— group. The parameters determined and the suggested structure are

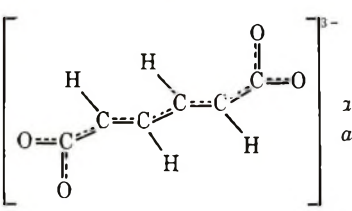

g = 2.00334
$a_2^H = a_5^H$ = 5.72 G (triplet)
$a_3^H = a_4^H$ = 2.72 G (triplet)

III

The asignment of the 5.7 and 2.7-G triplets to the hydrogens in the 2,5 and 3,4 positions, respectively, can be made by comparison to the molecular orbital calculations for butadiene anion radicals (see below).

(10) P. Neta and R. W. Fessenden, *J. Phys. Chem.*, **74**, 2263 (1970).
(11) R. W. Fessenden, *J. Chem. Phys.*, **37**, 747 (1962).
(12) H. Fischer, *Z. Naturforsch.*, **19a**, 866 (1964).

The other two radicals produced from muconic acid are the result of addition of OH and of H to a double bond

$^{-}O_2CCH_2CHCH{=}CHCO_2^{-}$ (1 2 3 4 5 6) IV

$g = 2.00307$
$a_2^H = 12.13$ G (triplet)
$a_3^H, a_5^H = 13.95, 12.48$ G
$a_4^H = 3.59$ G

$^{-}O_2CCH(OH)CH{=}CHCO_2^{-}$ V

$g = 2.00302$
$a_2^H, a_3^H, a_5^H = 13.11, 12.31, 12.01$ G
$a_4^H = 3.68$ G

The addition of H and OH takes place on the α carbon, at least to a major extent, because the radicals produced show esr parameters which are characteristic of allyl-type radicals.[13] Addition on the β carbon would form radicals in which the unpaired electron is not conjugated with the other double bond, *i.e.*, substituted alkyl radicals, and which will have larger hyperfine constants. The assignment of the 3.6-G splitting to the proton on C_4 is certain because this carbon is the center of the allylic stucture. The assignment of the 12.13-G triplet splitting in radical IV is also obvious. However, all the other hyperfine constants are of similar magnitudes and cannot be assigned to specific protons.

β-Hydromuconic Acid. This compound ($^{-}OOCCH_2CH{=}CHCH_2COO^{-}$) does not contain a conjugated system and is not expected to yield a stable electron adduct. Moreover, because the carboxyl groups are not adjacent to the double bond its reactivity toward e_{aq}^- is expected to be low.[3] The results show that the reactivity is, indeed, very low and no electron adduct was detected. This compound was irradiated at pH 12 in the presence of formate as OH scavenger. The spectrum recorded contained only a single line which was identified as that of $C_2O_4^{3-}$ previously reported.[9] This radical is formed by the reaction of e_{aq}^- with oxalate formed as a radiation product from formate ($HCO_2^- + OH \rightarrow CO_2^- + H_2O$; $2CO_2^- \rightarrow C_2O_4^{2-}$). The fact that $C_2O_4^{3-}$ was observed indicates that 10^{-2} M β-hydromuconic acid does not compete for e_{aq}^- with $\sim 10^4$ M oxalate $k_{e_{aq}^- + oxalate} = 4.8 \times 10^7$ M^{-1} sec^{-1})[14] accumulated during irradiation and, therefore, that the rate constant for the reaction of e_{aq}^- with the hydromuconate (pH 12) must be $< 10^6$ M^{-1} sec^{-1}.

An attempt to observe the electron adduct to 2,4-hexadienoic acid ($CH_3CH{=}CHCH{=}CHCO_2^-$) was not successful because only very weak lines were observed which could not be analyzed.

Chelidonic Acid (4-Pyrone-2,6-dicarboxylic Acid). The spectrum of the electron adduct recorded at pH 12 in the presence and in the absence of formate consisted of a 1.2-G triplet of very intense lines; at pH 6.3 it consisted of a 1.8-G triplet of 0.4-G doublets. At pH 7–9 the spectrum consisted of a superposition of both sets of lines. Clearly a protonation took place and the suggested forms of this radical are

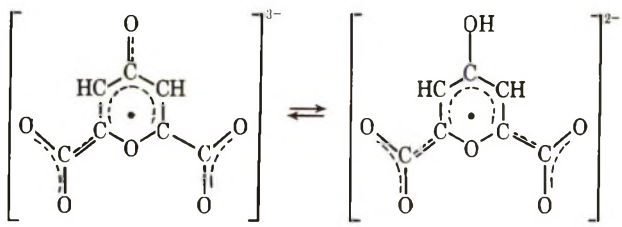

VI
$g = 2.00402$
$a^H = 1.24$ G (triplet)

VII
$g = 2.00384$
$a^H = 1.82$ G (triplet)
$a^H = 0.43$ G

The signal intensity of the spectrum in the case of radical VI was 40 times higher than that for radical VII indicating the large difference between the radical–radical reaction rate constant for the triply and doubly charged radicals. The pK for the dissociation of VII is estimated to be 8 from the pH at which comparable signal intensities are observed from the two forms. (The forward and reverse rates of the equilibrium are assumed to be faster than the disappearance reactions.)

Maleic Acid. A solution of 0.01 M maleic acid containing 0.5 M *tert*-butyl alcohol as OH scavenger was irradiated at 10 different pH values. The spectra recorded at pH 9.2, 12.6, 13.7, and 14 were identical. They were analyzed in terms of two equivalent protons with 6.7 G-hyperfine splitting and one proton with 0.6-G splitting. At lower pH values (6–7) the two protons with the large splitting become inequivalent and an additional small hyperfine constant for a single proton appears. These findings can be explained by the structures

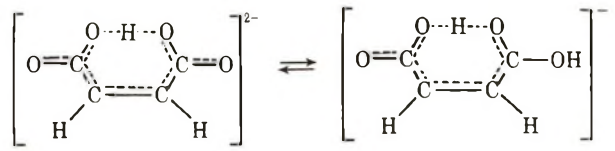

VIII
$g = 2.00347$
$a_2^H = a_3^H = 6.74$ G (triplet)
$a_{COOH}^H = 0.65$ G

IX
$g = 2.00341$
$a_2^H = 8.12$ G
$a_3^H = 5.06$ G
$a_{COOH}^H = 0.76$ G
$a_{COOH}^H = 0.59$ G

Structure VIII has previously been suggested from experiments in neutral solutions[8] and the esr parameters determined here are in good agreement with the previous measurements. The equivalence of the two CH protons can mean either that the carboxylic proton undergoes a fast intramolecular exchange between two positions or that the structure is totally symmetric. The existence[15] of a single potential minimum for the

(13) R. W. Fessenden and R. H. Schuler, *J. Chem. Phys.*, 39, 2147 (1963).

(14) O. Micic and I. Draganic, *Int. J. Radiat. Phys. Chem.*, 1, 287 (1969).

(15) See discussion in K. Nakamoto, Y. A. Sarma, and G. T. Behnke, *J. Chem. Phys.*, 42, 1662 (1965).

proton in hydrogen maleate suggests that the latter possibility may be correct. The present results show that dissociation of the carboxylic proton in VIII does not take place even at pH 14. The parameters determined for radical IX are somewhat similar to those previously reported[8] within the accuracy of those measurements, but the inequivalence of the two protons with the small splittings was not detected in the earlier study.[8] This fact led the previous authors to an assignment different from IX, with no hydrogen bridge and two hydrogen atoms on one carboxyl group. However, the parameters determined here clearly suggest that the ring structure is still stable after the second protonation. The radical observed at pH 1 was also suggested to have a bridged structure such as would result from the protonation of IX. Even under those acid conditions the bridging proton does not exchange and displays a hyperfine splitting of 1.1 G.[8] The existence of bridged structures under both acidic and basic conditions strongly suggests such a structure (IX) under intermediate pH conditions.

The existence of one undissociated carboxylic proton in VIII even at pH 14 is surprising. When compared with the second dissociation in maleic acid itself (pK = 6.2) this represents a change of >8 units. In part the change can be caused by the greater overall charge of the electron adduct. However, because no such effect is evident in the electron adduct of fumarate which shows the same spectrum from pH 7 to 14 (assigned[7] to the triply charged form), most of the change in pK in the case of maleic acid must arise because of the internal hydrogen bond. The same type of effect has been noted[9] for the anion radical of *o*-nitrophenol.

Dihydroxyfumaric Acid. When this compound is dissolved in water it is expected to be in equilibrium with dihydroxymaleic acid through the keto form. Therefore, three different electron adducts might be formed. The spectra recorded with irradiated solutions at pH 7–8 consisted of weak broad lines which could not be easily analyzed. However, at pH 9–14 spectra of two radicals were observed. These spectra were present when formate or *tert*-butyl alcohol were added as OH scavengers and were absent when N_2O was added as an e_{aq}^- scavenger. The corresponding radicals must, therefore, be electron adducts. One spectrum has the parameters g = 2.00390 and a^H (2 protons) = 0.49 G. Because of the two equivalent protons the radical must be symmetric. The magnitude of the splitting is typical of OH protons so that the e_{aq}^- adduct to either dihydroxymaleate or dihydroxyfumarate could be responsible. As no dissociation occurs to pH 14 a bridged structure as in the case of maleate is likely. (Note that the somewhat related radical VII has a pK near 8.) The e_{aq}^- adduct of dihydroxyfumarate which can be written as

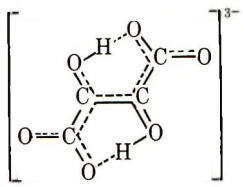

X

g = 2.00390

a^H = 0.49 G (triplet)

is suggested as the best possibility.

The second species produced in dihydroxyfumarate solution has a doublet spectrum with the parameters g = 2.00413 and a^H = 2.77 G. This splitting seems too large to be that of an OH proton so the e_{aq}^- adduct of the keto form must be considered

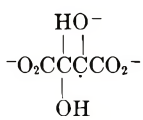

XI

g = 2.00413

a^H = 2.77 G

This form for the radical is confirmed by the fact that an identical spectrum is obtained by H abstraction from tartrate.[16] The small value of a_β^H is a result of loss of spin density onto the O^- [16] and a preferred rotational configuration which places the β hydrogen near the nodal plane of the p orbital in the α carbon.

Acetylenedicarboxylic Acid. Spectra of two radicals were observed in irradiated aqueous solutions of acetylenedicarboxylic acid. Each consisted of an intense doublet which did not change with pH between 7 and 14. The first, a 50-G doublet practically disappeared with the addition of N_2O. The other, an 18-G doublet increased in intensity with the addition of N_2O and disappeared in the presence of *tert*-butyl alcohol. The radicals responsible for these spectra are, therefore, produced by the reactions of e_{aq}^- and OH, respectively. The electron adduct evidently undergoes rapid protonation even at pH 14 and the result is a vinyl-type radical

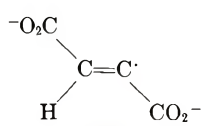

XII

g = 2.00283

a^H = 49.79 G

The *trans* configuration is evident from the large splitting.[13] The radical produced by OH reaction shows a hyperfine splitting which is too large for a hydroxyl proton and much closer to the size of the α-proton splitting in substituted alkyl radicals. Therefore, the spectrum is assigned to the keto form of the radical

(16) G. P. Laroff and R. W. Fessenden, *J. Chem. Phys.*, **55**, 5000 (1971), and unpublished results.

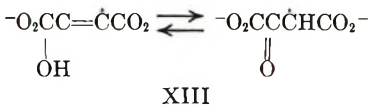

XIII

$g = 2.00451$
$a^H = 17.76$ G

This assignment is confirmed by preparing the radical from oxalacetic acid ($^-O_2CCOCH_2CO_2^-$) *via* hydrogen abstraction. Irradiation of this compound in N_2O saturated solution at pH 9 produced a spectrum, one component of which was a doublet with $g = 2.00450$ and $a^H = 17.73$ G in agreement with the esr parameters assigned to radical XIII.

Discussion of the Esr Parameters. The e_{aq}^- adducts of maleic (or fumaric) and muconic acids can be regarded as substituted anion radicals of ethylene and butadiene; the adduct of chelidonic acid is essentially a substituted pentadienyl radical. Consequently, it is of interest to compare hyperfine constants with these simpler radicals in order to estimate the loss of spin density to the substituents. Ethylene anion radical is not known experimentally but a radical closely related to VIII has been reported in irradiated potassium hydrogen maleate.[17,18] The radical proposed to explain the spectrum obtained in those solid phase experiments can be regarded as VIII with two electrons less. The two respective radicals are formed from hydrogen maleate by, respectively, loss or attachment of an electon. Interestingly the (C–H) hyperfine constants and g factor are the same within the accuracy obtainable for the solid. Although it is known[19] that positive and negative radical ion of aromatic molecules have similar spectra we would like to suggest that the radical observed in the solid may be the same as VIII. Toriyama and Iwasaki[18] do in fact write e^- as the precursor of this radical (designated by them T_π). With either interpretation it can be concluded from the hyperfine anisotropy that the spin density on the central carbons is 0.26.[18] The isotropic splitting of 6.7 G is, therefore, describable by a Q_α of 6.7/0.26 = 25.8 G, which is in the normal range of values. Approximately one half of the spin density resides on the ethylenic part of the radical.

The anion radical of butadiene is known[20] so a detailed comparison with the e_{aq}^- adduct to muconate (III) can be made. Molecular orbital theory for butadiene anion predicts[20] a larger spin density for the terminal carbon atoms and the splittings for III have been assigned accordingly. The splittings for butadiene anion are 7.62 and 2.80 G and by comparison with those for III (5.72 and 2.72 G) we see that only the larger one is changed by the substitution. The fractional loss of spin density is 1.98/(7.62 + 2.80) = 0.19. This change is much smaller than that of ~50% for the radical VIII from maleate.

With the e_{aq}^- adduct to chelidonic acid, a comparison can best be made with the C_5 conjugated system in cyclohexadienyl radical.[13] In this case the comparison is for the small splittings at positions of negative spin density so that less precise results are expected. The ratio 1.82/2.65 = 0.69 would suggest about a 30% loss to the two carboxyl groups. Although the results for the three radicals differ considerably, all suggest a rather large contribution of the carboxyl groups to the orbital for unpaired electron. This large contribution is expected to enhance the stability of the more conjugated anion radicals and offers an explanation for the rapid protonation of the acrylate electron adduct where only one carboxyl group can be involved.

Conclusions

The radicals produced by e_{aq}^- reaction with a number of unsaturated carboyxlate ions have been studied. With highly conjugated compounds such as muconic, chelidonic, maleic, and dihydroxyfumaric acids relatively stable anion radicals are produced. Protonation of these radicals in neutral and acid solutions takes place on the carboxylate groups. On the other hand, the e_{aq}^- adducts to acrylate and acetylenedicarboxylate were found even in strong base to protonate rapidly on carbon to produce the radicals $CH_3\dot{C}HCO_2^-$ and $^-O_2CCH{=}\dot{C}CO_2^-$, respectively. From this result it can be concluded that conjugation of two carboxylate groups is necessary to stabilize the anion radicals against protonation on carbon. (In the case of acetylenedicarboxylate the anion radical may be a σ radical, and, hence, not conjugated.) The anion radical from maleate is stable even with ~50% of the spin density on the ethylenic portion of the molecule. The intramolecular hydrogen bonds in the anion radicals of maleate and dihydroxyfumarate were found to be resistant to dissociation even at pH 14.

(17) H. C. Heller and T. Cole, *J. Amer. Chem. Soc.*, **84**, 4448 (1962).
(18) M. Iwasaki and K. Itoh, *Bull. Chem. Soc. Jap.*, **37**, 44 (1964); K. Toriyama and M. Iwasaki, *J. Chem. Phys.*, **55**, 2181 (1971).
(19) J. R. Bolton and G. K. Fraenkel, *ibid.*, **40**, 3307 (1964).
(20) D. H. Levy and R. J. Myers, *ibid.*, **41**, 1062 (1964).

Concentrated Electron Scavenger Effects on the Yields of Trapped Species in γ-Irradiated Alkaline Glass

by John D. Zimbrick* and Michael K. Bowman

Department of Radiation Biophysics, University of Kansas, Lawrence, Kansas 66044 *(Received September 10, 1971)*

Publication costs borne completely by The Journal of Physical Chemistry

The γ radiolysis of aqueous alkaline glass at 77°K produces significant yields of solvated electrons, hydrogen atoms, and oxygen radical anions ($O\cdot^-$) which are trapped in the glassy matrix. Epr techniques were used to measure the relative yields of these three species as a function of NO_3^- concentration. The yields of trapped hydrogen atoms (H_t) were determined in the absence of NO_3^- as a function of OH^- concentration, ice phase, and radiation dose. The paramagnetic relaxation behavior of H_t was measured as a function of radiation dose and OH^- concentration. The formation of $NO_3\cdot^{2-}$ *via* e_m^- scavenging by NO_3^- increased linearly with $[NO_3^-]^{1/3}$ up to a NO_3^- concentration of 0.1 M at which point the slope of the curve decreased and $G(NO_3\cdot^{2-}) = 3.4$. At NO_3^- concentrations above 0.1 M, the yield of $NO_3\cdot^{2-}$ continued to increase linearly up to a G value of 4.9 at 3 M. The $G(H_t)$ was not reduced below the value obtained in the absence of NO_3^- until $[NO_3^-]$ reached concentrations of ≥ 0.1 M. $G(O\cdot^-)$ increased linearly with $[NO_3^-]^{1/3}$ until a NO_3^- concentration of 0.1 M was reached. Just as in the case of $G(NO_3\cdot^{2-})$, the $O\cdot^-$ yield curve exhibited a negative change in slope at $[NO_3^-] = 0.1$ M, above which $G(O\cdot^-)$ increased slowly up to $[NO_3^-] = 3$ M. Paramagnetic relaxation measurements indicated that the local concentration of H_t decreased with increasing radiation dose in the same dose region in which the sample-average concentration of H_t increased. All of these data support the hypothesis that a significant fraction of electrons produced in alkaline glass by radiation do not become hydrated before they react in spurs. These electrons can be scavenged by NO_3^- and are responsible for the formation of a major fraction of the observed yield of H_t.

I. Introduction

In the γ radiolysis of water the initial species produced are H_2O^+ (holes), e^-, and possibly H_2O^*. At times approximately 10^{-11} sec after passage of the radiation, the species present are nonhomogeneously distributed and consist of solvated electrons (e_{aq}^-), hydroxyl radicals ($OH\cdot$), hydrogen atoms ($H\cdot$), and molecular hydrogen (H_2). The subsequent chemical reactions of these species are described adequately by the spur diffusion model.[1] The question of whether the chemical reactions occurring within spurs at times earlier than 10^{-11} sec can be altered by concentrated scavengers or observed by spectroscopic techniques was raised several years ago by Magee,[2] who discussed e^- (unsolvated electron) and postulated that it could not react with H^+. More recently, Hamill[3] has incorporated e^- in a model for the radiolysis of water. Several subsequent reports have discussed data obtained from pulsed and steady-state radiolysis studies of aqueous solutions containing concentrated electron scavengers in light of possible e^- reactions.[4-13]

If evidence for reactions of e^- with concentrated scavengers can be obtained in aqueous solutions then it should be possible to obtain analogous evidence in a suitable solid aqueous matrix by, for example, trapping the products of e^- reactions and studying these products in detail by conventional spectroscopic techniques. Steen, *et al.*,[12] have measured the decrease in optical absorption of trapped electrons (e_t^-) as a function of electron scavenger concentration in X-irradiated ethylene glycol–water glass at 77°K. The kinetics of disappearance of the absorption were not homogeneous and this finding was used as indirect evidence to support the hypothesis that e^- reactions with the scavengers were occurring with different, generally lower efficiencies than those with e_m^-.

Epr spectroscopic techniques can be used to obtain more direct evidence regarding possible e^- reactions in solid matrices. The yields and kinetics of all para-

(1) H. A. Schwartz, *J. Phys. Chem.*, **73**, 1928 (1969).

(2) Summary of proceedings of the 4th Informal Conference on the Radiation Chemistry of Water, University of Notre Dame, March 23–25, 1961, p 62.

(3) W. H. Hamill, *J. Phys. Chem.*, **73**, 1341 (1969).

(4) T. Sawai and W. H. Hamill, *ibid.*, **74**, 3914 (1970).

(5) P. L. T. Bevan and W. H. Hamill, *Trans. Faraday Soc.*, **66**, 2533 (1970).

(6) G. V. Buxton, F. C. R. Cattell, and F. S. Dainton, *Chem. Commun.*, 25 (1971).

(7) G. V. Buxton, F. C. R. Cattell, and F. S. Dainton, *Trans. Faraday Soc.*, **67**, 687 (1971).

(8) M. J. Bronskill, R. K. Wolff, and J. W. Hunt, *J. Chem. Phys.*, **53**, 4201 (1970).

(9) R. K. Wolff, M. J. Bronskill, and J. W. Hunt, *ibid.*, **53**, 4211 (1970).

(10) T. I. Balkos, J. H. Fendler, and R. H. Schuler, *J. Phys. Chem.*, **74**, 4497 (1970).

(11) E. Pelad, U. Mirski, and G. Czapski, *ibid.*, **75**, 31 (1971).

(12) H. B. Steen, O. Kasphus, and M. Kongshaug, *ibid.*, **75**, 31 (1971).

(13) H. B. Steen, *ibid.*, **74**, 4059 (1970).

magnetic species in the matrix can be examined simultaneously as a function of electron scavenger concentration and, in particular, the formation of the scavenger anion can be studied in detail. Concentrated alkaline glass at 77°K is an ideal matrix for such studies since e_m^-, $O\cdot^-$, and H· produced by radiolysis are all trapped with yields that are easily detectable by epr. (e_m^- is the traditional mobile electron observed in irradiated aqueous glasses.) The trapped species in γ-irradiated alkaline glass have been the subjects of numerous investigations which have been summarized in several recent reviews.[14-16] The e_t^- and $O\cdot^-$ yields are approximately the same[14] ($G \simeq 1.9$ in 10 M NaOH). Paramagnetic relaxation data indicate that the e_t^- are located within "expanded spurs" of radii approximately 40 Å.[17,18] In the present work, we report studies on the effect of high concentrations of NO_3^-, a well-known e_{aq}^- scavenger and recently postulated to be an efficient e^- scavenger,[3,7,12] on the yields of e_t^-, $O\cdot^-$, and H· in alkaline glass at 77°K. We also characterize the yields and spatial distribution of H· in the absence of NO_3^- since these data are necessary for complete interpretation of the scavenging results.

II. Experimental Section

A. Sample Preparation. Reagent grade chemicals were used without further purification. All solutions were made with singly distilled water.

Samples were prepared by pipetting drops of the solutions into liquid nitrogen, where they froze into uniform spheres of approximately 3-mm diameter. The spheres were transferred to small glass tubes in which they were irradiated and stored in darkness at 77°K. For epr measurement, the spheres were transferred without warming to a quartz dewar insert filled with liquid nitrogen.

The γ irradiation was carried out at 77°K in a ^{60}Co source with a dose rate of 88,800 rads/hr as calibrated by ferrous sulfate dosimetry.

B. Epr Measurements. The epr measurements were made with a Varian V-4502 EPR spectrometer system. First derivative absorption spectra were recorded at 77°K using a field modulation frequency of 100 kHz, a sweep rate of 20 G/min, and a modulation amplitude of 3 G. The AFC was locked on the cavity while the spectrometer was in the low power configuration with a microwave termination on the high-power arm. Power saturation measurements were made with a field modulation of 100 kHz. The microwave power incident on the cavity was measured by techniques described previously.[17-19]

During the epr measurements, the dewar insert was loosely stoppered to prevent the accumulation of ice crystals in the dewar. Liquid nitrogen boiling around the sample was prevented by cooling the nitrogen to approximately 73°K with a stream of helium gas.

The high-field H-atom line was used exclusively for all $G(H_t)$ analyses. The yield was determined by taking the peak-to-peak height (h) and the width (w) at maximum slope from the first derivative spectrum and calculating hw^2 which is proportional to the area under the absorption curve. Samples of glassy 8.7 M H_2SO_4 were irradiated and measured as a standard for determining G values. The G value for production of trapped hydrogen atoms in glassy 8.7 M H_2SO_4 was taken to be 1.66.[20]

The spectra of $O\cdot^-$ and $NO_3\cdot^{2-}$ overlapped to some extent. In order to determine separate values of $G(O\cdot^-)$ and $G(NO_3\cdot^{2-})$, the low-field slope of the $O\cdot^-$ line and the high-field line of the $NO_3\cdot^{2-}$ triplet were measured since these portions of the spectra were not perturbed.

III. Results

A. Yields of Trapped Hydrogen Atoms vs. Molarity and Radiation Dose. Figure 1 shows a plot of the yield of trapped hydrogen atoms (H_t) against the molarity of NaOH. The yields are relatively small (≤ 0.035) and are of the same order of magnitude as those found by Henriksen.[21] The apparent discontinuity near 5 M occurs in the region of the phase change from a visibly polycrystalline to a visibly glass matrix. The increase in H_t yield associated with the change from polycrystalline to glassy matrix is in contrast to Henriksen's

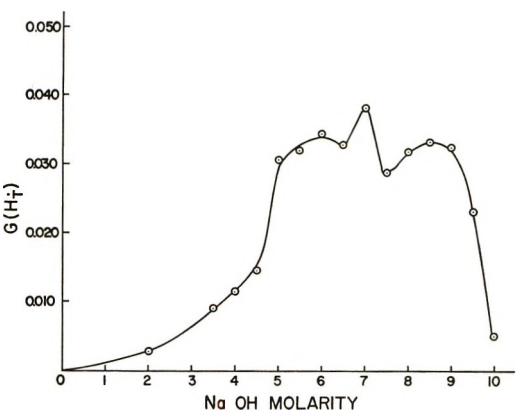

Figure 1. Yield of H_t [$G(H_t)$] *vs.* molar concentration of NaOH in alkaline ice at 77°K. Epr measurements made on high-field line of H_t doublet. ^{60}Co γ dose = 500 krads. Phase transition from polycrystalline to glassy matrix occurs in the region 4.5–5.5 M.

(14) L. Kevan in "Radiation Chemistry of Aqueous Systems," G. Stein, Ed., Wiley-Interscience, New York, N. Y., 1968, p 21.

(15) B. G. Ershov and A. K. Pikaev, *Radiat. Res. Rev.*, **2**, 1 (1969).

(16) D. Schulte-Frohlinde and K. Vacek in "Current Topics in Radiation Research," Vol. V, M. Ebert and A. Howard, Ed., Wiley-Interscience, New York, N. Y., 1969, p 39.

(17) J. Zimbrick and L. Kevan, *J. Chem. Phys.*, **47**, 2364 (1967).

(18) L. Kevan and D. H. Chen, *ibid.*, **49**, 1970 (1968).

(19) B. L. Bales and L. Kevan, *ibid.*, **52**, 4644 (1970).

(20) R. Livingston and A. J. Weinberger, *ibid.*, **33**, 499 (1960).

(21) T. Henriksen, *Radiat. Res.*, **23**, 63 (1964).

results which show a decrease in yield with the phase change in samples of the same molarity.[21] The general shape of his yield *vs.* molarity curve is different from that found here and may reflect the effects of very different experimental procedures; *e.g.*, his method of production of a polycrystalline matrix by thermally annealing a glassy matrix is in contrast with ours in which the phase was determined solely by NaOH molarity.

It can be seen from Figure 1 that the H_t yield data vary erratically in the region of 7 *M* NaOH. In this regard it must be noted that each data point is the average of several experiments. The precision of these experiments is such that the standard deviations of the averages generally are no larger than the diameters of the data points. Thus the sharp fluctuations in H_t yield shown on the graph cannot be attributed to statistical error. They occur in the concentration region in which single hydrated crystals of $NaOH \cdot 7H_2O$ can be grown.[22] It is possible that the ices, though visibly glassy, may contain local regions which possess the structure of the hydrated crystal and these regions perturb the observed $G(H_t)$.

When the radiation dose was increased, H_t production increased linearly in the region from 0 to about 0.5 Mrad and then leveled off and decreased as shown in Figure 2. This behavior shows that a relatively efficient back reaction which destroys the H_t is occurring at the higher radiation doses. The decrease in concentration of H_t cannot be attributed to thermal decay since many samples were stored in darkness at 77°K for over a week with no detectable decrease in H_t concentration during that time.

B. Paramagnetic Relaxation of H_t vs. Radiation Dose. In order to assess the spatial uniformity of H_t, the product of spin–lattice and spin–spin relaxation time (T_1T_2) was determined as a function of radiation dose and NaOH molarity by progressively power-saturating the high-field H_t line. From the plots of epr signal intensity *vs.* microwave magnetic field, the value of microwave field at which half-saturation occurs, $H_{1/2}$, was measured. (T_1T_2) was calculated from $H_{1/2}$ by the Portis equation[17] assuming that the H_t lines are ideal cases of homogeneous broadening.[23] This application of the Portis equation is not strictly valid since the H_t epr lines are nonideal cases of homogeneous broadening, and fast passage conditions had to be used to detect the low yield of H_t. Nevertheless, the relative values of (T_1T_2) are considered valid indicators of spatial uniformity or nonuniformity within a given system.[17-19,23-25]

The relaxation time data are plotted in Figure 3 as $(T_1T_2)^{1/2}$ *vs.* radiation dose for 5 and 7.5 *M* NaOH. $(T_1T_2)^{1/2}$ increases with increasing dose for both NaOH molarities. Recall from section B, Figure 2, that the sample-average H_t concentration increases with radiation dose to at least 0.5 Mrad. Since changes in $(T_1T_2)^{1/2}$

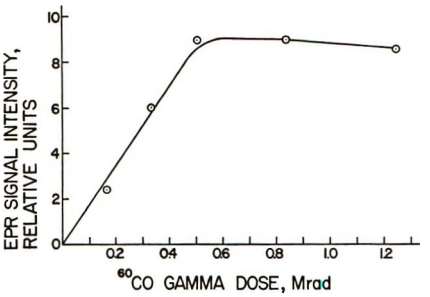

Figure 2. Relative concentration of H_t *vs.* ^{60}Co γ dose in glassy alkaline ice at 77°K. NaOH concentration = 7.5 *M*.

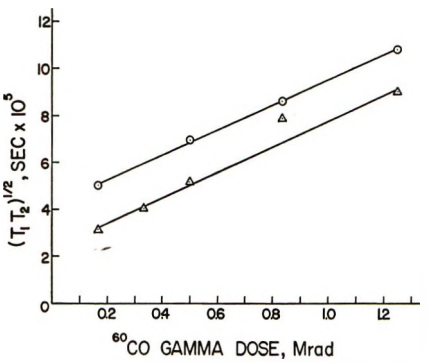

Figure 3. Relaxation time product, $(T_1T_2)^{1/2}$, *vs.* ^{60}Co γ dose for H_t in 5.0 *M* (○) alkaline ice and 7.5 *M* (△) alkaline ice at 77°K. ν_m = 100 kHz.

have been shown[17,18,23,25] to be due to changes in T_2 and since the magnitude of T_2 is inversely proportional to the average *local* H_t concentration, the increase in $(T_1T_2)^{1/2}$ with dose suggests that the local H_t concentration is decreasing at the same time that the sample average concentration is increasing.

C. Effects of Bleaching with Visible Light. The phenomenon of bleaching e_t^- with visible light is well documented in the literature.[14-16] Visible light mobilizes the trapped electrons such that they become available to react with remaining e_t^- or with other species. A 500-W projection lamp was used to irradiate the ice samples at 77°K in the epr cavity. The H_t high-field line, the $O\cdot^-$ line at g = 2.06, and the e_t^- singlet were scanned repeatedly during bleaching. The H_t and $O\cdot^-$ concentrations decrease by approximately 20% during the first minutes of bleaching, then level off while the e_t^- concentration continues to decrease sharply. Hamlet and Kevan[26] have also observed significant decreases in $O\cdot^-$ during optical bleaching.

D. Electron Scavenger Effects on e_t^-, H_t, and $O\cdot^-$ Yields. A series of samples of 7.5 *M* MaOH were pre-

(22) H. Barzynski and D. Schulte-Frohlinde, *Z. Naturforsch.*, **22a**, 2131 (1967).
(23) J. Zimbrick and L. Kevan, *J. Chem. Phys.*, **47**, 5000 (1967).
(24) H. Hase and L. Kevan, *ibid.*, **52**, 3183 (1970).
(25) H. Hase and L. Kevan, *J. Amer. Chem. Soc.*, **90**, 6875 (1968).
(26) P. Hamlet and L. Kevan, *J. Chem. Phys.*, **54**, 908 (1971).

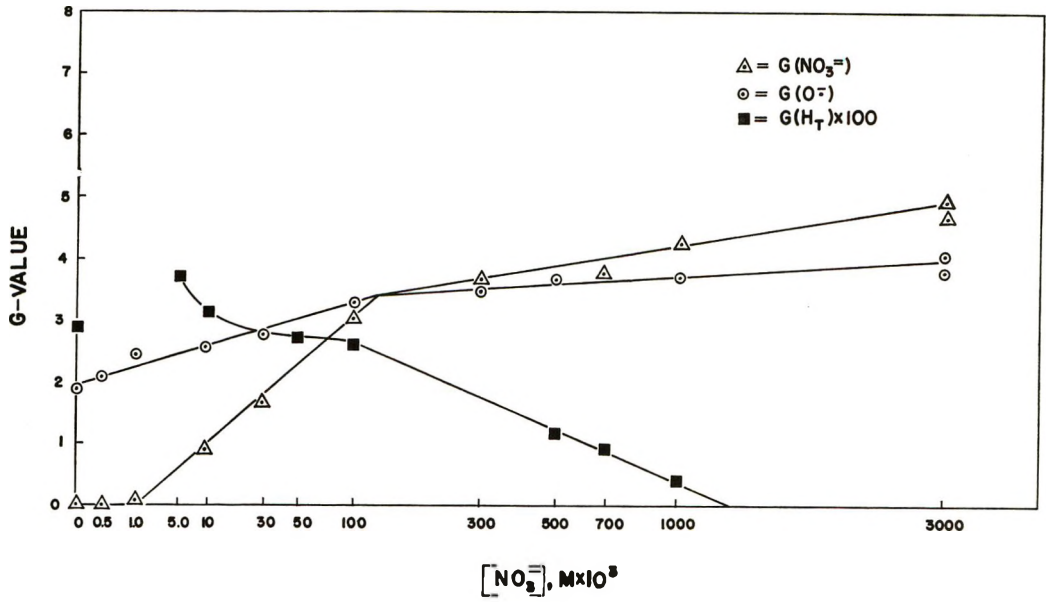

Figure 4. Yields of $NO_3 \cdot^{2-}$, $O \cdot^-$, and H_t (G values) as a function of $[NO_3^-]^{1/3}$. Numerical values of NO_3^- concentration shown on abscissa are molar concentrations $\times 10^3$. The yield of H_t is expressed as $G(H_t) \times 100$. ^{60}Co γ dose = 500 krads.

pared with varying concentrations of $NaNO_3$. The results of these experiments are shown graphically in Figure 4, as plots of G value *vs.* the cube root of NO_3^- concentration. The cube root plots were chosen since they allow the use of 0 molarity at the origin and since Kupperman[27] has calculated a cube root dependency for bimolecular reactions in "ideal" solutions. Kevan[14] has reported that only 0.05 M NO_3^- is needed in 6.0 M NaOH ices to reduce the $G(e_t^-)$ by one-half. In the present work, no trace of e_t^- (no blue color and no epr singlet at $g = 2.0023$) is left at a $NaNO_3$ concentration of 0.1 M, while there is an insignificant decrease in H_t and an actual increase in $O \cdot^-$. Recent optical absorbance measurements on e_t^- at λ_{max} 5850 Å at 77°K indicate that 0.1 M NO_3^- scavenges more than 99% of the e_t^-.[28] $NO_3 \cdot^{2-}$ could not be detected by epr at NO_3^- concentrations below 0.001 M. At low concentrations of NO_3^- there is a pronounced increase in the yield of H_t over that found in the absence of scavenger. At concentrations of NO_3^- above 0.1 M, the H_t concentration decreases while the $O \cdot^-$ and $NO_3 \cdot^{2-}$ concentrations increase linearly up to 3 M NO_3^-, the highest concentration studied. The epr spectrum of the paramagnetic nitrate species consisted of a triplet centered at $g = 2.004$ with approximately 40-G peak-to-peak splittings between the lines, and was identical with the one published previously by Ayscough and Collins.[29] This spectrum was studied in detail at NO_3^- concentrations above and below 0.1 M to determine whether any changes occur which might indicate that $NO_3 \cdot$ or $NO_2 \cdot$ were being formed from H_2O^+ reactions at high NO_3^- concentrations. No changes were found and it is concluded that $NO_3 \cdot^{2-}$ is the sole product of scavenger reactions present throughout the concentration range of NO_3^- used in this work. Also, ionic strength effects of the high concentrations of $NaNO_3$ were ruled out by the observation that 3 M NaCl added to 7.5 M NaOH glass produced no effect on the yields of H_t, e_t^-, and $O \cdot^-$.

IV. Discussion

The scavenging data in Figure 4 indicate that $G(NO_3 \cdot^{2-})$ increases linearly with $[NO_3]^{-1/3}$ from 0.001 M up to approximately 0.1 M NO_3^-. Above this concentration, $G(NO_3 \cdot^{2-})$ continues to increase linearly but with a reduced slope. Plots of $G(NO_3 \cdot^{2-})$ *vs.* NO_3^- molarity and ln (NO_3^- molarity) also exhibit a break at approximately 0.1 M NO_3^-. If $NO_3 \cdot^{2-}$ were formed only by reaction with e_m^-, then it would be expected that $G(NO_3 \cdot^{2-})$ would rise with increasing NO_3^- concentration until $G(NO_3 \cdot^{2-}) = G(e_m^-)$. If it is assumed that at low concentrations of NO_3^-, $G(NO_3 \cdot^{2-}) = G(-e_t^-)$, then the change in slope in the $G(NO_3 \cdot^{2-})$ curve occurs at $G(NO_3 \cdot^{2-}) = 3.4$, and at the the highest NO_3^- concentration used, $G(NO_3 \cdot^{2-}) = 4.9$ and is still increasing. Since $G(NO_3 \cdot^{2-})$ continues to increase at a slower rate above the change in slope at 0.1 M NO_3^-, this increase must be due to the formation of $NO_3 \cdot^{2-}$ by reaction with a reducing species other than e_m^-. The two possible candidates for this reducing species are e^- and H_2O^*. There is little experimental evidence available which supports either the existence or reactions of H_2O^*. Since no data obtained in these experiments or from other published studies are inconsistent with the

(27) A. Kupperman in "The Chemical and Biological Actions of Radiations," M. Hoissinsky, Ed., Academic Press, London, 1961, pp 158, 159.

(28) J. D. Zimbrick, unpublished data.

(29) P. B. Ayscough and R. G. Collins, *J. Phys. Chem.*, 70, 3128 (1966).

hypothesis that the mobile e^- is the reducing species responsible for $NO_3 \cdot^{2-}$ formation at high NO_3^- concentrations, we conclude that e^- is most probably the species involved. With this assumption, the data support the additional hypotheses that (a) the total yield of electrons produced by radiation is ≥ 4.9, and (b) NO_3^- reacts with both e_m^- and e^- but the efficiency of reaction with e^- is lower than with e_m^-. The latter hypothesis is supported by the recent work of Steen, *et al.*,[12,13] in ethylene glycol–water glasses. Very recently, Buxton, *et al.*,[6,7] have reported the results of some microsecond pulse radiolysis experiments on 10 *M* alkaline solutions as a function of temperature; their data on the yields of e_{aq}^- at the end of 0.2-μsec pulses of 3-MeV electrons are relevant to the interpretation of our present epr results. They find $G(e_{aq}^-) \simeq 3.3$ at room temperature and this yield increases slowly as the temperature is reduced until a maximum yield of $G(e_{aq}^-) \simeq 5$ is reached at 220°K. Below 220°K, $G(e_{aq}^-)$ decreases steadily until the temperature at which the solution freezes to a glass is reached (approximately 150°K). The yield in the temperature range 77–150°K is constant at $G(e_{aq}^-) \simeq 2.7$, and is within the range of reported values for $G(e_t^-)$ which have been measured by epr techniques.[14-16] Considering the wide range of published values of $G(e_t^-)$, and the possible differences between e_{aq}^- and e_m^-, this value of $G(e_{aq}^-)$ is also in reasonable agreement with our $G(NO_3 \cdot^{2-}) = 3.4$ measured at the point (Figure 4) where the yield curve changes slope. Thus, between the temperatures of 220 and 150°K the data of Buxton, *et al.*,[6,7] indicate an apparent "loss" of yield of $G(-e_{aq}^-) \simeq 2.3$. Since the physical interaction of the radiation with the 10 *M* alkaline solution produces the same initial yield of e^- regardless of temperature, the finding of an apparent loss of $G(e_{aq}^-)$ reflects a change in some process or reaction occurring after this interaction phase of irradiation or some change in instrument response during measurment of e_{aq}^-. Buxton, *et al.*, attribute the variation of $G(e_{aq}^-)$ with temperature to a variation of the relative rates of solvation and recombination of e^-. Our epr data on NO_3^{2-} formation at 77°K are consistent with this hypothesis and also indicate that e^- is capable of undergoing reactions other than recombination.

It can be seen from Figure 4 that the presence of NO_3^- in 7.5 *M* NaOH glass significantly increases the observed yield of $O \cdot^-$. $G(O \cdot^-)$ rises linearly with increasing $[NO_3]^{-1/3}$ in the concentration range 0–0.13 *M*. At the latter concentration there is a significant decrease in the slope of the $G(O \cdot^-)$ curve; this decrease occurs with the same NO_3^- concentration at which $G(NO_3 \cdot^{2-})$ exhibits a decrease in slope. At concentrations of NO_3^- above 0.13 *M*, $G(O \cdot^-)$ increases linearly at a lower rate than the linear increase of $G(NO_3 \cdot^{2-})$. The lower rate of $G(NO_3 \cdot^{2-})$ increase may reflect hole reactions competing with $O \cdot^-$ formation. The initial increase in $G(O \cdot^-)$ with addition of NO_3^- is due to a decrease in the number of e_m^- available to destroy $O \cdot^-$ *via* reaction 1.

$$e_m^- + O \cdot^- \longrightarrow O^{2-} \qquad (1)$$

Further support for reaction 1 comes from the bleaching studies reported here in section IIIC and elsewhere.[26] The observed $G(O \cdot^-)$ decreases significantly during photobleaching when only e_t^- are being mobilized. At NO_3^- concentrations above 0.13 *M*, the increase in $G(O \cdot^-)$ with $G(NO_3 \cdot^{2-})$ indicates that NO_3^- is preventing the destruction or enhancing the formation of $O \cdot^-$ by scavenging e^-. The formation of $O \cdot^-$ occurs[14] *via* reactions 2–5. Thus

$$H_2O \xrightarrow{h\nu} H_2O^+ + e^- \qquad (2)$$

$$H_2O^+ + H_2O \longrightarrow H_3O^+ + OH \cdot \qquad (3)$$

$$H_2O^+ + OH_{aq}^- \longrightarrow H_2O + OH \cdot \qquad (4)$$

$$OH \cdot + OH_{aq}^- \longrightarrow H_2O + O \cdot^- \qquad (5)$$

scavenging e^- prevents the destruction of H_2O^+, $OH \cdot$, $O \cdot^-$ as in the reactions

$$e^- + H_2O^+ \longrightarrow H_2O^* \longrightarrow H_2O \qquad (6)$$

$$e^- + OH \cdot \longrightarrow OH^- \qquad (7)$$

$$e^- + O \cdot^- \longrightarrow O^{2-} \qquad (8)$$

If a "best estimate" value[14] of 1.9 is taken for $G(O \cdot^-)$ in the absence of NO_3^-, then $G(O \cdot^-) = 4.0$ at 3 *M* NO_3^-.

The yields of H_t are changed markedly by the addition of NO_3^- to 7.5 *M* NaOH glass. In Figure 4, $G(H_t)$ in glass which contains 5×10^{-3} *M* NO_3^- is actually higher than in glass without NO_3^-. Since photobleaching e_t^- also reduces $G(H_t)$, the initial increase in $G(H_t)$ with small concentrations of added NO_3^- is attributed to the scavenging by NO_3^- of e_m^- which escape the spurs in which they were formed, thus preventing H_t destruction as in reaction 9. A fraction of $H \cdot$ produced by radiolysis very likely has intraspur e_m^- as a precursor in a reaction such as (10)

$$e_m^- + H_t \xrightarrow{H_2O} H_2 + OH^- \qquad (9)$$

$$e_m^- + H_3O^+ \longrightarrow H \cdot + H_2O \qquad (10)$$

so that increasing concentrations of NO_3^- in the range 5×10^{-3} to 0.1 *M* scavenge some of the e_m^- and cause a decrease in $G(H_t)$. This scavenging is not especially efficient, however, since a concentration of 0.1 *M* NO_3^- only reduces $G(H_t)$ to its value which obtains in the absence of NO_3^-. Above $[NO_3^-] = 0.1$ *M* a dramatic increase in efficiency of reduction of $G(H_t)$ by NO_3^- occurs. These high NO_3^- concentrations are scavenging all e_m^- plus some e^- so that the decrease of $G(H_t)$ indicates that a significant fraction of the observed H_t has an e^- precursor. Hamill[3] has postulated that e^-

forms H· in spurs according to reaction 11 whereas e_m^- produces H· in spurs by reaction 12.

$$e^- + H_3O^+ + OH\cdot \longrightarrow 2H\cdot + 2OH\cdot \quad (11)$$

$$e_m^- + H_3O_{aq}^+ + OH\cdot \longrightarrow H\cdot + OH\cdot + H_2O \quad (12)$$

Due to the alkalinity of the matrix, H_3O^+ and $H_3O_{aq}^+$ are likely to be quickly neutralized by a nearby OH^- to $2H_2O$. The effectiveness of this neutralization process can be observed by examination of Figure 1 which shows that $G(H_t)$ drops sharply as $[OH^-]$ is increased above 9 *M*.

The validity of reactions 11 and 12 can be tested in more detail by examining the spatial distribution of H_t as deduced from paramagnetic relaxation data. Figure 3 shows that $(T_1T_2)^{1/2}$ for H_t increases with radiation dose. Since the H_t epr spectrum does not overlap the spectra of the other radicals present, the variation in $(T_1T_2)^{1/2}$ measures the local concentration of only H_t and not the other radicals. These data indicate that the local H_t concentration is decreasing at the same time that the sample average concentration is increasing (Figure 2). This behavior is consistent with the production of H_t by reaction 11. Reaction 11 predicts the pairwise formation of H· in spurs. The H· pairs are very likely trapped as $2H_t$ in or near the spurs in which they are produced since the probability for their destruction by OH^- *via* reaction 13 increases with the distance traveled before trapping. Intraspur spin–spin relaxation between the paired H_t, especially at very low radiation doses, makes a significant contribution to T_2 and thus to $(T_1T_2)^{1/2}$. As the radiation dose is increased, some of the H_t are destroyed by reaction

$$H\cdot + OH_{aq}^- \dashrightarrow e_m^- + H_2O \quad (13)$$

with another species (as evidenced by dose saturation of H_t concentration at 0.6 Mrad) and, on the average, only one member of each H_t pair would be expected to undergo such reaction until very high radiation doses are reached. The effect of increasing the radiation dose in the region 0–0.6 Mrad, then, is to increase the sample average H_t concentration and to lower the local H_t concentration which in turn decreases spin–spin relaxation and increases $(T_1T_2)^{1/2}$ as is observed.

The species which destroys individual members of the H_t pairs during irradiation must be mobile, since the H_t are stable indefinitely at 77°K after irradiation. The most likely candidate for the mobile species is e_m^- which could react according to eq 9. As discussed above, the effect of bleaching e_m^- on the observed H_t concentration supports this hypothesis.

V. Conclusions

The data obtained in this study support the following hypotheses. (a) At 77°K in concentrated alkaline glass a significant fraction of electrons produced by radiation do not become hydrated before they react in spurs. These electrons can be scavenged by NO_3^-. (b) A major fraction of the observed yield of H_t is produced by e^- reaction within spurs. (c) The efficiency of scavenging e^- by NO_3^- is lower than that of e_m^- by NO_3^-. We find no inconsistencies between the data presented here and the spur diffusion model.

Acknowledgments. This research was supported in part by a University of Kansas General Research Grant No. 3221-5038 and by the National Science Foundation. We are grateful to the Kansas University Chemistry Department for use of epr equipment. M. B. is grateful to the National Science Foundation for a summer research participant award, made under Grant No. GY-7411.

Nitrogen-14 Magnetic Relaxation of Dimethylformamide Solutions Containing Nickel(II), Cobalt(II), and Manganese(II) Ions

by Tzeng-ming Chen[1]

Contribution No. 2500 from the Department of Chemistry, University of California at Los Angeles, Los Angeles, California 90024 *(Received November 29, 1971)*

Publication costs borne completely by The Journal of Physical Chemistry

Nitrogen-14 spin relaxation rates in solutions of Co(II), Ni(II), and Mn(II) ions have been studied as functions of temperature and frequency by nmr techniques. The "excess" ^{14}N spin relaxation in these systems is governed by the rate of first shell relaxation for most of the temperature ranges studied. For Ni(II) and Co(II) ions, ^{14}N quadrupole interactions dominate the relaxation mechanism; however, for Mn(II) ion, the isotropic spin exchange plays the most significant role.

Introduction

It is well known that nuclear magnetic relaxation in liquids is greatly enhanced by the presence of paramagnetic ions. Proton relaxation in water containing ions of the iron group elements has been the subject of extensive work in the literature.[2] Studies have also been made upon paramagnetic ions in nonaqueous solvents,[3-8] but few studies have been concerned with the ^{14}N spin relaxation in solutions containing transition metals.

A ^{14}N nucleus has a nuclear spin $I = 1$, and in addition to a magnetic dipole moment, it has an electric quadrupole moment. If paramagnetic metal ions are added to dimethylformamide (DMF) solutions, the ^{14}N nuclear spins will relax through nuclear–electron spin–spin dipolar interactions, isotropic nuclear–electron spin exchange (Fermi contact interaction), and electric quadrupole interactions. These mechanisms dominate provided that fast chemical exchange occurs between the bulk solvent and the first solvation shell of the ions, and provided that the chemical shifts are small; in this case a resonance is observed which is the average of the resonances of nuclei in the free and bonded molecules.

Previous authors have studied the proton relaxation times of DMF solutions of Ni(II), Co(II), and Mn(II) ions.[7,8] They attempted to determine the relaxation mechanisms, the relaxation times, and the activation energies associated with the proton relaxation processes. Garrett, *et al.*,[9] observed esr line broadening for Mn(II)–DMF complex ion at high temperatures which he attributed to a strong perturbation caused by chemical exchange.[8,9] In the present paper, we have studied the ^{14}N spin relaxation in similar systems and have correlated the proton and ^{14}N spin relaxation studies.

Theory

The nuclear resonance spectra of DMF in solutions of paramagnetic ions in DMF can lead to much insight into the nature of the chemical exchange of DMF between coordinated sites on the paramagnetic ion and free sites in the bulk solvent. The nmr line widths arising from DMF nuclei depend on τ_h, the lifetime of a DMF molecule bound to a paramagnetic ion.

For fast ligand exchange

$$\tau_h \ll T_{2M} \tag{1}$$

Swift and Connick's equation[10] can be reduced to

$$\frac{1}{T_{2p}} = \left(\frac{1}{T_2}\right)_{ob} - \frac{1 - P_M}{T_{2l}} = \frac{P_M}{T_{2M}}\left[\frac{1 + T_{2M}\tau_h\Delta\omega_M{}^2}{1 + \tau_h{}^2\Delta\omega_M{}^2}\right] \tag{2}$$

where $T_{2P}{}^{-1}$ is the "excess" line width due to the presence of the paramagnetic ions; T_{2M} and T_{2l} are the transverse relaxation times of the resonant nucleus in the first coordination shell of complex ion and in free DMF, respectively; $\Delta\omega_M$ is the frequency difference

(1) Address correspondence to the author at the Polytechnic Institute of Brooklyn, Brooklyn, N. Y. 11201.

(2) N. Bloembergen and L. O. Morgan, *J. Chem. Phys.*, **34**, 842 (1961), and references cited therein.

(3) (a) H. Yoshioka and L. Fujita, *J. Phys. Soc. Jap.*, **14**, 1717 (1959); (b) Z. Luz and S. Meiboom, *J. Chem. Phys.*, **40**, 1058, 1066, 2686 (1964).

(4) Z. Luz, *ibid.*, **41**, 1748, 1756 (1964).

(5) D. Geschke and H. Pfeifer, *Strukt. Khim.*, **5**, 201 (1964).

(6) R. Sperling and H. Pfeifer, *Z. Naturforsch.*, **19a**, 1342 (1964).

(7) N. A. Matwiyoff, *Inorg. Chem.*, **5**, 788 (1966).

(8) R. C. Phillips and L. O. Morgan, submitted for publication.

(9) B. B. Garrett and L. O. Morgan, *J. Chem. Phys.*, **44**, 890 (1966).

(10) T. J. Swift and Robert E. Connick, *ibid.*, **37**, 307 (1962).

between the resonant nucleus in free DMF and coordinated DMF; P_M is the probability of the nucleus being in the first coordinated sphere. Equation 2 can be further simplified by considering the two limiting cases.

(*A*) *Small Chemical Shift.* T_{2P}^{-1} is controlled by the rate of first shell relaxation.

$$T_{2M}^{-1}\tau_h^{-1} \gg \Delta\omega_M^2 \tag{3}$$

$$\tau_h^{-2} \gg \Delta\omega_M^2 \tag{4}$$

then

$$\frac{1}{T_{2P}} = \frac{P_M}{T_{2M}} \tag{5}$$

(*B*) *Large Chemical Shift.* T_{2P}^{-1} is controlled by the rate of relaxation through the large chemical shift

$$\tau_h^{-2} \gg \Delta\omega_M^2 \tag{6}$$

$$T_{2M}^{-1}\tau_h^{-1} \ll \Delta\omega_M^2 \tag{7}$$

then

$$\frac{1}{T_{2P}} = P_M\tau_h\Delta\omega_M^2 \tag{8}$$

For the (A) case, the observed relaxation of a ^{14}N nucleus in the coordinated sphere could occur through nitrogen–electron spin–spin dipolar interactions $(1/T_2)_{DD}$,[11] isotropic nitrogen–electron spin exchange (Fermi contact interaction) $(1/T_2)_{HF}$,[12] and ^{14}N quadrupole interaction $(1/T_2)_Q$.[13]

$$\frac{1}{T_{2P}} = \left(\frac{1}{T_2}\right)_{DD} + \left(\frac{1}{T_2}\right)_{HF} + \left(\frac{1}{T_2}\right)_Q \tag{9}$$

where

$$\left(\frac{1}{T_2}\right)_{DD} = \frac{1}{15}\frac{S(S+1)g^2\beta^2\gamma_I^2P_M}{r^6}\left[7\tau_c + \frac{13\tau_c}{1+\omega_S^2\tau_c^2}\right] \tag{10}$$

$$\left(\frac{1}{T_2}\right)_{HF} = \frac{1}{3}\frac{S(S+1)A^2P_M}{\hbar^2}\left[\tau_e + \frac{\tau_e}{1+\omega_S^2\tau_e^2}\right] \tag{11}$$

$$\left(\frac{1}{T_2}\right)_Q = \frac{3}{8}\left(1+\frac{\xi^2}{3}\right)\left(\frac{e^2Q}{\hbar}V_{zz}\right)^2P_M(\tau_r^{-1}+\tau_h^{-1})^{-1} \tag{12}$$

where indexes I and S refer to the nitrogen and electron spins, respectively; γ is the gyromagnetic ratio of the nitrogen nucleus; r is the electron–nitrogen distance; A is the spin-exchange constant; τ_c, τ_e, and τ_r are the correlation times for dipolar, spin-exchange interactions, and tumbling of the complexed ion, respectively; ξ indicates the asymmetry of the electric field gradient

$$\xi = \frac{V_{xx} - V_{yy}}{V_{zz}} \tag{13}$$

where $V_{\alpha\alpha}$ is the second derivative of the electric potential with respect to axes fixed in the molecule. Q is the quadrupole moment of the nucleus.

The correlation times in eq 10 and 11 are related by the relations

$$\tau_c^{-1} = \tau_s^{-1} + \tau_r^{-1} + \tau_h^{-1} \tag{14}$$

$$\tau_e^{-1} = \tau_s^{-1} + \tau_h^{-1} \tag{15}$$

where τ_s is the electron spin-relaxation time.

The electron spin-relaxation time for Mn(II) can be approximated by the expression[2]

$$\frac{1}{\tau_s} = \frac{12C_2^2\hbar^{-2}}{5S(S+1)}\left[\frac{\tau_v}{1+\omega_S^2\tau_v^2} + \frac{4\tau_v}{1+4\omega_S^2\tau_v^2}\right] \tag{16}$$

where

$$C_2^2 = \frac{2}{225}(2S+1)S^2(S+1)^2 \times \left[1 - \frac{3}{4S(S+1)}\right][2\langle D^2\rangle_{av} + 3\langle E^2\rangle_{av}] \tag{17}$$

D and E are zero-field splittings of the complex ion; τ_v is the solvent-fluctuation correlation time.

The splitting $\Delta\omega_M$ is given by the relation[12]

$$\frac{\Delta\omega_M}{\omega} = \frac{S(S+1)}{3kT}\frac{\gamma_e}{\gamma_N}A \tag{18}$$

where A is the scalar coupling constant and the other symbols have been described previously.

Experimental Section

Metal–DMF complexes were prepared by the following procedure.[14,15] The aquated metal perchlorates were dehydrated with 100% excess of 2,2-dimethoxypropane by stirring with a magnetic stirrer for 20 hr at room temperature. The resulting rust-colored solutions were treated with a 15-fold mole excess of the ligand. A large quantity of anhydrous ether was added to precipitate the product. The crystalline product was collected on a Büchner filter equipped with a vacuum pump, washed with several portions of anhydrous ether, and dried with a stream of dry nitrogen. All metal–DMF complexes were hygroscopic and could only be handled in a drybox.

Reagent grade DMF and 2,2-dimethoxypropane were dried with CaO by stirring for several days. They were distilled from CaO at reduced pressure and the middle fraction was collected.

The ^{14}N resonance signals were recorded with a Varian Associates Model V-4200 wide-line spectrom-

(11) L. Solomon, *Phys. Rev.*, **99**, 559 (1955).

(12) N. Bloembergen, *J. Chem. Phys.*, **27**, 572, 595 (1957).

(13) A. Abragam, "The Principles of Nuclear Magnetism," Oxford University Press, London, 1961, Chapter 8.

(14) J. H. Bright, R. S. Drago, D. M. Hart, and S. K. Madan, *Inorg. Chem.*, **4**, 18 (1965).

(15) K. Stark, *J. Inorg. Nucl. Chem.*, **11**, 77 (1959).

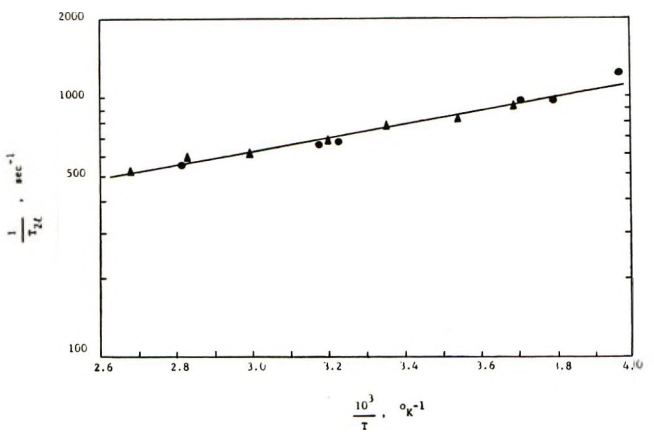

Figure 1. Temperature dependence of ^{14}N magnetic relaxation time of DMF: ▲, data taken at 2.8 MHz; ●, data taken at 2.3 MHz.

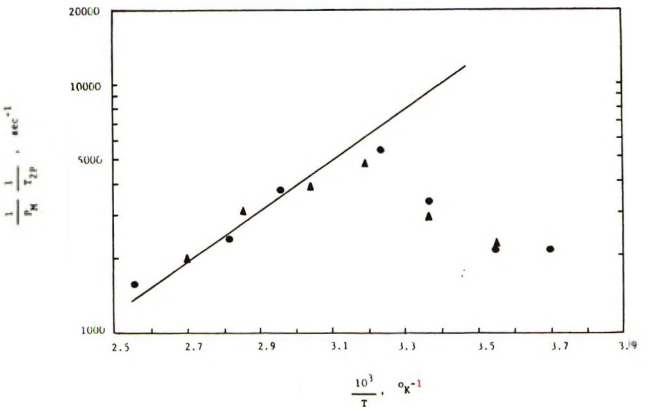

Figure 2. Temperature dependence of ^{14}N magnetic relaxation time in DMF solutions of Ni(II) ion: ▲, data taken at 2.8 MHz; ●, data taken at 2.3 MHz.

eter operated at 2.3 and 2.8 MHz. The temperature dependence studies were carried out by flowing thermostated nitrogen gas through a Varian wide-line variable temperature accessory. The temperature was measured with a copper–constantan thermocouple to an accuracy of 0.2° and kept constant within ±0.5°.

Special care was taken to avoid modulation and saturation broadening. All samples were degassed by a freeze–thaw method and sealed under vacuum.

Results and Discussion

Since the results vary greatly for the different cases studied, each one is considered separately.

(*A*) *Pure DMF.* Figure 1 shows the temperature dependence of the DMF ^{14}N transverse relaxation time T_{2l} at 2.3 and 2.8 MHz. Since intra- and intermolecule dipole–dipole interactions are very small, it can be safely assumed that the transverse relaxation times of the ^{14}N nuclei in DMF are determined primarily by the quadrupole interaction (see eq 12). The ^{14}N quadrupole coupling constant has not been determined for DMF and therefore must be taken from an analogous compound. The ^{14}N coupling constant, $(e^2Q/h)V_{zz}$ = 3.6 MHz, is taken from the microwave value for formamide.[16] The ^{14}N coupling constant is probably independent of internal rotation and temperature. Wallach and Huntress[17] pointed out recently that the rate of internal rotation of DMF is much slower than both overall molecular rotation and the ^{14}N relaxation rates. Therefore, the effect of the internal rotation on the ^{14}N relaxation times is negligible. The relaxation rates are frequency independent and depend exponentially on temperature with an activation energy of 1.17 kcal/mol. Inserting the ^{14}N coupling constant and neglecting the asymmetry parameter in eq 12, we calculate τ_r to be 4×10^{-12} sec at 25°.

(*B*) *Ni(II) and Co(II) in DMF.* Figures 2 and 3 show the temperature as well as the frequency dependence of the ^{14}N spin relaxation times in DMF solutions of Ni(II) and Co(II) ions, respectively. Since τ_h,[7] $\Delta\omega_M$ (see Table I) and P_M (P_M = 0.044 for both ions) can be estimated by independent experiments, we can show that the observed ^{14}N line widths are compatible only with the fast exchange limit formulas (A) case, except possibly for the low-temperature data on $Ni(DMF)_6^{2+}$. The ^{14}N relaxation rates are almost frequency independent which implies that the relaxation mechanisms are dominated by the rate of first shell relaxation (eq 5) since the shift $\Delta\omega_M$ in eq 8 is frequency dependent. Deviation from the linear part at low temperature ($10^3/T \geq 3.2$) in Figure 2 indicates that other relaxation processes might be responsible for that region. The conditions, $T_{2M}^{-1}\tau_h^{-1} \gg \Delta\omega_M^2$ and $\tau_h^{-2} \gg \Delta\omega_M^2$, for case (A) may no longer be true at lower temperature for $Ni(DMF)_6^{2+}$. The complex behavior including a shift-broadening term might be responsible for this low-temperature region. The shift-broadening mechanism would contribute only a part of the total effect in the intermediate region so that frequency effects are expected to be relatively small.

In order to estimate the contribution $(1/T_2)_{DD}$ of the nitrogen–electron spin dipole–dipole interaction to the line width, the bond angles and distances listed by

Table I: Temperature and Frequency Dependence of $\Delta\omega_M$, Hz[a]

	Temp, °C	
	25	50
$Ni(DMF)_6^{2+}$	223 (290)	250 (300)
$Co(DMF)_6^{2+}$	892 (1070)	1000 (1210)
$Mn(DMF)_6^{2+}$	3500 (4000)	3600 (4100)

[a] First figures were obtained at 2.3 MHz and those in parentheses at 2.8 MHz. All shifted to downfield.

(16) R. J. Knowland and E. B. Wilson, *J. Chem. Phys.*, **27**, 585 (1957).

(17) D. Wallach and W. T. Huntress, Jr., *ibid.*, **50**, 1219 (1969).

Vilkov, Akishin, and Presnyakova[18] were used. The Co(II)–O and Ni(II)–O internuclear distances were estimated from the ionic radii for octahedrally coordinated Co(II) ion (0.72 Å), Ni(II) ion (0.68 Å) and O^{2-} ion (1.40 Å).[19] We assume that the C_2NCOH frame in DMF is planar.[18,20] The correlation time (τ_c) for the dipolar interaction is determined according to eq 14 by the more rapid of the two processes: electron spin relaxation (τ_S) and the tumbling of the complex (τ_r), since they are probably much shorter than τ_h. Matwiyoff[7] has estimated that τ_S is 5×10^{-13} sec for $Co(DMF)_6^{2+}$ and 3×10^{-12} sec for $Ni(DMF)_6^{2+}$ at 25°; τ_r is probably of the order[2] of 10^{-11} sec at 25°. In the discussion which follows we have assumed $\tau_c = \tau_S$, but the qualitative conclusions are not changed by assuming τ_c values as large as 10^{-11} sec. Small values of τ_S are consistent with the observations that $Co(DMF)_6^{2+}$ and $Ni(DMF)_6^{2+}$ do not exhibit electron spin resonance signals even at 77°K. By means of eq 10, $(1/T_2)_{DD}$ was estimated to be 1.4×10^{-3} and 3.5×10^{-2} sec^{-1} for $Co(DMF)_6^{2+}$ and $Ni(DMF)_6^{2+}$, respectively. This cannot account for the observed line widths.

Because of the great width of the resonances, accurate chemical shifts, $\Delta\omega_M$, could not be obtained, but $\Delta\omega_M$ was estimated by measuring the chemical shift between complexed and pure DMF solution (see Table I). Fermi contact contribution can be estimated: the scalar coupling constant A was estimated by means of eq 18, τ_e was set equal to τ_S in eq 15 since $\tau_h \gg \tau_S$, and $(1/T_2)_{HF}$ was estimated to be the order of 0.1 sec^{-1} for both ions. This effect also cannot account for the observed line widths. It is, therefore, reasonable to assume that the spin relaxations in the linear regions of Figures 2 and 3 are entirely controlled by quadrupole relaxation. The slopes of the linear regions give an activation energy of *ca.* 3.90 kcal/mol for $Co(DMF)_6^{2+}$ and *ca.* 4.57 kcal/mol for $Ni(DMF)_6^{2+}$, which are reasonable values for ion tumbling. For comparison, the temperature as well as frequency dependence of the line widths of the diamagnetic complex species, $Zn(DMF)_6^{2+}$, are shown in Figure 4. Clearly, ^{14}N quadrupole interactions play the dominant role in spin relaxation in this diamagnetic species, and the similarity among Figures 2, 3, and 4 supports the assumption above that quadrupolar relaxation dominates at high temperature for the Ni and Co solutions.

By employing eq 12, τ_r were determined to be 1.67×10^{-11} and 4.76×10^{-11} sec at 25° for $Co(DMF)_6^{2+}$ and $Ni(DMF)_6^{2+}$, respectively, compared to the value of 2.9×10^{-11} sec for $Mn(DMF)_6^{2+}$.[8]

Stengle, *et al.*,[21] also measured ^{17}O relaxation in the same solutions. They estimated the kinetic rates for DMF in the coordination spheres of $Co(DMF)_6^{2+}$ and $Ni(DMF)_6^{2+}$ solutions and obtained results which differ slightly from the previously reported rate parameters of Matwiyoff.[7] However, a qualitative conclusion would not make any change for this study. The conditions (A) are also not valid for $Ni(DMF)_6^{2+}$ at lower temperature.

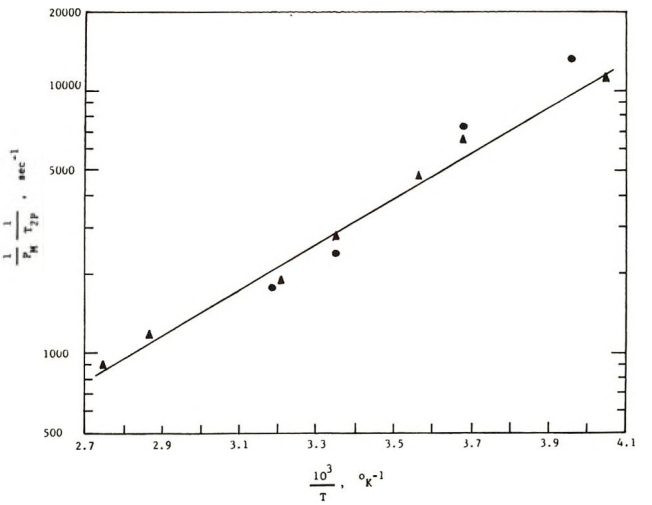

Figure 3. Temperature dependence of ^{14}N magnetic relaxation time in DMF solutions of Co(II) ion: ▲, data taken at 2.8 MHz; ●, data taken at 2.3 MHz.

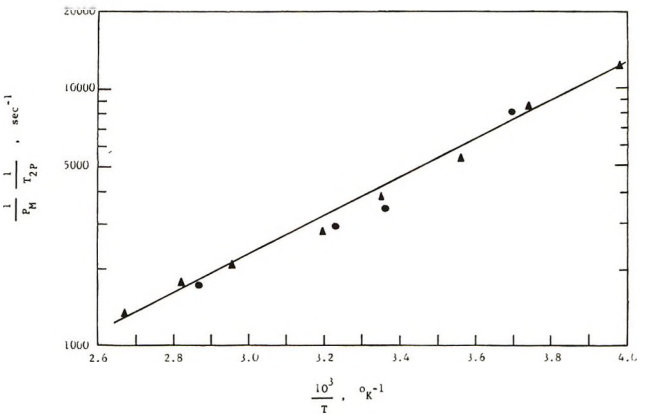

Figure 4. Temperature dependence of ^{14}N magnetic relaxation time in DMF solutions of Zn(II) ion: ▲, data taken at 2.8 MHz; ●, data taken at 2.3 MHz.

(C) *Mn(II) in DMF.* As for Ni(II) and Co(II) ions described in the previous section, the observed ^{14}N line widths for Mn are also compatible with the fast exchange condition. For Mn(II) in DMF (see Figure 5) the correlation time τ_S can be estimated from esr measurements to be about 10^{-9} sec;[9] since $\tau_h \approx 4.2 \times 10^{-7}$ sec[8] at 25°, in the temperature range studies for Mn(II) in DMF we can set $\tau_c \approx \tau_r$. We can then use eq 10 to estimate $(1/T_2)_{DD} \approx 0.2$ sec^{-1}, a predicted ^{14}N

(18) L. V. Vilkov, P. A. Akishin, and V. M. Presnyakova, *Strukt. Khim.*, **3**, 5 (1962).

(19) H. A. Wells, "Structural Inorganic Chemistry," 3rd ed, Oxford University Press, London, 1963.

(20) C. C. Costain and J. M. Douling, *J. Chem. Phys.*, **32**, 158 (1960).

(21) J. S. Babiec, Jr., C. H. Langford, and T. R. Stengle, *Inorg. Chem.*, **5**, 1362 (1966).

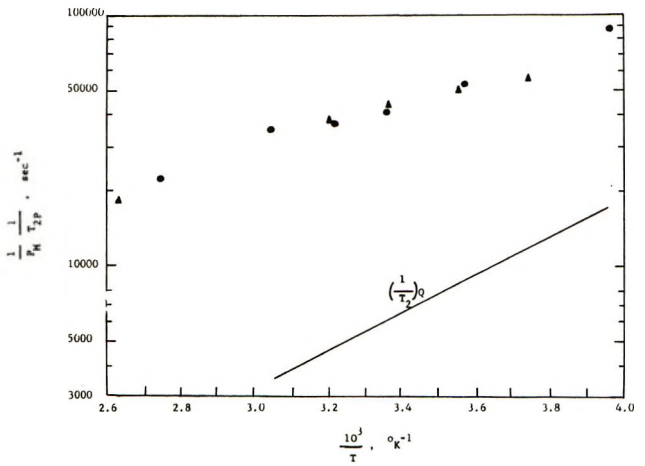

Figure 5. Temperature dependence of ^{14}N magnetic relaxation time in DMF solutions of Mn(II) ion: ▲, data taken at 2.8 MHz; ●, data taken at 2.3 MHz.

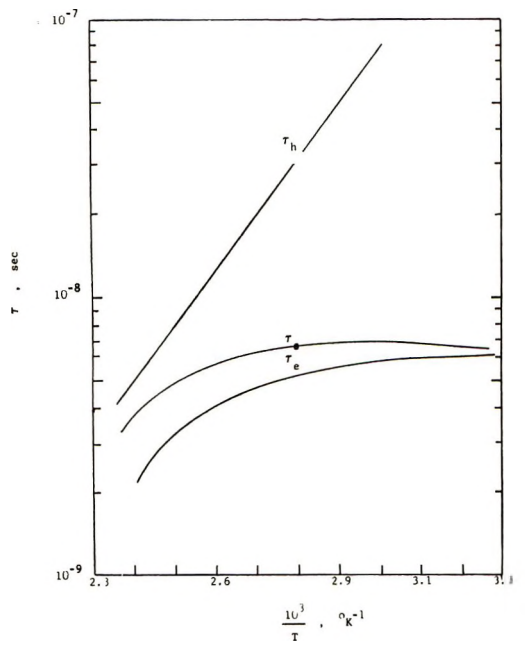

Figure 6. Plots of ln τ *vs.* $1/T$ for Mn(II)–DMF solution at V_i = 2.3 MHz.

line width is much smaller than that observed. Swift and Connick[10] in their ^{17}O spin-relaxation studies on enriched ^{17}O solution of $MnSO_4$, concluded that dipole–dipole relaxation mechanisms were negligible. These results support our conclusion that dipole–dipole interactions do not contribute significantly in our case since our dipole–dipole distance (4.3 Å) is larger than theirs (2.8 Å).

We estimate $(1/T_2)_Q$ by means of eq 12 and the parameters discussed in the last section; $(1/T_2)_Q \approx 27$ sec^{-1} at 25° and the activation energy, estimated from the proton spin relaxation data,[8] should be about 3.5 kcal/mol.

In order to calculate τ_S and τ_e, we have used the temperature dependence data of esr line widths of Mn(DMF)$_6^{2+}$ taken from the work of Garrett and Morgan.[9] Although the electron spin relaxation time τ_S may be slightly different at nmr and at esr frequencies, the solvent fluctuation time τ_v in eq 16 is probably so short ($\sim 2 \times 10^{-12}$ sec) that this frequency dependence is negligible. Figure 6 shows τ_S plotted as a function of temperature over the temperature range studied. τ_h was estimated from ^1H nmr data[8] to be 4.2×10^{-7} sec at 25° with an activation energy of 9.1 kcal/mol. As a result, τ_e could be evaluated by means of eq 15. (See Figure 6.)

If $(1/T_2)_Q$ is subtracted from the observed ^{14}N relaxation rates, the remaining line width is presumably due to contributions from the isotropic nitrogen-electron spin exchange (see Figure 5). A check on this conclusion was made by measuring the chemical shift between complex and pure DMF solutions and estimating $A/\hbar$ with the aid of eq 18; the result of $A/\hbar$ was 9.7×10^5 sec^{-1}, in agreement with the value 1.07×10^6 sec^{-1} at 2.8 MHz, obtained from eq 11, τ_e, and experimental relaxation rate.

Conclusion

The temperature as well as the frequency dependence of the ^{14}N spin relaxation rates in solutions of DMF containing Co(II), Ni(II), and Mn(II) ions, respectively, indicate that the excess line width, $1/T_{2P}$, is controlled by the rate of first shell relaxation for most of the temperature range studied; *i.e.*, $T_{2M}^{-1}\tau_h^{-1} \gg \Delta\omega_M^2$ and $\tau_h^{-2} \gg \Delta\omega_M^2$. The relaxation rates arising from electron–nitrogen dipolar interaction play a negligible effect for these ions. Further analyses of Ni(II) and Co(II) ions show that ^{14}N quadrupole interactions dominate the relaxation mechanisms; but with Mn(II) ion, the isotropic spin-exchange interaction plays the most significant role.

Acknowledgments. The author wishes to thank Professor D. Kivelson and Professor B. McGarvey for the hospitality of their laboratories during the course of this study and for their supervision and encouragement. Acknowledgments are also made to Professor M. E. Baur for his helpful discussions and Mr. R. Gillespie for his assistance with the electronics. This work was supported under Grant No. GM 11125, U. S. Public Health Service.

Proton Magnetic Relaxation in *N*-Methyl-γ-butyrolactam and Hexamethylphosphoric Triamide Solutions Containing Manganese(II) Ions[1a]

by Tzeng-ming Chen*[1b] and L. O. Morgan

Department of Chemistry, The University of Texas at Austin, Austin, Texas 78712 *(Received December 13, 1971)*

Publication costs assisted by the Robert A. Welch Foundation and the National Science Foundation

Temperature dependence of the "excess" proton spin relaxation rates for Mn(II)–NMBuL and Mn(II)–HMPA solutions has been studied by NMR A-60 techniques. The "excess" proton spin relaxation in these systems is governed by first solvation sphere relaxation at higher temperature and chemical exchange near frozen temperature. Further analyses of data indicate that dipolar interactions dominate the first solvation sphere relaxation. Kinetic parameters, various activation energies, and various correlation times were also determined. Electron spin resonance line widths of solvated Mn(II) ion in these systems have been measured as a function of temperature. Solvent fluctuations about the complex ion proposed by Bloembergen and Morgan were applicable to low-temperature data. However, evidence for a second relaxation mechanism was observed at high temperature. Highly hindered rotation of ligand molecules about the Mn(II)–O bond in the Mn(II)–NMBuL complex ion and free rotation of the bulky methyl groups about N–P bond and ligand exchange in the Mn(II)–HMPA complex ion were postulated for high-temperature broadening.

Introduction

It is well known that nuclear magnetic relaxation in liquids is greatly enhanced by the presence of paramagnetic ions. Proton nuclear spin will relax through proton–electron spin–spin dipolar interactions and isotropic proton–electron spin exchange (Fermi contact interaction). These mechanisms dominate provided that fast chemical exchange occurs between the bulk solvent and the first solvation shell of the ion, and provided that the chemical shifts are small with respect to first shell solvent relaxation rate and solvent chemical exchange rate; in this case a resonance is observed which is the average of the resonances of protons in the free and bonded molecules.

Proton relaxation in water containing ions of the iron group elements has been the subject of extensive work in the literature.[2] Studies were also made upon paramagnetic ions in nonaqueous solvents.[3–8] The present study was undertaken in an attempt to determine the various relaxation mechanisms, the correlation times, and the various activation energies associated with processes in solutions of *N*-methyl-γ-butyrolactam (hereafter referred to as NMBuL), $CH_3N(CH_2)_3CO$, or hexamethylphosphoric triamide (hereafter referred to as HMPA), $((CH_3)_2N)_3PO$, containing Mn(II) ion. Morgan and his coworkers[8,9] observed epr line broadening for Mn(II)–dimethylformamide complex ion at high temperature which they attributed to a strong perturbation caused by chemical exchange and free rotation of methyl groups around OC–N bonds in the complex ion. It would be interesting to see the effect of the cyclic structure of NMBuL and the effect of the partial double bond character of HMPA on epr line widths for Mn(II) complex ions at high temperature.

Theory

The temperature dependence of the line width broadening of the free solvent protons can be conveniently analyzed using the equations developed by Swift and Connick.[10] For the exchange of solvent between the bulk solvent and the complex ion, the applicable equation is

$$\frac{1}{T_{2P}} = \left(\frac{1}{T_2}\right)_{ob} - \frac{1 - P_M}{T_{21}} = \frac{P_M}{\tau_h}\left[\frac{(T_{2M}^{-1} + \tau_h^{-1})T_{2M}^{-1} + \Delta\omega_M^2}{(T_{2M}^{-1} + \tau_h^{-1})^2 + \Delta\omega_M^2}\right] \quad (1)$$

where T_{2P}^{-1} is the "excess" line width due to the presence of the paramagnetic ions; T_{2M} and T_{21} are the transverse relaxation times of the resonant nucleus in the first solvation shell of complex and in free solvent,

(1) (a) This work was supported by the Robert A. Welch Foundation and the National Science Foundation. (b) Address correspondence to the author at the Polytechnic Institute of Brooklyn, Brooklyn, N. Y. 11201.

(2) N. Bloembergen and L. O. Morgan, *J. Chem. Phys.*, **34**, 842 (1961), and references cited therein.

(3) H. Yoshioka and L. Fujita, *J. Phys. Soc. Jap.*, **14**, 1717 (1959).

(4) (a) Z. Luz and S. Meiboom, *J. Chem. Phys.*, **40**, 1058, 1066, 2686 (1964); (b) Z. Luz, *ibid.*, **41**, 1948, 1956 (1964).

(5) D. Gescke and H. Pfeifer, *Z. Naturforsch.*, **19a**, 1342 (1964).

(6) R. Sperling and H. Pfeifer, *Strukt. Khim.*, **5**, 201 (1964).

(7) N. A. Matwiyoff, *Inorg. Chem.*, **5**, 788 (1966).

(8) R. C. Phillips Ph.D. Thesis, The University of Texas at Austin, Austin, Texas, 1967.

(9) B. B. Garrett and L. O. Morgan, *J. Chem. Phys.*, **44**, 890 (1966).

(10) T. J. Swift and Robert E. Connick, *ibid.*, **37**, 307 (1962).

respectively; $\Delta\omega_M$ is the frequency difference between the resonant nucleus in free solvent and coordinated solvent; P_M is the probability of the nucleus being in the first coordinated sphere; and τ_h is the lifetime of a solvent in the first coordinated sphere.

For small chemical shift

$$\Delta\omega_M^2 \ll T_{2M}^{-2} \tag{2}$$

$$\Delta\omega_M^2 \ll T_{2M}^{-1}\tau_h^{-1} \tag{3}$$

$$\Delta\omega_M^2 \ll \tau_h^{-2} \tag{4}$$

Equation 1 can be reduced to

$$\frac{1}{T_{2P}} = \frac{P_M}{T_{2M} + \tau_h} \tag{5}$$

Equation 5 can be further simplified by considering the two extremes. (A) Ligand exchange is fast with respect to the first shell solvent relaxation time; T_{2P}^{-1} is controlled by the rate of first shell relaxation.

$$T_{2M} \gg \tau_h \tag{6}$$

then

$$\frac{1}{T_{2P}} = \frac{P_M}{T_{2M}} \tag{7}$$

(B) Ligand exchange is slow with respect to the first shell solvent relaxation time; T_{2P}^{-1} is controlled by the rate of chemical exchange.

$$\tau_h \gg T_{2M} \tag{8}$$

then

$$\frac{1}{T_{2P}} = \frac{P_M}{\tau_h} \tag{9}$$

For the (A) case, the observed relaxation of a proton nucleus in the coordinated sphere could occur through proton–electron spin–spin dipolar interactions $(1/T_2)_{DD}$[11] and isotropic proton–electron spin exchange (Fermi contact interaction)$(1/T_2)_{HF}$.[12]

$$\frac{1}{T_{2P}} = \left(\frac{1}{T_2}\right)_{DD} + \left(\frac{1}{T_2}\right)_{HF} \tag{10}$$

where

$$\left(\frac{1}{T_2}\right)_{DD} = \frac{1}{15}\frac{S(S+1)g^2\beta^2\gamma_I^2 P_M}{r^6} \times \left[7\tau_c + \frac{13\tau_c}{1+\omega_s^2\tau_c^2}\right] \tag{11}$$

$$\left(\frac{1}{T_2}\right)_{HF} = \frac{1}{3}\frac{S(S+1)A^2P_M}{\hbar^2}\left[\tau_e + \frac{\tau_e}{1+\omega_s^2\tau_e^2}\right] \tag{12}$$

where indexes I and S refer to the proton and electron spins, respectively, γ_I is the gyromagnetic ratio of the proton nucleus; τ_c and τ_e are the correlation times for dipolar and spin exchange interactions, respectively; r is the electron–proton distance; and A is the spin exchange constant.

The correlation times in eq 11 and 12 are related by the relations

$$\tau_c^{-1} = \tau_s^{-1} + \tau_r^{-1} + \tau_h^{-1} \tag{13}$$

$$\tau_e^{-1} = \tau_s^{-1} + \tau_h^{-1} \tag{14}$$

where τ_r and τ_s are the correlation times associated with tumbling of the complex ion and electron spin relaxation.

The equation suggested[2] as a basis for correlation of frequency dependence of electron spin relaxation for Mn(II) is

$$\frac{1}{\tau_s} = \frac{12C_2^2\hbar^{-2}}{5S(S+1)}\left[\frac{\tau_v}{1+\omega_s^2\tau_v^2} + \frac{4\tau_v}{1+4\omega_s^2\tau_v^2}\right] \tag{15}$$

where

$$C_2^2 = \frac{2}{225}(2S+1)S^2(S+1)^2 \times \left[1 - \frac{3}{4S(S+1)}\right](2\langle D^2\rangle_{av} + 3\langle E^2\rangle_{av}) \tag{16}$$

D and E are zero-field splittings of the complex ion; τ_v is the correlation time for the impact of solvent molecules upon the solvated ion. It depends upon the symmetry of solvent molecules and temperature.

The splitting $\Delta\omega_M$ is given by the relation[12]

$$\frac{\Delta\omega_M}{\omega} = \frac{S(S+1)}{3kT}\frac{\gamma_e}{\gamma_I}A \tag{17}$$

where k is the Botzmann constant and T is the absolute temperature; other symbols were defined previously.

The variation of τ_h with temperature is given[13] by

$$\frac{1}{\tau_h} = K_M = \frac{kT}{h}e^{[(\Delta S^{\pm}/R) - (\Delta H^{\pm}/RT)]} \tag{18}$$

where K_M is a first-order rate constant and $\Delta S^{\pm}$ and $\Delta H^{\pm}$ are the entropy and enthalpy of activation for the exchange.

Experimental Section

NMBuL and HMPA complexes were prepared by the following general procedure.[14,15] The aquated metal perchlorates were dehydrated with 100% excess of 2,2-dimethoxypropane by stirring with a magnetic stirrer for 20 hr at room temperature. The resulting rust-colored solutions were treated with a 15-fold mole excess of the ligand. A large quantity of anhydrous ether was added to precipitate the product. The crystalline product was collected on a Büchner filter equipped with a vacuum pump, washed with several

(11) L. Solomon, *Phys. Rev.*, **99**, 559 (1955).

(12) N. Bloembergen, *J. Chem. Phys.*, **27**, 572, 595 (1957).

(13) S. Glasstone, K. Laidler, and H. Eyring, "The Theory of Rate Processes," McGraw-Hill, New York, N. Y., 1941.

(14) K. Stark, *J. Inorg. Nucl. Chem.*, **11**, 77 (1959).

(15) J. H. Bright, R. S. Drago, D. M. Hart, and S. K. Madan, *Inorg. Chem.*, **4**, 18 (1965).

portions of anhydrous ether, and dried with a stream of dry nitrogen. All the samples are hygroscopic and should be handled in a drybox.

Anal. Calcd for $Mn(HMPA)_4(ClO_4)_2$: C, 29.40; H, 7.43; N, 17.30. Found: C, 29.40; H, 7.40; N, 17.10. Calcd for $Mn(NMBuL)_6(ClO_4)_2$: C, 42.46, H, 6.41; N, 9.90. Found: C, 42.42; H, 6.46; N, 9.91.

Proton nmr spectra were obtained at 60 MHz using a Varian A-60 spectrometer equipped with a variable temperature probe and a Varian temperature controller. The temperature was monitored by measuring the peak separations of methanol or ethylene glycol and could be held to within ±1° at a given temperature. The magnetic fields scanned with the spectrometer were calibrated using an audiooscillator monitored by a frequency counter. Line positions were reproducible to within ±1 Hz and line widths to within ±0.2 Hz. All samples were degassed by a freeze–thaw method and sealed under vacuum.

For epr data on Mn(II) solutions in NMBuL and HMPA, a Varian V-153 Klystron (output 300 mV) and employing 100-kHz field modulation was used. The variable temperature unit (Varian V-4540) was calibrated with a chromel–alumel thermocouple. Infrared spectra were obtained using a Baird Model 4-55 spectrophotometer calibrated with polysterene film. The visible spectra were recorded by a Perkin-Elmer Model 202 spectrometer.

Results and Discussion

(1) *Mn(II)–NMBuL.* Figure 1 shows the nmr spectrum of NMBuL, for which the proton assignments are indicated. Protons B, adjacent to a nitrogen atom, lie at the lowest field; the triplet peaks, separated by 6.5 ± 0.5 Hz, with intensity ratios 1:2:1, arise from coupling with protons C. The protons A are far away from the nitrogen atom and protons B, and only one peak has been observed. The magnetic fields of protons C and D are too close to be observed separately. Therefore, we confine our attention to peaks A and B.

The introduction of Mn(II) to NMBuL solution enhances the proton relaxation; that is, the peaks are broadened by electron–proton dipolar and isotropic spin-exchange interactions. In order to analyze the complex spectra, it is convenient to introduce some equations.

The line-shape function $g(\nu)$ derived[16] from the steady-state solution of the Block equations in which M_z is constant and the transverse components rotate with the applied ratio frequency field H_1, is

$$g(\nu) = \frac{g(\nu)_{max}}{1 + 4\pi^2 T_2^2(\nu_0 - \nu)^2} \tag{19}$$

where T_2 is the transverse relaxation time and ν_0 and ν are the resonant frequencies at maximum height and at any instance, respectively. Define

$$T_2 = \frac{1}{2\pi(\nu_0 - \nu)_{1/2}} \tag{20}$$

and substitute eq 20 into eq 19. Then

$$\frac{g(\nu)}{g(\nu)_{max}} = \frac{1}{1 + \dfrac{(\nu_0 - \nu)^2}{(\nu_0 - \nu)^2_{1/2}}} \tag{21}$$

where $(\nu_0 - \nu)_{1/2}$ = half line width at half-maximum height in hertz. Set $(\nu_0 - \nu)_{1/2} = 1$; then

$$\frac{g(\nu)}{g(\nu)_{max}} = \frac{1}{1 + (\nu_0 - \nu')^2} \tag{22}$$

If several assumptions are made, namely that (1) each component of the multiplet shifts isotropically, (2) the coupling constant for the complex is the same as that of the free ligand, and (3) absorption can be best described by a Lorentzian curve, then by trial and error techniques the line width at half-maximum height for each component can be evaluated using eq 22 from best fit of theoretical and observed curves. Figure 2 illustrates the triplet resolution. All peaks were taken on the expanded scale.

Relaxation rates were obtained for 0.01, 0.005, 0.003, and 0.002 *M* solutions. Most temperature dependences of relaxation rates over the normal liquid temperature range of NMBuL were obtained for 0.005 *M* solution. Within experimental accuracy, the relaxation rates of individual proton resonances are linear with Mn(II) concentration.

Since $\Delta\omega_M$ is so small ($\Delta\omega_M = 4 \times 10^3$ radians/sec for A protons and 6×10^3 radians/sec for B protons at 300°K), we can show that the observed line widths are compatible only with eq 5. In Figures 3 and 4,

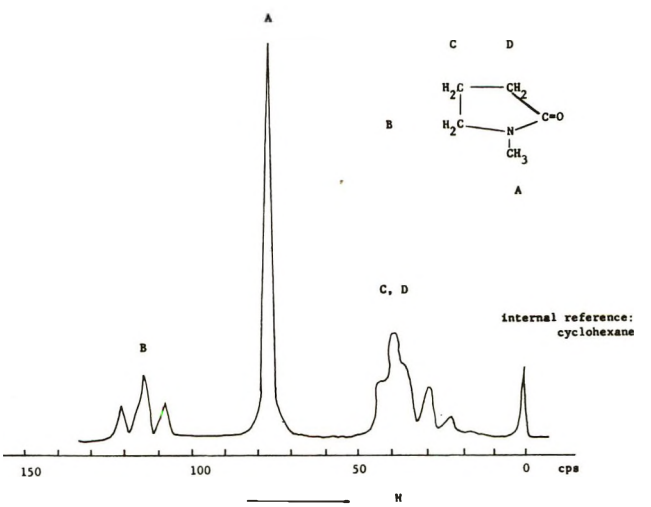

Figure 1. Nmr spectrum of NMBuL; spectrum measured at 20°.

(16) J. A. Pople, W. G. Schneider, and H. J. Bernstein, "High-Resolution Nuclear Magnetic Resonances," McGraw-Hill, New York, N. Y., 1959, p 35.

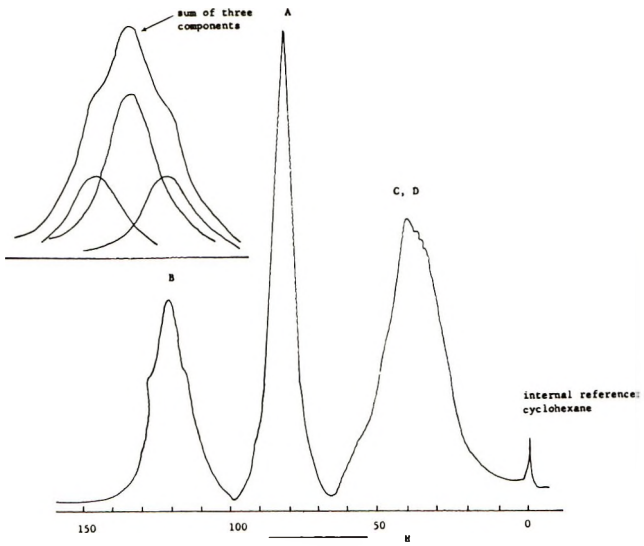

Figure 2. Analysis of nmr spectrum of Mn(II)–NMBuL solution.

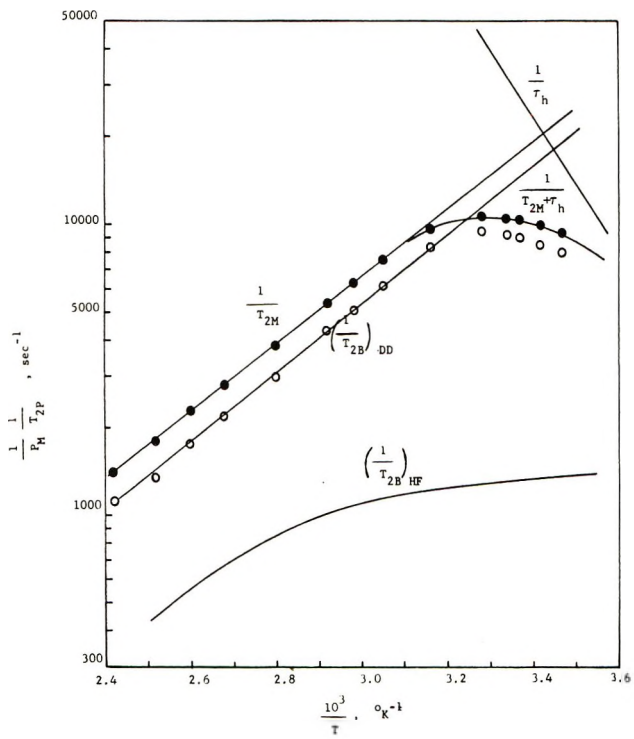

Figure 3. Temperature dependence of B proton relaxation rate in Mn(II)–NMBuL solution.

the straight lines with activation energies of $\sim$ 5 kcal/mol observed for the solutions at high temperature ($10^3/T < 3.06$) represent the case in which the relaxation rate is dominated by $T_{2M}{}^{-1}$ through fast chemical exchange (eq 7). Lines resulting from the curve fitting are shown in Figures 3 and 4. As a result of curve fitting, a linear region with an activation energy of 9.20 $\pm$ 1.40 kcal/mol at low temperature was calculated in which the relaxation rate is controlled by the rate of chemical exchange through fast T_{2M} relaxation

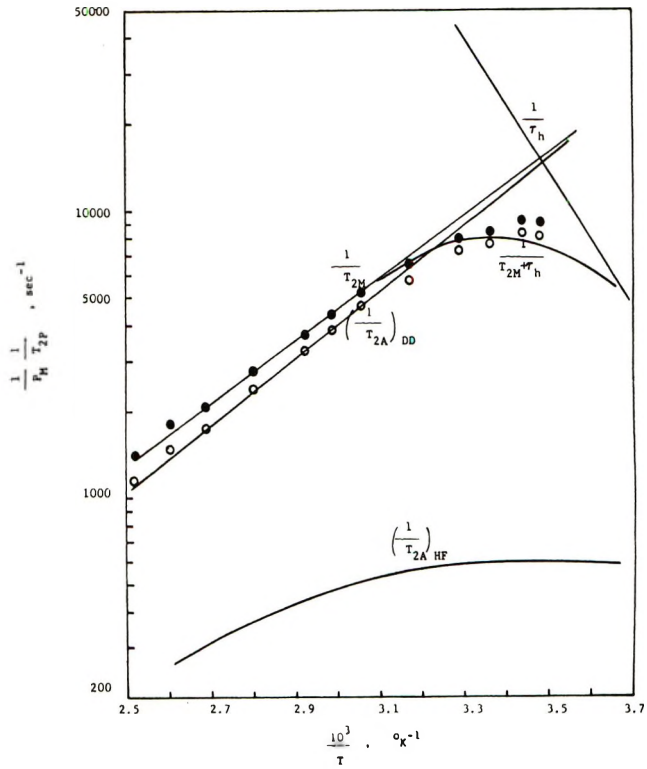

Figure 4. Temperature dependence of A proton relaxation rate in Mn(II)–NMBuL solution.

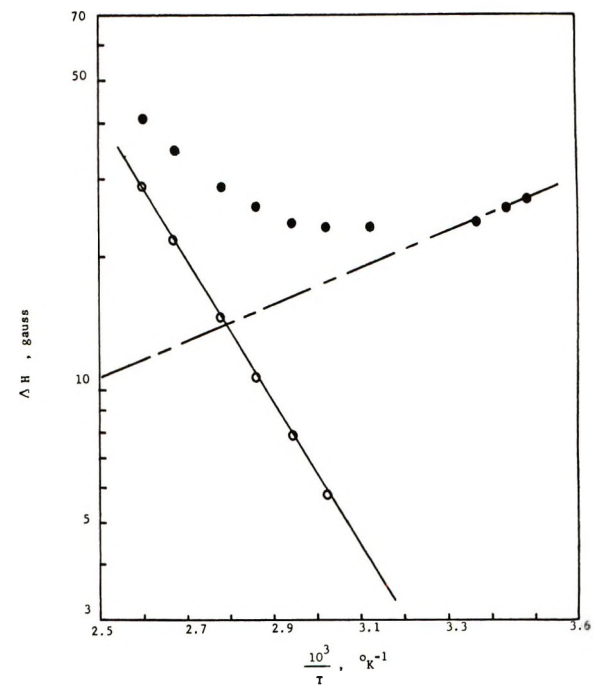

Figure 5. Plot of ln (epr line widths) *vs.* $1/T$ for Mn(II)–NMBuL solution at epr frequency of 8.92 kMHz.

(eq 9). At the low temperature, the line widths are broad and overlapping somewhat with neighbor line widths. The observed line width error for B protons is $\pm$1 Hz. Low-temperature data for A protons are less accurate than those for B protons because of partial

overlap resulting from A protons with C (or D) and B protons; therefore we used the value of τ_h estimated from B protons as the curve fitting.

The epr spectrum of a Mn(II)–NMBuL solution shows six lines and each line consists of five superposed components. We chose the fourth line width from the downfield end of the spectrum for consideration because of being the least affected by enhanced (inhomogeneous) broadening.[17] The temperature dependence of epr line widths of NMBuL solutions containing Mn(II) is shown in Figure 5. Fluctuations of the solvent environment about the solvated ions first proposed by Bloembergen and Morgan[2] can explain the low-temperature data. The activation energy, V_v, was found to be 1.83 kcal/mol, using low-temperature data. With eq 15 and 16, τ_v was estimated. Bleaney and Ingram[18] found $D = 0.018\ cm^{-1}$ and $E = 0$ for $MnSiF_6 6H_2O$ crystals and $D = 0.024\ cm^{-1}$ and $E \approx 0.01\ cm^{-1}$ for the Tutton salt, $(NH_4)_2Mn(SO_4)_2 6H_2O$, from an epr spectrum at room temperature. In these substances the Mn(II) ion is surrounded by an octahedron of water molecules in a manner similar to that proposed for the hydrated ion in solution. For lack of other information, we used the values of $D = 0.018\ cm^{-1}$ and $E = 0$ in eq 16 to estimate C_2^2. Best fit is obtained when $\tau_v = 2.96 \times 10^{-12}$ sec at 25°. Residual line widths obtained from substracting line widths due to the solvent-fluctuation process from observed line widths show a linear temperature dependence with a slope corresponding to 7.35 kcal/mol.

By correcting the frequency factor between epr frequency of 8.92 kMHz (≈13.6 MHz for proton) and proton nmr frequency of 60 MHz as indicated in eq 15, the low- and high-temperature electron relaxation times denoted by τ_{s1} and τ_{s2}, respectively, are used to obtain the total electron spin relaxation time τ_s shown in Figure 6 using the relation $\tau_s^{-1} = \tau_{s1}^{-1} + \tau_{s2}^{-1}$. If τ_h is estimated from nmr data, then from eq 14 τ_e is approximately equal to τ_s, since τ_s is much shorter than τ_h. If τ_h is assumed to be τ_{s2}, that is the ligand exchange acts as a strong perturbation to produce epr line broadening, τ_h is found to be 4×10^{-8} sec at 25° compared to 3.80×10^{-5} sec from nmr data. Because the nmr value is almost certainly associated with molecular ligand exchange, we must conclude that the epr high-temperature relaxation process is not that process.

Spin-exchange constants $A/\hbar$ were obtained from paramagnetic shifts and eq 17. The values of $A/\hbar$ are 2.26×10^5 and 3.40×10^5 Hz for A and B protons, respectively. These values of $A/\hbar$ remain constant within experimental error and are independent of concentration throughout the temperature range. At low temperatures, where chemical exchange becomes too slow to allow rapid mixing between the first solvation shell and the bulk solvents, the shift was observed to

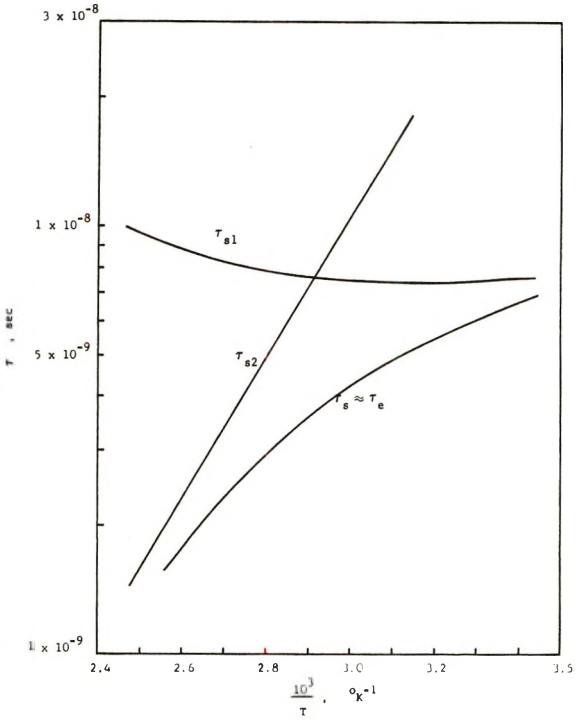

Figure 6. Plot of ln τ *vs.* $1/T$ at $\omega_I = 60$ MHz for Mn(II)–NMBuL solution.

decrease. As pointed out by several authors,[10] the coupling constant $A/\hbar$ is dependent on covalent bonding in the metal ion–ligand bond, for an ionic bonding cannot give rise to electron delocalization. No conclusion could be drawn from this study about covalency because there are several bonds between metal ion and the resonant nuclei which make it impractical to evaluate the overlaps. The contributions of $(1/T_2)_{HF}$ to the overall relaxation rates can be calculated from $A/\hbar$, τ_e, and eq 12. $(1/T_2)_{HF}$ is subtracted from the overall interactions. Figures 3 and 4 also show the contributions of $(1/T_2)_{HF}$ and $(1/T_2)_{DD}$ as a function of temperature. Within the experimental error, the activation energies for the dipolar interactions for A and B protons are 5.37 kcal/mol, which are reasonable values for ion tumbling.

The nature of the high-temperature electron spin relaxation processes is open to question. Garrett and Morgan[9] postulated a second process due to ligand exchange to interpret high-temperature line broadening for Mn(II) ions in the solvents: dimethylformamide (DMF), diethylformamide (DEF), and dimethyl sulfoxide (DMSO); however, lack of high-temperature line broadening for the water system was taken to be evidence for a concerted exchange mechanism. After reinspection of Garrett and Morgan data by Phillips,[8] it was found that only those solvents containing a

(17) R. G. Hayes and R. L. Meyers, *J. Chem. Phys.*, **40**, 877 (1964).
(18) B. Bleaney and D. J. E. Ingram, *Proc. Roy. Soc., Ser. A*, **205**, 336 (1951).

double bond, and hindered rotation of proton groups in the solvated ion, exhibit the high-temperature line-broadening behavior. Another process, namely, distortion of the octahedral symmetry of the complex ion by free rotation of the bulky methyl groups, was also proposed. If it were true, the cyclic structure of NMBuL would not be expected to exhibit the enhanced line broadening due to the impossibility of free rotation about the C–N bond even at high temperature, so another mechanism is required to explain the electron spin relaxation processes in the present study.

A complex ion model was constructed partly with the aid listed by Vilkov, Akishin, and Presnyakova[19] for the bond angles and distances of the amide structure in DMF. The Mn–O internuclear distance was assumed to be the sum of ionic radii for octahedrally coordinated Mn(II) ion (0.82 Å) and O^{2-} ion (1.40 Å).[20] The nitrogen is assumed to be tetrahedral in this model. The average distances between the various protons and the Mn(II) ion for Mn–O–C angles are summarized in Table I. There is excellent agreement between the experimental data and those calculated from models with Mn–O–C angles between 90 and 130° using varying extents of deviation from the mean plane of the NMBuL molecule. Nonlinear models for DMF molecules coordinated to Mn(II) (angle Mn–O–C = 109–120°) and Co(II) (angle Co–O–C = 140°) have also been reported by nmr techniques.[7,8] Cotton and Soderberg[21] found the angle Co–O–P to be 136° from an X-ray crystallagraphic study on $Co(C(CH_3)_3PO)_2(NO_3)_2$. No explanations can be offered for the variation in bond angles for the several cases. However, we feel the model deduced from nmr line-broadening techniques is merely suggestive because of the many assumptions inherent in the application of eq 11.

One of the assumptions made in the preceding interpretation was that the bonding about the nitrogen atom is essentially tetrahedral, in contrast with the trigonal arrangement in the free ligand. Distribution of electrons is certainly different in the two cases and the positive character of the central metal ion should result in removal of electronic constraints to planarity at the nitrogen atom in the complex. Experimentally, Mn–H distances obtained from dipolar relaxation data would require that the Mn–O–C angle be less than 90° if the nitrogen is trigonal planar. Such an angle is not compatible with the requirements for packing six ligands about the central atom. The tetrahedral arrangement for nitrogen bonds allows much more reasonable Mn–O–C bond angles to be chosen.

Linearity of the temperature dependence for dipolar interaction of A and B protons implies constancy of average distanced between the individual protons and the metal ion in the high-temperature relaxation processes and rules out the possibility of rotation about the carbonyl bond. Rotation of NMBuL molecules in the solvated ion about the oxygen–metal ion bond, which acts as a strong perturbation, might be responsible for the high-temperature electron relaxation. Drago and his coauthors[22] have studied a series of amides of the type $R_1C(CO)NR_2R_3$. It was found that whenever R_1 and R_2 are both alkyl groups, lower values for Dq and β result for the six coordinate nickel complexes than when either R_1 or both R_2 and R_3 are hydrogens. It was proposed that a steric effect exists between neighboring coordinated amide molecules in metal complexes. The same conclusion was reached for a series of lactam complexes.[15] The hindered rotation of the ligand about the oxygen–metal bond would result in a marked distortion of the octahedral symmetry of the complex.

(2) *Mn(II)–HMPA.* The proton magnetic resonance spectrum of HMPA was found to consist of two peaks of equal intensity separated by 9.7 ± 0.3 Hz. The doublet could be due to phosphorus–hydrogen coupling or to nonequivalent methyl groups. No evidence was seen for rotational isomerism which could be manifested in this spectrum as a further splitting of the two components of the doublet. Mortimer[23] has explained the doublet observed in the fundamental stretching band at 1290 cm^{-1} for the PO bond of $(CH_3O)_3PO$ by invoking rotational isomerism. No splitting of the P–O fundamental stretching band at 1300 cm^{-1} for HMPA was observed in the present study. Pople[24] has pointed out recently there is no guarantee that the protons of any given pair of rota-

Table I: Calculated Ion–Proton Internuclear Distances for the Mn(II)–NMBuL Complex Ion[a]

Mn–O–C angle, deg	r_A, Å	r_B, Å	r_A/r_B
90[b]	5.00	4.80	1.042
180[b]	4.25	6.00	0.71
130[c]	5.00	4.80	1.042
Experimental[d]			1.042

[a] Mn–O bond is trans to C–N bond with respect to C=O bond. [b] All configurations are taken to be a plane formed by NMBuL molecule except for the hydrogen atoms of methylene groups and the methyl group. [c] Calculated from the model: planar with maximum deviation of 0.17 Å from the mean plane, except for the hydrogen atoms of methylene groups and methyl group. [d] Calculated from dipolar relaxation rates at $10^3/T$ = 3.1 (see Figures 3 and 4) and the dipolar term in eq 11.

(19) L. V. Vilkov, P. A. Akishin, and V. M. Presnyakova, *Strukt. Khim.*, 3, 5 (1962).

(20) H. A. Wells, "Structural Inorganic Chemistry," Oxford University Press, London, 1962.

(21) F. A. Cotton and R. H. Soderberg, *J. Amer. Chem. Soc.*, 85, 2402 (1963).

(22) R. S. Drago, D. W. Meek, M. D. Joeston, and L. Laroche, *Inorg. Chem.*, 2, 124 (1963).

(23) F. S. Mortimer, *Spectrochimica*, 9, 270 (1957).

(24) J. A. Pople, *Mol. Phys.*, 1, 3 (1959).

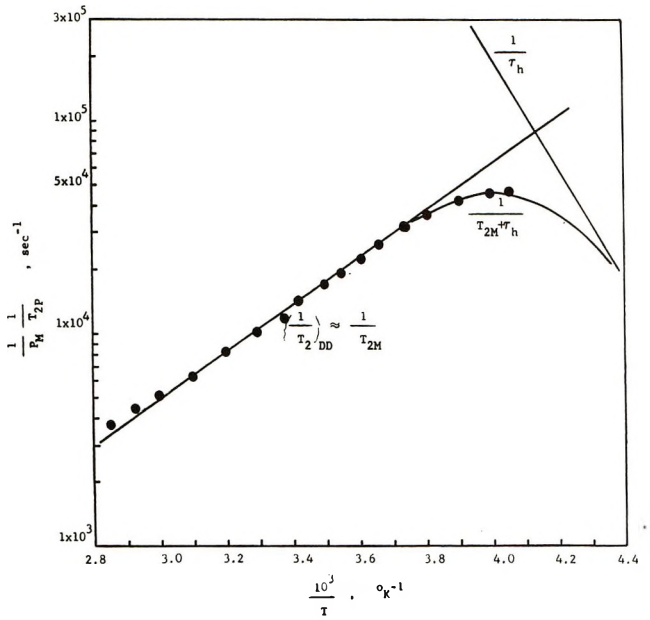

Figure 7. Temperature dependence of proton relaxation rate in Mn(II)–HMPA solution.

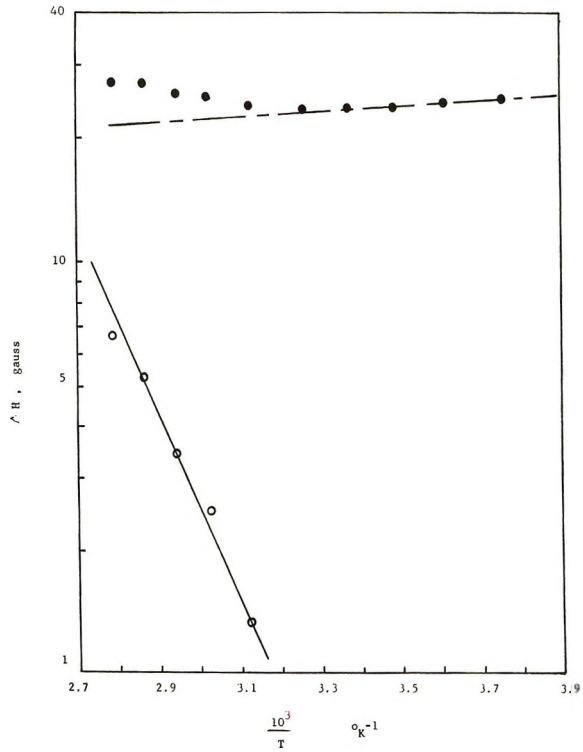

Figure 8. Plot of ln (epr line widths) *vs.* $1/T$ for Mn(II)–HMPA solution at epr frequency of 8.92 kMHz.

tional isomers will be magnetically nonequivalent or that the rotational isomers will have lifetimes long enough that they may be observed by nmr. The temperature variation of the doublet separation was found to be 9.7 ± 0.3 Hz in the temperature range 25–150°, and the proton magnetic resonance spectrum of an HMPA solution of $Zn(HMPA)_4(ClO_4)_2$ comprises a doublet separated by 9.8 Hz. That is good evidence that the doublet arises from coupling between phosphorus and hydrogen, for the nonequivalence of the two methyl groups would not be expected to have temperature independence of splitting or be identical in the complex and pure HMPA. Values for J_{P-H} of approximately 10 Hz have also been reported for similar compounds.[25,26]

The nmr spectra of Mn(II)–HMPA complex consist of only one peak. The line width of the methyl resonance in the 0.01 *M* $Mn(HMPA)_4^{2+}$ solution at 120° is 10 Hz, and no hump could be observed even at low solute concentrations where quite narrow spectra are obtained. The doublet resonance also was not observed in the Ni(II)–HMPA complex.[27] The phosphorus must be decoupled from hydrogen by some process in the paramagnetic complex. The delocalization of the unpaired electron of Mn(II) ion places odd electron density in the ligands. The unpaired electron in the phosphoryl orbitals must be strongly coupled with the phosphorus nuclear spin causing very rapid relaxation, thus effectively decoupling the phosphorus from the methyl protons.

The temperature dependence of proton relaxation in Mn(II)–HMPA solutions is shown in Figure 7. Most of the data were obtained for 0.10 *M* solution. Analyses of these data were described in the preceding section.

The temperature dependence of epr line width in Mn(II)–HMPA solution is plotted in Figure 8. The solvent-fluctuation electron relaxation process proposed by Bloembergen and Morgan[2] also serves to interpret our low-temperature data. The low value of the activation energy, V_v = 0.32 kcal/mol, is inconsistent with expectation. The highly symmetrical HMPA solvation ion should have a high value, since activation energy is a measure of the distortion barrier of complex ion. However, due to large repulsions among six methyl groups, internal ligand processes may result in lowering the value. Residual line widths at high temperature show linear temperature dependence with a slope of 10.7 kcal/mol. The value of τ_h estimated from nmr data is 1.00×10^{-7} sec at 25° compared with epr relaxation, 1.6×10^{-7} sec. The ligand exchange might play a very important role in the high-temperature broadening. Free rotation of the bulky methyl groups about partial double bond character of N–P bonds (see next paragraph) could also contribute to the high-temperature broadening.

The visible spectra of iodine and HMPA–iodine solutions are shown in Figure 9. The absorption band maximum for iodine (core plus $\sigma^2\pi^4\pi^{*4}$) occurs at about 524 mμ in the solvent CCl_4 and has been assigned to

(25) A. H. Cowley and R. P. Pinnell, *J. Amer. Chem. Soc.*, 87, 4454 (1965).

(26) N. Muller, P. C. Lauterbau, and J. Goldenson, *ibid.*, 78, 3557 (1956).

(27) B. B. Wayland and R. S. Drago, *ibid.*, 87, 2372 (1965).

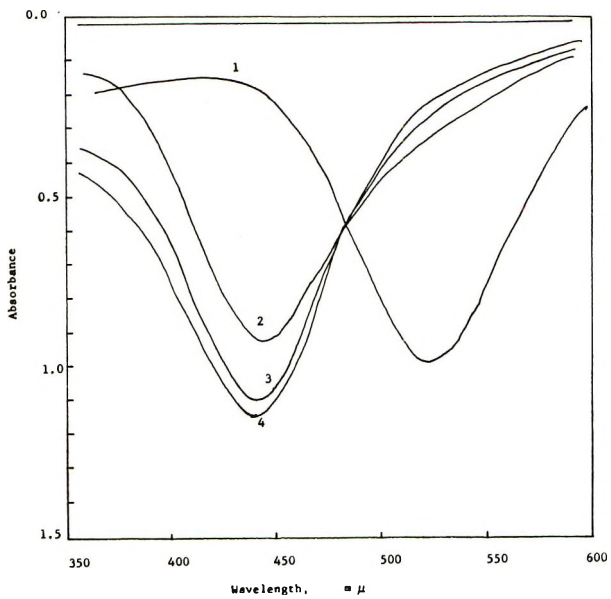

Figure 9. Spectra of iodine and HMPA–iodine solutions: 1, 0.00108 M I_2 in CCl_4; 2, 0.05710 M HMPA in CCl_4; 3, 0.11420 M HMPA in CCl_4; 4, 0.17130 M HMPA in CCl_4. All data taken at 25° in visible region; 2, 3, and 4 solutions are same I_2 concentration (0.00108 M I_2).

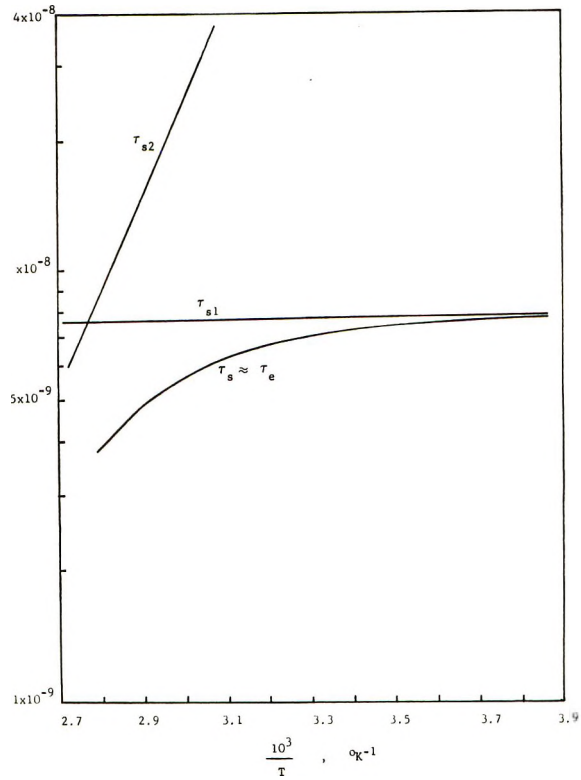

Figure 10. Plot of ln τ *vs.* $1/T$ at ω_I = 60 MHz for Mn(II)–HMPA solution.

a $\pi^* \rightarrow \sigma^*$ transition, while a blue shift is observed from 524 mμ in pure solvent to 440 mμ in the HMPA–iodine solutions and the band assigned to a $\pi_c^* \rightarrow \sigma^*$ transition.[28] The existence of an isosbestic point at 484 mμ indicates that there are two absorption species in the system: presumably free iodine and the iodine complex. From the variation in intensity at 440 mμ as a function of HMPA added, the equilibrium constant was calculated to be 25, and the molar extinction coefficient of the complex was 2×10^3 l./mol at 25°, by employing Drago's equation.[29] The O–H stretching frequency shift of phenol upon complexation with HMPA was also observed to be 460 cm^{-1}. For lack of information about a suitable series, it is impossible to compare donor properties of phosphoryl oxides; but they are apparently greater than those of $(CH_3O)_3PO$ (the equilibrium constant with I_2, 3.3, and O–H stretching frequency shift of phenol, 130 cm^{-1}). Cowley and Pinnell[25] have shown that J_{PNCH} is larger than the J_{PCH} in the methyl-substituted aminophosphines and concluded that some double bonding exists between the nitrogen and phosphorus atom, so we say that there is some double bonding between the nitrogen and phosphorus atoms which presumably involves P_π–d_π bonding between a filled nitrogen 2p orbital and empty phosphorus 3d orbital.

Figure 10 shows the behavior of τ_e as a function of temperature. τ_{s1} was corrected to 60 MHz using the values of D = 0.018 cm^{-1} and E = 0, eq 15 and 16. The spin-exchange constant, $A/\hbar$, was found from paramagnetic shifts and eq 17 to be 7×10^4 Hz. With τ_e, $A/\hbar$, and eq 12, $(1/T_2)_{HF}$ was calculated. It may be concluded from these values that $(1/T_2)_{HF}$ is negligible in the temperature range studied. The dipolar activation energy, V_c, was found to be 5.54 kcal/mol.

Not all possible mechanisms for electron relaxation can be determined from these studies. However, in addition to the solvent-fluctuation process, the electron relaxation mechanisms at high temperature might depend on one (or some combination) of the following factors: (1) the symmetry of the ligand; (2) the rotation about metal–ligand bond axis; (3) ligand exchange; or (4) restricted rotation of particular groups about partial double bonds in the ligand.

Summary and Conclusions

Temperature dependence of $1/T_{2P}$ for Mn(II)–NMBuL and Mn(II)–HMPA solutions was measured by nmr techniques. The "excess" relaxation rates were analyzed in terms of dipolar and spin exchange (negligible for Mn(II)–HMPA) at high temperature; chemical exchange and spin exchange (negligible for Mn(II)–HMPA) at near frozen temperature. Chemical exchange and ion tumbling activation energies (V_h and V_r) were determined from these data, as well as chemical exchange correlation time, τ_h, and ion tum-

(28) R. S. Drago, "Physical Methods in Inorganic Chemistry," Reinhold, New York, N. Y., 1965, p 156.

(29) N. J. Rose and R. S. Drago, *J. Amer. Chem. Soc.*, **81**, 6138 (1959).

Table II: Comparison of Relaxation Rate Parameters of Mn(II)–NMBuL and Mn(II)–HMPA Solutions with Mn(II)–DMF Solution[a]

Solvent parameters	NMBuL	HMPA	DMF[b]
V_r, kcal/mol	5.37	5.54	3.50
τ_r, sec	6.10×10^{-11}		2.90×10^{-11}
V_h, kcal/mol	9.20 ± 1.40	12.20	9.10
τ_h, sec	$(3.80 \pm 0.70) \times 10^{-5}$	1.00×10^{-7}	4.20×10^{-7}
V_v, kcal/mol	1.83	0.32	2.20
τ_v, sec	2.96×10^{-12}	2.97×10^{-12}	2.50×10^{-12}
τ_s, sec	6.50×10^{-9}	7.20×10^{-9}	5.85×10^{-9}
$\Delta H^{\pm}$, kcal/mol	9.20 ± 1.40	12.20	8.90
$\Delta S^{\pm}$, eu	-5.85 ± 2.90	10.30	0.73

[a] All values at 25°. [b] Data from ref 8.

bling correlation time, τ_r. Results of these determinations are summarized in Table II, where they are compared to those made in Mn(II)–DMF solutions.

Paramagnetic shifts were measured as a function of temperature to permit calculation of spin-exchange constants. The constants were temperature independent throughout most of the experimental temperature range except at low temperature. At low temperatures, where chemical exchange becomes too slow to allow rapid mixing between the first solvation shell and the bulk solvent, the shift was observed to decrease.

The visible spectra of I_2 and HMPA–I_2 solutions and the infrared spectra of OH stretching frequency shift of phenol upon complexation with HMPA show that there is some double bonding between the nitrogen and phosphorus atoms. The doublet of the proton magnetic resonance spectrum of HMPA is confirmed to be coupling from the phosphorus nucleus.

Temperature dependence of electron spin resonance line widths of solvated Mn(II) ion in the NMBuL solution was determined. Solvent fluctuations about the complex ion proposed by Bloembergen and Morgan were applicable to low-temperature data. However, evidence for a second relaxation mechanism was observed at high temperature with an activation energy of 7.35 kcal/mol. It is proposed that highly hindered rotation of ligand molecules about the Mn(II)–O bond in the complex ion results in a marked increase in perturbation of the ion symmetry without necessarily influencing the chemical exchange rate.

The variation in epr line widths of Mn(II)–HMPA solutions was also measured. Low-temperature data were interpreted by the solvent-fluctuation electron process. However, due to large repulsions among the six methyl groups of HMPA, intramolecular processes may lead to perturbations having a low value of V_v. For high-temperature data, free rotation of the bulky methyl groups about the N–P bond and ligand exchange may act as a strong perturbation which is responsible for high-temperature broadening, if the Mn–O–P bond angle is assumed to be 180°. On the other hand, if that angle is less than 180°, hindered rotation about the Mn–O bond may be responsible for high-temperature electron relaxation, as in the NMBuL case. Dipolar relaxation rates cannot be used to evaluate the bond angle from geometry of the complex ion because of uncertainty as to orientation of the methyl groups in the microcrystalline unit.

Vapor-Phase Electron Donor–Acceptor Complexes of Tetracyanoethylene and of Sulfur Dioxide[1]

by Ichiro Hanazaki[2]

The Laboratory of Molecular Structure and Spectra, Department of Physics, University of Chicago, Chicago, Illinois 60637
(Received August 16, 1971)

Publication costs assisted by the University of Chicago

The electron donor–acceptor complexes of benzene, toluene, *o*-xylene, and naphthalene with tetracyanoethylene (TCNE) and of *trans*-2-butene with sulfur dioxide were investigated spectrophotometrically in the vapor phase. The results obtained at various temperatures were analyzed simultaneously by a modified least-squares treatment of the Scott equation. The results show that the differences between the thermodynamic and spectral properties obtained in the vapor phase and those obtained in solution are in accordance with general tendencies observed so far. However, in contrast to previous results, the intensity of the charge-transfer (CT) absorption band of the TCNE complexes with methylbenzenes is found to increase upon methyl substitution, in parallel with the heat of formation. This is in accordance with the theoretical prediction derived on the assumption that the donor–acceptor bond is mainly of CT nature. Attempts to study vapor-phase CT spectra in a number of other systems were made but were unsuccessful. A brief discussion is based on these results.

Introduction

Since the necessity for the vapor-phase study of electron donor–acceptor molecular complexes was recognized, several investigations have been performed on this subject,[3-7] including iodine complexes with ethyl ether,[4] benzene,[4,5a] *p*-xylene, mesitylene,[5b] dimethyl sulfide,[7] diethyl sulfide,[5a,7] and tetrahydrothiophene;[7] tetracyanoethylene complexes[7] with *p*-xylene, *o*-xylene, mesitylene, and durene; and carbonyl cyanide complexes with ethyl ether, dioxane, benzene, and toluene.[6] However, it seems to be necessary to accumulate more vapor-phase data so as to provide a sound basis for theoretical considerations on the nature of the bonding and for the study of the solvation effect. In addition, there are some questions about the accuracy of the existing vapor-phase data, indicating a necessity for a more detailed examination of the experimental error.[3]

In the present work, the vapor-phase study of tetracyanoethylene (TCNE) complexes is extended to those with benzene, toluene, and naphthalene as electron donors. Because of experimental difficulty in the vapor-phase study, we have a relatively large error in separating the equilibrium constant (K) and molar extinction coefficient (ϵ) from their product. For instance, the two independent studies[5a,7] of the iodine–diethyl sulfide system show remarkable discrepancies in K and ϵ, though they give almost the same value for the $K\epsilon$ product. In view of this, the TCNE–*o*-xylene system has been reinvestigated in the present work and is compared with the previous result.[7]

The experimental difficulty is mainly due to the low concentration (vapor pressure) of one of the component substances (usually donor). The donor substances which are favorable for the optical determination of the equilibrium usually have lower vapor pressures around the room temperature, so that it is necessary to undertake the measurement at relatively high temperatures. This experimental condition often accelerates chemical reaction. Furthermore, the K and ϵ values must be extrapolated to room temperature in order to be compared with solution values. This might cause a large error. From this point of view, several donor–acceptor systems with relatively high vapor pressures were examined in addition to the TCNE complexes, in the hope to observe complex formation around room temperature. However, stable complex formation could not be observed except for the sulfur dioxide–olefin system reported here.

Experimental Section

Materials. TCNE (Eastman) was sublimed twice under high vacuum at 60–70°, and stored in a vacuum desiccator over phosphorus pentoxide. Sulfur dioxide (Matheson) was dried by passing it through a tube containing phosphorus pentoxide, and it was fractionally distilled. Benzene and toluene were purified

(1) This research was supported by the Office of Naval Research under Contract N00014-67-A-0285-0001.

(2) Address correspondence to the author at The Institute of Physical and Chemical Research, Wako-shi, Saitama, Japan.

(3) (a) R. S. Mulliken and W. B. Person, "Molecular Complexes," Wiley-Interscience, New York, N. Y., 1969; (b) R. Foster, "Organic Charge Transfer Complexes," Academic Press, New York, N. Y., 1969.

(4) F. T. Lang and R. L. Strong, *J. Amer. Chem. Soc.*, **87**, 2345 (1965).

(5) (a) M. Tamrès and J. M. Goodenow, *J. Phys. Chem.*, **71**, 1982 (1967); (b) J. W. K. Duerksen and M. Tamres, *J. Amer. Chem. Soc.*, **90**, 1379 (1968).

(6) J. Prochorow and A. Tramer, *J. Chem. Phys.*, **44**, 4545 (1966).

(7) M. Kroll, *J. Amer. Chem. Soc.*, **90**, 1097 (1968).

by the standard method[8] and were fractionally distilled twice. *o*-Xylene was refluxed with sodium metal and was fractionally distilled twice. Naphthalene was recrystallized twice from ethanol and sublimed twice. *trans*-2-Butene (Phillips) was passed through anhydrous calcium sulfate and sodium metal sputtered on glass wool.

Apparatus and Procedure. The spectrophotometer, absorption cell, and electric furnace used for the present measurements are the same as those used by Kroll,[7] with some minor modifications.

The amount of TCNE was determined in the following manner. A small ampoule (*ca.* 20 × 6 mm ϕ) with a breakable end was attached to the 10-mm glass tube (Figure 1). It was evacuated and weighed. An approximate amount of TCNE was placed in this ampoule in a drybox. It was then evacuated again, cooled by liquid nitrogen, and sealed off at A. The ampoule and glass tube were reweighed and the difference gave the amount of TCNE after an approximate correction for the buoyancy. The correction was about 0.2 mg, which was ~1–2% of the net amount of TCNE.

An approximate desired amount of benzene or toluene was transferred into a small bulb with a break-seal by vacuum distillation through a phosphorus pentoxide tube. It was then degassed, frozen, and sealed off. The difference between the weights gave the amount of the donor (0.5–5 g) after the buoyancy correction (less than 1% of the amount of donor). *o*-Xylene and naphthalene were transferred directly in a drybox into a bulb with break-seal.

In the measurement on the TCNE complex, the acceptor and donor were placed in the absorption cell as shown in Figure 1. After being evacuated with baking out, the cell was sealed off from the vacuum line (at 10^{-4} to 10^{-5} mm), and the base line of absorbance was measured on the spectrophotometer. The ampoule and break-seal were then crushed by the breaker, and TCNE and donor were condensed in B and D, respectively, by lightly flaming the side arms. The side arms were then sealed off at C and E.

In the measurements on the sulfur dioxide complex, the amount of donor and acceptor was determined by measuring the vapor pressure in a thermostated glass bulb of known volume. A correction for gas imperfection was applied. The donor and acceptor are transferred by vacuum distillation through a tube containing drying reagent (sodium for the acceptor and phosphorus pentoxide for the donor) into the side arms of the absorption cell. A stopcock was used when the acceptor absorption was measured. It was sealed off from the cell before the measurement of the equilibrium was made.

After the absorption cell (*ca.* 90 cm path length) containing the donor–acceptor mixture was sealed off, it was placed in the oven together with the reference cell,

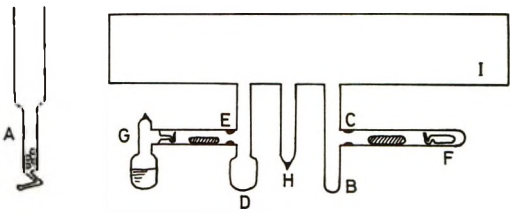

Figure 1. Illustration of the procedure to introduce donor and acceptor. An ampoule containing TCNE is placed at F. The small bulb containing donor (G) is connected to the absorption cell (I) through a break-seal. The cell is then evacuated through H and sealed off.

and the oven was heated to the highest temperature necessary in the measurement. It was left until the absorption spectrum showed no change. The temperature was then lowered by steps of 10–20°, and the absorption spectrum was recorded at least twice at each temperature. The fluctuation of the temperature with time and the deviation along the absorption cell were less than 0.5°, which corresponds to an error of ~1% of the K value.

Analysis of the Data

The data obtained in the present work were fitted to the modified Scott equation[5a,9]

$$adl/\Delta D = (1/\Delta\epsilon)(d + a) + 1/(K_c\Delta\epsilon) \qquad (1)$$

where a and d are the initial concentrations (mol/l.) of the acceptor and donor, respectively, l is the optical path length (cm), and K_c is the equilibrium constant defined on the basis of concentration. ΔD and $\Delta\epsilon$ are defined by

$$\begin{aligned} \Delta D &= D - D_A - D_D \\ \Delta\epsilon &= \epsilon_C - \epsilon_A - \epsilon_D \end{aligned} \qquad (2)$$

where ϵ_C, ϵ_A, and ϵ_D are the molar extinction coefficients of the complex, acceptor, and donor, respectively, D is the optical density, and D_A and D_D are the absorbances due to the acceptor and donor, respectively, corresponding to their initial concentrations.

Since the accurate determination of ϵ_C or $\Delta\epsilon$ is difficult in vapor-phase work, the ϵ values obtained from the slope of eq 1 for various temperatures (*cf.* Figures 3 and 4) are usually averaged to give the "best" value. However, this procedure causes some ambiguities in the estimated error limit (*e.g.*, standard deviation). Therefore, in the present work, a modified least-squares treatment of eq 1 was employed for the purpose of removing those ambiguities.

If we define new quantities; $y_{ij} = adl/\Delta D$, $x_i = a + d$, $\alpha = 1/\Delta\epsilon$, and $\beta_j = 1/(K_c\Delta\epsilon)$, eq 1 is rewritten in the form

$$y_{ij} = \alpha x_i + \sum_k \delta_{kj}\beta_k \qquad (3)$$

(8) A. Weissberger and E. S. Proskauer, "Organic Solvents," 2nd ed, Interscience, New York, N. Y., 1967.

(9) R. L. Scott, *Recl. Trav. Chim.*, **75**, 787 (1956).

Table I: Experimental Conditions Employed for the TCNE Complexes

	Benzene	Toluene	*o*-Xylene	Naphthalene
Temperature, °C	105 ~ 140	118 ~ 170	120 ~ 180	160 ~ 210
Concentration,[a] *M*				
Donor	$5.78 \times 10^{-3} \sim 3.66 \times 10^{-2}$	$5.19 \times 10^{-3} \sim 3.65 \times 10^{-2}$	$5.45 \times 10^{-3} \sim 2.00 \times 10^{-2}$	$2.12 \times 10^{-3} \sim 7.76 \times 10^{-3}$
TCNE	$4.68 \times 10^{-5} \sim 1.06 \times 10^{-4}$	$3.72 \times 10^{-5} \sim 4.07 \times 10^{-4}$	$5.45 \times 10^{-5} \sim 1.44 \times 10^{-4}$	$1.13 \times 10^{-4} \sim 5.85 \times 10^{-4}$
λ_0[b]	345	370	390	480

[a] Two concentrations connected by ~ indicate the lowest and highest concentrations employed in the measurement. [b] Wavelength (mμ) at which the least-squares analysis was made.

Table II: Thermodynamic and Spectroscopic Data of the TCNE Complexes of Benzene, Toluene, and *o*-Xylene

	Benzene			Toluene		*o*-Xylene		
	Vap[e]	Soln[f]	Soln[g]	Vap[e]	soln[g]	Vap[e]	Vap[h]	Soln[g]
ν_{max}, 10^3 cm^{-1} [a]	28.95	26.1	26.0	27.1	24.6	25.39	25.38	23.3
$\Delta\nu_{1/2}$, 10^3 cm^{-1} [b]	5.90	5.55	...	6.6	...	6.4	6.1	...
ϵ_{max}, l. mol^{-1} cm^{-1}	770 ± 120	2330	3570	1150 ± 140	3330	1730 ± 230	1100 ± 350	3860
f[c]	0.019 ± 0.003	...	...	0.033 ± 0.004	...	0.048 ± 0.006	0.029 ± 0.009	0.11
K_c (25°), l. mol^{-1}	49 ± 30	0.938	0.12	76 ± 11	0.23	197 ± 12	350 ± 120	0.45[i]
K_c (100°), l. mol^{-1}	6.6 ± 3.6	...	...	8.1 ± 1.0	...	14.0 ± 0.7	23.6 ± 6.4	...
$K_c\epsilon$ (25°), 10^3 l.^{2} mol^{-2} cm^{-1}	38 ± 23	2.2	0.44	87 ± 13	0.76	340 ± 20	...	...
$K_c\epsilon$ (100°), 10^3 l.^{2} mol^{-2} cm^{-1}	5.0 ± 2.7	...	...	9.3 ± 1.2	...	24.2 ± 1.2	26.0 ± 1.9	...
ΔU, kcal mol^{-1} [d]	−6.0 ± 0.3	...	...	−6.63 ± 0.07	...	−7.80 ± 0.03	−8.0 ± 0.5	...
ΔH, kcal mol^{-1} [i]	−6.6 ± 0.3	−3.12	−2.30	−7.22 ± 0.07	−2.72	−8.39 ± 0.03	−8.7 ± 0.5	...
ΔS, eu	−12.2 ± 0.7	−10.6	−11.9	−13.6 ± 0.2	−12.1	−15.64 ± 0.07	−17.0 ± 2.0	...

[a] Maximum of the CT absorption band. [b] Half-width. [c] Oscillator strength. The error limit was estimated assuming that the relative error was the same as that of ϵ_{max}. [d] Standard change of the internal energy based on the standard state of 1 mol/l. [e] This work. The error limit shown is the standard deviation obtained in the least-squares treatment. [f] Reference 10. In carbon tetrachloride. The data are given for 25° (calculated from the original data given at 20°). [g] Reference 11. Methylene chloride solution. The data are given for 25° (calculated from the original data given at 22°). The K_c values are calculated from the original data given for K_x (equilibrium constant based on mole fraction) [W. C. Herndon and R. D. Goodin, *J. Phys. Chem.*, **73**, 2793 (1969)]. [h] Reference 7. [i] Value at 25°. The vapor-phase value of ΔH was calculated from ΔU assuming the ideal-gas behavior; $\Delta H = \Delta U - RT$. [j] Value at 22°.

where δ_{kj} is the Kronecker δ, the subscript i denotes the measurement characterized by the combination of a and d, and the subscript j denotes the temperature at which the measurement is made. Taking y_{ij}, x_i, and δ_{kj} as known variables, and α and β_k as unknowns to be determined, the data obtained at various temperatures can be treated simultaneously by a single least-squares treatment, on the assumption that $\Delta\epsilon$ is independent of temperature.

Results

The experimental conditions employed for TCNE complexes with benzene, toluene, *o*-xylene, and naphthalene are summarized in Table I. Results are given in Tables II and III, together with those obtained in solution.[10,11]

The relative absorbance of the TCNE–benzene complex at a given wavelength to that at 345 mμ, where the least-squares analysis was made, was calculated for one of the eight measurements. Since the calculated relative absorbance shows little temperature dependence, the results were averaged over temperatures, giving the best relative absorption curve. From this and the value ϵ_C = 766 l. mol^{-1} cm^{-1} at 345 mμ, obtained by the least-squares analysis, the CT absorption band was determined as shown in Figure 2.

The result of the Scott plot for the TCNE–toluene system is shown in Figure 3. The Liptay analysis[12] was also made for seven measurements obtained at 148.0°. The ζ matrix shows that the deviation from the average value, $\bar{\zeta}_\lambda$, at given wavelength λ, is less than 2% for 320–430 mμ. From $\bar{\zeta}_\lambda$ and the absorbance

(10) G. Briegleb, J. Czekalla, and G. Reuss, *Z. Phys. Chem.* (*Frankfurt am Main*), **30**, 316, 333 (1961).

(11) R. E. Merrifield and W. D. Phillips, *J. Amer. Chem. Soc.*, **80**, 2778 (1958).

(12) W. Liptay, *Z. Elektrochem.*, **65**, 375 (1961).

Table III: Thermodynamic and Spectroscopic Data of the TCNE–Naphthalene Complex[a]

	Band I			Band II		
	Vap[b]	Soln[c]	Soln[d]	Vap[b]	Soln[c]	Soln[d]
ν_{max}, 10^3 cm^{-1}	20.97	18.2	18.2	26.05	23.4	23.4
$\Delta\nu_{1/2}$, 10^3 cm^{-1}	4.0	3.95	...	5.1	4.05	...
ϵ_{max}, l. mol^{-1} cm^{-1}	575 ± 167	1640	1240	610 ± 117	1660	1120
f	0.010 ± 0.003	...	...	0.014 ± 0.004	...	...
K_c (25°), l. mol^{-1}	381 ± 73	2.93	0.75			
K_c (100°), l. mol^{-1}	35 ± 6	...	...			
$K_{c\epsilon}$ (25°), 10^3 l.^{2} mol^{-2} cm^{-1}	219 ± 41	4.8	...			
$K_{c\epsilon}$ (100°), 10^3 l.^{2} mol^{-2} cm^{-1}	20 ± 3	...	...			
ΔU, kcal mol^{-1}	−7.08 ± 0.09	...	...			
ΔH, kcal mol^{-1}	−7.67 ± 0.09	−3.84	...			
ΔS, eu	−11.9 ± 0.2	−10.8	...			

[a] See the footnotes to Table II for the definitions of symbols. [b] This work. The error limit indicated is the standard deviation. [c] Reference 10. In carbon tetrachloride. The data for 25° were calculated from the original ones given for 20°. [d] Reference 11. Measured in methylene chloride at 22°. See footnote *g* in Table II.

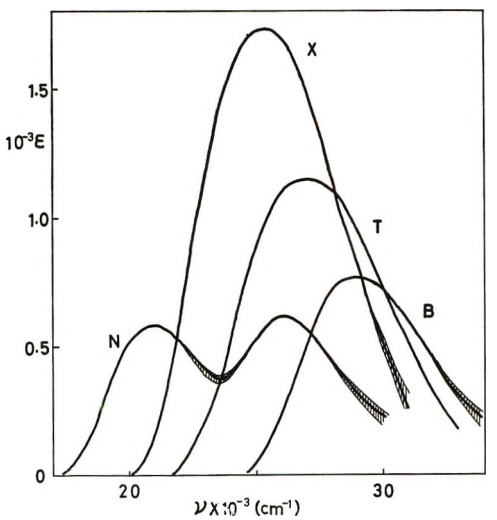

Figure 2. CT absorption spectra of the TCNE complexes with benzene (B), toluene (T), *o*-xylene (X), and naphthalene (N). The shaded parts indicate the relative change of ϵ_C with temperature.

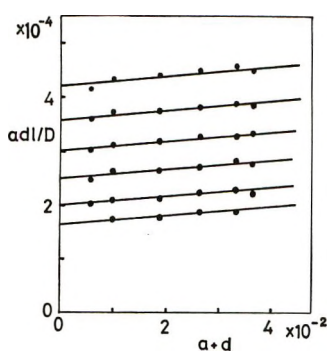

Figure 3. The Scott plot for the TCNE complex with toluene. The temperatures are (from the top) 167.4, 157.8, 148.0, 138.0, 127.2, and 118.2°.

at λ, the estimated absorbance at 370 mμ was computed for each measurement, averaged over λ, giving the best values of the absorbance in each measurement. The

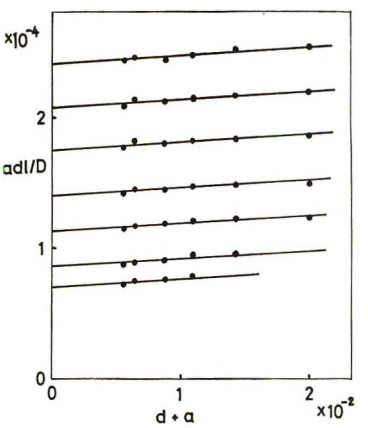

Figure 4. The Scott plot for the TCNE complex with *o*-xylene. The temperatures are (from the top) 175.3, 167.4, 159.1, 148.7, 139.4, 127.8, and 119.5°.

difference between the best value and the original absorbance at 370 mμ was less than 1% in all measurements.

The Scott plot for the TCNE–*o*-xylene system is shown in Figure 4. For one of the seven measurements, relative absorbances were computed at various temperatures. The deviation with temperature was less than 1%. The best relative absorbance curve, obtained by averaging the relative absorbances over temperature, combined with the least-squares value, ϵ_C = 1720 at 390 mμ, gives the CT absorption curve shown in Figure 2.

The Liptay analysis was applied to all seven measurements for the TCNE–naphthalene system at 179.1°. The deviation of ζ at given λ from the average value, $\bar{\zeta}_\lambda$, is less than 3% for 370–540 mμ. The difference between the best absorbance at 480 mμ and the original absorbance was less than 2% for each measurement. From this best relative absorbance, combined with the least-squares value ϵ_C = 573.0 at 480 mμ, the CT absorption curve was obtained as shown in Figure 2.

The temperature dependence of the relative absorption was also examined for one of the measurements. The deviation from the average value was less than 3% between 360 and 540 mμ.

For all TCNE complexes studied here, the light absorption due to the free TCNE molecule does not affect the absorbance due to the CT transition, whereas a small correction was necessary for the absorption due to the free donor.

The sulfur dioxide–*trans*-2-butene system was investigated at temperatures 30–90° for donor and acceptor concentrations of 3.68×10^{-2} to 6.49×10^{-2} and 1.93×10^{-4} to 3.08×10^{-4} mol/l., respectively. Since the wavelength region between 255 and 300 mμ could not be studied with these acceptor concentrations, because of the strong absorbance due to the sulfur dioxide, the 230–250-mμ region, where the sulfur dioxide absorption is relatively weak ($\epsilon_A \sim 30$, absorbance below 0.7), was examined in the present work. The absorption in this region clearly increases upon mixing with the donor. The net increase of absorption ΔD (eq 2) decreases with increasing temperature. Since the sulfur dioxide absorption increases with temperature, the temperature dependence of ϵ_A was determined in advance and corrected for D_A at each temperature.[13]

A question arises as to whether the apparent increase of the acceptor absorbance is due to the pressure effect of the foreign gas. In order to clarify this point, dry nitrogen gas (~1 atm) was introduced in the absorption cell containing 2.75×10^{-4} mol/l. of sulfur dioxide. The apparent increase of the sulfur dioxide absorption in the 235–250-mμ region was less than 2% at room temperature in contrast to the increase of 50–150% when mixed with the donor. The apparent increase becomes larger with rising temperature in contrast to the definite decrease of ΔD with temperature when mixed with the donor. The Liptay analysis was applied by use of the absorbance ΔD in the 235–250-mμ region, where the effect of foreign gas is negligibly small. The deviation of the relative absorbance, ζ, from the average value, $\bar{\zeta}$, is less than 4% in this wavelength region. The least-squares treatment was made by use of the best absorbance at 240 mμ obtained by the Liptay analysis at temperatures 30–70°, assuming that $\Delta\epsilon$ is independent of temperature.[14] The results are summarized in Table IV, in which the ϵ_C value for 245 mμ is shown, though it is not quite clear if this corresponds to the CT absorption maximum (see the discussion below).

For the purpose of examining the possibility of observing the vapor-phase equilibrium of donor–acceptor systems with relatively high vapor pressures, some other donor–acceptor systems have been examined. Among them, the systems sulfur dioxide–ammonia, carbon tetrachloride–trimethylamine, and iodine–pyridine seem to undergo irreversible chemical reactions.

Table IV: Thermodynamic and Spectroscopic Data on the Sulfur Dioxide–*trans*-2-Butene Complex[a]

	Gas[b]	Soln[c]
ν_{max}, 10^3 cm^{-1}	41?	38.2, (33.9)[e]
ϵ_{max}, l. mol^{-1} cm^{-1}	120 + 40[d]	2290, (1960)[e]
K_c (25°), l. mol^{-1}	3.1 ± 0.5	0.082 ± 0.009
$K_c \cdot \Delta\epsilon$ (25°), 10^3 l.^{2} mol^{-2} cm^{-1}	0.290 ± 0.049[f]	0.116 ± 0.007[d]
ΔU, kcal mol^{-1}	−2.52 ± 0.07	...
ΔH, kcal mol^{-1}	−3.11 ± 0.07	−1.37 ± 0.12
ΔS, eu	−6.2 ± 0.2	−9.55 ± 0.5

[a] See the footnotes to Table II for the definition of symbols. [b] This work. The result of the Liptay analysis. [c] Reference 24. In *n*-hexane solution. [d] At 245 mμ. [e] Absorption band due to the LE transition in sulfur dioxide. [f] At 240 mμ.

The sulfur hexafluoride–trimethylamine system shows no change of the electronic absorption spectrum upon mixing. The sulfur dioxide–diethyl sulfide and sulfur dioxide–dimethyl sulfide systems show very weak absorption bands around 300 mμ, which cannot be attributed to the absorption due to the donor or acceptor molecule. The origin of the absorption band is likely the locally excited (LE) transition in sulfur dioxide modified by complex formation. Unfortunately, the apparent absorptions are too weak to be analyzed quantitatively in the vapor phase.

Discussion

In view of the fact that the K_c and ϵ values for the iodine complex with diethyl sulfide obtained by Kroll[7] and those of Tamres and Goodenow[5a] show large differences, it is interesting to compare the present result for TCNE–*o*-xylene with that obtained by Kroll.[7] As can be seen in Table II, the two independent studies give coincident values for the energy of the CT transition, ν_{max}, and thermodynamic quantities ΔU, ΔH, and ΔS which agree within experimental uncertainties. They also give almost the same value for the $K_c\epsilon$ product, whereas the separated values of K_c and ϵ show relatively large differences in the two measurements. However, the lower limit of the ϵ value obtained by the present work is 1730 − 230 = 1500, which is only slightly larger than the upper limit of Kroll's ϵ, 1100 + 350 = 1450. It is not clear if this indicates the presence of some systematic error. A possible cause of the systematic error accounting for this discrepancy is the procedure to weigh TCNE. If some amount of atmospheric moisture was introduced in the course of

(13) The weak absorbance due to the donor was also taken into account in computing ΔD. Its temperature dependence was negligibly small in the wavelength range studied here.

(14) Strictly speaking, this assumption is not valid for this complex, since $\Delta\epsilon$ includes ϵ_A which varies with temperature. However, the change of ϵ_A with temperature (30–70°) is at most 1 l. mol^{-1} cm^{-1} at 235–250 mμ, corresponding to an error of less than 1% of the ϵ_C value.

weighing, it would react with TCNE upon heating, resulting in a lower absorbance due to the CT transition. The Scott plot would then shift upward. Since a smaller amount of the acceptor is usually employed as the donor concentration becomes larger, in order to obtain an appropriate absorbance, the effect of water should be more appreciable for a larger $a + d$ value. This makes the slope of the Scott plot $(1/\epsilon)$ too large whereas it brings relatively small error in the intercept (hence in the $K_\epsilon\epsilon$ product). In this respect, the present treatment is believed to be more reliable since, compared with the previous work,[7] it has much less possibility that the moisture is absorbed on TCNE during the weighing procedure.

The Liptay analysis for the TCNE complexes with toluene and naphthalene shows no indication of the existence of the 1:2 complex, or any other one with higher stoichiometry. Perhaps the same holds in the case of the benzene and *o*-xylene complexes. It has been claimed, however, that this cannot be taken as evidence for the nonexistence of higher-order complexes.[3b] It has also been suggested[15a] that the 1:2 complex will strongly affect the observed K value even for relatively low concentrations of donor and acceptor as employed in the present vapor-phase study if the equilibrium constant, K_2, for the 1:2 complex formation is assumed, for example, to be of the same order of magnitude as that (K_1) of the 1:1 complex formation. The effect of higher-order complexes may be detected by the wavelength dependence of K[15b] and, possibly, by the temperature dependence of absorption intensity. However, the former is not observed in the present study. For example, the K values for the TCNE–toluene system at 148° are 3.0 ± 1.0, 3.6 ± 0.7, and 3.2 ± 1.0 at 320, 370, and 420 mμ, respectively, which are constant within the experimental uncertainty. The temperature dependence of ϵ_{max} and of the band shape also is not observed in the present study.[16] Therefore even a more sophisticated method of data analysis[17] would give no evidence for higher-order complexes (if any) because of a relatively large experimental error which is inevitable in the vapor-phase study.

Although the magnitude of K_2 is quite uncertain, the K values, obtained in the present study at relatively high temperatures, is expected to be much less affected by the 1:2 complex (if any) than the corresponding solution values measured at lower temperatures and with higher concentrations of donor and acceptor. This is because K_2 should decrease much more rapidly with increasing temperature than K_1, since the heat of formation for the 1:2 complex must be considerably larger than that for the 1:1 complex. This might be one of the reasons for the remarkable difference between the solution and vapor-phase values of K.

The two absorption bands observed for the TCNE–naphthalene complex have been ascribed to the CT transitions from the highest- and next highest-occupied MO's of naphthalene. This has also been confirmed by theroretical calculations.[18a,18b] The TCNE complexes of *p*-xylene and durene are also known to exhibit two overlapping absorption bands in the vapor phase as well as in solution.[7,11] They have been interpreted as two CT transitions from the highest occupied MO's of benzene which split due to methyl substitution.[18b,18c] Voigt suggested[18d] the overlapping of two CT bands also in the spectra of the toluene and *o*-xylene complexes in solution for which a single band is apparently observed. This was confirmed later for the latter by the low-temperature absorption spectrum.[19] Since the complexes of toluene and *o*-xylene in the vapor phase exhibit spectra similar to those in solution, with relatively large half-width (6600 and 6400 cm^{-1}, respectively, in contrast to those of 5900 cm^{-1} in the benzene complex, and 4000 and 5100 cm^{-1} in the naphthalene complex), two CT bands are likely overlapping each other, giving an apparent single band. In order to explain the appearance of two CT bands with nearly equal intensities in the solution spectra, the existence of 1:1 isomers has been discussed.[20a] A model has also been proposed in which the TCNE molecule rotates almost freely on the donor.[20b] However, the existence of 1:1 isomers seems to be excluded in view of the fluorescence study; upon exciting the second CT band, the same fluorescence spectrum was observed with high quantum yield as that observed by exciting the first band, indicating the existence of a single species in a rigid glass solution.[19] The temperature independence of the absorption intensity observed in the present study (Figures 2, 3, and 4) is also negative for the existence of isomer.[15b] The free-rotation model is also excluded in view of the fact that the complexes exhibit similar absorption spectra to those in solution even in a frozen solution.[19]

From this point of view, the displaced arrangement of donor and acceptor seems to be most plausible for the molecular geometry of the TCNE complexes in the vapor and liquid phases; *i.e.*, TCNE lies on the benzene ring with its molecular center displaced with respect

(15) (a) C. C. Thompson, Jr., *Can. J. Chem.*, **47**, 2605 (1969); (b) G. D. Johnson and R. E. Bowen, *J. Amer. Chem. Soc.*, **87**, 1655 (1965).

(16) Figure 2 shows clearly that the relative intensity is independent of temperature. The temperature independence of ϵ_{max} was assumed in the present analysis of data. However, the good fit of the data at various temperatures to a single ϵ_{max} value seems to confirm the initial assumption of temperature independence (see Figures 3 and 4).

(17) For example, L. P. Varga and F. C. Veatch, *Anal. Chem.*, **39**, 1101 (1967).

(18) (a) A. R. Lepley and C. C. Thompson, Jr., *J. Amer. Chem. Soc.*, **89**, 5523 (1967); (b) A. R. Lepley, *ibid.*, **86**, 2545 (1964); (c) L. E. Orgel, *J. Chem. Phys.*, **23**, 1352 (1955); (d) E. M. Voigt, *J. Amer. Chem. Soc.*, **86**, 3930 (1964).

(19) (a) J. Prochorow and A. Tramer, *J. Chem. Phys.*, **47**, 775 (1967); (b) J. Prochorow, *Bull. Acad. Pol. Sci., Ser. Sci., Math., Astron. Phys.*, **15**, 37 (1967).

(20) (a) A. R. Lepley, *Tetrahedron Lett.*, **39**, 2823 (1964); (b) E. M. Voigt and C. Reid, *J. Amer. Chem. Soc.*, **86**, 3611 (1964).

to the sixfold axis of the latter, or alternatively, that in which the center of TCNE lies on the sixfold axis but rotated by some intermediate angle. In either model, the symmetry of the complex is reduced, making both transitions allowed for a single geometrical configuration. A semiempirical calculation on the electronic structure of the TCNE–naphthalene complex indicates that the second CT band is almost forbidden if the geometrical configuration of the complex in crystal[21] is assumed (the center of TCNE lies on the center of one of the benzene rings of naphthalene with the C=C axis perpendicular to the long axis of the latter).[22a] The polarized crystal spectrum[22b] seems to support this viewpoint. This result is not necessarily in contradiction to the above viewpoint, since the geometry of the complex in a single crystal may be different from those in the vapor and liquid phases and in a rigid solution.

In contrast to the data for the TCNE complex with methylbenzenes in solution,[11] the previous work in the vapor phase shows no clear increase of the intensity with methyl substitution whereas ΔH increases steadily.[7] The present results for the TCNE complexes with benzene, toluene, and *o*-xylene show, however, a steady increase of the intensity, as well as ΔH, upon methyl substitution. This result is in accordance with the theoretical prediction derived on the assumption that the donor–acceptor bond is mainly of CT nature,[3] though it is not quite clear if this fact can be taken as a definite evidence for the CT bonding.[23]

If the TCNE complex with naphthalene is compared with the methylbenzene complexes, the intensity of the CT bands of the former is somewhat too low in view of the relatively high heat of formation. A possible explanation accounting for this fact is the stronger interaction of the CT excited state with upper excited states in the naphthalene complex; for instance, the first CT state can interact with the low-lying α band of naphthalene. Since the latter is a symmetry-forbidden transition in naphthalene, the intensity of the CT band is partly taken away by the latter. Secondly, relatively low-lying upper CT configurations may contribute to the ground state, making $-\Delta H$ larger than that expected for the interaction of the ground state only with the lowest two CT configurations, whereas this effect diminishes the intensity of the first two CT absorption bands. Another possible explanation is a stronger electrostatic contribution in the ground state of the naphthalene complex, since a larger conjugated system in naphthalene results in a higher polarizability than that of the methylbenzenes.

The CT bands of the TCNE complexes studied here show maxima at higher energy than the corresponding solution data by 2000–3000 cm^{-1}, in accordance with the previous investigations.[3-7] The magnitude of the red shift on going from vapor to solution decreases with methyl substitution on benzene. This tendency can be understood if the bond compression due to the internal pressure of solvent accounts for the observed red shift, since the compression becomes more difficult as the methyl substitution increases the donor–acceptor bond strength.[6]

As discussed above, the examination of the pressure effect on the sulfur dioxide absorption and its temperature dependence clearly exclude the possibility that the increase of the absorbance upon the introduction of *trans*-2-butene is due to a simple pressure effect caused by the foreign gas. The least-squares analysis of the Scott equation on the basis of the result of the Liptay analysis shows a relatively small but definite absorbance due to the complex in the 240–250-mμ region. Unfortunately, the absorbance due to the complex could not be determined in the 250–310-mμ region because of interference by the absorption due to the uncomplexed sulfur dioxide. The absorption in the 240–250-mμ region seems to be a shoulder band overlapping on the tail of another band at ~290 mμ (a modified LE transition localized on the acceptor molecule in the complex). In order to check the similarity to the solution measurement, the light absorption due to the complex of sulfur dioxide with 2,3-dimethyl-2-butene was examined in the vapor phase. The system shows a new absorption band around 300 mμ corresponding to the band observed at 325 mμ in solution.[24] Hence the shoulder band observed for the *trans*-2-butene complex in the 240–250-mμ region is probably due to the same kind of transition as that observed in solution at 262 mμ, which has been assigned to the CT transition on the basis of correlation with the donor ionization potential.[24]

The remarkable difference of ϵ_{max} between the vapor and solution data for this weak complex should be explained on the basis of the strong effect of the solvent cage,[6,25] or incorporation of contact CT absorption in the solution spectrum.[26] If we adopt the former model, the extent of the CT force in the ground state should be larger in solution than in the vapor phase. Actually, the contribution of the CT interaction is estimated to be only a few per cent of the total binding energy in the vapor phase, on the basis of the simplified resonance theory[3] and of the observed intensity ratio. This means that the donor and acceptor molecules are bound to each other mainly by the van der Waals and/or electrostatic forces. The resultant binding is therefore loose and nonspecific, the relative orientation

(21) R. M. Williams and S. C. Wallwork, *Acta Cryst.*, **22**, 899 (1967).

(22) (a) T. Ohta, T. Kunii, and H. Kuroda, *Theoret. Chim. Acta*, **19**, 167 (1970); (b) H. Kuroda, T. Amano, I. Ikemoto, and H. Akamatsu, *J. Amer. Chem. Soc.*, **89**, 6056 (1967).

(23) (a) D. Atack and O. K. Rice, *J. Phys. Chem.*, **58**, 1017 (1954); (b) M. W. Hanna, *J. Amer. Chem. Soc.*, **90**, 288 (1968); M. W. Hanna and D. E. Williams, *ibid.*, **90**, 5358 (1968); J. L. Lippert, M. W. Hanna, and P. J. Trotter, *ibid.*, **91**, 4035 (1969).

(24) D. Booth, F. S. Dainton, and K. J. Ivin, *Trans. Faraday Soc.*, **55**, 1293 (1959).

(25) P. J. Trotter, *J. Amer. Chem. Soc.*, **88**, 572 (1966).

(26) L. E. Orgel and R. S. Mulliken, *ibid.*, **79**, 4839 (1957).

of the donor to the acceptor not being uniquely determined. Hence most of the complex in the vapor phase may not contribute to the light absorption in the 240–250-mμ region.

Finally, the change of the entropy of formation, ΔS, needs some discussion. In contrast to the TCNE complexes, ΔS is much more negative in solution for the sulfur dioxide–*trans*-2-butene complex. This fact indicates that the donor and acceptor are bound to each other more rigidly and specifically in solution than in the vapor phase, in accordance with the bond-compression model. On the other hand, in the case of TCNE complexes with aromatic hydrocarbons, $-\Delta S_{vapor}$ is only slightly larger than $-\Delta S_{soln}$, indicating that the complex retains almost the same geometrical configuration in the vapor phase as that in solution.

Acknowledgments. It is my pleasure to thank Professor Robert S. Mulliken for a number of stimulating discussions and for his encouragement during my stay in Chicago. I also wish to thank Professors Milton Tamres and Saburo Nagakura for many helpful discussions.

Hydrogen-Bonded Complex–Ion-Pair Equilibria in 3,4-Dinitrophenol–Amine–Aprotic Solvent Systems[1]

by R. A. Hudson, R. M. Scott,[2] and S. N. Vinogradov*[3]

Biochemistry Department, Wayne State University School of Medicine, Detroit, Michigan 48207
(Received December 22, 1971)

Publication costs assisted by the National Institutes of Health, U. S. Public Health Service

The formation of hydrogen-bonded complexes and of ion pairs in solutions of 3,4-dinitrophenol with triethylamine, tri-*n*-propylamine, tri-*n*-butylamine, di-*n*-butylamine, and *n*-butylamine was investigated spectrophotometrically in benzene and benzene–cyclohexane mixtures. In benzene, addition of *n*-butylamine or di-*n*-butylamine results in a shift of the 3,4-dinitrophenol absorption band at 2850 and 3150 Å associated with the formation of a 1:1 hydrogen-bonded complex. At amine concentrations higher than 0.01 *M*, the progressive ionization of 3,4-dinitrophenol is indicated by the appearance of a band of 3700–3900 Å, which grows with an increase in amine concentration until ionization appears to be complete. Addition of a tertiary amine to a benzene solution of 3,4-dinitrophenol leads directly to the appearance of an anion band at *ca.* 3750 Å; the 1:1 stoichiometry suggests the formation of an ion pair. At concentrations of amine higher than 0.1 *M* a hypsochromic shift of the 3,4-dinitrophenol spectrum occurs to about 3250 Å in pure amine. This change is probably associated with a reversal of ionization and the formation of amine-solvated hydrogen-bonded complexes. In the presence of a large excess of tertiary amine in benzene–cyclohexane mixtures, a similar hypsochromic shift is observed with decrease in benzene concentration. The observed spectral changes are interpreted in terms of a solvent-induced shift of a $O–H\cdots N \rightleftharpoons O^-\cdots H–N^+$ equilibrium. The thermodynamic parameters for the formation of the two types of complexes show that in this case, no enthalpy difference and only a small free energy difference exists between a hydrogen-bonded complex and an ion pair.

Introduction

Of the many factors that influence the position of the simple prototropic equilibrium

$$\underset{\text{I}}{R–A–H\cdots B} \rightleftharpoons \underset{\text{II}}{R–A^-\cdots H–B^+}$$

where RAH and B are Brönsted acid and base, respectively, the effect of solvent environment is one of the most subtle and least predictable. The experimental study of an equilibrium between a hydrogen-bonded complex I and a hydrogen-bonded ion pair II is frequently hindered by a marked preponderance of one of the two types of complexes and by the presence of competing equilibria, which, depending on the concentration ranges of the acid and base employed, include the self-association of either or both moieties and the formation of homoconjugate and heteroconjugate ions. Furthermore, in solvents of low dielectric constant,

(1) This work was partially supported by Grant HE 14063 from the National Institutes of Health, U. S. Public Health Service.

(2) Chemistry Department, Eastern Michigan University.

(3) To whom requests for reprints should be addressed.

the formation of triple ions, quadropoles, and multipoles of higher order can cause substantial difficulties. While the carboxylic acid–amine complexes in aprotic solvents exhibit the presence of several competing equilibria,[4,5] we have sought among the nitrophenols and the simple aliphatic amines acid–base pairs which could be studied at low enough concentrations of the acid to avoid its self-association. The use of dinitrophenols unsubstituted at the ortho positions avoids intramolecular hydrogen bonding, and in aprotic solvents, should afford a study of some of the equilibria in the general scheme below.

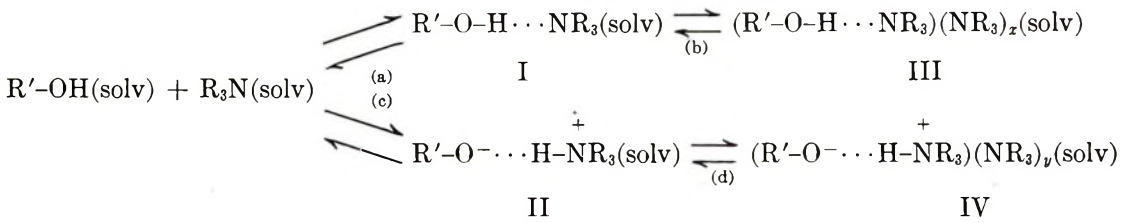

3,4-Dinitrophenol is a weak acid (pK_a = 5.42)[6] relative to dinitrophenols where one or both ortho positions are substituted by a nitro group, but it is known to form an ion pair with triethylamine in benzene.[7] We report below the results of a spectrophotometric study of the formation of hydrogen-bonded and ion-pair complexes of 3,4-dinitrophenol with several aliphatic amines in benzene and in benzene–cyclohexane mixtures.

Results and Discussion

Nitrophenols with neither ortho position substituted by a proton acceptor group exhibit a characteristic series of bathochromic shifts in their ultraviolet absorption spectra in going from free acid to a hydrogen-bonded complex, to an ion pair, to a solvated ion pair or a solvated anion. The $\pi \rightarrow \pi^*$ transition of the intramolecular charge transfer type[8,9] of *p*-nitrophenol located at 2850 Å in cyclohexane is shifted to 3050 Å in the presence of excess triethylamine or dioxane.[10] In the presence of excess triethylamine, this band occurs at 3900 and 4260 Å in 1,2-dichloroethane and in acetonitrile, respectively.[11] The corresponding band of 3,4-dinitrophenol shifts from 2850 Å in the free acid in benzene, to 3150 Å in the presence of small quantities of *n*-butylamine, and to 3850 Å in the presence of a large excess of *n*-butylamine (Figure 1). The absorption maximum of the 3,4-dinitrophenolate anion is at 4000 Å, while the undissociated 3,4-dinitrophenol absorbs at *ca.* 3100 Å in aqueous solution (Figure 1).

The addition of triethylamine, tri-*n*-propylamine, or tri-*n*-butylamine to 3,4-dinitrophenol in benzene leads directly to the formation of an ion pair II possessing an absorption maximum at 3750 Å with an isosbestic at 3030 Å (Figure 2). Plots of log [A]/[AH] *vs.* log [B] employing the absorbances at 3750 and 3250 Å are linear (Figure 3) and indicate a simple one to one stoichiometry for equilibrium c (Table I). At concentrations of tertiary amine greater than about 0.1 *M*, a hypsochromic shift occurs in the absorption spectrum of 3,4-dinitrophenol (Figure 2) which suggests the reversal of the ionization process and the formation of amine-solvated hydrogen-bonded complex III. This behavior culminates in the virtual disappearance of any absorption due to ion pairs at 3750 Å in the pure trialkylamine. The disappearance of absorption due to ionized *p*-nitrophenol in liquid trialkylamine solutions has been observed previously.[12]

In contrast to the case observed in the presence of tertiary alkylamines, the addition of *n*-butylamine or di-*n*-butylamine to a solution of 3,4-dinitrophenol in benzene leads first of all to the formation of hydrogen-bonded complexes only (Figure 1). Equilibria a and c appear to coexist in the presence of amine concentrations higher than about 0.01 *M*. The formation of ion pairs becomes predominant at concentrations of amine

Table I: Results of Some of the Log-Log Plots for 3,4-Dinitrophenol in Benzene[a]

Amine	λ, Å	Slope	Log *K*	Complex
Triethylamine	3750	0.98	3.36	Ion pair
Tributylamine	3750	1.05	3.20	Ion pair
Tributylamine	3250	1.08	3.15	Ion pair
Tributylamine	3750	0.98[b]	2.49[b]	Ion pair
Dibutylamine	3200	0.98	3.15	Hydrogen bonded
n-Butylamine	3200	1.00	3.45	Hydrogen bonded
n-Butylamine	3500	1.02	3.46	Hydrogen bonded
n-Butylamine	4200	1.77	0.92	Solvated ion pair

[a] At 25°. [b] At 45°.

(4) M. M. Davis, "Acid–Base Behavior in Aprotic Organic Solvents," National Bureau of Standards Monograph 105, 1968, p 64.

(5) D. F. DeTar and R. W. Novak, *J. Amer. Chem. Soc.*, **92**, 1361 (1970).

(6) R. A. Robinson, M. M. Davis, M. Paabo, and V. E. Bower, *J. Res. Nat. Bur. Stand., Sect. A*, **64**, 347 (1960).

(7) M. M. Davis, *J. Amer. Chem. Soc.*, **84**, 3623 (1962).

(8) S. Nagakura, *J. Chem. Phys.*, **23**, 1441 (1955).

(9) A. J. Parker and D. Brody, *J. Chem. Soc.*, 4061 (1963).

(10) R. A. Hudson, R. M. Scott, and S. N. Vinogradov, *Spectrochim. Acta, Part A*, **26**, 337 (1970).

(11) H. Baba, A. Matsuyama, and H. Kokubun, *ibid.*, **25**, 1709 (1969).

(12) R. Scott, D. DePalma, and S. N. Vinogradov, *J. Phys. Chem.*, **72**, 3192 (1968).

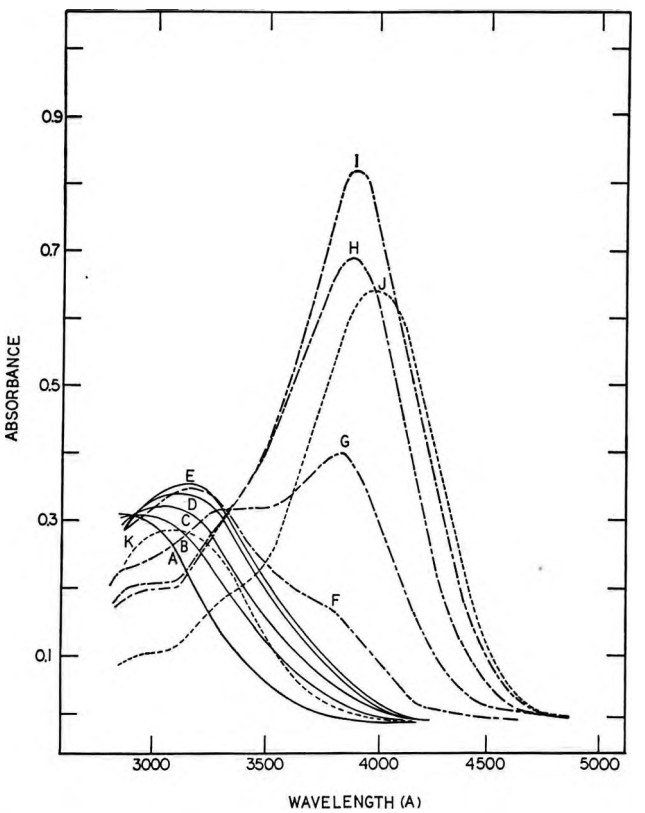

Figure 1. The absorption spectra of 2.6×10^{-5} *M* 3,4-dinitrophenol in benzene (curve A) and in the presence of *n*-butylamine (curves B through I) and in aqueous solution at pH 11.4 (curve J) and pH 3.4 (curve K); 2-cm cell, 25°. B, 4.05×10^{-4} *M*; C, 1.44×10^{-3} *M*; D, 2.83×10^{-3} *M*; E, 1.90×10^{-2} *M*; F, 1.19×10^{-1} *M*; G, 3.13×10^{-1} *M*; H, 6.74×10^{-1} *M*; I, 1.476 *M*.

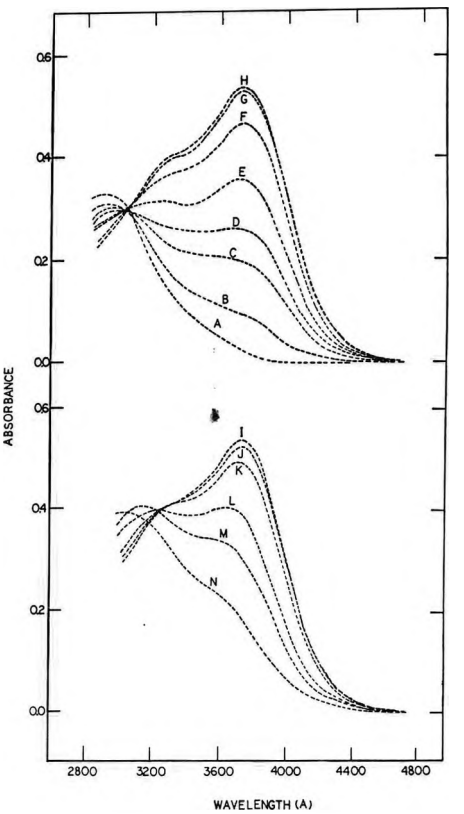

Figure 2. The absorption spectra of 5.44×10^{-5} *M* 3,4-dinitrophenol in benzene (curve A) and in the presence of tri-*n*-butylamine (curves B through N); 1-cm cell, 25°. B, 2.10×10^{-4} *M*; C, 6.30×10^{-4} *M*; D, 1.05×10^{-3} *M*; E, 2.10×10^{-3} *M*; F, 6.30×10^{-3} *M*; G, 8.40×10^{-2} *M*; H, 1.68×10^{-1} *M*; I, 0.084 *M*; J, 0.42 *M*; K, 0.84 *M*; L, 2.1 M, 3.15 *M*; N, 4.2 *M* (pure tributylamine).

higher than about 0.3 *M* (Figure 1). The continuous shift of the peak assigned to the hydrogen-bonded ion pair II to longer wavelengths and the increase in intensity associated with the increase in amine concentration should probably be attributed to the occurrence of amine solvation equilibria d. This conclusion is supported by the fact that the log–log plots obtained employing absorbances at 3750 Å possess slopes higher than unity (Table I). At low primary or secondary amine concentrations, the log–log plots provide the expected 1:1 stoichiometry for the formation of hydrogen-bonded complexes I (Figure 3, Table I).

The addition of either a primary, a secondary, or a tertiary amine to a cyclohexane solution of 3,4-dinitrophenol leads solely to the formation of a hydrogen-bonded complex I. The investigation of cyclohexane solutions is hampered by the very low solubility of 3,4-dinitrophenol and the marked tendency towards the occurrence of opalescence on addition of small quantities of amines.

In the case of the trialkylamines, at a concentration of amine sufficient to ensure the complete formation of the hydrogen-bonded complex I in cyclohexane and of the ion pair II in benzene, about 0.05 to 0.1 *M*, it is observed that both types of complexes coexist in benzene–cyclohexane solutions. Figure 4 illustrates the absorption spectra of 3,4-dinitrophenol in the presence of a 950-fold excess of tri-*n*-butylamine. The equilibrium between ion pairs and hydrogen-bonded complexes shifts gradually in favor of the former with increase in benzene content of the binary solvent mixture.

We have determined the thermodynamic parameters of formation of complexes of 3,4-dinitrophenol with several of the foregoing amines by a modification of the Rose–Drago method.[13] The results are presented in Table II. Representative thermodynamic parameters of formation of the hydrogen-bonded ion pairs II are shown in the first six lines of the table. The remainder of the results are thermodynamic parameters of formation of hydrogen-bonded complexes I. Contrary to expectations, no obvious relationship can be discerned between the thermodynamic parameters on one hand and the shift from ion pairs to hydrogen-bonded complexes on the other. It is probable that an increase in ΔH° and ΔG° of formation of 3,4-dinitrophenol–tri-*n*-butylamine hydrogen-bonded complex occurs in going

(13) N. J. Rose and R. S. Drago, *J. Amer. Chem. Soc.*, **81**, 6138 (1959).

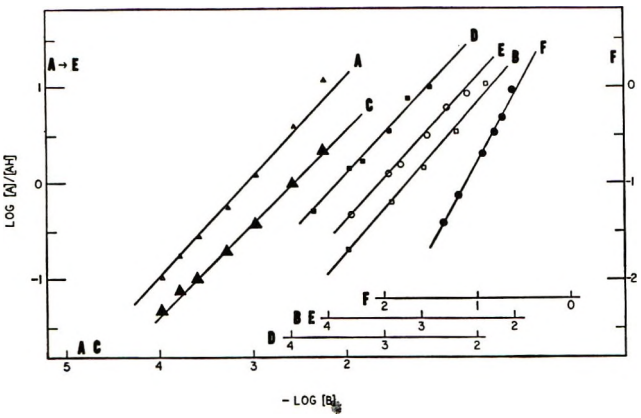

Figure 3. The results of spectrophotometric titrations of 3,4-dinitrophenol in benzene with tri-*n*-butylamine (curves A through C) and with *n*-butylamine (curves D through F), plotted as log [A]/[AH] *vs.* log [B]. A, 3750 Å, 25°; B, 3250 Å 25°; C, 3750 Å, 45°; D, 3200 Å, 25°; E, 3500 Å, 25°; F, 4200 Å, 25°.

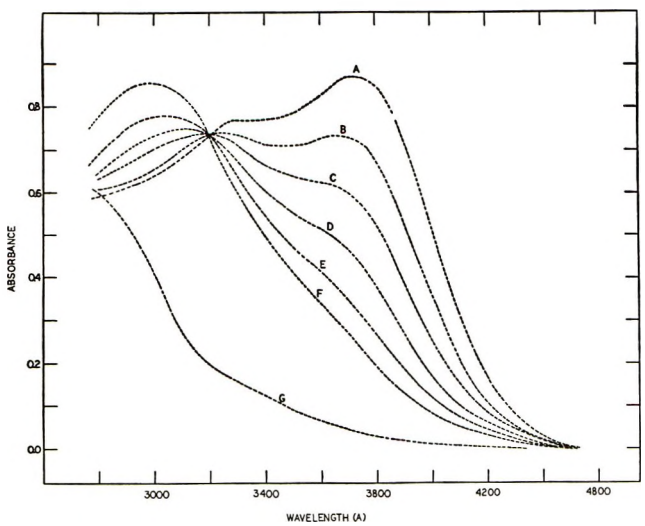

Figure 4. The shift of the hydrogen-bonded complex–ion-pair equilibrium as a function of benzene concentration in benzene–cyclohexane mixtures in the case of 1.24×10^{-4} *M* 3,4-dinitrophenol in the presence of 0.118 *M* tri-*n*-butylamine; 1-cm cell, 25°. A, benzene; B, 82.5 mol % benzene; C, 64.4 mol % benzene; D, 49.5 mol % benzene; E, 23.4 mol % benzene; F, cyclohexane; G, cyclohexane, no tri-*n*-butylamine.

from the 14.4 mol % benzene–cyclohexane mixture to pure cyclohexane. However, this region of solvent composition is not the one where the transition from hydrogen-bonded complex to ion pair is found to occur. The thermodynamic parameters of formation of the two types of complexes at 33.1 mol % benzene and at 75 mol % benzene, respectively, the limiting binary mixtures where the presence of the other type of complex could be neglected, are surprisingly similar, with the exception of a slightly higher ΔG° of the hydrogen-bonded complex. The values of the free energies and enthalpies of formation of hydrogen-bonded complexes of 3,4-dinitrophenol with amines show that the O–H···N hydrogen bonds involved are among the strongest hydrogen bonds known.[14] The strength of the hydrogen bond in the 3,4-dinitrophenol–tri-*n*-butylamine complex is greater than that of the hydrogen bond in the *p*-nitrophenol–triethylamine complex in cyclohexane,[10] a result consistent with the lower pK_a of 3,4-dinitrophenol (5.42 relative to 7.15). The values of the thermodynamic parameters of formation of 3,4-dinitrophenol–amine ion pairs are in general agreement with the corresponding values for ion pairs formed by more acidic dinitrophenols with amines.[4,15]

Complexes of 3,4-dinitrophenol with tertiary amines in benzene–cyclohexane mixtures and with primary amines in benzene represent a unique case of a delicately poised equilibrium between hydrogen-bonded and ion-pair complexes. Its investigation by dielectric titration and by pmr spectroscopy, now in progress, should provide some insight into the movement of the proton between the oxygen and nitrogen atoms of the two moieties of the complex.

Experimental Section

3,4-Dinitrophenol was prepared by nitration of *m*-nitrophenol by the method of Sidgewick and Aldos.[16] Fractional crystallization of the mixture of isomeric dinitrophenols from benzene–hexane mixtures gave a pure sample of 3,4-dinitrophenol (mp 134–134.5° uncor) whose spectra agreed with the published results.[6] Potentiometric titration showed it to have a pK_a = 5.37 compared to the literature value of 5.42.[6]

The amines were reagent grade chemicals distilled prior to use. The benzene was Matheson Coleman and Bell or Baker spectrograde. The cyclohexane was Matheson Coleman and Bell spectrograde or reagent grade material purified by treatment with concentrated sulfuric acid.[17]

The spectra of solutions prepared by weighing on the same day were obtained employing a 1-cm quartz cell thermostated to better than 0.1° and a Cary Model 15 spectrophotometer. For each concentration of 3,4-dinitrophenol, six to ten solutions were prepared of different amine concentration. The equilibrium constant K for the formation of a 1:1 complex was obtained from the absorbances at a given wavelength, at each temperature, by the method of Rose and Drago.[13] The following equation

$$\frac{1}{K} = \frac{a_c - a_{AH}}{A - a_{AH}c_{AH}^\circ}c_{AH}^\circ c_B^\circ + \frac{A - a_{AH}c_{AH}^\circ}{a_c - a_{AH}} - c_{AH}^\circ - c_B^\circ$$

(14) S. N. Vinogradov and R. H. Linnell, "Hydrogen Bonding," Van Nostrand Reinhold, Princeton, N. J., 1971, Chapter 5.

(15) D. Neerinck, A. Van Audenhaege, L. Lamberts, and P. Huyskens, *Nature*, **218**, 461 (1968).

(16) N. V. Sidgewick and W. M. Aldos, *J. Chem. Soc.*, **119**, 1001 (1921).

(17) S. N. Vinogradov, *Can. J. Chem.*, **40**, 2170 (1962).

Table II: Thermodynamic Parameters of Formation of Complexes of 3,4-Dinitrophenol with Amines

Amine	Solvent	λ, Å	$-\Delta H°$, kcal/mol	$-\Delta G°_{298}$, kcal/mol	$-\Delta S°_{298}$, eu
Triethylamine	Benzene	3750	8.1 ± 1.7	4.77 ± 0.11	11.1 ± 5.9
Tripropylamine	Benzene	3750	9.2 ± 1.3	3.89 ± 0.04	17.7 + 4.4
Tributylamine	Benzene	3750	10.3 ± 0.2	3.98 ± 0.01	21.2 ± 0.6
Tributylamine	90 mol % benzene–cyclohexane	3750	9.6 ± 0.2	3.91 ± 0.01	19.0 ± 0.8
Tributylamine	83.3 mol % benzene–cyclohexane	3750	10.7 ± 0.7	4.03 ± 0.03	22.5 ± 2.4
Tributylamine	75.0 mol % benzene–chlorohexane	3750	10.2 ± 0.7	4.02 ± 0.04	20.6 ± 2.3
Tributylamine	33.1 mol % benzene–cyclohexane	3300	10.4 ± 0.5	4.21 ± 0.02	20.8 ± 2.8
Tributylamine	25.1 mol % benzene–cyclohexane	3300	9.8 ± 1.7	4.24 ± 0.09	18.8 ± 6.0
Tributylamine	14.4 mol % benzene–cyclohexane	3300	8.4 ± 0.8	4.43 ± 0.03	13.3 ± 2.6
Tributylamine	Cyclohexane	3300	11.2 ± 1.2	5.45 ± 0.09	19.2 ± 4.3
Tributylamine	Cyclohexane	3200	10.9 ± 0.6	5.41 ± 0.04	18.3 ± 2.1
Di-*n*-butylamine	Benzene	3100	9.4 ± 0.7	4.77 ± 0.03	15.6 ± 2.4
n-Butylamine	Benzene	3100	7.5 ± 1.3	4.57 ± 0.05	9.8 ± 4.5

(where $c_{AH}°$ and $c_B°$ are the initial concentrations of the 3,4-dinitrophenol and amine, respectively, A is the observed absorbance at a given wavelength, and a_c and a_{AH} are the absorptivities of the complex and of the free 3,4-dinitrophenol, respectively, at the same wavelength) was solved for all pairs of solutions. The calculated equilibrium constants were subjected to Chauvenet's rejection criterion[18] and averaged. The enthalpies, free energies, and entropies of formation of the complexes were obtained from the least-squares equations for the linear plots of log K *vs.* T^{-1}.

(18) H. D. Young, "Statistical Treatment of Experimental Data," McGraw-Hill, New York, N. Y., 1962, p 78.

The Association of Copper(II), Vanadyl, and Zinc(II) 4,4′,4″,4‴-Tetraalkylphthalocyanine Dyes in Benzene

by Alan R. Monahan,* James A. Brado, and Allen F. DeLuca

Xerox Rochester Research Center, Rochester, New York 14603 *(Received January 28, 1972)*

Publication costs assisted by the Xerox Corporation

Analyses of the absorption spectra of three phthalocyanine dyes in the 12,000-32,000-cm^{-1} region demonstrate the existence of monomer-dimer equilibrium in the concentration range from 10^{-6} to 10^{-4} M. The dimerization constants in benzene, $K_{eq} = C_d/C_m^2$, are $(1.58 \pm 0.09) \times 10^4$ M^{-1}, $(1.09 \pm 0.23) \times 10^6$ M^{-1}, and $(2.01 \pm 0.49) \times 10^6$ M^{-1} for the Cu(II)-, Zn(II)-, and vanadyl-4,4′,4″,4‴-tetraoctadecylsulfonamidophthalocyanines, respectively. The absorption spectra of pure monomer and pure dimer in benzene are calculated for each dye. The relative dye–dye interaction as measured from the Davydov splitting in the dimer and the equilibrium constant for dimerization were found to be reasonably consistent for the three metallophthalocyanine dye molecules.

Introduction

Metal-free 4,4′,4″,4‴-tetrasulfophthalocyanine (H_2-TSP) and its Cu(II), Co(II), Zn(II), Fe(III), and VO(II) analogs are known to dimerize in water.[1] The stability of the dimers decreases in the order CuTSP > H_2TSP > FeTSP ≥ (VO)TSP ∼ ZnTSP > CoTSP and the stability as measured by the equilibrium constant for dye association varies by roughly two orders of magnitude within the series. The lower stability of the Co and Zn phthalocyanines was tentatively explained on the basis of axially coordinated water molecules inhibiting dye association. However, it has recently been found that both Fe^{III}TSP and VO^{II}TSP, which have coordination numbers greater than 4, are more stable than the Zn and Co analogs. Hence it may be concluded that other factors which have not been previously taken into account[1b] are operative in controlling phthalocyanine dye aggregation processes. The major difficulty in evaluating dye association processes in water is that the strong solvent–solvent interaction is the dominant force causing the molecules to associate rather than the dye–dye interaction.

In a previous paper[2] we reported a study on the monomer–dimer equilibria of a phthalocyanine dye molecule of the structure

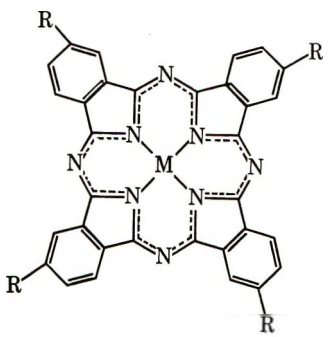

where R is $SO_2NH(CH_2)_{17}CH_3$ and M is Cu(II). The equilibrium studies were carried out in benzene and CCl_4 in the concentration range 10^{-6} to 10^{-4} M. Using this alkylated phthalocyanine dye molecule the dimerization process could be studied in solvents of low dielectric constant where the dye–dye interaction is maximized. The resolved solution dimer spectrum in both solvent systems was virtually identical with that of the solid-state spectrum. This indicated that interactions operative in the solid state can be simulated in solution if the solvent system and structure–solubility characteristics of the dye are matched properly.

In this paper we report a preliminary attempt to evaluate the effect of metal atom on the dimerization of a phthalocyanine dye molecule in benzene using previously reported spectroscopic computer techniques.[3] In this study M is Cu(II), (CuPc), Zn(II), (ZnPc), and VO(II), (VOPc). In all three molecules the association constants were measured spectrophotometrically at 25° in the 10^{-6} to 10^{-4} M concentration region. In addition, the resolved monomer and dimer spectra were obtained. Thus, the relative interaction energy could be obtained from the size of the Davydov splitting in the dimer. The approximate dye–dye interaction as obtained from Davydov theory and the magnitude of the dye–dye interaction as measured from the equilibrium constant for dimerization were found to be reasonably consistent for the three metallophthalocyanine dye molecules.

(1) (a) K. Bernauer and S. Fallab, *Helv. Chim. Acta*, **44**, 1287 (1961); (b) H. Sigel, P. Waldmeier, and B. Prijs, *Inorg. Nucl. Chem. Lett.*, **7**, 161 (1971).

(2) A. R. Monahan, J. A. Brado, and A. F. DeLuca, *J. Phys. Chem.*, **76**, 446 (1972).

(3) A. R. Monahan and D. F. Blossey, *ibid.*, **74**, 4014 (1970); A. R. Monahan, N. J. Germano, and D. F. Blossey, *ibid.*, **75**, 1227 (1971).

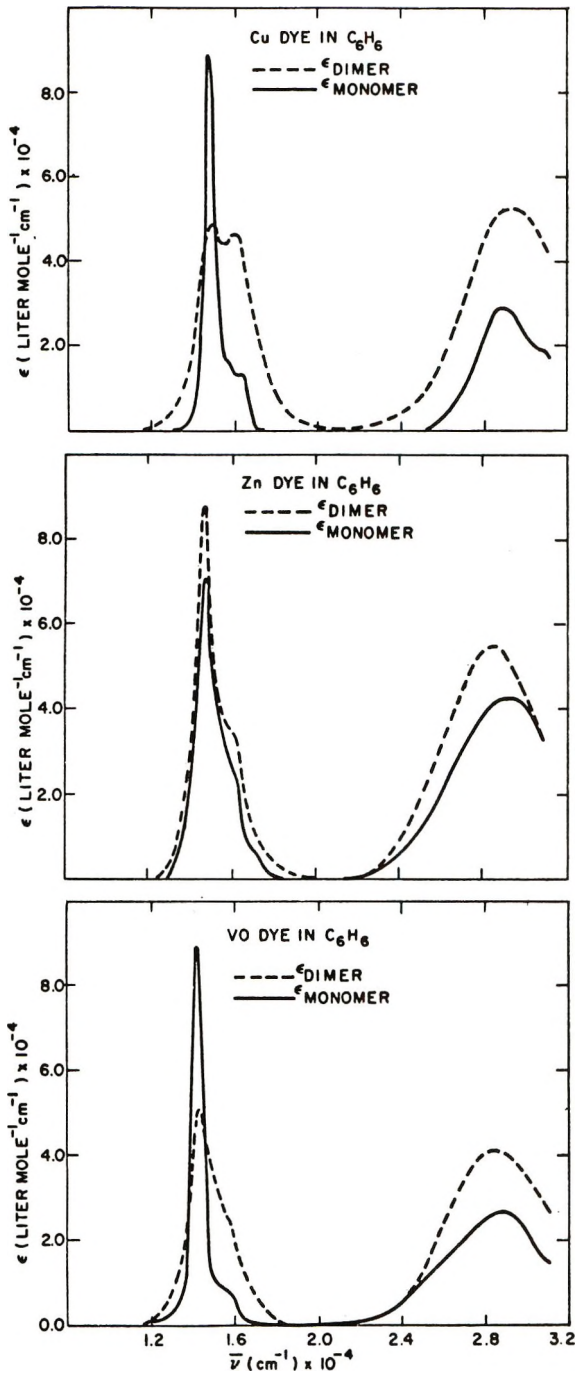

Figure 1. Calculated absorption spectra of phthalocyanine monomers and dimers in benzene.

Experimental Section

The preparation and characterization of copper(II)–4,4′,4″,4‴ - tetraoctadecylsulfonamidophthalocyanine was reported previously,[2] as well as solution preparation techniques and measurement of absorption spectra. The corresponding vanadyl and zinc compounds were prepared by a similar procedure.

Anal. Calcd for ZnPc dye: C, 65.6; H, 8.7; N, 8.8; Zn, 3.4. Found: C, 65.6; H, 8.9; N, 8.5; Zn, 3.5. Calcd for VOPc dye: C, 65.6; H, 8.7; N, 8.8; V, 2.7. Found: C, 65.3; H, 8.8; N, 8.6; V, 2.5.

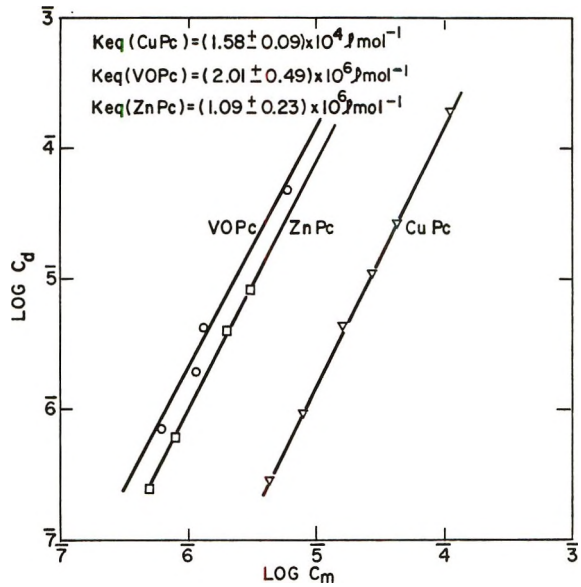

Figure 2. Plot of log C_d *vs.* log C_m for phthalocyanine dyes in benzene. Solid lines are drawn with theoretical slopes of 2.

Results and Discussion

The concentration dependence of the copper phthalocyanine dye in benzene was published in a previous paper.[2] Similar spectral dependences were found as a function of total dye concentration for the VO and Zn molecules. For each set of spectral data the equilibrium constant and pure component monomer and dimer spectrum can be calculated using an iterative computer technique.[3] For each total dye concentration, the monomer concentration C_m, dimer concentration C_d, and equilibrium constant K_{eq} can be found. The calculation is made assuming the monomer–dimer equilibria follow the law of mass action where $K_{eq} = C_d/C_m^2$. The best-fit monomer and dimer spectra for the three dyes are shown in Figure 1. The monomer and dimer spectra were used to calculate the equilibrium constants for each total dye concentration. Figure 2 shows the fit to a simple monomer–dimer equilibrium by graphical display of the mass law equation. The best fits were obtained at equilibrium constants of $K_{eq} = (1.58 \pm 0.09) \times 10^4\ M^{-1}$ for the CuPc dye, $(1.09 \pm 0.23) \times 10^6\ M^{-1}$ for the ZnPc dye and $(2.01 \pm 0.49) \times 10^6\ M^{-1}$ for the VOPc dye.

According to the theory of molecular excitons,[4] the size of the splitting of an allowed transition is a measure of the interaction energy between molecules in the dimer. The VO and Zn dimers are characterized by larger exciton splittings (*ca.* 1500 cm^{-1}) than the Cu dimer (1100 cm^{-1}). The splittings were obtained by means of a computer curve fitting calculation. The absorption spectra of the dyes at 77°K in hydrocarbon matrices (*ca.* $10^{-4}\ M$) and as solid phase melt cast films[2]

(4) A. S. Davydov, "Theory of Molecular Excitons," Nauka Press, Moscow, 1968, p 56.

confirmed the magnitudes of the calculated exciton splittings. The association constants also reflect the stronger intermolecular interactions in the VO and Zn dimers relative to the Cu dimer. The interaction energy in the Zn dimer is in all probability larger than in the Cu pair because the filled $3d_{z^2}$ orbital in Zn contracts relative to Cu and allows for a stronger interplanar interaction.[5] The VO dimer is the most stable probably because of the formation of a relatively strong interplanar OV···OV or OV···N bond. Dickson and Petrakis[6] have studied the bonding of a vanadyl mesoporphyrin using infrared spectroscopy and demonstrated the existence of specific types of coordinated VO bonds with relatively large bonding energies (*ca.* 17 kcal mol^{-1}). The equilibrium constants obtained in benzene solution seem to give a fairly accurate indication of the true dye–dye interaction since the relative intermolecular interactions of the three phthalocyanine dye molecules are reasonable in terms of previously proposed intermolecular bonding schemes.

In marked contrast to our study in a nonpolar solvent, the previous studies of CuTSP and ZnTSP in water[1] demonstrated that the Cu dimer associates to a greater extent than the Zn pair. In water as a solvent, the dye–dye interaction is not the major driving force for aggregation. Instead the strong solvent–solvent interaction tends to exclude the dye molecules from solution and forces them to aggregate. In addition, complications arising from metal–water complexation may be operative. Solid-state studies on unsubstituted Cu and Zn pigments by Day and Williams[5] show that the Zn phthalocyanine is two orders of magnitude more conducting than the Cu pigment. Also the Davydov splitting in the crystal is 2230 cm^{-1} for the Zn and 1890 cm^{-1} for the Cu, indicating a larger interaction energy in the Zn crystal. Thus, the relative magnitudes of the interactions in the solid state agrees qualitatively with our studies in benzene. Therefore, molecular association processes in solvents of low dielectric constant perhaps reflect the ordering of the dye–dye interactions in the solid more accurately than in aqueous systems, where the solvent–solvent interaction is the major driving force for self-association.[3]

Acknowledgment. Informative discussions with Drs. M. S. Walker and D. F. Blossey are acknowledged with pleasure.

(5) P. Day and R. J. P. Williams, *J. Chem. Phys.*, **37**, 567 (1962).
(6) F. E. Dickson and L. Petrakis, *J. Phys. Chem.*, **74**, 2850 (1970).

The Dissociation Constant of the 9-Anthroic Acidium Cation in the Lowest Excited Singlet State

by Stephen G. Schulman* and Irene Pace

College of Pharmacy, University of Florida, Gainesville, Florida 32601 *(Received December 17, 1971)*

Publication costs borne completely by The Journal of Physical Chemistry

The large red shift of the fluorescence of 9-anthroic acid in moderately concentrated acid solutions has been investigated and attributed to prototropic equilibrium in the ^1La state between 9-anthroic acid and its conjugate cation. Comparison of pK_a* values for the latter equilibrium, obtained by fluorometric titration and by Förster cycle calculations, is used to evaluate thermal relaxation processes in ground and electronically excited states. Conversion of the fluorescence of 9-anthroic acid to that of the conjugate anion is found to be static. The excited-state reaction apparently is too slow to compete with fluorescence.

The fluorescences of 9-anthroic acid and the 9-anthroate anion have been studied recently.[1,2] The large Stokes shift of the acid has been well characterized as the result of rotation of the carboxyl group from perpendicularity, with the anthracene ring[2] in the anion, to coplanarity in the neutral acid. The previous studies also attempted to draw conclusions about the acidity of the acid in the lowest excited singlet state (the ^1La state), relative to that of the ground state, by means of Förster cycle calculations.[3] Förster cycle calculations of the dissociation constant of 9-

(1) E. Vander Donckt and G. Porter, *Trans. Faraday Soc.*, **64**, 3218 (1968).
(2) T. C. Werner and D. M. Hercules, *J. Phys. Chem.*, **73**, 2005 (1969).
(3) T. Förster, *Z. Elektrochem.*, **54**, 42 (1950).

anthroic acid in the lowest excited singlet state (pK_a^*), which employed the averages of absorption and fluorescence maxima for both conjugate species[1] and which indicated that the excited acid is much weaker than the ground-state acid,[4] were criticized[2] on the grounds that the excited-state rotation of the carboxyl group of the neutral acid probably results in violation of the assumption of equal protonation entropies in ground and excited states. In order to test this hypothesis, attempts were made, in this laboratory, to perform fluorometric titrations of 9-anthroic acid. In the course of these studies, emission was observed from the conjugate acid to 9-anthroic acid, a phenomenon that in itself is rather interesting since 9-anthroic acid is known to decarboxylate rather rapidly in strong acid media.[5]

Experimental Section

9-Anthroic acid was purchased from Aldrich Chemical Co. Inc., Milwaukee, Wis., and purified by multiple recrystallization from ethanol. Solutions for fluorometric titration were prepared by delivering 100 μl of 1.00×10^{-3} M 9-anthroic acid in ethanol to 10.00 ml of the appropriate perchloric or sulfuric acid, acetate, phosphate, or borate buffer solution.

Fluorescence spectra were taken on a Perkin-Elmer MPF-2A fluorescence spectrophotometer whose monochromators were calibrated against the line emission spectrum of xenon. Correction of spectral output for variability of response with wavelength of monochromators and photodetector was accomplished by means of a rhodamine B quantum counter.

Results and Discussion

Fluorometric titration of the 9-anthroate anion with H^+ showed the blue, structured fluorescence of the 9-anthroate anion to change to the green, diffuse emission of the neutral 9-anthroic acid in the pH region 5–1. The midpoint of this interconversion occurred at pH 3.0 and coincides with the ground-state pK_a of 9-anthroic acid. It would appear that prototropism during the lifetime of the lowest excited singlet states of 9-anthroic acid and its conjugate base is exceedingly slow compared with the rates of radiative deactivation of the species under consideration. Consequently, no definitive information concerning the thermodynamic significance of the rotation of the carboxyl group in the lowest excited singlet state was to be had from this approach. The spectral properties of 9-anthroic acid are summarized in Table I.

As the acidity of the anthroic acid solutions was increased, it was observed that the green, diffuse fluorescence of the neutral 9-anthroic acid red-shifted reversibly. The new emission was structureless and had its maximum at 1.78×10^4 cm^{-1}. The appearence of the emission at 1.78×10^4 cm^{-1} and the disappearance of the emission at 2.11×10^4 cm^{-1} both depended on the Hammett acitity H_0 in such a way as to fit the Henderson–Hasselbach equation. No change in the absorption spectra of the acid solutions employed in this fluorometric titration was observed. Consequently, the red-shifting of the 9-anthroic acid fluorescence with increasing acidity is attributed to protonation of the carboxyl group in the lowest excited singlet state, the yellow fluorescence at 1.78×10^4 cm^{-1} originating from the excited 9-anthroic acidium cation. The quantum yield of fluorescence of the latter species was determined by the method of Parker and Rees,[6] employing quinine bisulfate in 0.1 N H_2SO_4 as a standard, and found to be 0.19. The pK_a^* of the 9-anthroic acidium cation is estimated to be -1.4, the Hammett acidity at midpoint of the fluorometric titration. In solutions of Hammett acidity more negative than -6, the 0–0 band of the structured absorption spectrum of the neutral 9-anthroic acid, which appears at 2.61×10^4 cm^{-1} in dilute acid, red-shifted to 2.57×10^4 cm^{-1}, a shift which is probably due to the protonation of the neutral acid in the ground state. Accompanying the shift of the absorption spectrum, there was a decrease in the intensity of the yellow fluorescence of the 9-anthroic acid cation and the corresponding appearance and increase of a blue, structured fluorescence with 0–0 band at 2.48×10^4 cm^{-1}. Upon standing for about 2 hr, precipitation of small particles from the concentrated acid solutions ($H_0 = -8.1$[7]) was noted. A workable amount of the precipitate was collected, washed with water, and recrystallized from ethanol. The absorption and fluorescence spectra of the purified precipitate, as well as its melting point, indicated that it was anthracene. Since at acidities great enough to produce the excited cation of 9-anthroic acid but not to produce the ground-state cation, the fluorescence of the cation is stable for several hours, it is apparent that decarboxylation occurs in the ground

Table I: Absorption and Fluorescence Spectral Maxima of the Cation and Neutral Species Derived from 9-Anthroic Acid

	$10^{-4}\bar{\nu}_{abs}$, cm^{-1}	$10^{-4}\bar{\nu}_{flu}$, cm^{-1}
Cation (in concentrated $HClO_4$)	2.53[a]	1.78
Cation (in 1 M CCl_3COOH in $CHCl_3$)		1.88
Neutral species (in 0.1 M $HClO_4$ in water)	2.61[b]	2.11
Neutral species (in $CHCl_3$)	2.62[b]	2.11

[a] Estimated position of the 0–0 band of the cation absorption spectrum. [b] 0–0 band.

(4) A. Weller, *Progr. React. Kinet.*, **1**, 187 (1961).
(5) H. Schenkel and M. Schenkel-Rudin, *Helv. Chim. Acta*, **31**, 514 (1948).
(6) C. A. Parker and W. T. Rees, *Analyst (London)*, **85**, 587 (1960).
(7) K. Yates and H. Wai, *J. Amer. Chem. Soc.*, **86**, 5408 (1964).

state of 9-anthroic acid subsequent to protonation. Attempts to study the fluorescence of the cation and to complete the ground-state pK_a determination in sulfuric acid solutions of higher acidity than the perchloric acid media were thus unsuccessful. However, extrapolation of the protonation red shift of the absorption spectrum observed in perchloric acid yielded an approximate pK_a of -7.4 and indicated that the 0–0 absorption band of the isolated cation occurred at about 2.53×10^4 cm^{-1}.

Förster cycle calculations of the pK_a^* of the 9-anthroic acidium cation were performed, employing shifts of fluorescence spectra, absorption spectra, and the averages of absorption and fluorescence spectra. These results are summarized in Table II.

Table II: Ground (pK_a) and Lowest Excited Singlet State Dissociation Constants of the 9-Anthroic Acidium Cation

pK_a	pK_a^*(abs)[a]	pK_a^*(flu)[b]	pK_a^*(0–0)[c]	pK_a^*(FT)[d]
−7.4	−5.7	−0.5	−3.1	−1.4

[a] Calculated from the shift in the absorption spectra. [b] Calculated from the shift in the fluorescence spectra. [c] Calculated from the shift in the averages of the absorption and fluorescence spectra for each species. [d] Calculated from fluorometric titration.

The pK_a^* calculated from the fluorescence shift is in best agreement with that obtained from the fluorometric titration. The pK_a^* calculated from the absorption shift shows the poorest agreement with the fluorometric titration. These results can be rationalized from the following arguments. The pK_a^* determined from the fluorometric titration represents a thermodynamic parameter, calculated from the equilibrium distributions of two well-defined chemical entities, each having a particular geometrical structure, electronic configuration, and solvent cage. In the ^{1}La state both acid and conjugate base have the carboxyl group coplanar with the anthracene ring, a heavy concentration of electronic change in the carboxyl group, and a solvent cage which is in equilibrium with the excited molecule. All of these factors contribute to the chemical potential of each electronically excited species and thus to the difference in chemical potential between them (*e.g.*, the pK_a^*). In the ground state the carboxyl groups of both the cation and the neutral molecule are perpendicular to the anthracene ring (or nearly so), the electron density on each carboxyl group is not as great as in the ^{1}La state, and the solvent cages are characteristic of the ground-state geometries and electronic configurations. Owing to the differences in charge distributions, thermal rotation energies, and solvation energies, the relative chemical potentials and hence the equilibrium distributions of the ground- and excited-state acid and conjugate base and thus the pK_a and pK_a^* are generally different. Both the absorption and emission processes are very fast (10^{-15} sec), so that while fluorescence transitions originate and terminate in the excited-state geometrical and solvent configurations and by their intensities reflect the excited-state species distributions, absorptive transitions occur in molecules having the ground-state geometrical and solvent configurations and reflect the ground-state distributions. Thermal relaxation occurs in either terminal state subsequent to transition and is not reflected in the transition.

The Förster cycle enables rigorous calculation of pK_a^*, as a chemically significant quantity, only if the electronic transition energies employed in the calculation account for all differences in energy between the thermally relaxed ground- and excited-state species involved in the cycle. In other words, the free energies of ground- and excited-state dissociations and the electronic transition energies of acid and conjugate base must conform to a closed cycle. Assuming the entropies of dissociation to be identical in ground and excited states, this approach works well for conjugate acid–base pairs which do not undergo dramatic relaxation processes subsequent to excitation or emission. However, if thermal relaxation phenomena are appreciable in magnitude, in ground or excited states, and are unequal for conjugate acid and base, pK_a^* values calculated from absorption band shifts will be in error by the difference in thermal relaxation energy of acid and conjugate base in the excited state. Similarly, pK_a^* values calculated from fluorescence band shifts will be in error by the difference in thermal relaxation energy between acid and conjugate base in the ground state. The choice of whether to use absorption or fluorescence shifts to calculate the best value of pK_a^* will depend upon whether thermal relaxation discrepancies are greatest in excited or ground states. In molecules which are more polar in the excited state, thermal relaxation errors are usually more pronounced in the excited state and thus the calculation of pK_a^* from fluorescence shifts provides the best estimate of pK_a^*. In molecules which are more polar in the ground state absorption shifts might be expected to yield the best estimate of pK_a^*.

The averaging of absorption and fluorescence maxima of acid and conjugate base, respectively, to locate the 0–0 bands of the transitions[8] to be used in Förster cycle calculations was introduced in order to minimize vibrational relaxation errors in the calculations. However, this technique also averages into the calculation the solvent and configurational relaxation errors which are usually greater than vibrational errors. Thus the intelligent choice of fluorescence or absorption shifts will normally provide the best rapid estimation of pK_a^*.

(8) W. L. Levshin, *Z. Phys.*, **43**, 230 (1931).

While it is difficult to determine unambiguously the differences in thermal relaxation energies between the cation and neutral species derived from 9-anthroic acid, due exclusively to rotation of the carboxyl group and conjugation with the anthracene ring in ground and excited states, the much greater sensitivity of the position of the fluorescence maxima to protonation and dissociation suggests that this effect is more pronounced in the excited state. Moreover, it is possible to estimate the differences in solvent cage relaxation energies by observing the effect of a low dielectric solvent upon the fluorescence maxima. Thus in chloroform the fluorescence maximum of the neutral molecule is the same as in water while the fluorescence maximum of the cation lies 1000 cm^{-1} to higher frequencies than in water (Table I). This establishes that the cation is more polar in the excited state than in the ground state and that a solvent relaxation error of 2.1 units in pK_a^* from this source alone would be incurred if absorption shifts alone, or an error of 1.1 units would occur if the averaging technique were employed to calculate pK_a^*. Thus because the employment of absorption shifts in the Förster cycle fails to account for substantial differences in rotational, conjugative, and solvational stabilization of the excited cation and neutral molecule derived from 9-anthroic acid, the employment of fluorescence shifts produced by excited-state prototropism provides the best estimation of pK_a^*.

Dielectric Properties of Quaternary Ammonium Salt Hydrates

by George T. Koide*[1] and Edwin L. Carstensen

Department of Electrical Engineering, College of Engineering and Applied Science, University of Rochester, Rochester, New York *(Received February 24, 1972)*

Publication costs assisted by the University of Rochester

The quaternary ammonium halide hydrates undergo dielectric dispersion in the frequency range 10^2 to 10^7 Hz. Low-frequency dielectric constants, which can be attributed to bulk properties of the sample material rather than electrode phenomena, range from less than 100 to values in excess of 1000. The dielectric data expressed as a function of hydration number show a discontinuity near critical hydration numbers which are in close agreement with values which have been obtained by X-ray diffraction. In general, the low-frequency limit of the dielectric constant increases with temperature—in some cases with marked changes occurring near 0°. It appears that the dominant contribution to the dielectric polarization at low frequencies comes from dipoles created by movement of anions either in liquid or crystalline water relative to cations which have been trapped in the clathrate structure. Of all the hydrates studied, only that of tetra-*n*-butylammonium hydroxide hydrate relaxes at frequencies above 10 MHz. The polarization, the high conductivities, and high relaxation frequencies of this hydrate are probably related to the high effective mobility of the hydroxyl ion in the crystalline structure.

Introduction

Water in several structural forms has been studied by dielectric techniques. In the liquid state, near 0°, water has a relaxation frequency of approximately 9 GHz.[2] With the phase transition to hexagonal ice, its relaxation frequency falls abruptly to 7 kHz.[3] Although the relaxation frequency changes by many orders of magnitude, the low-frequency limit of the dielectric constant is affected very little by the phase transition and, in fact, to a good approximation goes as the reciprocal of the absolute temperature both above and below 0°. Davidson and his coworkers have found that several "gas" clathrate hydrates and high pressure ices have relaxation frequencies which are near 1 MHz, if extrapolated to 0°.[4-10]

Dielectric studies of protein solutions show a dispersion at uhf–vhf frequencies.[11-15] Pennock and Schwan suggest that the disperion above 100 MHz re-

(1) Address correspondence to this author at the Department of Electrical Engineering, Rochester Institute of Technology, Rochester, N. Y.

(2) C. H. Collie, J. B. Hasted, and D. M. Ritson, *Proc. Phys. Soc.*, **60**, 145 (1948).

(3) L. Onsager and M. Dupuis in "Electrolytes," Pergamon Press, New York, N. Y., 1962.

(4) D. W. Davidson and G. J. Wilson, *Can. J. Chem.*, **41**, 1424 (1963).

(5) G. J. Wilson and D. W. Davidson, *Can. J. Chem.*, **41**, 264 (1963).

(6) G. J. Wilson, P. K. Chan, D. W. Davidson, and E. Whalley, *J. Chem. Phys.*, **43**, 2384 (1965).

(7) A. D. Potts and D. W. Davidson, *J. Phys. Chem.*, **69**, 996 (1965).

(8) R. E. Hawkins and D. W. Davidson, *ibid.*, **70**, 1889 (1966).

sults from a rotational relaxation of the water bound to the protein. Since the protein itself may contribute to the relaxation in this frequency range, it is difficult to show unequivocally which of the components—protein or bound water—are responsible for the dispersion at uhf frequencies. In fact, there is no clear evidence as yet that water in any of its forms relaxes at uhf frequencies.

The clathrate hydrates are fascinating structural forms of water. Under the stabilizing influence of appropriate guest molecules, water is able to form open crystalline cages which are stable at temperatures above 30° in certain cases. In fact, it has been suggested that the bound water of proteins may have a crystalline structure similar to the clathrate hydrates.[16] The quaternary ammonium salt hydrates differ from the gas hydrates both in crystal structure and in the fact that ions are involved. The cations serve as guest molecules in the clathrate cavities and the anions are believed to be included in the clathrate water structure.[17]

This study was initiated to determine whether the kind of structural water found in the quaternary ammonium salt hydrates would provide a clear example of water with a rotational relaxation frequency in the uhf range. Instead, the dielectric propeties of these hydrates are dominated by a low-frequency relaxation which is probably related to the movement of ions in trapped liquid or protons in the crystalline structure.

Experimental Section

Methods and Materials. The salts used in this study were supplied by Distillation Products Industries, Division of Eastman Kodak Co. Water concentrations were determined by drying the samples under vacuum at 100° for 24 hr. In this investigation measurements were carried out on hydrates which in some cases contain more and in other cases less water than the amount required to form a complete clathrate structure around each of the cations. The term *hydration number* here is used to mean simply the ratio of the number of water molecules to the number of solute molecules in a given sample. The precise hydration number required to provide a complete clathrate shell for each guest molecule is called the *critical hydration number*. In this report, the hydration number follows the name of the salt; *e.g.*, tetraisoamylammonium chloride 41 indicates a sample of this salt with a hydration number of 41.

Precise measurements of the concentration of tetra-*n*-butylammonium hydroxide by the dry weight method were not possible because the compound sublimes. In this case samples with roughly the critical hydration number were prepared by first forming the hydrates at low temperature in an excess of water. The mixture of hydrate and water was filtered and the crystals were collected and dried on blotter paper for approximately 1 hr at 5°. These samples were then melted and poured into the measuring cell and recrystallized for measurements.

A simple calorimeter for measurements with the hydrates consisted of a 5-ml beaker containing the sample, heating elements, and a thermistor. This assembly was placed in a dewar. Starting at −20°, a power of about 50–100 mW was applied to the heating coil and the temperature of the sample was monitored as a function of time. The unit was calibrated with water.

Dielectric measurements in the frequency range 1–200 MHz were made using a Boonton Measurements Corp. 250A RX meter, those in the frequency range 0.1–4 MHz were made on a Wayne Kerr capacitance–conductance bridge B201, and those at low frequencies were performed with a special admittance bridge using techniques which have been described previously.[18–21] Observations of the dielectric properties of doped ice have been interpreted in part as an electrode phenomenon.[22] In our case the apparent low-frequency dielectric properties of the materials studied were shown to be independent of electrode spacing for separations ranging over a factor of 10. Thus the data reported here refer to the properties of the materials which constitute the samples and are independent of sample geometry and properties of the electrodes. In a few cases with highly conducting samples there was evidence that electrode polarization[23] affected the data at low frequencies. In these cases, data were corrected by standard techniques to remove the influence of polarization.[20]

(9) E. Whalley, D. W. Davidson, and J. B. R. Heath, *J. Chem. Phys.*, **45**, 3976 (1966).

(10) A. Venkateswaran, J. R. Easterfield, and D. W. Davidson, *Can. J. Chem.*, **45**, 884 (1967).

(11) H. P. Schwan, *Advan. Biol. Med. Phys.*, **5**, 147 (1957).

(12) H. P. Schwan, *Ann. N. Y. Acad. Sci.*, **125** (2), 344 (1965).

(13) M. W. Aaron, E. H. Grant, and S. E. Young, *Chem. Soc. Spec. Publ.*, **20**, 77 (1966).

(14) E. H. Grant, *Phys. Med. Biol.*, **2**, 17 (1957).

(15) B. E. Pennock and H. P. Schwan, *J. Phys. Chem.*, **73**, 2600 (1969).

(16) I. M. Klotz in "Protein Structure and Function," Brookhaven Symposia in Biology, No. 13, 1960, p 25.

(17) G. A. Jeffrey, *Sonderduck Dechema-Monogr.*, **47**, 849 (1962).

(18) H. Pauly and H. P. Schwan, *Biophys. J.*, **6**, 621 (1966).

(19) H. P. Schwan and K. Sittel, *IEEE Trans. Commun. Electron.*, **72**, 114 (1953).

(20) H. P. Schwan in "Physical Techniques in Biological Research," Vol. 6, Part B, W. L. Nastuk, Ed., Academic Press, New York, N. Y., 1963, p 323.

(21) C. W. Einolf, Jr., and E. L. Carstensen, *Biochim. Biophys. Acta*, **148**, 506 (1967).

(22) M. Ida and S. Kawada, *J. Phys. Soc. Jap.*, **21**, 561 (1966).

(23) This particular study and the general question of electrode polarization and space charge effects are discussed in detail in an internal report (Electrical Engineering Technical Report No. GMO9933-13, "The Dielectric Properties of Structured Water," by G. T. Koide and E. L. Carstensen) which may be made available to the interested reader. This is also available from University Microfilms, Ann Arbor, Mich., order no. 70-2884.

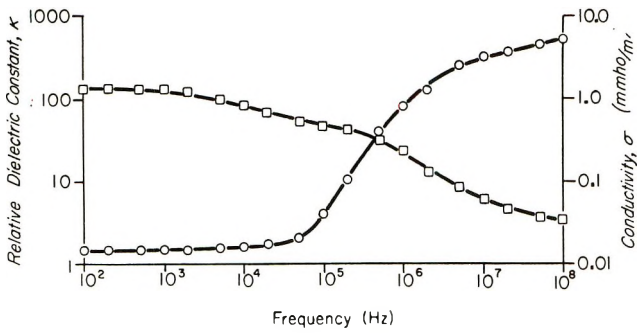

Figure 1. Dielectric constant (□) and conductivity (○) of tetraisoamylammonium chloride 36 hydrate; temperature 5°.

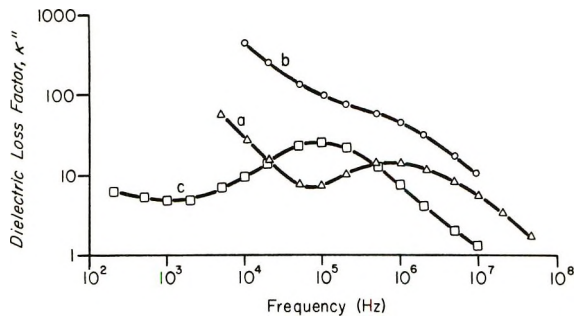

Figure 2. Dielectric loss factor κ'' for hydrates of tetraisoamylammonium chloride: a, hydration number, 36; temperature, 5°; b, hydration number, 41; temperature 5°; c, hydration number, 41; temperature, −18°.

Experimental Observations

This investigation included dielectric studies of hydrates formed with both the tetra-*n*-butylammonium cation and the tetraisoamylammonium cation as guests in the clathrate structure and the anions F^-, Cl^-, Br^-, $C_2O_4^-$, $C_2H_3O_3^-$, NO_3^-, and OH^- as a part of the water structure. In many cases, the measurements extended from 20 Hz to 200 MHz and included a wide range of temperature and solute concentrations. Of all the quaternary ammonium salt hydrates studied thus far, only one, tetra-*n*-butylammonium hydroxide, shows a relaxation in the uhf range. Even this may not represent rotational relaxation of water. However, in all the other quaternary ammonium hydrates studied, it is clear that water is either irrotational or characterized by relaxation frequencies of the order of 1 MHz or less. In all of the hydrates, there are low-frequency dispersion processes. The data presented here are intended to illustrate the great diversity which is found in the dielectric behavior of this class of hydrates.[24]

Frequency Dependence. Figure 1 gives the relative dielectric constant and conductivity for the hydrate of tetraisoamylammonium chloride with approximately the critical amount of water necessary to form the complete clathrate structure for all of the solutions. The conductivity at low frequencies in this hydrate is unusually low. However, because of this fact, it is possible to see a relaxation at around 0.5 MHz which may be present in other samples but is simply obscured by the high static conductivity. The relative loss factor curves in Figure 2 show the phenomenon.[25] For the same solute but with a slight excess of water the conductivity at 5° increases so much that the maximum in the κ'' curve is almost obscured. However, when this sample is cooled to −18° the low-frequency conductivity drops by nearly two orders of magnitude and the maximum in κ'' reappears this time shifted to about 0.1 MHz. As mentioned above, the tetraisoamylammonium chloride hydrate is the exception rather than the rule. In general, the quaternary ammonium salt hydrates have higher conductivities and appear to have a broad distribution of relaxation fre-

Table I: Low-Frequency Limits of the Dielectric Constants of Samples of Quaternary Ammonium Hydrates for Various Temperatures[a]

Sample	*T*, °C	Low-freq. limit for κ
Tetra-*n*-butyl-	−34	800
ammonium	−15	850
bromide 12	−10	900
	−5	1000
	1	1100
	5	500
Tetra-*n*-butyl-	−25	280
ammonium	−15	300
chloride 32	−6	350
	5	700
Tetraisoamyl-	−34	650 (100 Hz)
ammonium	−20	975 (100 Hz)
bromide 41	−11	1600 (100 Hz)
	2	4000 (100 Hz)
Tetraisoamyl-	−30	50
ammonium	−15	250
chloride 35	−8	250
	6	250
	10	250
	15	340
	20	500
Tetraisoamyl-	−34	50
ammonium	−18	50
chloride 41	−10	50
	1	150
	3	350
	10	350
	15	380
	20	420

[a] Asymptotic values corrected for electrode polarization where it exists are reported. At low frequencies the tetraisoamylammonium bromide hydrate did not show electrode polarization but neither did it appear to be approaching a static limit. The 100-Hz data give an indication of the properties of these samples.

(24) A much more complete description of these hydrates and their dielectric properties is given in the internal report mentioned in footnote 23.

(25) The relative loss factor $\kappa'' = \sigma/\epsilon_0\omega$ where σ is the conductivity, $\epsilon_0 = 8.85 \times 10^{-12}$ F/m is the permittivity of free space, and ω is the angular frequency.

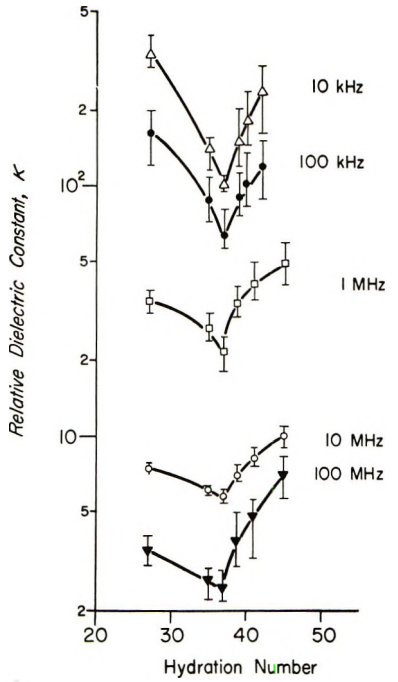

Figure 3. Relative dielectric constant of hydrates of tetraisoamylammonium chloride; temperature, 5°. Note the sharp minimum near the critical hydration number for this salt.

quencies extending up to roughly 10^6 Hz. The results of a large number of observations are summarized in Table I by giving just the low-frequency limit of the dielectric constant of the hydrate samples. Note that the dielectric constant is reduced at low temperatures.

Concentration. The critical hydration number for most of the quaternary ammonium hydrates shows clearly in the dielectric data. The dielectric constants for tetraisoamylammonium chloride (Figure 3) are typical for most of the samples studied. In these there is a sharp minimum in the dielectric constant when the water content of the sample reaches the critical value. An exception to the general pattern is found in the data for tetra-*n*-butylammonium bromide (Figure 4). In this case, the dielectric constant increases monotonically with hydration number but has an abrupt increase after passing beyond the critical number. At low temperatures, where presumably most of the liquid water has been frozen out (Figure 4b), the dielectric behavior is qualitatively different. Not only are the dielectric constant values significantly lower at all frequencies but there are no longer marked discontinuities in the data associated with the critical hydration number.

Temperature Dependence. The dielectric constants of all the samples increase with temperature. For most of the salts this increase is more or less continuous up to the melting temperature of the hydrates at which point the dielectric constant takes on the fre-

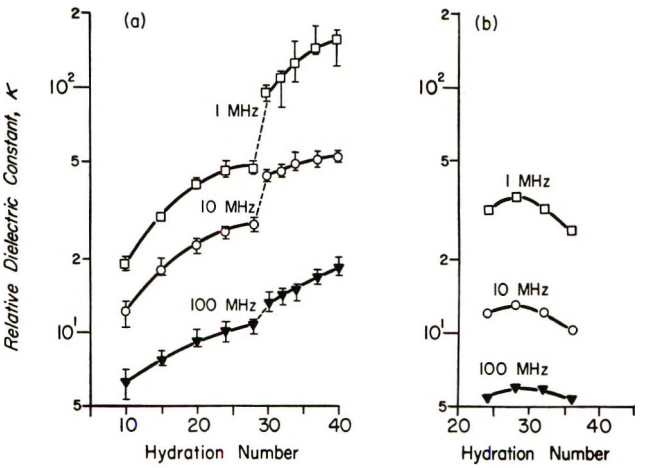

Figure 4. Relative dielectric constant for hydrates of tetra-*n*-butylammonium bromide: a, temperature, 5°; b, temperature, −20°. The discontinuities in the curves at high temperatures occur near the critical hydration number for this salt.

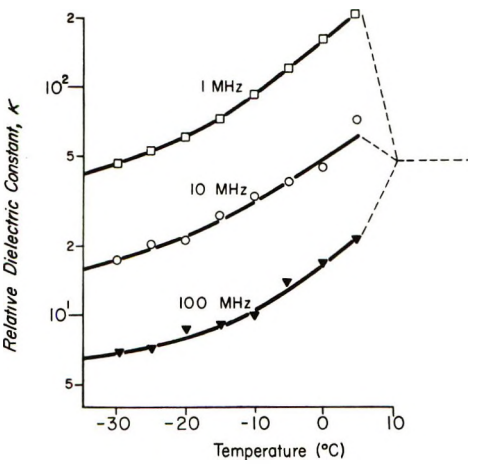

Figure 5. Relative dielectric constant for tetra-*n*-butylammonium chloride 36 hydrates. The dashed line at high temperatures is the frequency-independent dielectric constant which is characteristic of this sample in its liquid state.

quency independent value of the liquid solution. The data for tetra-*n*-butylammonium chloride with a hydration number of 36 in Figure 5 is fairly representative of most of the samples tested. In contrast, data for tetraisoamylammonium chloride 41 show an almost discontinuous increase of about 300 units in the relative dielectric constant near 0°. This must be related to the thawing of the excess liquid water in the sample (See Table I and Figure 6). There is a similar, although less marked, discontinuity near 0° in the low-frequency dielectric constant data for tetraisoamylammonium bromide 40.

As discussed below, the low-frequency dielectric constants appear to be related in part to movement of ions in liquid. With calorimetry it is possible to dem-

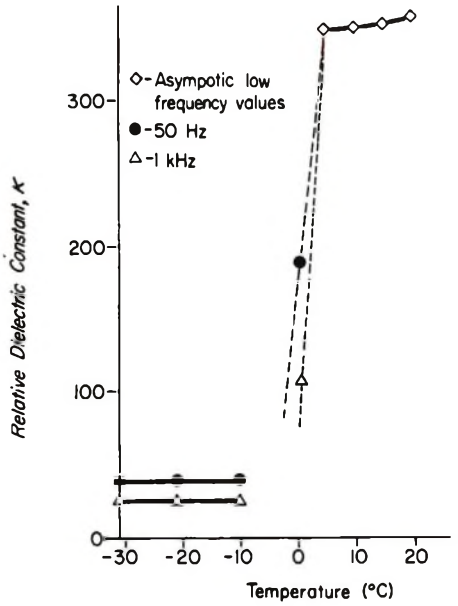

Figure 6. Relative dielectric constant for tetraisoamylammonium chloride 41 hydrates.

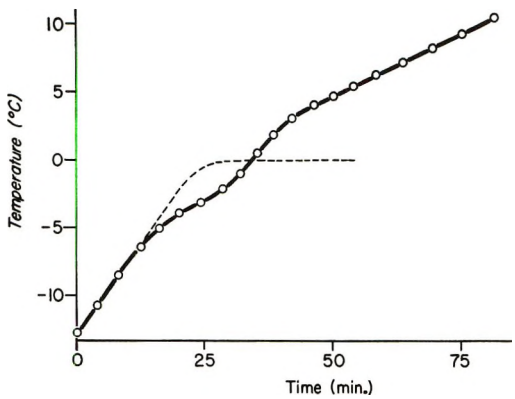

Figure 7. Heating curve for tetraisoamylammonium chloride 40; sample weight, 4.4 g; input heat, 56 mW. The dashed curve is that for a sample with the same amount of water (2.9 g) as contained in the hydrate sample and with 56 mW input heat.

onstrate that some water exists in the liquid state in the samples at temperatures well below 0°. Figure 7 shows the heating curve for tetraisoamylammonium chloride 40. Note the slope change which begins at about −7° indicating that some of the water begins to change state at this temperature. All samples tested showed evidence of liquid forming at temperatures below 0° with the exception of tetra-*n*-butylammonium bromide at below critical hydration numbers. The hydrates of this compound were unique in that the dielectric constants for samples of low water content were lower than those for samples near the critical hydration number (Figure 4).

The Hydroxide Hydrates. Tetra-*n*-butylammonium hydroxide hydrates are unique among the samples studied. Not only are the conductivities of these hydrates an order of magnitude or more higher than the others but from the appearance of the data in Figure 8 the relaxation frequency at temperatures around 0° must occur well above 100 MHz. The dielectric properties of tetraisoamylammonium hydroxide hydrates are similar to those of the halide hydrates.

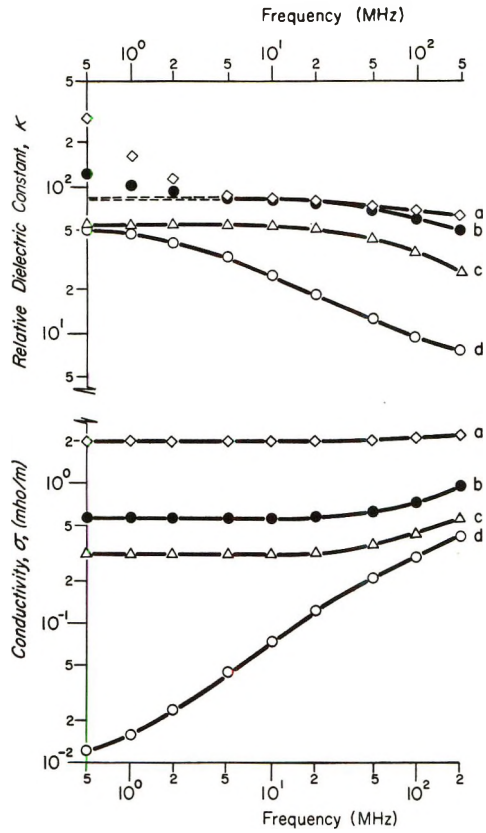

Figure 8. Dielectric constants and conductivities of tetra-*n*-butylammonium hydroxide hydrate: a, 5°; b, −6°; c, −20°; d, −38°. See Methods section for preparation of the sample and estimates of hydration number. The apparent dispersion in the dielectric constant below 5 MHz in curves a and b probably results from electrode polarization.

Discussion

Let us consider two general classes of relaxation processes which can lead to dispersion in the frequency range of these observations. One involves the preferred orientation of preexisting molecular dipoles; the other arises from the creation of dipoles by the displacement of ions of opposite sign relative to each other.[26,27]

In pure water only the first of these is important. The phenomenon of the rotation of polar molecules in the liquid state has been treated with some success

(26) Maxwell–Wagner[27] relaxation arising from the presence of conducting liquid "pockets" in an insulating solid would contribute minimally to the dispersion; *e.g.*, if 10% of the medium were highly conducting, the magnitude of the dispersion in the dielectric constant $\Delta\kappa$ would be only 1.05 κ_1 where κ_1 is the relative dielectric constant of the insulating portion of the medium.

(27) K. W. Wagner, *Arch. Elektrotech. (Berlin)*, **3**, 83 (1914).

by Onsager,[28] Kirkwood,[29] Debye,[30] and others. In the solid state, an answer to the question of how the molecules are able to "rotate" in the crystalline structure has been given by Bjerrum[31] in terms of lattice defects. Even though the relaxation frequency changes by many orders of magnitude with the changes in state of water, the contribution of the polar molecules to the low-frequency limit of the dielectric constant is of the order of 80–100 in all cases.

The presence of ions in liquid water has only a minor effect on rotational relaxation frequency[32] and the magnitude of the dielectric constant. The case for ice is somewhat different. The movement of ionic defects in ice may actually result in rotation of water molecules in a direction opposite to the electric field. As a consequence, the contribution of molecular dipoles to the dielectric constant is reduced.[33] Jaccard predicts a reduction in dielectric constant with an increase in ion concentration. The effect has been observed in ice doped by HF.[34,35] Thus, whereas in pure ice and water the rotation of permanent molecular dipoles is the only mechanism which contributes to the polarization, this effect can be reduced in ice by even small concentrations of ions.

The other general class of polarization phenomena, the creation of dipoles by relative motion of ions, is not understood in detail but there are numerous examples of this kind of process in the work of others. The Schwarz[36] mechanism, involving the movement of counterions relative to fixed surface charges, would fall into this category. There are many examples of high dielectric constants for doped ice (*e.g.*, ice doped with KOH and ice doped with NH_3).[37,38] In the most general terms, one would expect for this mechanism a low-frequency dielectric constant which would depend more or less directly upon the concentration of mobile ions and a relaxation frequency which is roughly proportional to the mobility of the counterions. In the case of the quaternary ammonium salt hydrates, since the cation is trapped in the clathrate structure, it is most reasonable to assume that the mobile ions are the anions. Halide ions in ice have mobilities which are lower by a factor of 10^4 than in water.[39] Thus halide ions can be considered mobile only if they are able to move in liquid water. On the other hand, hydronium and hydroxyl ions have an even higher effective mobility in ice than in water.[39] Assuming that the mobility characteristics of the ions are the same in the clathrate structure as in ice, it appears that a very wide range of dielectric constants and relaxation frequencies might be anticipated for the quaternary ammonium hydrates.

The studies reported in the preceding section were designed to determine whether rotational relaxation of water contributes to the dispersion of the quaternary ammonium hydrates and insofar as possible to determine the pathway for the movement of ions. Since it is apparent simply from the magnitudes of the low-frequency dielectric constants of the hydrates that rotational relaxation of water alone cannot explain the dielectric phenomena, let us first consider the mechanism involving ion movement.

Movement of Ions. From the relatively crude calorimetry illustrated in Figure 7, it is clear that many of the hydrate samples contain liquid water at temperatures as low as $-10°$. There is other evidence to suggest that liquid water may provide a pathway for the movement of ions in these samples, The abrupt shift in the low-frequency dielectric constants of tetraisoamylammonium chloride 41 with change in temperature near 0° (Table I) would be difficult to explain on any other basis. The gradual increase in dielectric constant with temperature up to 0° of most of the samples summarized in Table I would be consistent with a thawing of the hexagonal ice in the samples. On the other hand, although tetra-*n*-butylammonium bromide 32 seems to have a pronounced shift in relaxation frequency with temperature, its low-frequency dielectric constant holds at roughly 1000 independent of temperature (Table I). In this case it appears that the concentration of relaxing elements is relatively constant but that the mobility of the charge carriers depends strongly on temperature. The ions involved in this relaxation cannot be identified with any assurance from these studies. The possibility that the bromide ions move in trace amounts of liquid water cannot be ruled out but it is difficult to see that very much liquid water could remain in the samples at temperatures below $-30°$. Assuming that some liquid is present at these low temperatures, it would appear likely that a large fraction of the counterions would be immobilized as the freezing out process continues. Yet the magnitude of the dielectric constant remains above 800 even at the lowest temperature of observation. In fact, all halide hydrates measured with the exception of tetraisoamylammonium chloride have low-frequency–low-temperature dielectric constants well above 100.

Liquid samples of tetra-*n*-butylammonium bromide and chloride had pH values close to 7. Among the

(28) L. Onsager, *J. Amer. Chem. Soc.*, **58**, 1486 (1936).

(29) J. G. Kirkwood, *J. Chem. Phys.*, **7**, 911 (1939).

(30) P. Debye, "Polar Molecules," Dover Publications, New York, N. Y., 1929.

(31) N. Bjerrum, *Science*, **115**, 385 (1952).

(32) G. H. Harris, J. P. Hasted, and T. S. Buchanan, *J. Chem. Phys.*, **20**, 1452 (1952).

(33) C. Jaccard, *Helv. Phys. Acta*, **32**, 89 (1959).

(34) A. Steinmann and H. Granicher, *ibid.*, **30**, 553 (1957).

(35) H. Granicher, *Phys. Kondens. Mater.*, **1**, 1 (1963).

(36) A. Schwarz, *J. Phys. Chem.*, **66**, 2636 (1962).

(37) M. Ida and S. Kawada, *J. Phys. Soc. Jap.*, **21**, 561 (1966).

(38) A. Arias, L. Levi, and L. Lubert, *Trans. Faraday Soc.*, **62**, 1955 (1966).

(39) M. Eigen and L. DeMaeyer, *Proc. Roy. Soc., Ser. A*, **247**, 505 (1958).

tetra-*n*-butylammonium salt hydrates, hydroxyl hydrates have a melting temperature which is significantly higher than chloride and bromide hydrates. It is conceivable that upon lowering temperature, hydroxide hydrates are formed from the small number of hydroxyl ions in the solution in preference to the halide ions. As tetra-*n*-butylammonium hydroxide hydrates are formed more hydroxyl ions are created to satisfy the equilibrium constant. Thus, for the tetra-*n*-butylammonium salt hydrates, it may be possible that a higher concentration of hydroxide hydrates exist than would be anticipated from the pH of the liquid sample. This might account for the high conductivity and relaxation frequency of these hydrates.

Rotational Relaxation of Water. It appears that the dominant contribution to dielectric polarization at low frequencies comes from dipoles created by the movement of ions either in liquid or crystalline water. Whether there is any contribution from rotational relaxation of water is difficult to tell in the presence of the ionic mechanism. If a liquid pathway were important for the movement of these ions, it might be possible to suppress the low-frequency mechanism by "freezing out" this water. This would not be expected to reduce the magnitude of the rotational relaxation of the clathrate water, but merely to shift its relaxation frequency. Of the experiments described in the previous sections this technique was "successful" only for the tetraisoamylammonium chloride samples. With tetraisoamylammonium chloride 36 at 5° (Figure 2) there appears to be a maximum in κ'' at about 500 kHz. The dielectric constant (around 100 at 100 kHz) is too high to be accounted for by the amount of water present in the sample. When a little more water is present in the sample (tetraisoamylammonium chloride 41, Figure 2) the low-frequency dielectric constant and conductivity increase and the maximum in κ'' nearly disappears. When the temperature of this sample is reduced to $-18°$ the maximum in κ'' again appears, this time at about 100 kHz. The dielectric constant is low enough at this temperature that it could be accounted for by the amount of water present in the sample. This evidence is far from conclusive but it leaves open the possibility that a rotational relaxation exists in the quaternary ammonium salt hydrates which is similar to that found by Davidson and coworkers for the gas clathrates and high-pressure ices.

Hydroxide Hydrates. The movement of ions in crystalline water was suggested above as a possible mechanism for the observed dispersion in the halide hydrates at temperatures below freezing. It is clear that such a mechanism must be considered with the hydroxide hydrates. The hydroxyl ion has a high mobility in ice.[39] If it has a similar mobility in the clathrates this may explain the high conductivities and high relaxation frequencies of tetra-*n*-butylammonium hydroxide hydrate. Whether rotational relaxation of the water molecules is involved at all is open to question. Since roughly 40% of the clathrate is occupied by the nonpolar quaternary ammonium cation, the dielectric constant of the samples above $-6°$ is too high to be accounted for by the water present in the sample.

Conclusions

The magnitude of the dielectric constant at low frequencies in most samples is too great to be accounted for by the preferred orientation of molecular dipoles. Instead it appears that the polarization results from the creation of dipoles by movement of ions relative to other ions which have been trapped in the crystal structure. Calorimetry has shown that liquid water exists in the samples at temperatures somewhat below 0°. Thus it is possible that some of the ions may move in liquid water. Movement of hydronium or hydroxyl ions in the crystal structure may also contribute to the polarization.

The relaxation frequencies of tetra-*n*-butylammonium hydroxide hydrate are higher than those of the halide hydrates. The polarization, the high conductivities, and high relaxation frequencies of these hydrates are probably related to the high concentration and effective mobility of the hydroxyl ions in the crystalline structure.

In all of the observations there is no clear-cut evidence for rotational relaxation of the polar water molecules. It may exist but could simply be obscured by the ionic mechanism. The experiment with tetraisoamylammonium chloride 41 keeps this possibility open. However, this study of the quaternary ammonium salt hydrates contributes no positive support to the postulate that bound water is responsible for the relaxation of protein solutions at vhf–uhf frequenies. All of the clathrates relax at much lower frequencies with the exception of the tetra-*n*-butylammonium hydroxide hydrate. Even in the hydroxide hydrate it is unlikely that the vhf dispersion results from a simple rotational relaxation of water.

Acknowledgments. The authors are indebted to Mr. R. W. Smearing and Mr. J. Lozina for extensive help in the initial stages of this investigation and to Mrs. Sally Child for continued technical assistance throughout the investigation. The authors wish to thank Dr. D. W. Davidson, National Research Council, Ottawa, Canada, Dr. W. Y. Wen of Clark University, Drs. W. F. Newman, S. Shapiro, D. W. Healy, Jr., W. Streifer, and J. A. Kampmeier, all of the University of Rochester for helpful discussions. This work was supported in part by U.S. P. H. S. Grant No. GMO9933. Dr. Koide was an N. I. H. Fellow under U. S. P. H. S. Grant No. 2TIGN540.

Excitation of Molecular Vibration on Collision. Simultaneous Vibrational and Rotational Transitions in Hydrogen + Argon at High Collision Velocities[1]

by Hyung Kyu Shin

Contribution No. 1037 from the Theoretical Chemistry Group, Department of Chemistry, University of Nevada, Reno, Nevada 89507 *(Received February 3, 1972)*

Publication costs assisted by the U. S. Air Force Office of Scientific Research

Simultaneous vibrational and rotational transitions in H_2 + Ar at high collision velocities have been studied by use of the sudden approximation. The probabilities of $0 \rightarrow 1$, $0 \rightarrow 2$, and $1 \rightarrow 2$ vibrational transitions simultaneously occurring with the rotational change of $jm = 00$ to 00, 20, or 40 at zero impact parameter in the velocity range of 10^6 to 10^7 cm/sec have been calculated. The perturbation energy has been derived from high-velocity beam experiments. Each simultaneous transition probability takes a maximum value at the neighborhood of 10^6 cm/sec, and then always decreases with increasing velocity. For a given vibrational transition, the $00 \rightarrow 20$ rotational change produces the largest energy transfer above 10^6 cm/sec. Only important rotational transitions are found to be $00 \rightarrow 20$ and $00 \rightarrow 40$. Calculation is extended to the collision taking place at velocities lower than 10^6 cm/sec to find the undulatory variation of the simultaneous transition probabilities. The vibrational transition probabilities at collinear and perpendicular orientations are also calculated. In the limit of high collision velocities, the collinear transition probability is larger than the orientation-averaged probability by a factor of 5.6 for both $0 \rightarrow 1$ and $1 \rightarrow 2$, and by 10 for $0 \rightarrow 2$; at lower velocities the factors seriously deviate from these values and furthermore they depend strongly on the velocity indicating that the orientation dependence of the vibrational transition probability cannot be given by any simple steric factor.

I. Introduction

In the studies of vibrational energy transfer in molecular collisions, we often encounter the dependence of energy transfer probabilities on molecular orientations.[2-6] The coupling between rotation and vibration is usually strong, so that the rotational state generally changes before the vibrational transition occurs. If the interaction energy is strongly orientation dependent, the molecules may take a particular orientation during the collision; this problem of vibrational transitions at preferred orientations has been investigated in ref 6. Rotational transitions affect vibrational energy transfer by enabling the orientation-dependent part of the potential to contribute. Also, rotational transitions can alter the translational energy, thus affecting the transition probability. Sometimes, the final form of vibrational transition probability is integrated over all possible molecular orientations to obtain the orientation-averaged probability. This procedure is equivalent to a sum over all rotational transitions. Wartell and Cross[7] have investigated the problem of vibrational energy transfer in H_2 + He in the energy range of 0.17–17 eV by including effects of concurrent rotationally inelastic scattering and the orientation dependence of the potential. Although extensive consideration has been given to both the purely vibrational and purely rotational transitions, the problem of simultaneous vibrational and rotational transitions has not been subjected to critical investigation. Such problems can be particularly important in collision systems involving hydrogen molecules.

In recent years knowledge of short-range interaction potential energies between atoms, between an atom and a molecule, and between molecules has become available from measurements for the scattering of high-velocity beams.[8,9] In addition, with the advent of large memory high-speed computers, accurate *a priori* interaction potential functions are also becoming available.[10-13]

(1) This work was supported by the U. S. Air Force Office of Scientific Research, Grant AFOSR-72-2231.

(2) (a) K. F. Herzfeld and T. A. Litovitz, "Absorption and Dispersion of Ultrasonic Waves," Academic Press, Inc., New York, N. Y., 1958, Chapter 7; (b) T. L. Cottrell and J. C. McCoubrey, "Molecular Energy Transfer in Gases," Butterworths, London, 1961, Chapter 6.

(3) K. Takayanagi, *Advan. At. Mol. Phys.*, **1**, 149 (1965).

(4) D. Rapp and T. Kassal, *Chem. Rev.*, **69**, 61 (1969).

(5) H. Shin, *J. Chem. Phys.*, **47**, 3302 (1967); *J. Phys. Chem.*, **73**, 4321 (1970).

(6) H. Shin, *J. Chem. Phys.*, **49**, 3964 (1968).

(7) M. A. Wartell and R. J. Cross, *Chem. Phys. Lett.*, **5**, 477 (1970). Also see R. J. Cross, *J. Chem. Phys.*, **47**, 3724 (1967).

(8) E. A. Mason and J. T. Vanderslice in "Atomic and Molecular Processing," D. R. Bates, Ed., Academic Press, New York, N. Y., 1962, pp 663–695.

(9) (a) S. O. Colgate, J. E. Jordan, I. Amdur, and E. A. Mason, *J. Chem. Phys.*, **51**, 968 (1969); also see references therein. (b) J. E. Jordan, S. O. Colgate, I. Amdur, and E. A. Mason, *ibid.*, **52**, 1143 (1970).

(10) C. S. Roberts, *Phys. Rev.*, **131**, 203 (1963).

(11) M. Krauss and F. H. Mies, *J. Chem. Phys.*, **42**, 2703 (1965).

(12) M. D. Gordon and D. Secrest, *ibid.*, **52**, 120 (1970).

(13) W. A. Lester, *ibid.*, **53**, 1511, 1611 (1970); **54**, 3171 (1971).

These studies provide analytical forms of interaction potential energy which are needed in investigating the problem of vibrationally inelastic scattering. Some of the reported potential functions[8,9] often obey the approximate form of $U(r) = K/r^s$, where r is the relative separation between the colliding partners, and K and s are the potential parameters. Since such explicit potential functions are available, we can now make rigorous calculations of molecular energy transfer probabilities.

In the present paper we shall report the study of simultaneous vibrational and rotational transitions in H_2 + Ar for which the interaction potential function is available from high-velocity beam experiments. We shall use the sudden approximation[7,14-18] with the assumptions of constant relative velocity and linear trajectory; the approximation is valid in the velocity range where the vibrational period is long compared to the collision time. While the approximation is not valid at thermal energies, it should be fairly good at energies in the electron-volt range where there are data on interaction potentials. For this collision system, the potential function determined by Colgate, Jordan, Amdur, and Mason[9a] will be used. We shall calculate the probabilities of $0 \rightarrow 1$, $0 \rightarrow 2$, and $1 \rightarrow 2$ vibrational transitions occurring simultaneously with the change in rotational states $jm \rightarrow j'm'$, where j and m are the rotational and orientational quantum numbers, at high collision velocities. The collision model will be developed for arbitrary impact parameters, but the formulation and calculation of transition probabilities will be made for the case of a rotating oscillator with zero impact parameter. In addition, we shall report the calculation of orientation-averaged transition probabilities as well as the probabilities at collinear and perpendicular collisions.

II. Interaction Potential Function

The interaction potential function determined by Colgate and coworkers from high-velocity beam scattering experiments is[9a]

$$U(r) = 159/r^{6.28} \text{ eV} \quad (1)$$

This expression represents the spherically symmetric part of the H_2 + Ar interaction, and it does not produce vibrational and/or rotational transitions. However, we can derive an approximate overall form of the H_2 + Ar interaction energy which includes eq 1 as its unperturbed part. For this purpose we write the overall potential as a function of the two Ar···H distances r_1 and r_2, which are defined in Figure 1

$$V(r_1,r_2) = A/r_1^s + A/r_2^s \quad (2)$$

Since the distances are

$$r_{1,2} = [r^2 \mp (d + \xi)r \cos\Theta + {}^1/_4(d + \xi)^2]^{1/2} \quad (3)$$

the overall interaction potential becomes

$$V(r,\Theta,\xi) = A\{[r^2 - (d + \xi)r \cos\Theta + {}^1/_4(d + \xi)^2]^{-s/2} + [r^2 + (d + \xi)r \times \cos\Theta + {}^1/_4(d + \xi)^2]^{-s/2}\} \quad (4a)$$

which by expanding the denominators in a power series of $(d + \xi)/r$, can be reduced to

$$V(r,\Theta,\xi) = \frac{2A}{r^s} + \frac{s(s + 2)A}{4r^{s+2}} \times \left(\cos^2\Theta - \frac{1}{s + 2}\right)(d + \xi)^2 + \ldots \quad (4b)$$

Notice that when the denominators in eq 4a are expanded, all terms in odd powers of $(d + \xi)/r$ of the first part cancel with those of the second. The zero- and second-order terms are shown in eq 4b. The fourth- and high-order terms make much less important contribution to the overall interaction energy. Equation 4b can also be written as

$$V(r,\Theta,\xi) = \frac{K}{r^s} - \frac{sd^2K}{8r^{s+2}} + \frac{s(s + 2)d^2K}{8r^{s+2}} \cos^2\Theta + \frac{s(s + 2)dK}{4r^{s+2}}\left(\cos^2\Theta - \frac{1}{s + 2}\right)\left(\xi + \frac{\xi^2}{2d}\right) \equiv U(r) + U(r,\Theta) + U(r,\Theta,\xi) \quad (5)$$

where $K = 2A$. When we set $K = 159$ eV Å$^{6.28}$ and $s = 6.28$, the spherically symmetric term, $U(r)$ =

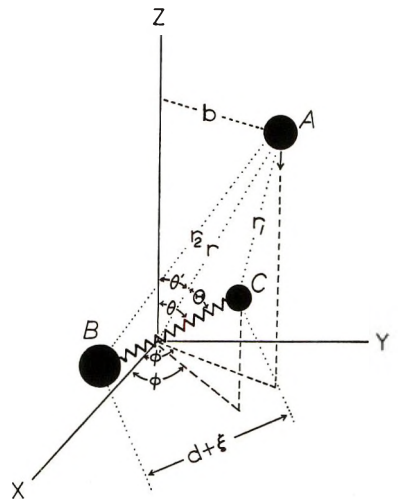

Figure 1. Collision geometry for the approach of the incident atom A toward the rotating, vibrating molecule BC; ξ represents the displacement of the oscillator amplitude from the equilibrium value.

(14) K. Alder and A. Winther, "Coulomb Excitation," Academic Press, New York, N. Y., 1966, pp 209–280; the original article appeared in *Kgl. Dan. Vidensk. Selsk., Mat. Fys. Medd.*, **32**, 8 (1960).

(15) K. H. Kramer and R. B. Bernstein, *J. Chem. Phys.*, **40**, 200 (1960); **44**, 4473 (1966); R. W. Fenstermacker and R. B. Bernstein, *ibid.*, **47**, 4417 (1968).

(16) J. P. Toennis, *Z. Phys.*, **193**, 76 (1966).

(17) H. Shin, *J. Phys. Chem.*, **75**, 923 (1971).

(18) H. Shin, *ibid.*, **75**, 3185 (1971).

$159[1 - 0.785(d/r)^2]r^{-6.28}$ eV, which represents the unperturbed interaction, closely reproduces the experimental result given by eq 1. Note that the experimental data were obtained for 1.89 Å $< r <$ 2.31 Å, so that the additional term $-0.785(d/r)^2$ in the square brackets of $U(r)$ is very small compared to unity; since $d = 0.741$ Å, the correction term changes from -0.120 to -0.0807. The second term $U(r,\Theta)$ of eq 5 produces purely rotational transitions and the third $U(r,\Theta,\xi)$ the transitions involving both vibrations and rotations. Therefore, to investigate simultaneous vibrational and rotational transitions in H_2 + Ar, we take the perturbation energy as

$$U(r,\Theta,\xi) = \frac{13dK}{r^{8.28}}(\cos^2\Theta - 0.1207)\left(\xi + \frac{\xi^2}{2d}\right) \quad (6)$$

with $K = 159$ eV Å$^{6.28}$ and $s = 6.28$. The equilibrium bond distance d is 0.741 Å, or $1.4a_0$, and the range of vibrational amplitude of interest is perhaps $\pm 0.2a_0$. Thus we can take $2d \gg \xi$ and neglect the term $\xi^2/2d$ in eq 6.

From the collision geometry shown in Figure 1, the relative orientation angle can be related to the molecular rotation angles θ, ϕ, and the impact parameter b as

$$\cos\Theta = \frac{z\cos\theta + b\sin\theta\cos\phi}{(b^2 + z^2)^{1/2}} \quad (7)$$

By rotating the coordinate system about the z axis, the azimuthal angle ϕ' has been eliminated from eq 7. We use the linear trajectory and constant relative velocity approximation for the present high-velocity collision system; *i.e.*, $r^2 = b^2 + z^2$ and $z \simeq vt$, where v is the relative velocity. For the impact parameter zero, eq 7 simply reduces to $\cos\Theta = \cos\theta$, the relation which will be used in the following formulation of transition probabilities.

III. Transition Probabilities

A. Simultaneous Vibrational and Rotational Transitions. According to the sudden approximation, the probability of simultaneous vibrational ($n \rightarrow n'$) and rotational ($jm \rightarrow j'm'$) transitions takes the form[7,14-18]

$$P_{nn'}^{jmj'm'} = |\langle n'j'm'|\exp[2i\eta(v,b,\Theta,\xi)]|njm\rangle|^2 \quad (8)$$

where the phase shift is given by

$$\eta(v,b,\Theta,\xi) = -\frac{1}{2\hbar}\int_{-\infty}^{\infty} U(r,\Theta,\xi)\,dt \quad (9)$$

Equation 8 therefore involves the evaluations of vibrational and rotational matrix elements. For the zero impact parameter collision, $\Theta = \theta$. For the present system it is now necessary to modify the lower integration limit; we choose the coordinate system in which the incident atom comes in along the z axis with the velocity v and strikes the target molecule. However, the atom cannot approach the distance closer than the "hard-sphere collision diameter." We shall denote this distance by l and replace the lower integration limit by l. This procedure is equivalent to setting $r = l + vt$ and writing the integral as $\int_0^\infty (l + vt)^{-8.28}\,dt$.

The integration of eq 9 with the perturbation energy given by eq 6 is trivial; the result is

$$\eta(v,\theta,\xi) = -\frac{0.4464d^2K}{\hbar v l^{7.28}}\cos^2\theta - \frac{0.8929dK}{\hbar v l^{7.28}}(\cos^2\theta - 0.1207)\xi \quad (10)$$

where we set $b = 0$ and $\Theta = \theta$. The first term of this expression is due to the rotational motion and produces purely rotational transitions; it does not contribute directly to vibrational transitions. Then, the transition probability of simultaneous vibrational and rotational transitions takes the form

$$P_{nn'}^{jmj'm'} = \left|\left\langle n'j'm'\left|\exp\left[-\frac{1.785dKi}{\hbar v l^{7.28}} \times (\cos^2\theta - 0.1207)\xi\right]\right|njm\right\rangle\right|^2 \quad (11)$$

We shall use the harmonic oscillator wave functions in eq 11. Then, the vibrational matrix element can be evaluated as[19]

$$\left\langle n'\left|\exp\left[-\frac{1.785dKi}{\hbar v l^{7.28}}(\cos^2\theta - 0.1207)\xi\right]\right|n\right\rangle = \exp(\alpha^2)\left[\frac{n!}{n'!}2^{n'-n}\right]^{1/2}|\alpha|^{n'-n}\mathfrak{L}_n^{n'-n}(-2\alpha^2) \equiv \mathcal{U}^{nn'} \quad (12)$$

where

$$\alpha = -\frac{1.262dKi}{(2M\hbar\omega)^{1/2}vl^{7.28}}(\cos^2\theta - 0.1207)$$

and $\mathfrak{L}_n^{n'-n}$ is the Laguerre polynomial with $n' \geq n$; M and ω are the reduced mass and vibrational frequency of H_2, respectively. We must note that the formula $\mathcal{U}_{nn'}$ for the matrix elements given by Rapp and Sharp[19] is not valid for complex argument of the exponential. For the odd values of $|n - n'|$ the matrix elements given by them must be multiplied by $-i$, and for the even values by -1. However, this situation does not affect the expectation values of these matrix elements which appear in the final form of the transition probability. Equation 11 may then be simplified as

$$P_{nn'}^{jmj'm'} = |\langle j'm'|\mathcal{U}_{nn'}|jm\rangle|^2 \quad (13)$$

For the first three vibrational transitions, we have

$$P_{01}^{jmj'm'} = |\langle j'm'|F\exp(-{}^1/_2F^2)|jm\rangle|^2$$

$$P_{02}^{jmj'm'} = {}^1/_2|\langle j'm'|F^2\exp(-{}^1/_2F^2)|jm\rangle|^2$$

$$P_{12}^{jmj'm'} = 2|\langle j'm'|F(1 - {}^1/_2F^2)\exp(-{}^1/_2F^2)|jm\rangle|^2$$

(19) D. Rapp and T. E. Sharp, *J. Chem. Phys.*, **38**, 2641 (1963).

where

$$F = \frac{1.785dK}{(2M\hbar\omega)^{1/2}vl^{7.28}}(\cos^2\theta - 0.1207)$$

Because of the complicated v dependence of vibrational matrix elements, eq 13 cannot be integrated to analytical forms; we shall integrate the rotational matrix elements numerically in the numerical section below.

B. Orientation-Averaged Transition Probabilities. The orientation-averaged transition probability can be defined as the square of the vibrational matrix element integrated over all possible values of θ and ϕ

$$P_{nn'}^{\text{ave}} = \frac{1}{4\pi}\int_0^{2\pi}\int_0^{\pi}|\mathcal{U}_{nn'}|^2 \sin\theta \, d\theta \, d\phi \qquad (14)$$

The average is exactly equivalent to a sum over rotational transitions and an average over initial m states. Since for the present zero-b collision, F is a function only of θ, the ϕ integration is simply 2π. The θ integration will have to be carried out numerically.

C. Collinear and Perpendicular Collisions. We shall also investigate the vibrational transitions at the collinear and perpendicular collisions. From eq 8 and 13 we notice that the square of the vibrational matrix element represents the vibrational transition probability at a specific molecular orientation θ (or Θ); we shall denote the θ-dependent probability as

$$P_{nn'}^{\theta} = |\mathcal{U}_{nn'}|^2 \qquad (15)$$

Then the collinear and perpendicular collision probabilities will be denoted by $P_{nn'}^{0°}$ and $P_{nn'}^{90°}$, respectively.

For these two types of collisions, the function F which is contained in the vibrational matrix element can be obtained in the forms which are somewhat different from the one given above. For $\theta = 0°$, the interaction distances are $r_1 = r - {}^1/_2(d + \xi)$ and $r_2 = r + {}^1/_2(d + \xi)$. When these distances are introduced in eq 2, the overall interaction potential can be obtained as

$$V(r,\xi) = \frac{K}{r^{6.28}}\left(1 + 5.71\frac{d^2}{r^2}\right) + \frac{11.4dK}{r^{8.28}}\xi \qquad (16)$$

so that the vibrational matrix element is

$$\mathcal{U}_{nn'} = \left\langle n'\left|\exp\left[-\frac{1.566dKi\xi}{\hbar vl^{7.28}}\right]\right|n\right\rangle \qquad (17)$$

Therefore, the function F is

$$F = \frac{1.566dK}{(2M\hbar\omega)^{1/2}vl^{7.28}} \qquad (18)$$

On the other hand, for the perpendicular collision, the distances are $r_1 = r_2 = [r^2 + {}^1/_4(d + \xi)^2]^{1/2}$, and the overall potential is

$$V(r,\xi) = \frac{K}{r^{6.28}}\left(1 - 0.785\frac{d^2}{r^2}\right) - \frac{1.570dK}{r^{8.28}}\xi \qquad (19)$$

The vibrational matrix element is

$$\mathcal{U}_{nn'} = \left\langle n'\left|\exp\left[\frac{0.215dKi\xi}{\hbar vl^{7.28}}\right]\right|n\right\rangle \qquad (20)$$

and the F function is

$$F = \frac{0.215dK}{(2M\hbar\omega)^{1/2}vl^{7.28}} \qquad (21)$$

Equations 18 and 21 will be introduced in eq 15 for the collinear and perpendicular collisions, respectively.

D. Comparison with Forced-Oscillator Transition Probabilities. Before concluding the derivation of vibrational transition probabilities, it is important to recognize that the square of the vibrational matrix element is in a form identical with the vibrational transition probability obtained from the solution of the time-dependent[20,21] or time-independent[22] wave equation for the forced harmonic oscillator. This solution gives

$$P_{nn'} = n!n'!\exp(-\epsilon_0)\epsilon_0^{n+n'} \times \left[\sum_{j=0}^{k}\frac{(-1)^j\epsilon_0^{-j}}{(n' - j)!j!(n - j)!}\right]^2 \qquad (22)$$

where k is the lesser of n and n' and ϵ_0 is the energy absorbed by the oscillator measured in units of the vibrational energy quantum $\hbar\omega$. Therefore, if we set $F^2 = \epsilon_0$, then eq 22 is identical with the transition probability given by eq 15.

The classically calculated energy transfer in units of $\hbar\omega$ is [2b-4]

$$\epsilon_0 = \frac{1}{2M\hbar\omega}\left|\int_{-\infty}^{\infty}\mathcal{F}(t)\exp(i\omega t)dt\right|^2 \qquad (23)$$

where the time-dependent perturbation force can be obtained from eq 5 as $U(r,\Theta,\xi) = -\mathcal{F}[r(t)]\xi$, *i.e.*

$$\mathcal{F}(t) = -\frac{s(s + 2)dK}{4[r(t)]^{s+2}}\left(\cos^2\Theta - \frac{1}{s + 2}\right) \qquad (24)$$

Then the energy transfer is

$$\epsilon_0 = \frac{1}{32M\hbar\omega}\left[s(s + 2)dK\left(\cos^2\Theta - \frac{1}{s + 2}\right)\right]^2 \times \left|\int_{-\infty}^{\infty}\frac{\exp(i\omega t)}{[r(t)]^{s+2}}\,dt\right|^2 \qquad (25)$$

The last integral is

$$\int_{-\infty}^{\infty}\frac{\exp(i\omega t)}{(l + vt)^{s+2}}\,dt = \frac{1}{vl^{7.28}}\int_0^{\infty}\frac{\cos(\beta z)}{(1 + z)^{8.28}}\,dz \qquad (26)$$

where $\beta = \omega l/v$. The integral in the right-hand side of eq 26 can be integrated by parts to obtain the recursion relation

(20) E. Kerner, *Can. J. Phys.*, **36**, 371 (1958).
(21) C. E. Treanor, *J. Chem. Phys.*, **43**, 532 (1965); **44**, 2220 (1966).
(22) H. Shin, *Chem. Phys. Lett.*, **3**, 125 (1969).

$$I_J = \int_0^\infty \frac{\cos(\beta z)}{(1+z)^{J+1}}\,dz = \frac{1}{J} - \frac{\beta^2}{J(J-1)} I_{J-2} \quad (27a)$$

where $J = 7.28$. The completion of the integration results in six terms containing β^0, β^2, β^4, β^6, and β^8. For high-velocity collisions, β is not greatly different from unity, and then we can approximate[23]

$$\int_0^\infty \frac{\cos(\beta z)}{(1+z)^{J+1}}\,dz \simeq \frac{1}{J} \quad (27b)$$

which leads to the expression of ϵ_0 that is identical with F^2 given above. At low velocities where β can be very large compared to unity and where the difference between ϵ_0 and F^2 becomes serious, the latter being much larger than the former, the use of the sudden approximation cannot be justified.

IV. Numerical Results and Discussion

To calculate transition probabilities we need to estimate the value of l. By taking the van der Waals radius of Ar to be 1.5 Å, the equilibrium bond distance 0.74 Å, and the crystal radius[24] of hydrogen 0.25 Å, we estimate the value as 2.1 Å. The vibrational frequency[25] ($\omega = 2\pi\nu$) is 7.83×10^{14} sec^{-1}. For the present zero b collision the interaction energy is independent of ϕ, and we shall consider the rotational transitions from $jm = 00$ to $j'm' = 00$, 20, and 40 for the $0 \rightarrow 1$, $0 \rightarrow 2$, and $1 \rightarrow 2$ vibrational transitions in the velocity range of 10^6 to 10^7 cm/sec, which corresponds approximately to the energy range of 1 to 100 eV; the results for this velocity range are shown in Figures 2, 4, and 6 for $0 \rightarrow 1$, $0 \rightarrow 2$, and $1 \rightarrow 2$ vibrational transitions, respectively. Although the applicability of the sudden approximation is doubtful, we shall extend the calculation to velocities below 10^6 cm/sec to obtain qualitative information on the variation of transition probabilities in low velocity collisions; see Figures 3, 5, and 7.

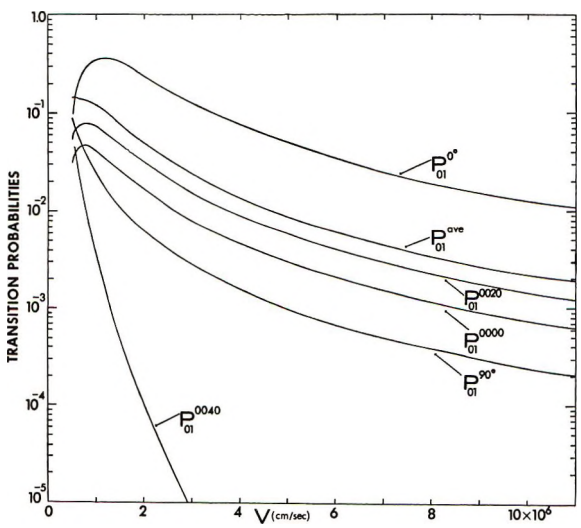

Figure 2. Plots of the simultaneous vibrational and rotational transition probabilities, orientation-averaged transition probability, and transition probabilities for collinear and perpendicular collisions for the $0 \rightarrow 1$ vibrational transition in the velocity range 5×10^5–10^7 cm/sec. The lower velocity region is enlarged in Figure 3.

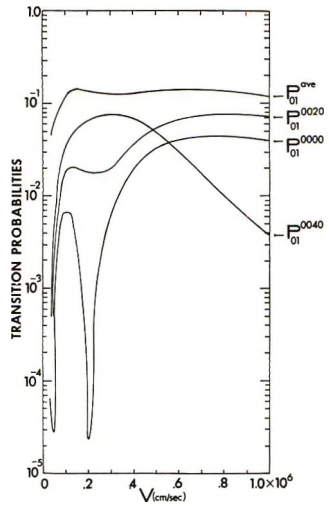

Figure 3. Enlarged plots of the simultaneous and orientation-averaged transition probabilities for $0 \rightarrow 1$ at velocities below 10^6 cm/sec.

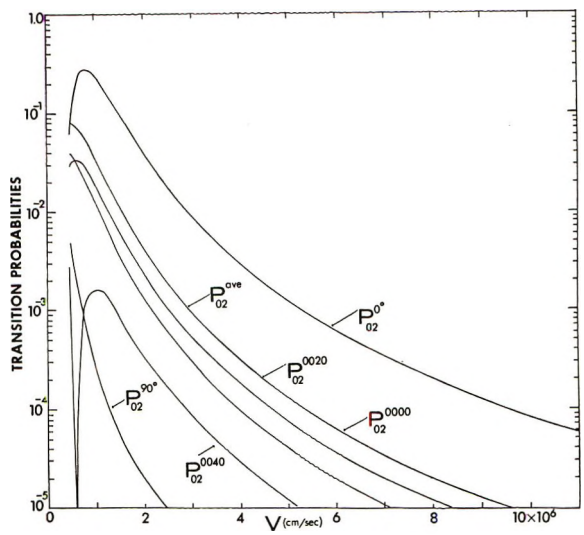

Figure 4. Same plots as Figure 2 for the $0 \rightarrow 2$ vibrational transition. The lower velocity region is enlarged in Figure 5.

The integration over rotational states is carried out by use of Simpson's $^1/_3$ rule on an XDS Sigma-7 computer. The different spacings and Richardson's extrapolations are used to improve the result.[26]

(23) M. Abramowitz and I. A. Stegun, Ed., "Handbook of Mathematical Functions," (National Bureau of Standards, Applied Mathematics Series, No. 55, Washington, D. C., 1964), pp 232, 233.

(24) M. Karplus and R. N. Porter, "Atoms and Molecules," W. A. Benjamin, Inc., New York, N. Y., 1970, Table 4.2.

(25) G. Herzberg, "Spectra of Diatomic Molecules," D. Van Nostrand Co., Princeton, N. J., 1950, Table 39.

(26) J. M. McCormick and M. G. Salvadori, "Numerical Methods in Fortran," Prentice-Hall, Englewood Cliffs, N. J., 1964, pp 312–317.

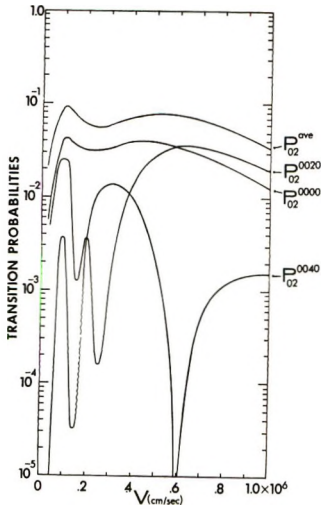

Figure 5. Enlarged plots of the simultaneous and orientation-averaged transition probabilities for 0 → 2 at velocities below 10^6 cm/sec.

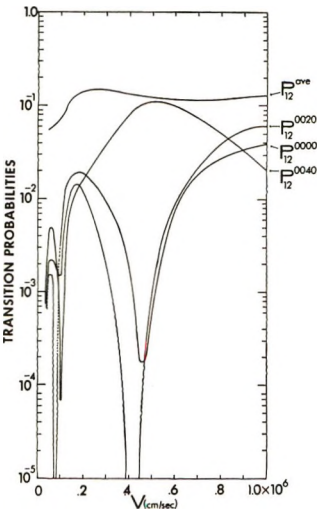

Figure 7. Enlarged plots of the simultaneous and orientation-averaged transition probabilities for 1 → 2 at velocities below 10^6 cm/sec. The curve for P_{12}^{0000} at lower velocities is dotted to avoid confusion.

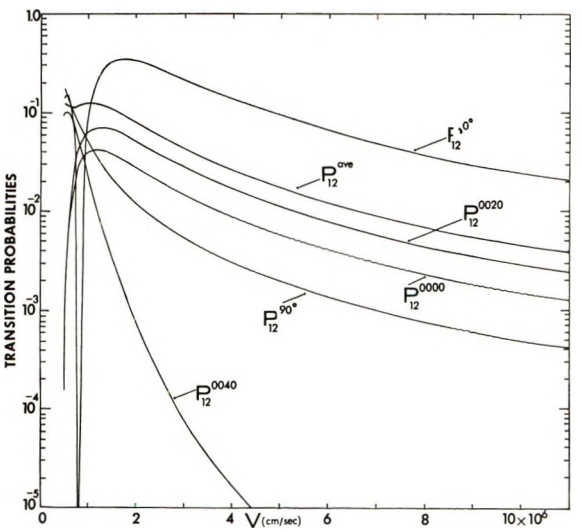

Figure 6. Same plots as Figure 2 for the 1 → 2 vibrational transition. The lower region is enlarged in Figure 7.

A. 0 → 1 Vibrational Transition. Figures 2 and 3 show the rotational transitions 00 → 00, 00 → 20, and 00 → 40 for the 0 → 1 vibrational transition. The 00 → 00 transition probability takes a sharp maximum value at $v = 10^5$ cm/sec; after reaching a maximum value at 2×10^5 cm/sec, it increases to another maximum value at 8×10^5 cm/sec as the velocity increases. Beyond this velocity the probability of 00 → 00 transition, as well as those of 00 → 20 and 00 → 40, is a decreasing function of velocity. Such an undulatory behavior of the transition probability at low collision velocities is also seen for 00 → 20 and 00 → 40 transitions, the latter having only one maximum value. The first-order perturbation approximation yields the selection rules $\Delta j = 0, \pm 2$ and $\Delta m = 0, \pm 2$. However, in the present treatment for which the perturbation energy is independent of ϕ, we find the selection rules $\Delta j = 0$, $2n^*$ (n^* = integer) and $\Delta m = 0$. The 00 → 40 transition probability is larger at low collision velocities, but decreases very rapidly as the velocity increases; above 2×10^6 cm/sec it is negligibly small compared to 00 → 00 and 00 → 20 probabilities.

An important result found in Figure 2 is that the 0 → 1 vibrational transition probability with the rotational change 00 → 20 is largest above 5×10^5 cm/sec; below this velocity that with 00 → 40 is now largest. The orientation-averaged transition probability, which is also plotted in Figures 2 and 3 is always greater than any of the three probabilities. As shown in Table I, the average transition probability is essentially equal to the sum of the three transition probabilities above 10^6 cm/sec; the table lists the values of the ratios $P_{01}^{jmj'm'}/P_{01}^{ave}$. The deviation of the sum of the ratios from unity becomes significant at lower velocities due to the important contribution of other rotational transitions which are not considered here.

The vibrational transition probability at the collinear collision is very large above 5×10^5 cm/sec, and it takes the maximum value of $1/e$ at 1.2×10^6 cm/sec. As shown in Table I the ratio $P_{01}^{0°}/P_{01}^{ave}$ increases from 3.02 at 10^6 cm/sec to 5.67 at 10^7 cm/sec. (Below this velocity range, the ratio becomes very small; *e.g.*, at 5×10^5 cm/sec the ratio is only 0.216.) The introduction of the so-called steric factor $^1/_3$ to the result of the collinear collision at the end of the calculation is then obviously an unsatisfactory procedure. The perpendicular collision also shows the maximum value of $1/e$, but it now occurs at a lower velocity (2×10^5 cm/sec). As the velocity increases, the perpendicular probability decreases very rapidly; *e.g.*, it is as small as 9.79×10^{-4} at 5×10^6 cm/sec, while the collinear collision leads to the probability 4.90×10^{-2}. The

Table I: Ratios of the Simultaneous, Collinear, and Perpendicular Transition Probabilities to the Orientation-Averaged Probability for 0 → 1 over the Velocity Range 10^6–10^7 Cm/Sec

	v^a									
	1	2	3	4	5	6	7	8	9	10
$P_{01}^{0000}/P_{01}^{ave}$	0.345	0.341	0.339	0.338	0.337	0.337	0.337	0.337	0.337	0.337
$P_{01}^{0020}/P_{01}^{ave}$	0.621	0.656	0.659	0.662	0.663	0.663	0.663	0.663	0.663	0.663
$P_{01}^{0040}/P_{01}^{ave}$	3.21 (2)[b]	1.95 (3)	3.80 (4)	1.18 (4)	4.79 (5)	2.27 (5)	1.20 (5)	6.90 (6)	4.20 (6)	2.68 (6)
Sum[c]	0.998	0.998	0.998	1.00	1.00	1.00	1.00	1.00	1.00	1.00
$P_{01}^{0°}/P_{01}^{ave}$	3.02	4.91	5.35	5.51	5.57	5.60	5.62	5.64	5.65	5.67
$P_{01}^{90°}/P_{01}^{ave}$	0.202	0.128	0.116	0.112	0.111	0.110	0.109	0.109	0.109	0.109

[a] Velocity in units of 10^6 cm/sec. [b] Numbers in parentheses denote the negative power of 10; *e.g.*, 3.21 (2) = 3.21×10^{-2}. [c] Sum of the ratios for simultaneous transition probabilities.

Table II: Ratios of the Simultaneous, Collinear, and Perpendicular Transition Probabilities to the Orientation-Averaged Probability for 0→2 over the Velocity Range 10^6–10^7 Cm/Sec

	v^a									
	1	2	3	4	5	6	7	8	9	10
$P_{02}^{0000}/P_{02}^{ave}$	0.371	0.326	0.318	0.316	0.315	0.313	0.313	0.313	0.313	0.313
$P_{02}^{0020}/P_{02}^{ave}$	0.574	0.585	0.587	0.586	0.587	0.587	0.586	0.586	0.587	0.587
$P_{02}^{0040}/P_{02}^{ave}$	4.46 (2)[b]	8.67 (2)	9.41 (2)	9.70 (2)	9.84 (2)	9.93 (2)	1.00 (2)	1.00 (1)	1.00 (1)	1.00 (1)
Sum[c]	0.989	0.997	0.999	0.999	0.999	0.999	0.999	0.999	1.00	1.00
$P_{02}^{0°}/P_{02}^{ave}$	6.63	9.24	9.74	9.93	10.0	10.0	10.1	10.1	10.0	10.0
$P_{02}^{90°}/P_{02}^{ave}$	8.46 (3)	4.53 (3)	4.03 (3)	3.86 (3)	3.79 (3)	3.75 (3)	3.73 (3)	3.70 (3)	3.70 (3)	3.70 (3)

[a–c] See footnotes of Table I.

values of the ratio $P_{01}^{90°}/P_{01}^{ave}$ are also listed in Table I; the ratio is 0.202 at 10^6 cm/sec and levels off to 0.109 as the velocity continues to increase.

B. 0 → 2 Vibrational Transition. The results for the 0 → 2 vibrational transition taking place simultaneously with $jm \rightarrow j'm'$ are plotted in Figures 4 and 5; the ratios $P_{02}^{0000}/P_{02}^{ave}$, $P_{02}^{0020}/P_{02}^{ave}$, and $P_{02}^{0040}/P_{02}^{ave}$ are shown in Table II. Since the process is a two-vibrational quantum transition, the probabilities are very small compared to those of the 0 → 1 vibrational transition, and they decrease very sharply with increasing velocity above 10^6 cm/sec. It is also seen that the transition probabilities are sharply peaked compared to 0 → 1. At low collision velocities, the undulatory variation of probabilities with v is also seen as in the case of 0 → 1. The sum of the three simultaneous transition probabilities is essentially equal to P_{02}^{ave} over the velocity range of 10^6 to 10^7 cm/sec as shown in Table II.

The collinear collision produces the largest energy transfer and leads to the transition probabilities which are significantly larger than P_{02}^{ave} above 10^6 cm/sec; *e.g.*, the ratio $P_{02}^{0°}/P_{02}^{ave}$ is 6.63 at 10^6 cm/sec and approaches the limiting value 10.1 as the velocity increases. This result then indicates the introduction of a steric factor of $^1/_3$ to the collinear vibrational transition probability is erroneous particularly for multiquantum transitions; furthermore, the ratio is not even a constant. The perpendicular collision is less efficient in transferring vibrational energy by four orders of magnitude. The limiting value of the ratio $P_{02}^{90°}/P_{02}^{ave}$ is 3.70×10^{-3}. The efficient energy transfer at the collinear orientation is certainly expected because the present collision takes place at zero impact parameter. We should note that for large impact parameters the perpendicular collision can produce the largest energy transfer. The maximum value of $P_{02}^{0°}$, as well as that of $P_{02}^{90°}$, is $2/e^2$.

C. 1 → 2 Vibrational Transition. The results of simultaneous vibrational (1 → 2) and rotational transitions (00 → 00, 00 → 20, or 00 → 40) are shown in Figures 6 and 7. All simultaneous transition probabilities are quite large and have broad maxima which move out to higher v compared to both the 0 → 1 and 0 → 2 vibrational transitions. This indicates that the 1 → 2 vibrational transition becomes increasingly important at high collision velocities. At 10^6 cm/sec the 0 → 1 vibrational transition probabilities with 00 → 00, 00 → 20, and 00 → 40 are 4.05×10^{-2}, 7.30×10^{-2}, and 3.75×10^{-3}; for 1 → 2, they are 3.96×10^{-2}, 6.32×10^{-2}, and 2.19×10^{-2}; for 0 → 2, the three transition probabilities are 1.28×10^{-2}, 1.98×10^{-2}, and 1.54×10^{-3}. The orientation-averaged transition probabilities are 1.17×10^{-1}, 3.45×10^{-2}, and 1.25×10^{-1}, respectively, for the 0 → 1, 0 → 2, and 1 → 2 vibrational transitions. At 5×10^6 cm/sec, the simultaneous transition probabilities for 1 → 2 are larger than those for 0 → 1; the three probabilities for 1 → 2 take the

Table III: Ratios of the Simultaneous, Collinear, and Perpendicular Transition Probabilities to the Orientation-Averaged Probability for 1 → 2 over the Velocity Range 10^6–10^7 Cm/Sec

	v^a									
	1	2	3	4	5	6	7	8	9	10
$P_{12}^{0000}/P_{12}^{ave}$	0.316	0.344	0.341	0.340	0.340	0.340	0.338	0.337	0.337	0.336
$P_{12}^{0020}/P_{12}^{ave}$	0.505	0.645	0.656	0.659	0.659	0.660	0.662	0.663	0.663	0.664
$P_{12}^{0040}/P_{12}^{ave}$	0.175	9.13 (3)[b]	1.81 (3)	6.12 (4)	2.77 (4)	1.51 (4)	9.29 (5)	6.31 (5)	4.59 (5)	3.54 (5)
Sum[c]	0.996	0.998	0.998	0.999	0.999	1.00	1.00	1.00	1.00	1.00
$P_{12}^{0°}/P_{12}^{ave}$	0.714	4.14	5.00	5.31	5.47	5.58	5.57	5.60	5.62	5.62
$P_{12}^{90°}/P_{12}^{ave}$	0.372	0.151	0.126	0.117	0.114	0.112	0.113	0.110	0.110	0.109

[a–c] See footnotes of Table I.

values 5.79×10^{-3}, 1.13×10^{-2}, and 4.72×10^{-6}, while those for 0 → 1 are 2.97×10^{-3}, 5.82×10^{-3}, and 4.21×10^{-7}, respectively. The average transition probabilities are $P_{12}^{ave} = 1.70 \times 10^{-2}$ and $P_{01}^{ave} = 8.79 \times 10^{-3}$ at 5×10^6 cm/sec. Although the processes involve the change of one-quantum state as in 0 → 1, Figure 7 shows a complicated undulatory behavior of transition probabilities at low collision velocities. The figure also shows that the 00 → 40 probability is very large over the velocity range of 2×10^5 to 10^6 cm/sec, while the 00 → 00 and 00 → 20 probabilities are very small; *e.g.*, at 4.5×10^5 cm/sec, the probabilities for 00 → 00 and 00 → 20 are 1.72×10^{-4} and 2.55×10^{-5}, respectively, while it is as large as 9.89×10^{-2} for 00 → 40. However, above 10^6 cm/sec, the 00 → 40 probability becomes very small.

Both the ratios $P_{12}^{0°}/P_{12}^{ave}$ and $P_{12}^{90°}/P_{12}^{ave}$ are very close to those of 0 → 1 at higher velocities, indicating that the ratios are fairly insensitive to the initial vibrational state of the oscillator as long as the transition involves only a one-quantum change. A particularly small value of the former ratio at 10^6 cm/sec is due to a sharp decrease to a minimum value at the neighborhood of the velocity. (See Table III.)

V. Concluding Remarks

From the above results we can make the following concluding statements.

(i) A major portion of the transition probabilities arises from the high-velocity region (or strong interaction region) where the usual first-order perturbation approximations do not apply. The calculated probabilities do not exceed unity, in contrast to the results of the perturbation approximations. At the high collision velocities considered above, the perturbation approaches would lead to transition probabilities which are larger than unity. From the comparison of the present formulation with eq 22, we would expect, in the limit of weak interaction, F to be very small; such a situation would result when K is small and/or l is large. In this limit, we can then ignore the exponential part in the vibrational matrix element and obtain the result which may be identified as the first-order approximation expression; this expression would tend to exceed unity when used in high-velocity calculations. In the above calculation, the decrease in transition probabilities with increasing velocity is due to this exponential part.

(ii) During vibrational transitions in H_2 + Ar, the molecule also tends to change its rotational state. By comparing the magnitudes of the $n00 \rightarrow n'00$, $n00 \rightarrow n'20$, and $n00 \rightarrow n'40$ simultaneous probabilities, we find that a very large portion of the orientation-averaged transition probability, which may be regarded as a "total" transition probability since it is a sum of all rotational transitions, arises from the rotational change of $j = 0$ to $j' = 2$ in the velocity range of 10^6 to 10^7 cm/sec. At lower velocities, the $j = 0$ to $j' = 4$ change becomes also important. In all three vibrational transitions (0 → 1, 0 → 2, 1 → 2) only the important rotational changes are found to be 00 → 20 and 00 → 40.

(iii) The variation of the 1 → 2 vibrational transition probability is very similar to that of 0 → 1 above 10^6 cm/sec. At such velocities, simultaneous vibrational and rotational transition probabilities for 1 → 2 are always larger than those for 0 → 1. The orientation-averaged, collinear, and perpendicular probabilities for 1 → 2 are also larger than those for 0 → 1. For a given vibrational transition, 00 → 00, 00 → 20, orientation-averaged, collinear, and perpendicular probabilities decrease with increasing velocity at approximately the same rate above 3×10^6 cm/sec.

(iv) The collinear collision always produces the largest energy transfer above 10^6 cm/sec. The difference between $P_{nn'}^{0°}$ and $P_{nn'}^{ave}$ is not three as often assumed in introducing a steric factor to the collinear probability, but it is about 5.6 for 0 → 1 and 1 → 2, and about 10 for 0 → 2 above 3×10^6 cm/sec; the difference is particularly large for multi-quantum transitions. Below 10^6 cm/sec the differences seriously deviate from these limiting values, and furthermore they depend strongly on velocity. These results therefore indicate that the orientation dependence of vibrational transition probability cannot be given by any simple steric factor.

A van der Waals Equation for Nonspherical Molecules

by M. Rigby

Chemistry Department, Queen Elizabeth College, University of London, London W8 7AH, England
(Received January 13, 1972)

Publication costs borne completely by The Journal of Physical Chemistry

An equation of state of the van der Waals type is proposed for systems of nonspherical molecules. The hard-sphere repulsive term is replaced by a term appropriate to nonspherical convex hard molecules. The effects of this change are found to be similar to many of the experimentally observed effects of changes in molecular shape.

The effects of molecular shape on the bulk properties of fluids have been the subject of many investigations[1,2] and the experimental pattern has been well established. The work of Pitzer and his coworkers[1] has shown that variations from the corresponding states behavior characteristic of simple spherical molecules may be accurately correlated using a single additional parameter. This parameter, called by Pitzer the acentric factor, is determined by a number of factors and may include contributions from the effects of nonspherical attractive and repulsive intermolecular forces and from variations in the spherically symmetric force field. Attempts to relate the observed behavior to the presence of various types of nonspherical intermolecular interaction have tended to concentrate on the effects of contributions from nonspherical attractive terms, which may be treated as perturbations of a spherically symmetric reference potential. The effects of the presence of dipoles, quadrupoles, and higher multipoles have been investigated in this way and are now quite well understood.[2] The treatment of nonspherical repulsive forces is less easy. The energy perturbations associated with the nonspherical repulsive terms are much larger than those for attractive perturbations, and it seems desirable to seek an alternative approach. The success of recent extensions of the van der Waals type of model of the liquid has suggested one possible treatment of this problem.

Perturbation theories, whose physical basis is similar to that of the van der Waals equation, have been applied with great success to the description of simple fluids.[3-5] This work has shown that the principal factor determining the geometric structure of a fluid is the magnitude of the repulsive forces and that these may be adequately approximated using a hard sphere model. The structure of a real liquid is thus very similar to that of a hard-sphere fluid at an appropriate density, and the attractive intermolecular forces have little effect on the structure.

Equations of state embodying these principles may be written in the generalized form[5]

$$\frac{PV}{NkT} = \beta\left(\frac{N}{V}\right) - \frac{\alpha}{kT}\left(\frac{N}{V}\right) \tag{1}$$

where α and β are functions only of the density, N/V. The function β describes the equation of state of the hard-sphere fluid, and the correction due to attractive intermolecular forces is given by the function α. The simple approximate form of α used by van der Waals appears to be fairly adequate for many systems.

$$\alpha = \frac{aN}{V^2} \tag{2}$$

This form of α implies that the configurational internal energy of the fluid is directly proportional to the density. The original van der Waals form of β is less satisfactory, and recent work[6] has shown the advantages of using an accurate hard-sphere equation of state. One of the most convenient analytic representations of this is that derived from scaled particle theory,[7] which reproduces the data from Monte Carlo and molecular dynamics simulations well.

Since the hard-sphere model provides a good basis for the description of systems of real spherical molecules, it seemed interesting to investigate the adequacy of a similar approach to the study of systems of nonspherical molecules. This has been done by studying the properties of an equation of state of the general form of eq 1, retaining the van der Waals form of α, but utilizing a hard core term, β, which is applicable to convex hard molecules of generalized shapes. Using such an equation one may expect to establish the effects of nonspherical repulsive forces, separated from those

(1) K. S. Pitzer, D. Z. Lippmann, R. F. Curl, Jr., C. M. Huggins, and D. E. Petersen, *J. Amer. Chem. Soc.*, **77**, 3433 (1955).

(2) J. S. Rowlinson, "Liquids and Liquid Mixtures," 2nd ed, Butterworths, London, 1969, Chapter 8.

(3) J. A. Barker and D. Henderson, *J. Chem. Phys.*, **47**, 4714 (1967).

(4) B. Widom, *Science*, **157**, 375 (1967).

(5) M. Rigby, *Quart. Rev. Chem. Soc.*, **24**, 416 (1970).

(6) E. A. Guggenheim, *Mol. Phys.*, **9**, 199 (1965).

(7) H. Reiss, H. L. Frisch, and J. L. Lebowitz, *J. Chem. Phys.*, **31**, 369 (1959).

arising from nonspherical attractive terms. A suitable equation of state for convex hard cores has been derived by Gibbons,[8] using scaled particle theory, and may be written

$$\beta = \frac{PV}{NkT} = \frac{3 + d(3\gamma - 6) + d^2(3 - 3\gamma + \gamma^2)}{3(1 - d)^3} \quad (3)$$

where γ is a single parameter determined by the shape of the hard core. This is defined in terms of the volume, v, mean radius, $\bar{R}$, and surface area, S, of the hard core.

$$\gamma = \frac{\bar{R}S}{v} \quad (4)$$

The density, d, is defined by

$$d = \frac{Nv}{V} \quad (5)$$

This equation of state (3) appears to provide a good representation of the (rather meager) data presently available for nonspherical hard molecules.[9]

The complete van der Waals type equation using the forms of β and α defined in eq 3 and 2 is an example of a three-parameter corresponding states relationship, and it is of interest to see to what extent such an equation can reflect the experimentally observed deviations from simple (two-parameter) corresponding states behavior. These have been summarized by Pitzer[1] and Rowlinson.[2] Certain general trends are evident with increasing departure from spherical symmetry. These include variations in the reduced vapor pressure as a function of reduced temperature, increases in the slope of the rectilinear diameter line, decreases in the critical compressibility factor, and increases in the configurational heat capacities. Most of these changes are reproduced qualitatively by the present model.

Method

The equation of state shows the general characteristics observed with the van der Waals equation, and the critical point may be readily located in the usual manner. Because of the rather greater complexity of the equation, the solutions for several values of the shape factor γ were obtained numerically. The critical compressibility factor, $(PV/NkT)_c$, was evaluated for a wide range of values of γ, and the results are shown in Table I. In order to give a readily comprehended idea of the molecular shape associated with a given value of γ, the dimensions of the appropriate prolate spherocylinder (see Figure 1) are given also. This shape is selected for the purpose of illustration only, since a given value of γ is compatible with a wide range of shapes.

For each value of γ studied, the vapor pressure was determined over a temperature range from about $0.5T_c$ to T_c. The method of calculation used was a numerical one, based on the Maxwell equal area rule. The densities of the coexisting phases were determined at the same time, and the rectilinear diameter curve was established.

Table I: Critical Data for Nonspherical van der Waals Model

γ	R/σ	$(PV/NkT)_c$
3	0	0.3599
4	1.457	0.3574
5	2.826	0.3555
6	3.562	0.3539
7	4.582	0.3525
8	5.596	0.3514
9	6.606	0.3503
10	7.613	0.3494
15	12.633	0.3461

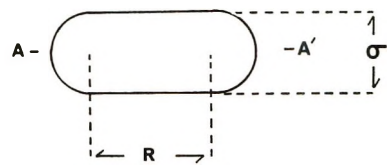

Figure 1. The prolate spherocylinder model. AA′ is the axis of rotation.

Results

Before considering in detail the results obtained, it must be emphasized that qualitative agreement with experimental trends is all that can be expected from such a model. Since the repulsive forces in real molecules are not infinite, the appropriate hard-core dimensions should presumably be temperature dependent, in analogy with the similar hard-sphere case.[3] The omission of this adjustment must modify the quantitative conclusions to some extent.

The critical compressibility factor is reported in Table I for a range of molecular shapes from spherical ($\gamma = 3$) to spherocylinders of length $R = 12.6\sigma$ (see Figure 1). The value of the critical compressibility factor for the spherical case is rather different from the experimental value for simple spherical molecules of around 0.28. This is clearly to some extent a comment on the simple modified van der Waals equation of state. As the shape of the molecules deviates increasingly from the spherical, the critical compressibility factor is seen to decrease slightly. This behavior is observed experimentally, when a series such as the alkanes is considered. However, the experimentally observed changes are quite large, *e.g.*, a change from 0.290 to 0.266 on passing from CH_4 to n-C_5H_{12}. This may be contrasted with the variation from 0.360 to 0.353 on changing from the spherical case, $R = 0$, to the case $R = 4\sigma$, a change which might be thought naively to

(8) R. M. Gibbons, *Mol. Phys.*, **17**, 18 (1969).
(9) M. Rigby, *J. Chem. Phys.*, **53**, 1021 (1970).

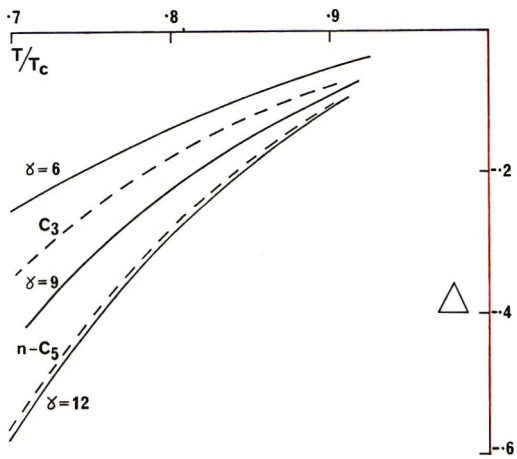

Figure 2. The reduced vapor pressure curves.

$$\Delta = \ln (P/P_c)_\gamma - \ln (P/P_c)_{\gamma=3}$$

Experimental data (relative to argon) are shown as dashed lines for C_3H_8 and n-C_5H_{12}.

be of the correct magnitude for the van der Waals model.

The results of the vapor pressure calculations are shown in Figure 2. Rowlinson[2] has illustrated the deviations of the reduced vapor pressure from the simple spherical molecule pattern and has shown how this may be correlated with nonspherical attractive terms. These deviations are conveniently displayed by plotting the difference in the logarithm of the reduced vapor pressure, P/P_c, for systems of nonspherical and spherical molecules, as a function of the reduced temperature, T/T_c. The typical experimental trend is shown in Figure 2, together with the results based on the modified van der Waals equation for several values of γ. It is seen that the van der Waals model reproduces qualitatively the observed effects of changing shape. The effects of moderate changes in the core shape are clearly significant, and any comprehensive treatment of shape must evidently include the effects of both attractive and repulsive contributions.

The study of the slope of the rectilinear diameter lines does not lead to any clear conclusion. For the spherical case, the van der Waals model gives a line whose slope greatly exceeds the appropriate experimental value. For nonspherical cores, this slope is increased, in agreement with experimental observation, but in view of the large discrepancy for the case of spherical molecules this agreement may be fortuitous.

The van der Waals model cannot adequately describe the heat capacity of a fluid, as the assumption of a uniform attractive energy field implies that the heat capacities have the ideal gas values, with zero configurational contributions. This is of course partly an artefact of the hard-core model, and repulsive contributions would be expected if a soft repulsive model were used for the core.

Conclusion

A simple equation of state for systems of nonspherical molecules is found to be able to reproduce many of the changes in behavior found experimentally as the shape deviates increasingly from the spherical. It is suggested that the contributions of repulsive nonspherical forces are significant and should not be neglected. However, the effects of both attractive and repulsive terms are qualitatively similar for many properties and it will probably prove difficult to separate the effects arising from different causes, from a study of experimental results.

Dissolution Lifetime of a "Hydrated" Solute Sphere[1]

by Daniel E. Rosner*[2] and W. S. Chang[3]

Department of Engineering and Applied Science, Yale University, New Haven, Connecticut 06520
(Received January 7, 1972)

Publication costs assisted by the U. S. Air Force Office of Scientific Research

An exact method is presented for calculating the total dissolution lifetime of a solvent-containing (*e.g.*, hydrated) sphere in terms of the corresponding lifetime of a solvent-free (pure solute) sphere. The resulting algorithm, which is free of the common quasi-steady and/or sparing solubility approximations, is illustrated herein for the dissolution of lithium iodide and its three hydrates ($LiI \cdot xH_2O$, $x = 1, 2, 3$) in water at 25°.

Introduction

Recent theoretical studies of diffusion-limited dissolution have provided quantitative results for the total lifetime of an isolated sphere[4,5] free of the well-known but overly restrictive quasi-steady and sparing solubility approximations. These lifetime predictions explicitly apply to the isothermal dissolution of a stationary, pure solute sphere in an otherwise quiescent, incompressible solvent fluid. Since the sphere/solvent density ratio, ρ_0/ρ, may be large, of order unity, or small, formal application to problems of solid–liquid, liquid (droplet)–liquid, and gas (bubble)–liquid dissolution is possible. In the present note we (i) demonstrate that these results may equally well be used to predict the lifetime of spheres initially containing a prescribed amount of solvent (as in the case of hydrated salts dissolving into water); (ii) illustrate the computational algorithm, using as an example the dissolution of lithium iodide and its three well-known hydrates, $LiI \cdot xH_2O$ ($x = 1, 2, 3$); and (iii) examine the inaccuracy of the familiar quasi-steady (QS) approximation when applied to this same class of problems.

Physicochemical and Mathematical Model

With the exception that we now allow the sphere to contain a constant fraction of solvent, our constant property, spherically symmetric continuum model is identical with that discussed in detail in ref 4 and 5. Thus, we visualize that at time $t = 0$ a sphere of initial radius $R_0 \equiv R(0)$ is immersed in an incompressible solvent, which is undersaturated with respect to the solute (at the prevailing temperature). For definiteness, we can consider the sphere to have the composition $A \cdot xH_2O$, where A represents the solute species, and use the phrase "hydrate," although it is clear that our arguments would be valid regardless of the identity of the solvent.[6] Throughout the ensuing dissolution process, during which $\dot{R} \equiv dR/dt < 0$, local saturation is assumed at the sphere–solvent interface, in the sense that the solute mass fraction, c, evaluated at $r = R(t)$, will be taken to be the constant,[7] c_{sat}. Owing to our basic assumptions concerning the direction of solute mass transfer, c_{sat} is furthermore assumed to be between the solute mass fraction, c_0 in the sphere,[8] and the value c_∞ pertaining to the solute-containing ambient solvent. As in the cases treated in ref 4 and 5, the following set of solute conservation equations, boundary conditions, and initial conditions suffices to determine the transient solute concentration field $c(r,t)$, and the associated sphere radius–time "history" $R(t)$

$$\frac{\partial c}{\partial t} + \frac{R^2}{r^2}\left(1 - \frac{\rho_0}{\rho}\right)\dot{R}\frac{\partial c}{\partial r} = \frac{D}{r^2}\frac{\partial}{\partial r}\left(r^2\frac{\partial c}{\partial r}\right) \quad (r \geq R(t)) \tag{1}$$

$$\rho_0\dot{R} = \frac{D\rho}{c_0 - c_{sat}}\left(\frac{\partial c}{\partial r}\right)_{r=R} \tag{2}$$

$$c[R(t),t] = c_{sat} = \text{constant} \tag{3}$$

$$c(\infty,t) = c_\infty = \text{constant} \tag{4}$$

$$c(r,0) = c_\infty = \text{constant} \tag{5}$$

$$R(0) = R_0 \tag{6}$$

from which the total sphere lifetime, t_{life}, is obtained, using the definition

(1) Supported by the Propulsion and Energy Conversion Division of the U. S. Air Force Office of Scientific Research under Contract F44620-70C-0026.

(2) Associate Professor, Chemical Engineering Group; to whom inquiries concerning this paper should be addressed.

(3) Max Planck Institut für Biophysikalische Chemie, Göttingen, West Germany.

(4) D. E. Rosner, *J. Phys. Chem.*, **74**, 4001 (1970).

(5) D. L. Duda and J. S. Vrentas, *Int. J. Heat Mass Transfer*, **14**, 395 (1971).

(6) Thus, for a fuel droplet evaporating into air, the "solvent" would be air and the initial fuel droplet could contain the saturated amount of air at the prevailing pressure and droplet temperature. In such cases the ratio of solvent to solute in the sphere is not restricted to integer (stoichiometric) values. Similarly, for the dissolution of a gas bubble into a liquid, we can now take due account of the nonzero solvent vapor pressure within the bubble.

(7) Only when interface kinetic limitations to the dissolution process cause significant interfacial undersaturations would the value of c at $r = R(t)$ itself be time dependent. For a discussion of the validity of the solute diffusion "control" assumption see, *e.g.*, D. E. Rosner, *J. Phys. Chem.*, **73**, 382 (1969). In what follows, D is the concentration-independent Fick diffusion coefficient for solute transport.

(8) For a hydrated salt $A \cdot xH_2O$, c_0 will by definition be given by $M_A/(M_A + 18.02x)$ where M_A is the molecular weight of the solute A and x is the *degree of hydration*. The mass density of the sphere, ρ_0, will usually depend on the degree of hydration.

$$R(t_{life}) \equiv 0 \tag{7}$$

The only difference between eq 1–7 and the equations of ref 4 and 5 is the appearance of c_0 (rather than unity) in the solute conservation boundary condition at $r = R(t)$, eq 2. This latter equation follows from the fact that, relative to a control volume straddling the interface, solute A flows *in* per unit area at the rate $\rho_0 c_0(-\dot{R})$ and hence must flow *out* at the equal rate: $\rho c_{sat}[v(R,t) - \dot{R}] - D\rho(\partial c/\partial r)_{r=R}$, where the second contribution is due to Fick diffusion. Combining this statement with overall mass conservation to eliminate the radial mean mass fluid velocity $v(R,t)$ gives eq 2.

Analysis

Because $c_0 < 1$ enters only eq 2 and, by hypothesis, remains constant, the present problem can be readily transformed to the problem recently solved in ref 4 and 5. Toward this end we introduce the ratios

$$\theta(r,t) \equiv (c - c_\infty)/(c_{sat} - c_\infty) \tag{8}$$

$$B \equiv (c_{sat} - c_\infty)/(c_0 - c_{sat}) \tag{9}$$

where, as noted in ref 7, when $c_\infty = 0$ the parameter defined by eq 9 has the following simple physical interpretation: *B is numerically equal to the solubility of the "hydrated" solute, expressed in grams of hydrate per gram of solvent.* When the present boundary-value problem is rewritten in terms of θ and the *effective solubility parameter* B, it becomes identical with that already solved in ref 4 and 5; hence the dimensionless lifetime function $\tau_{life}(\rho/\rho_0,B)$ introduced in ref 4 and 7 can be applied to the present problem as well, where

$$\tau_{life}(\rho/\rho_0,B) \equiv 2\frac{\rho}{\rho_0}[\ln(1 + B)]\frac{Dt_{life}}{R_0^2} \tag{10}$$

and now B is given by eq 9. Thus, as first suggested in ref 7, the mere introduction of a more general solubility parameter, eq 9, allows us to solve the "hydrated" sphere problem, making no approximations other than those already underlying the τ_{life} predictions of ref 4 and 5. In particular, since the transient term, $\partial c/\partial t$, in eq 1 has been retained, and c_{sat} has *not* been considered negligible compared to unity, the present results are free of the restrictive "quasi-steady" and "sparing solubility" ($B \ll 1$) approximations. In the following examples we will use $\tau_{life}(\rho/\rho_0,B)$ values taken from ref 5, based on an accurate finite-difference solution to eq 1–6 with $c_0 = 1$. These have been conveniently cross-plotted by Rosner in ref 9 and 10, to which the reader is referred for absolute values and interpolation purposes. Values of t_{life} will then follow from eq 10.

Numerical Example and Discussion

To illustrate (i) how to apply our computational algorithm and (ii) the effect of hydration on the mass-transfer-controlled lifetime, we consider the dissolution of lithium iodide crystal (LiI) and its well-known hydrates ($LiI \cdot xH_2O$ with $x = 1, 2, 3$) in pure water (*i.e.*, $c_\infty = 0$) at 25°. In ref 11, the densities of LiI and $LiI \cdot 3H_2O$ are given as 3.494 ± 0.015 g/cm³ and 3.48 g/cm³, respectively.[11] In the absence of additional data we therefore simply neglect the dependence of density ρ_0 on degree of hydration; *i.e.*, we put $\rho_0 \approx 3.49$ g/cm³ for LiI and each of its hydrates. The molecular weight of LiI is 133.84. The saturation mass fraction, c_{sat}, of LiI in the liquid water at 25° is[12] 0.626. It should be noted that this same value applies in the fluid phase, no matter what the degree of hydration is in the adjacent solid phase. Thus, in this particular example, the final form for the effective solubility parameter B is

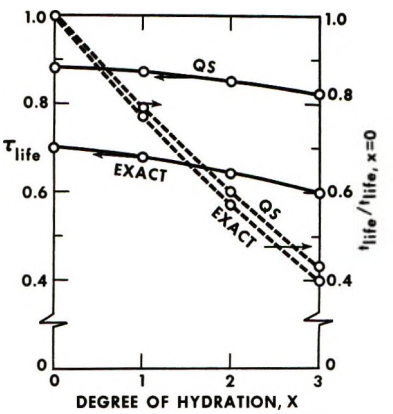

Figure 1. Exact and approximate diffusion-controlled total lifetime predictions for the dissolution of lithium iodide and its hydrates in water at 25°.

$$B = 0.626/(c_0 - 0.626) \tag{11}$$

where the solute mass fraction, c_0, in the sphere is obtained from

$$c_0(x) = 133.84/[133.84 + x\cdot(18.02)] \tag{12}$$

with $x = 0$ for pure lithium iodide crystal and $x = 1, 2, 3$ for the lithium iodide hydrates mentioned above. Since the solvent (H_2O) density is 1.0 g/cm³, the density ratio ρ/ρ_0 is approximately 0.29. Corresponding values of τ_{life} for $x = 0, 1, 2, 3$, estimated from Figure 2 of ref 9, are shown in Figure 1. Since the physical lifetime, t_{life}, is proportional to the ratio $\tau_{life}/\ln(1 + B)$ (*cf.* eq 10), corresponding values of the lifetime normalized by that of pure LiI are also included in Figure 1 (right-hand scale). Note that, all other things being equal, the trihydrate is expected to dissolve in a time which is only 40% of that required for a pure LiI sphere.

(9) D. E. Rosner, *J. Phys. Chem.*, **75**, 2969 (1971).

(10) D. E. Rosner and W. S. Chang, submitted for publication in *J. Phys. Chem.*

(11) C. D. Hodgman, R. C. Weast, and S. M. Selby, Ed., "Handbook of Chemistry and Physics," 47th ed, Chemical Publishing Co., Cleveland, Ohio.

(12) H. Stephen and T. Stephen, Ed., "Solubilities of Inorganic and Organic Compounds," Macmillan, New York, N. Y., 1968.

It is now interesting to compare these results with the corresponding predictions of the well-known quasi-steady (QS) state approximation. In accord with the QS procedure, the transient term in eq 1 is simply dropped and time is, accordingly, relegated to the role of a parameter. This leads to the following closed-form expression[13] for τ_{life}

$$\tau_{life,QS} = \frac{[1 - (\rho/\rho_0)] \ln (1 + B)}{\ln \{1 + [1 - (\rho/\rho_0)]B\}} \qquad (13)$$

[which is seen to be singular when $\rho/\rho_0 = (1 + B)/B$], and corresponding values of t_{life} can be obtained from the definition (10). QS values of t_{life} normalized by that of pure LiI are also shown dashed in Figure 1 (right-hand scale). Note that the use of the quasi-steady approximation systematically underestimates the effects of hydration on the sphere lifetime.[14] For the trihydrate this underestimate in $t_{life}/t_{life,x=0}$ amounts to about 9%.

Finally, it is interesting to inquire into the validity of our assumption of constant c_0 throughout the dissolution of a lower hydrate ($x \leq 2$ for the example above). In this connection we find that our model is valid provided *either:* (i) the temperature is high enough to ensure that no higher hydrate is thermodynamically stable at the sphere surface, *or* (ii) the Fick diffusion coefficient $D_{S\text{-}A}$ characterizing solvent transport through the ("hydrated") solute sphere is small enough so that $D_{S\text{-}A}t_{life}/R_0^2 \ll 1$. The first of these conditions rules out the possibility of an outer layer of higher hydrate purely on thermodynamic grounds, whereas the second precludes such outer layers based on their inadequate growth rate, even if they were thermodynamically feasible at the prevailing temperature.

Conclusions

We have demonstrated herein that recently obtained values of t_{life} for the dissolution of *pure* spheres[4,5] can be used to obtain t_{life} values for "hydrated"[6] spheres as well. Our computational algorithm and the magnitude of the hydration effect on the diffusion-controlled sphere lifetime have been illustrated for the isothermal dissolution of lithium iodide and its three hydrates in 25° water (*cf.* Figure 1). It is clear from this, and similar examples, that the quasi-steady-state approximation, rendered unnecessary by this work, leads to unacceptably large errors for this class of problems.

We conclude that our present method should provide useful predictions of the effects of initial solvent content on the total, diffusion-controlled dissolution time of a sphere, regardless of either the chemical nature of the solvent, or the sphere/solvent density ratio.

(13) W. S. Chang, Ph.D. dissertation, Department of Engineering and Applied Science, Yale University, 1972.

(14) It is clear from comparing $\tau_{life,x=0}$ to $\tau_{life,QS;x=0}$ that the QS-approximation underestimates t_{life} for *pure* LiI by 26% in this example.

The Hydrophile–Lipophile Balance (hlb) of Fluorocarbon Surfactants and Its Relation to the Critical Micelle Concentration (cmc)

by I. J. Lin

Department of Mineral Engineering, Technion–Israel Institute of Technology, Haifa, Israel *(Received December 21, 1971)*

Publication costs borne completely by The Journal of Physical Chemistry

A modified equation, based on Davies' theory, for determining the hlb value is given. Cmc and hlb values are correlated for ionic fluorocarbon surfactants. Several numerical examples are presented.

Theory

Hydrophile–Lipophile Balance. Surface-active agents are classified numerically according to the size and strength of the mutually counteractive hydrophilic and lipophilic groups in the molecule, whose balance is known as the hydrophile–lipophile balance or hlb.[1,2] By Davies' theory for ionic hydrocarbon surfactants, the hlb value is obtainable directly (using empirical group numbers[1]) from eq 1, in which both the structural

(1) J. T. Davies, *Proc. Int. Congr. Surface Activ., 2nd,* 1, 426 (1957).

(2) J. T. Davies and E. K. Rideal, "Interfacial Phenomena," 2nd ed, Academic Press, New York, N. Y., 1963.

layout of the molecule and the chemical formula are taken into account. For straight-chain hydrocarbon

$$\text{hlb} = \sum(\text{hydrophilic group numbers}) - \sum(\text{hydrophobic group numbers}) + 7 \quad (1)$$

surfactants with n CH_2 groups in the paraffinic chain molecule, eq 1 becomes

$$\text{hlb} = \sum(\text{hydrophilic group numbers}) - n(\text{group number per } CH_2) + 7 \quad (2)$$

and similarly for fluorocarbon surfactants with n CF_2 groups

$$\text{hlb} = \sum(\text{hydrophilic group numbers}) - n(\text{group number per } CF_2) + 7 \quad (3)$$

So far, the latter equation had no practical use in the absence of numerical data on the group number per CF_2. An attempt to remedy this situation is presented below.

On the basis of the correlation found[3,4] between the hlb and cmc values for hydrocarbon surfactants and of data on cohesive energy change (ϕ) in transferring of aliphatic chains from an aqueous to a nonpolar phase,[5] we obtain

$$n(\text{group number per } CH_2) = \phi/2.303kT \quad (4)$$

where k is the Boltzmann constant and T is the absolute temperature.

According to Davies,[1] the group number per CH_2 group equals 0.475; hence for a molecule of n carbon atoms—where $\phi = n\phi'$—eq 4 becomes

$$n0.475 = n\phi'_{CH_2}/2.303kT \quad (5a)$$

or

$$1.09kT = \phi'_{CH_2} \quad (5b)$$

This value may be compared with estimates from various sources. (a) Shinoda[6] found $1.08kT$ per methylene group from the change of critical micelle concentration of homologous paraffin chain salts *vs.* chain length under conditions of constant ionic strength. (b) Langmuir[7] found $(1.08–1.2)kT$ for the heat of adsorption of a methylene group in water. (c) Overbeek and Stigter[8] found $1.02kT$ for the standard free energy of micelle formation for sodium dodecyl sulfate at 25° in aqueous sodium chloride solutions. (d) Solubility data[9] for homologous aliphatic compounds in water yield $1.08kT$ per methylene group transferred from the aqueous to the oil phase. (e) Based on hemimicelle theory it was found[5] that the hydrophobic bonding is a linear function of the number of carbons in the alkyl chain with an incremental energy of approximately $1.0kT$ per CH_2 group. This hydrophobic energy is identical for removal of one CH_2 group from the aqueous phase into either the micellar or the hemimicellar state.

Correspondingly eq 2 yields

$$\text{hlb} = \sum(\text{hydrophilic group numbers}) - n\phi'/2.303kT + 7 \quad (6)$$

with ϕ' referring to the CH_2 or CF_2 group as the case may be. For a given homologous series of surfactants hlb decreases as the number of carbon atoms in the chain increases.

Critical Micelle Concentration. Shinoda[10] and other investigators[11–14] derived the following expressions for the critical micelle concentration, cmc, in aqueous solutions of long-chain hydrocarbon surfactants as functions of the total concentration of the counterions (gegenions), C_i, and the number of CH_2 groups, n, in the hydrocarbon chain. The change of cmc with ionic strength is given as

$$\log \text{cmc} = -K_g \log C_i + K' \quad (7)$$

where K_g is the number ratio of counterions to long-chain ions in the micelle[12] (ranging from 0.4 to 0.6 for hydrocarbon surfactants) and K' a negative empirical constant. Also, according to Shinoda,[15] for homologous series of paraffinic surface-active agents

$$\log \text{cmc} = -K_g \log C_i - n\phi'_{CH_2}/2.303kT + K_1 \quad (8)$$

where K_1 is another empirical constant and ϕ'_{CH_2} is the transfer energy per CH_2 group from aqueous environment to the interior of the micelle (free energy change due to micellization). If no inorganic salt is added, cmc = C_i, and eq 8 yields

$$\log \text{cmc} = -\frac{n\phi'_{CH_2}}{2.303kT(1 + K_g)} + K_2 \quad (9)$$

the cmc value depends on the number of carbon atoms of the paraffin or fluorocarbon chain and on temperature; at constant temperature, it decreases logarithmically as the number of carbon atoms in the chain increases. For the same polar group the longer hydrocarbon chains provide greater driving forces for micellization than short ones.

(3) I. J. Lin, *Isr. J. Technol.*, **9**, 621 (1971).
(4) I. J. Lin, *Trans. AIME*, **250**, 225 (1971).
(5) I. J. Lin and P. Somasundaran, *J. Colloid Interface Sci.*, **37**, 731 (1971).
(6) K. Shinoda, *J. Phys. Chem.*, **58**, 541 (1954).
(7) I. Langmuir, *J. Amer. Chem. Soc.*, **39**, 1883 (1917).
(8) J. T. G. Overbeek and D. Stigter, *Recl. Trav. Chim. Pays-Bas*, **75**, 1263 (1956).
(9) K. Shinoda, *Bull. Chem. Soc. Jap.*, **26**, 101 (1953).
(10) K. Shinoda, *J. Phys. Chem.*, **59**, 432 (1955).
(11) M. L. Corrin and W. D. Harkins, *J. Amer. Chem. Soc.*, **69**, 683 (1947).
(12) M. L. Corrin, *J. Colloid Sci.*, **3**, 333 (1948).
(13) E. D. Goddard, O. Harva, and T. G. Jones, *Trans. Faraday Soc.*, **49**, 980 (1953).
(14) E. K. Mysels and K. J. Mysels, *J. Colloid Sci.*, **20**, 20 (1965).
(15) K. Shinoda, "Colloidal Surfactants," Academic Press, New York, N. Y., 1963, Chapter 1.

Micelle formation is apparently controlled by two mutually opposite factors, namely, the cohesive forces between hydrophobic groups and the affinity of hydrophilic groups for the water molecules. At a given temperature, the balance between these factors produces a micelle of the corresponding size, shape, and charge. For a homologous series of surfactants, the cmc value may also be expressed by the well-known empirical equation given by Klevens[16] and Corrin[12]

$$\log \text{cmc} = A - Bn \tag{10}$$

where n is the number of carbon atoms in the hydrocarbon or fluorocarbon chain (also the equivalent effective number of CH_2 or CF_2 groups in a nonlinear chain[17]) and A and B are constants representing a particular temperature and homologous series. Equations 9 and 10 together yield

$$B = \frac{\phi'}{2.303kT(1 + K_g)} \tag{11}$$

with ϕ' again referring to the CH_2 or CF_2 group as the case may be, since the dependence of the cmc of fluorocarbon surfactants upon chain length is analogous to that of hydrocarbon compounds.[18–21]

Correlation between Cmc and Hlb. Equations 6 and 9 have a fundamental significance in terms of free energy of micellization. For straight-chain saturated derivatives n is the actual number of carbon atoms in the alkyl chain, and for nonlinear compounds n is assumed to be the effective chain length in terms of CH_2 or CF_2 units. Five different methods for determination of the effective number of CH_2 groups (n_{eff}) in long-chained surfactants are described elsewhere.[17]

Thus, eq 6 and 9 will become

$$\text{hlb} = \sum(\text{hydrophilic group numbers}) - n_{eff}\phi'/2.303kT + 7 \tag{12}$$

and

$$\log \text{cmc} = -\frac{n_{eff}\phi'}{2.303kT(1 + K_g)} + K_2 \tag{13}$$

Equations 6 and 9 or equations 12 and 13 provide a theoretical basis for the empirical equations (1) and (10).

In a homologous series of surface-active agents, chain length is a common determining parameter in the hlb and cmc equations and determines their numerical values. Accordingly, they can be correlated on the basis of Davies' modified formula (eq 6). Such a correlation was given for straight-chain hydrocarbon surfactants by Wacks and Hayano[22] and Lin[4] and is equally valid for the fluorinated compounds, *i.e.*

$$\log \text{cmc} = a + b(\text{hlb}) = a + \frac{\text{hlb}}{1 + K_g} \tag{14}$$

and

$$B/b = \phi'_{CF_2}/2.303kT$$

$$(A - a)/b = \sum(\text{hydrophilic group numbers}) + 7 \tag{15}$$

where a and b are constants at constant temperature for a given homologous series. Equation 14 makes possible a determination of the hlb for a homologous series of any surface-active agents from known cmc values.

Numerical Results

Arrington and Patterson[23] measured the cmc of a series of fluoroalkanoic acids, $H(CF_2)_nCOOH$, and their ammonium salts, $H(CF_2)_nCOONH_4$. The compounds are completely fluorinated except for the terminal hydrogen atom. Klevens and Raison[24] did the

Table I: Cmc of Fluorinated Surface-Active Agents

Compd	n	Cmc, M	Ref
$H(CF_2)_6COONH_4$	6	0.25, 0.11	23, 21
$H(CF_2)_8COONH_4$	8	0.038, 0.028	23, 21
$H(CF_2)_{10}COONH_4$	10	0.009	23
$H(CF_2)_6COOH$	6	0.15	23
$H(CF_2)_8COOH$	8	0.03	23
CF_3COOH	1	2.6	24
C_2F_5COOH	2	2.06	18
C_3F_7COOH	3	0.71, 0.74, 0.75	24, 21, 19
C_4F_9COOH	4	0.53	18
$C_5F_{11}COOH$	5	0.082, 0.051	24, *a*
$C_6F_{13}COOH$	6	0.05	18
$C_7F_{15}COOH$	7	0.0090, 0.0087	24, 19
$C_8F_{17}COOH$	8	0.0056	18
$C_9F_{19}COOH$	9	0.00089, 0.00085	24, 19, 21
$C_{10}H_{21}COOH$	10	0.00048	18
C_4F_9COOK	4	0.7	*b*
$C_5F_{11}COOK$	5	0.5	24
$C_6F_{13}COOK$	6	0.062	*b*
$C_7F_{15}COOK$	7	0.0263	24
$C_8F_{17}COOK$	8	0.0091	*b*
$C_9F_{19}COOK$	9	0.0009	24
$C_3F_7NH_2$	3	0.132	24
$C_3F_7NH_3Cl$	3	1.1	24

[a] H. B. Klevens and J. Vergnoble, *Proc. Int. Congr. Surface Activ., 2nd*, **1**, 395 (1957). [b] W. A. Zisman, "Encyclopedia of Chemical Technology," 2nd ed, 1963, pp 707–738.

(16) H. B. Klevens, *J. Phys. Colloid Chem.*, **52**, 130 (1948).

(17) I. J. Lin, P. Somasundaran, and B. M. Moudgil, paper presented at the AIME Annual Meeting, San Francisco, Calif., Feb 1972; I. J. Lin and A. Metzer, *J. Phys. Chem.*, **75**, 3000 (1971).

(18) H. B. Klevens, *Kolloid-Z.*, **158**, 53 (1958).

(19) H. M. Scholberg, R. A. Guenthner, and R. I. Coon, *J. Phys. Chem.*, **57**, 923 (1953).

(20) J. O. Hendricks, *Ind. Eng. Chem.*, **45**, 99 (1953).

(21) M. K. Bernett and W. A. Zisman, *J. Phys. Chem.*, **63**, 1911 (1959).

(22) V. W. Wacks and S. Hayano, *Kolloid-Z. Z. Polym.*, **181**, 139 (1962).

(23) C. H. Arrington and G. D. Patterson, *J. Phys. Chem.*, **57**, 247 (1953).

(24) H. B. Klevens and M. Raison, *J. Chim. Phys.*, **51**, 1 (1954).

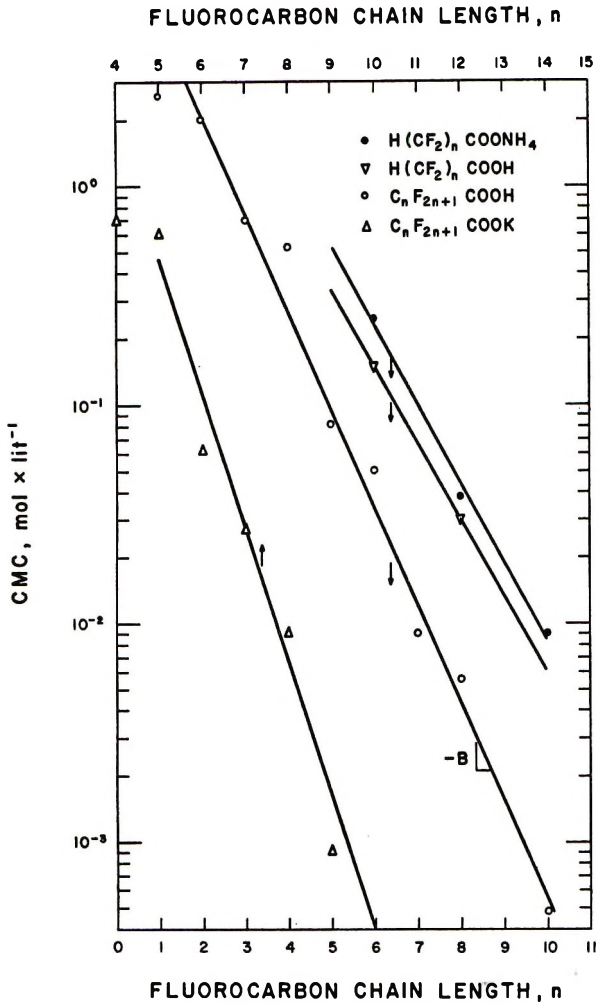

Figure 1. Plot of log cmc of fluorocarbon surfactants as a function of the number of CF_2 groups in the chain.

same for perfluoroalkanoic acids, $C_nF_{2n+1}COOH$, and their potassium salts, $C_nF_{2n+1}COOK$, as listed in Table I. Plots of log cmc against the number of carbon atoms in the chain are given in Figure 1, showing linearity in all cases.

Using eq 11 and literature values for K_g, ϕ'_{CH_2} was recalculated from the values of B given elsewhere.[5,15] Literature values of cmc as functions of n for different fluorocarbon reagents yielded B for the latter, and finally ϕ'_{CF_2} was determined from the average value obtained[25] for K_g according to eq 7. Results are presented in Table II along with the A and B values calculated from eq 10 and Figure 1.

The range obtained, 910–1190 cal/mol (1.53–2.00)-kT, is in fair agreement with literature data: Phillips[26] obtained 1300 cal/mol per CF_2 group for the adsorption energy calculated from cmc data, and Davies[2,27] reported 1490 cal/mol for the transfer between the bulk phase and the liquid–air interface. This is considerably greater than the value of about 600 cal/mol for the CH_2 group. Substituting an average of $2.0kT$ in eq 4, we obtain 0.870 for the lipophilic group number per

Table II: Values of A and B for a Homologous Series of Fluorocarbon Surfactants and Values for ϕ'_{CF_2}, Using Known K_g Values

Compd	A	B	ϕ'_{CF_2}	K_g
$H(CF_2)_nCOONH_4$	1.531	−0.361	$-1.58kT$ or 940 cal/mol	0.91[a]
$H(CF_2)_nCOOH$	1.273	−0.349	$-1.53kT$ or 910 cal/mol	0.91[a]
$C_nF_{2n+1}COOH$	1.165	−0.444	$-2.00kT$ or 1190 cal/mol	0.96[b]
$C_nF_{2n+1}COOK$	2.334	−0.572	$-2.00kT$ or 1190 cal/mol	0.52[b,c]

[a] After ref 25. [b] From eq 14. [c] The same K_g value was found for potassium perfluorooctanoate in the presence of potassium nitrate at 30°: K. Shinoda and K. Katsura, *J. Phys. Chem.*, **68**, 1568 (1964).

CF_2 group, compared with 0.475 for its CH_2 counterpart.

Hlb values were calculated from eq 6 and the data in Table III. For different n values in the $C_nF_{2n+1}COOK$ chain, the values of hlb are as follows: for $n = 5$, $21.1 - (5 \times 0.870) + 7 = 23.75$; for $n = 6$, 22.88; for $n = 7$, 22.01; for $n = 8$, 21.14; for $n = 9$, 20.27.

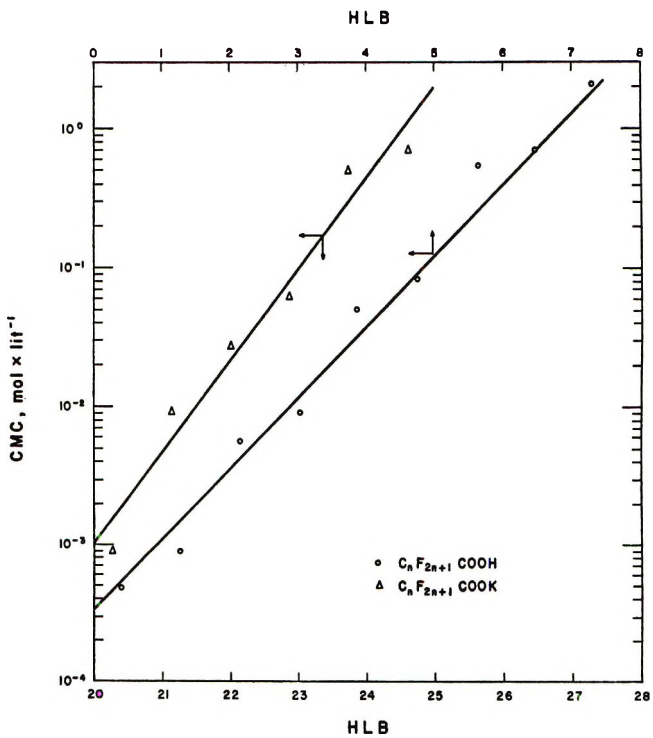

Figure 2. Cmc of fluorocarbon surfactants as a function of the corresponding hlb values.

(25) R. D. Kulkarni, P. Somasundaran, and I. J. Lin, unpublished work, Columbia University, New York, N. Y., 1971.

(26) J. N. Phillips, *Trans. Faraday Soc.*, 51, 561 (1955).

(27) H. B. Klevens and J. T. Davies, *Proc. Int. Congr. Surface Activ., 2nd*, 1, 31 (1957).

Table III: Hlb Group Numbers for Hydrophilic and Hydrophobic Groups (According to Davies[1])

Hydrophilic groups	Group no.	Lipophilic groups	Group no.
$-SO_4^-$, Na^+	38.7	-CH-	0.475
$-COO^-$, K^+	21.1	$-CH_2-$	0.475
$-COO^-$, Na^+	19.1	$-CH_3$	0.475
$-SO_3^-$, Na^+	11.0	=CH-	0.475
N(tertiary amine)	9.4		
-COOH	2.1		
-OH	1.9		
-O-	1.3		

The correlation between cmc and hlb according to eq 14 is directly obtainable from eq 15. Once A and B are known (Table II), the constants a, b, and K_g are readily eliminated. In Figure 2, log cmc is plotted against hlb for $C_nF_{2n+1}COOH$ and $C_nF_{2n+1}COOK$, showing linearity in both cases. For the two ionic fluorocarbon surfactants, eq 14 yields respectively the final relationships

$$\log \text{cmc} = -3.476 + 0.510(\text{hlb}) \quad (16)$$

where $K_g = 0.96$ and

$$\log \text{cmc} = -16.155 + 0.658(\text{hlb}) \quad (17)$$

where $K_g = 0.52$.

Conclusions

(1) The "lipophilic group number per CF_2 group" was found to be 0.870 for long-chain, unbranched polar molecules with terminal CF_2H or CF_3 groups.

(2) The empirical hlb values have a fundamental significance in terms of the free energy change per CH_2 or CF_2 group involved in chain transfer from the aqueous solution to the hydrocarbon or fluorocarbon medium.

(3) The correlation between cmc and hlb for fluorocarbon surfactants is identical with that for hydrocarbon surfactants.

(4) K_g is an important parameter in determining ϕ'_{CF_2} values. It is obtainable from the cmc of long-chain salts as functions of the counterion concentration (eq 7) or directly from eq 14.

(5) By means of Davies' theory of the hlb, the cohesive free energy change per methylene radical has been calculated to be $1.09kT$. This value is equal to the environmental energy change due to micellization.

Acknowledgment. The author wishes to thank Dr. A. Metzer for helpful discussions and the Faculty of Civil Engineering, Technion, Haifa, Israel, for financial support for this work.

A Critical Study Involving Water, Methanol, Acetonitrile, *N,N*-Dimethylformamide, and Dimethyl Sulfoxide of Medium Ion Activity Coefficients, γ, on the Basis of the $\gamma_{AsPh_4^+} = \gamma_{BPh_4^-}$ Assumption

by I. M. Kolthoff* and M. K. Chantooni, Jr.

School of Chemistry, University of Minnesota, Minneapolis, Minnesota 55455 *(Received January 20, 1972)*

Publication costs borne completely by The Journal of Physical Chemistry

A critical study has been made of solubility products, K^{sp}, of a host of salts in the solvents mentioned in the title, and the values compared with data, wherever available, in the literature. Based on the assumption that the medium activity coefficient ${}^{S_1}\gamma^{S_2}{}_i$ of the tetraphenylborate ion is equal to that of the tetraphenylarsonium ion, values of $p^M\gamma^S = -\log {}^M\gamma^S$ of a host of univalent cations and anions has been presented in Table IV (M = methanol, S = other title solvents). These have been obtained from pK^{sp} values and also from standard potential data (Table I) and, in a few instances, from polarographic half-wave potentiols. Conclusions are drawn in the discussion section regarding the relative solvation of the ions in the amphipratic solvents water and methanol on the one hand and the three aprotic polar solvents on the other. Values of $p\gamma_i$ obtained on the basis of the Strehlow assumption, that the potential of the ferrocene–ferricinium couple is constant in various solvents, differ from the data in Table IV by -1.3 units. With water as the reference solvent the difference is $+2.3$. Evidence is presented that the value of $p^W\gamma^{DMSO}{}_{H^+}$ obtained on the basis of the tetraphenylborate assumption is closer to the true value than that obtained by the ferrocene assumption. With reference to $p^M\gamma^{DMSO}{}_{H^+}$ it has been concluded in this paper that the tetraphenylborate assumption yields a value of $p^M\gamma^{DMSO}{}_{H^+}$ which closely agrees with that expected on the basis of ΔpK^d of a carban acid between M and DMSO.

In recent reviews,[1-3] the various extrathermodynamic assumptions which have been made to find a medium ion activity coefficient, ${}^{S_1}\gamma^{S_2}$, have been discussed. Among the most popular assumptions is that originated by Grunwald,[4] ${}^{S_1}\gamma^{S_2}{}_{PPh_4^-} = {}^{S_1}\gamma^{S_2}{}_{BPh_4^-}$, followed by similar assumptions, ${}^{S_1}\gamma^{S_2}{}_{TAB^+} = {}^{S_1}\gamma^{S_2}{}_{BPh_4^-}$[5] (TAB$^+$ is triisoamyl-*n*-butylammonium ion) and ${}^{S_1}\gamma^{S_2}{}_{AsPh_4^+} = {}^{S_1}\gamma^{S_2}{}_{BPh_4^-}$.[6] An extensive discussion of the various other assumptions has been given in Popovych's excellent review paper.[2] In a recent publication, Parker, *et al.*,[7] presented a list of solubility products, K^{sp}, at zero ionic strength of tetraphenylarsonium tetraphenylborate and a host of other salts in 14 organic solvents and gave values of log ${}^{AN}\gamma^S{}_{Ag^+}$, AN denoting acetonitrile. Water was not included because K^{sp} of $AsPh_4BPh_4$ and $AgBPh_4$ in water were unknown at that time. Popovych[8] calculated indirectly the solubility product of $TABBPh_4$ and Parker[7] of $AsPh_4BPh_4$ in water and the former author reported values of log ${}^W\gamma^M{}_i$ (W = water and M = methanol) of several univalent cations and anions, i. In the present work we have used the calculated value of pK^{sp} of $AsPh_4BPh_4$ of 17.3[9] (molar scale) and the experimentally determined value of $pK^{sp}{}_{AgBPh_4} = 17.2$ (molar scale) in water at 25°.[10] After our experimental work was concluded, Popovych, *et al.*,[11] sent us a preprint of a paper in which they present values of pK^{sp} of some alkali metal salts in water, methanol, ethanol, acetonitrile, and water–ethanol mixtures, and log ${}^W\gamma^S{}_i$ (S referring to the other solvents), using the three assumptions that the γ values of tetraphenylarsonium tetraphenylborate ($AsPh_4BPh_4$), tetraphenylphosphonium tetraphenylborate (PPh_4BPh_4), and triisoamyl-*n*-butylammonium tetraphenylborate ($TABBPh_4$) can be divided equally between their cations and anions. Excellent agreement is reported between the first two assumptions, while the third deviates in some water–ethanol mixtures from them as much as 0.5 unit. In connection with our studies of acid–base equilibria in W, M, AN,[12] *N,N*-dimethylformamide (DMF)[12] and

(1) A. J. Parker, *Chem. Rev.*, **69**, 1 (1969).

(2) O. Popovych, *Crit. Rev. Anal. Chem.*, **7**, 73 (1970).

(3) I. M. Kolthoff, *Pure Appl. Chem.*, **25**, 305 (1971).

(4) E. Grunwald, G. Baughman, and C. Kohnstam, *J. Amer. Chem. Soc.*, **82**, 5801 (1960).

(5) O. Popovych and A. J. Dill, *Anal. Chem.*, **38**, 588 (1966).

(6) R. Alexander and A. J. Parker, *J. Amer. Chem. Soc.*, **89**, 5539 (1967).

(7) R. Alexander, A. J. Parker, J. H. Sharp, and W. E. Waghorn, *ibid.*, **94**, 1148 (1972).

(8) O. Popovych and R. Friedman, *J. Phys. Chem.*, **70**, 1671 (1966).

(9) I. M. Kolthoff and M. K. Chantooni, Jr., *J. Amer. Chem. Soc.*, **93**, 7104 (1971).

(10) I. M. Kolthoff and M. K. Chantooni, Jr., *Anal. Chem.*, **44**, 194 (1972).

(11) O. Popovych, A. Gibofsky, and D. H. Berne, *ibid.*, in press.

(12) I. M. Kolthoff and M. K. Chantooni, Jr., *J. Amer. Chem. Soc.*, **93**, 3843 (1971).

dimethyl sulfoxide (DMSO), we have determined in the present work $p^{M}\gamma^{S}$ values of univalent inorganic cations and anions and of benzoate (Bz^-) and acetate (OAc^-). For the sake of brevity we use the notation $p^{S_1}\gamma^{S_2}{}_i$ instead of log ${}^{S_1}\gamma^{S_2}{}_i$, a negative value of the former indicating that in the transfer of the ion from S_1 to S_2 there is a decrease in free energy; in other words, the ion is stronger solvated in S_2 than in S_1. Although the notation p usually stands for $-\log$, we have used it in the above sense because a negative value has the same meaning as in the symbols used by Parker and Popovych.

Values are reported with reference to methanol because this solvent is close to isodielectric with the three aprotic solvents. However, since several French authors have used water as a reference solvent, we also present a table of $p^{W}\gamma^{S}$ of cations (Table V). Our data are based on the (Parker) assumption that $\gamma_{AsPh_4^+} = \gamma_{BPh_4^-}$, referred to as the tetraphenylborate assumption. Evidently the accuracy with which $p\gamma_{C^+}$ (C^+ is cation) or $p\gamma_{A^-}$ (A^- is anion) can be determined on the basis of this assumption depends upon the accuracy of the values of the solubility products, K^{sp}, of the corresponding salts. It is not a simple matter to find with accuracy K^{sp} values at zero ionic strength of many salts in organic solvents of intermediate dielectric constant because of some uncertainty involved in the values of ionic radii in the application of the Debye–Hückel expression, incomplete dissociation of the salts when K^{sp} is obtained from the total solubility, and of involved equilibria as a result of complexation of several silver and thallous salts. In the experimental part results of our values of pK^{sp} are reported and, wherever possible, compared with values found in the literature.

To find $p^{S_1}\gamma^{S_2}{}_{C^+}$ or $p^{S_1}\gamma^{S_2}{}_{A^-}$ use is made of the familiar relation

$$(pK^{sp}{}_{CA})_{S_2} - (pK^{sp}{}_{CA})_{S_1} = {}^{S_1}\Delta^{S_2}pK^{sp}{}_{CA} = p^{S_1}\gamma^{S_2}{}_{C^+} + p^{S_1}\gamma^{S_2}{}_{A^-} \quad (1)$$

Values of $p^{M}\gamma^{S}{}_{K^+}$ (S = W, AN) are used in the derivation of $p^{M}\gamma^{S}{}_{A^-}$ (S = W, AN) because the K^{sp} values of $KBPh_4$ in W, M, and AN are known in W, M, and AN with satisfactory accuracy. The high solubility of potassium and other alkali metal tetraphenylborates in DMF and DMSO does not allow an accurate determination of their solubility products in these solvents. Fortunately, values of $pK^{sp}{}_{AgBPh_4}$ are known with fair accuracy (± 0.2 unit) in W, M, AN, DMF, and DMSO. Values of $pK^{sp}{}_{CBPh_4}$ for cations different from K^+ or Ag^+ can be calculated from eq 2a and 2b and when available compared with experimental data, CA, KA (or AgA)

$${}^{M}\Delta^{S}pK^{sp}{}_{CBPh_4} = {}^{M}\Delta^{S}pK^{sp}{}_{CA} + {}^{M}\Delta^{S}pK^{sp}{}_{KBPh_4} - {}^{M}\Delta^{S}pK^{sp}{}_{KA} \quad (2a)$$

$${}^{M}\Delta^{S}pK^{sp}{}_{CBPh_4} = {}^{M}\Delta^{S}pK^{sp}{}_{CA} + {}^{M}\Delta^{S}pK^{sp}{}_{AgBPh_4} - {}^{M}\Delta^{S}pK^{sp}{}_{AgA} \quad (2b)$$

denoting slightly soluble salts. For the solvents, W, M, and AN it was possible to compare values of ${}^{W}\Delta^{S}pK^{sp}{}_{CBPh_4}$ obtained from each eq 2a and 2b and thus check the reliability of pK^{sp} values used. This was also done by calculating $p^{S_1}\gamma^{S_2}{}_{C^+}$ from the relation

$${}^{S_1}\Delta^{S_2}pK^{sp}{}_{CA} - {}^{S_1}\Delta^{S_2}pK^{sp}{}_{KA} \text{ (or } {}^{S_1}\Delta^{S_2}pK^{sp}{}_{AgA}) = p^{S_1}\gamma^{S_2}{}_{C^+} - p^{S_1}\gamma^{S_2}{}_{K^+} \text{ (or } p^{S_1}\gamma^{S_2}{}_{Ag^+}) \quad (3)$$

Examples are given in the experimental section. Using recommended values of $p^{M}\gamma^{S}{}_{C^+}$ in Table IV, values of $p^{M}\gamma^{S}{}_{A^-}$ were found using eq 1.

Since no suitable slightly soluble sodium salt NaA in water was available, $p^{M}\gamma^{W}{}_{Na^+}$ was found from the relation

$$p^{M}\gamma^{W}{}_{Na^+} - p^{M}\gamma^{W}{}_{K^+} = [(E^0{}_K - E^0{}_{Na})_M - (E^0{}_K - E^0{}_{Na})_W]/0.0591 \quad (\text{at } 25^\circ) \quad (4)$$

in which E^0 denotes the standard potential of the metal with reference to $E^0{}_H$ in the particular solvent. When values of $E^0{}_C$ were available in different solvents, values of $p^{S_1}\gamma^{S_2}{}_{C^+}$ obtained from equations analogous to eq 4 where C = Na and $E^0{}_K$, $p^{S_1}\gamma^{S_2}{}_{K^+}$ (or $E^0{}_{Ag}$, $p^{S_1}\gamma^{S_2}{}_{Ag^+}$) were compared with the average value of $p^{S_1}\gamma^{S_2}{}_{C^+}$ obtained from K^{sp} data. Values of E^0 of metals and the ferrocene–ferricinium couple are presented in Table I.

Some use for the calculation of $p^{S_1}\gamma^{S_2}{}_{C^+}$ using eq 5 has been made from differences between polarographic half-wave potentials, $E_{1/2}$, of a cation C^+ and $(E_{1/2})_K$, water being the reference solvent

$$\{[(E_{1/2})_C - (E_{1/2})_K]_W - [(E_{1/2})_C - (E_{1/2})_K]_S\}/0.0591 = p^{W}\gamma^{S}{}_{C^+} - p^{W}\gamma^{S}{}_{K^+} \quad (5)$$

A summary of $E_{1/2}$ data of univalent cations, which are reduced reversibly at the dme in W, M, AN, DMF, and DMSO, has been given in a previous paper.[3]

Values of $p^{M}\gamma^{S}{}_{H^+}$ cannot be found directly by application of eq 1 because there are no slightly soluble acids which are completely dissociated in the various solvents. Indirectly, $p^{M}\gamma^{S}{}_{H^+}$ values can be obtained using eq 6 from differences in dissociation constants of acids, $K^{d}{}_{HA}$, in various solvents, knowing ${}^{M}\gamma^{S}{}_{HA}$ from solubility determinations and ${}^{M}\gamma^{S}{}_{A^-}$ from K^{sp} of salts of the type CA

$$p^{M}\gamma^{S}{}_{H^+} = (pK^{d}{}_{HA})_S - (pK^{d}{}_{HA})_M - p^{M}\gamma^{S}{}_{A^-} + p^{M}\gamma^{S}{}_{HA} \quad (6)$$

Application of eq 6 is limited to those acids and salts which do not form crystalline solvates. Since $p^{M}\gamma^{S}{}_{A^-}$ is found from pK^{sp} data (eq 3), $p^{M}\gamma^{S}{}_{C^+}$ must be known.

Table I: Standard Potentials in Volts *vs.* $(E^0_H)_s$ of Alkali Metal Ions, Ag, Tl, and Ferrocene (Fc) in Various Solvents at 25° (Molar Scale)

Solvent	E^0_{Na}	E^0_K	E^0_{Rb}	E^0_{Tl}	E^0_{Ag}	E^0_{Fc}
Water	−2.714[a]	−2.925[a]	−2.925[a]	−0.336[a]	0.7996[e]	0.394[c]
						0.40[i]
						0.409[n]
MeOH	−2.728[d]	−2.921[b]	−2.912[b]	−0.379[d]	0.764[d]	0.501[n]
AN			−3.316[f]	−0.682[f,g]	0.096[c]	0.034[c]
						0.068[n]
DMF					0.785[m]	0.69[l]
					0.79[m']	
DMSO				−0.352[j,k]	0.680[j,k]	0.732[j,k]
					0.668[h]	

[a] W. Latimer, "Oxidation Potentials," 2nd ed, Prentice Hall, New York, N. Y., 1952. [b] K. Bräuer and H. Strehlow, *Z. Phys. Chem. (Frankfurt am Main)*, **17**, 346 (1958). [c] Reference 42. [d] P. Buckley and H. Hartley, *Phil. Mag.*, **8**, 320 (1929). [e] J. J. Lingane and W. Larson, *J. Amer. Chem. Soc.*, **58**, 2647 (1936). [f] J. F. Coetzee and J. Campion, *ibid.*, **89**, 2513 (1967). [g] Value based on E^0_{Ag} = 0.096 V in AN. [h] This work. [i] H. Koepp, H. Wendt, and H. Strehlow, *Z. Elektrochem.*, **64**, 483 (1960). [j] M. Le Démézet, *Bull. Soc. Chim. France*, 4550 (1970). [k] J. Courtot-Coupez, A. Laouenan, and M. Le Démézet, *C. R. Acad. Sci., Ser. C*, **267**, 1475 (1968). [l] Reference 46. [m] Value obtained in DMF from E^0_{Fc} (ref 48) and value of $E^0_{Fc} - E^0_{Ag} = -0.095$ V by Parker (ref 7). [m'] From $E^0_{Fc} - E^0_{Ag} = -0.099$ V reported by D. Leurs, *J. Inorg. Nucl. Chem.*, **33**, 2703 (1971). [n] Value calculated from $E^0_{Fc} - E^0_{Ag}$ reported by Parker (ref 7) and value of E^0_{Ag} in this table.

Values of pK^d_{HA} of a host of substituted benzoic acids and that of acetic acid are known in W, M,[13] and AN, DMF, and DMSO.[14]

Values of $p^M\gamma^S_{H^+}$ can also be obtained from standard potentials of metals, E^0_C, in different solvents and $^M\gamma^S_{C^+}$

$$p^M\gamma^S_{H^+} = [(E^0_C)_M - (E^0_C)_S]/0.0591 + p^M\gamma^S_{C^+} \quad (4a)$$

Unfortunately, few values of E^0_C are known in the various solvents (Table I). Wherever possible, values of $p^W\gamma^S_{H^+}$ obtained from eq 4a and 6 were compared (Table V). Note that all these $p^M\gamma^S_{H^+}$ values are based on the tetraphenylborate assumption.

Experimental Section

Chemicals. Solvents. Acetonitrile,[15] *N*,*N*-dimethylformamide,[16] dimethyl sulfoxide,[17] and methanol[18] were purified as described elsewhere.

Salts. Tetraphenylarsonium tetraphenylborate was prepared as described by Popov,[19] while potassium tetraphenylborate was prepared from metathesis of sodium tetraphenylborate with potassium chloride.[8] Sodium tetraphenylborate (Aldrich puriss. grade) was purified according to the method of Popov.[19] Thallium tetraphenylborate was prepared in the same way as the silver salt.[9] Potassium and cesium picrates were the products used previously,[20] while rubidium picrate was prepared from the bromide (Alpha Co.) in the same way as the cesium salt. Sodium and potassium halides were Merck Reagent grade. Cesium bromide was prepared from neutralization of the hydroxide with Baker hydrobromic acid. The hydroxide was prepared by passing a dilute solution of cesium perchlorate (G. F. Smith Co.) through a column of Dowex 1-X8 exchange resin. Potassium perchlorate was used previously,[20] while rubidium and tetraphenylarsonium perchlorates were prepared from neutralization of the hydroxides (prepared from the bromide by ion exchange) with Baker Co. perchloric acid. The alkali metal halides and perchlorates were recrystallized from water or water–ethanol mixtures. Thallous picrate, bromide, perchlorate, and benzoates were prepared by neutralizing an aqueous or ethanol solution of the corresponding acid with an aqueous thallous hydroxide solution prepared by passing thallous formate (Eastman Kodak Co.) solution through a column of Dowex I-X8 resin as above. Thallous nitrate and chloride were Fisher Co. products. All thallous salts were recrystallized from water. The procedure of Kolthoff, Lingane, and Larson[21] was used to prepare silver benzoate. Silver acetate was a Baker Co. product. Since *p*-bromobenzoic and *p*-dimethylaminobenzoic acids are slightly soluble even in ethanol, their alkali metal salts were prepared by adding an excess of the acid to a solution of the corresponding alkali metal hydroxide in hot water, cooling, filtering, and neutralizing the filtrate with hydroxide. The solutions were

(13) J. Juillard, *Bull. Soc. Chim.*, 1727 (1966).
(14) I. M. Kolthoff and M. K. Chantooni, Jr., *J. Amer. Chem. Soc.*, **92**, 7025 (1970).
(15) I. M. Kolthoff, S. Bruckenstein, and M. K. Chantooni, Jr., *ibid.*, **83**, 3927 (1961).
(16) I. M. Kolthoff, M. K. Chantooni, Jr., and H. Smagowski, *Anal. Chem.*, **42**, 1622 (1970).
(17) I. M. Kolthoff and T. B. Reddy, *Inorg. Chem.*, **1**, 189 (1962).
(18) I. M. Kolthoff and L. S. Guss, *J. Amer. Chem. Soc.*, **60**, 2516 (1938).
(19) A. I. Popov and R. Humphrey, *ibid.*, **81**, 2043 (1959).
(20) I. M. Kolthoff and M. K. Chantooni, Jr., *ibid.*, **87**, 4428 (1965).
(21) I. M. Kolthoff, J. J. Lingane, and W. D. Larson, *ibid.*, **60**, 2512 (1938).

taken to dryness and the salts were recrystallized from ethanol–ethyl acetate mixtures.

Ionic Solubility of Salts. Conductometric Determinations. The conductivity of the saturated solutions in the various solvents was determined without filtering, using the conductivity cell and bridge previously described.[15]

Potentiometric Determinations. The determination of pa_{Ag^+} in silver tetraphenylborate solutions in the presence of sodium tetraphenylborate in AN, DMF, and DMSO were carried out as in methanol.[9] Essentially the same technique was employed in pa_{Ag^+} determinations in solutions saturated with silver benzoate or acetate in AN and methanol in the presence or absence of the parent acid. Measurements of paH in these solutions with the glass electrode were performed in the same way as previously described.[20]

Total Solubility of Salts. All saturated solutions were filtered prior to the determination of total solubility. The total solubility of alkali halides and silver benzoate or acetate (both in absence and presence of parent acid) was determined by potentiometric titration with aqueous silver nitrate and sodium iodide, respectively, with the silver wire electrode after flooding an aliquot of the filtrate with 20 volumes of water. With acetonitrile solutions the solvent was removed first *in vacuo*. The total solubility of sodium acetate in DMSO and potassium *p*-bromobenzoate in DMF was found by conductometric titration with picric acid in the respective solvent, picric acid being practically completely dissociated in these solvents under the experimental conditions.[16,22] In a similar manner, the total solubility of silver benzoate and acetate in absence and presence of parent acid were determined in AN using 0.5 *M* perchloric acid (in acetic acid) and α-naphtholbenzein as indicator.[23] The total solubility of tetraphenylarsonium perchlorate in M and AN, potassium tetraphenylborate in AN, potassium *p*-bromobenzoate in M, thallous picrate in W and M, and thallous perchlorate and nitrate in M, were determined simply by evaporating the saturated solution to dryness and weighing the residue.

paH Measurements with the Hydrogen Electrode. The hydrogen electrode half-cell has been described by Bruckenstein.[24] Airco hydrogen was used with a Deoxo catalytic purifier. The same 0.010 *M* $AgNO_3$–Ag reference electrode, the silver nitrate solution being in the appropriate solvent, and Corning Model 10 pH meter were used as above.

Crystal Solvates of Salts. Possible solvate formation of the various salts was investigated as follows. (a) For the volatile solvents, M and AN, the dry salt was kept in a sealed canister saturated with solvent vapors for 2–4 days and any change in weight was noted. (b) A slurry consisting of 0.5–1 g of salt in 2 ml solvent was made, allowed to stand for 1–3 days, filtered, washed with at least ten 10-ml portions of hexane (AN, DMF as solvents) or anhydrous ethyl ether (*n*-butyronitrile, DMSO as solvents) "dried" in a current of nitrogen, and the residue dissolved in 0.5 ml of anhydrous acetic acid and the anion titrated in AN with perchloric acid.[23] As AN is volatile, solvate formation was checked with *n*-butyronitrile. The wash liquid (hexane, ethyl ether) was chosen such that its miscibility with the solvent (AN, DMF, etc.) was not too great that it removed the chemically bound solvent, but was sufficiently great to remove the excess adsorbed solvent. (c) This was the same procedure as (b) but the "dried" salt solvate was weighed before and after further drying *in vacuo* at 60° for 4 hr. As DMSO solvates of alkali halides are hygroscopic,[25] the above operations were carried out in a nitrogen atmosphere in a glove bag wherever possible. Crystal solvate studies of some salts in a few solvents have been made by Popovych, *et al.*[11]

Results

Conductometric Section. Use is made of the literature values of the mobilities of the various ions in the solvents employed in this study in the estimation of ionic solubilities of the salts from the conductivity of their saturated solutions. Ion mobilities of alkali metal, perchlorate, and halide ions have been reported in AN,[26–28] DMF,[29–31] in DMSO,[29,32,33] and in M.[29,34,35] That of Tl^+ has been given in AN[36] and DMF. Values of λ_0 for tetraphenylarsonium,[19] picrate,[37] and tetraphenylborate[19] have been reported in AN, while λ_0 of benzoates and acetates in AN was assumed equal to 100, that of 3,5-dinitrobenzoate.[38] Whenever literature values of λ_0 of these ions in solvents other than AN are not avail-

(22) I. M. Kolthoff, M. K. Chantooni, Jr., and S. Bhowmik, *J. Amer. Chem. Soc.*, **90**, 23 (1968).

(23) I. M. Kolthoff, M. K. Chantooni, Jr., and S. Bhowmik, *Anal. Chem.*, **39**, 1627 (1967).

(24) S. Bruckenstein and I. M. Kolthoff, *J. Amer. Chem. Soc.*, **78**, 2974 (1956).

(25) J. Kentamaa, *Suom. Kemistilehti B*, **33**, 179 (1960).

(26) P. Walden and E. Birr, *Z. Phys. Chem.*, **144**, 269 (1929).

(27) S. Minc and P. Werblan, *Electrochim. Acta*, **7**, 257 (1962).

(28) G. A. Forcier and J. W. Olver, *ibid.*, **14**, 135 (1969).

(29) J. E. Prue and P. J. Sherrington, *Trans. Faraday Soc.*, **57**, 1795 (1961).

(30) P. G. Sears, R. Wolford, and L. R. Dawson, *J. Electrochem. Soc.*, **103**, 633 (1956).

(31) D. P. Ames and P. G. Sears, *J. Phys. Chem.*, **59**, 16 (1955).

(32) P. G. Sears, G. R. Lester, and L. R. Dawson, *J. Phys. Chem.*, **60**, 1433 (1956).

(33) N. P. Yao and D. N. Bennion, *J. Electrochem. Soc.*, **118**, 1097 (1971).

(34) E. C. Evers and A. C. Knox, *J. Amer. Chem. Soc.*, **73**, 1739 (1951).

(35) R. E. Jervis, D. R. Muir, J. P. Bulter, and A. Gordon, *ibid.*, **75**, 2855 (1953).

(36) H. L. Yeager and B. Kratochvil, *J. Phys. Chem.*, **74**, 963 (1970).

(37) J. F. Coetzee and G. P. Cunningham, *J. Amer. Chem. Soc.*, **87**, 2529 (1965).

(38) I. M. Kolthoff and M. K. Chantooni, Jr., *ibid.*, **85**, 426 (1963).

Table II: Total Solubility, s_t, (Molarity), Specific Conductivity, £ (ohm^{-1} cm^{-1}) of Saturated Solutions, and Dissociation Constant, pK^d_{MA}, of Salts in Various Solvents at 25°

Salt	M			AN			DMF			DMSO		
	s_t	£ × 10^4	pK^d_{MA}	s_t	£ × 10^4	pK^d_{MA}	s_t	£ × 10^4	pK^d_{MA}	s_t	£ × 10^4	pK^d_{MA}
$AsPh_4BPh_4$							...	5.00	...	...	1.43	...
$AsPh_4ClO_4$	2.55×10^{-3}	2.54	s[a]	0.0251	25.6	s						
NaCl				0.85×10^{-4}	0.11[d]	3.8	5.02×10^{-3}	3.16	2.1	0.0857	...	1.25
Na *p*-dimethyl-aminobenzoate					*b*		...	0.422	...	...	1.61	...
Na benzoate					*b*		...	1.28	...			
Na acetate					*b*		...	0.357	...	0.0159	1.63	1.8
$KBPh_4$				0.0540	...	(s)						
KCl	0.0498	...	(s)	1.21×10^{-4}	0.179	s	2.04×10^{-3}	1.57	s		*c*	
KBr	0.141	59.7	(s)	1.96×10^{-3}	2.66	2.3	0.0732	33.7	s	0.60	...	(s)
K *p*-dimethyl-aminobenzoate					*b*					...	3.18	...
K *p*-bromobenzoate	0.242	...	0.82	...	*b*	...	9.63×10^{-3}	3.45	2.42	...	...	...
RbPi	...	15.5 (in W)	...	...	4.06	...						
RbBr	0.118	...	(s)	...	3.10	...	0.0466	...	(s)			
$RbClO_4$				...	10.6	...						
Rb *p*-dimethyl-aminobenzoate					*b*					...	3.45	...
CsPi	...	8.30 (in W)	...									
	...	2.74	...									
CsBr	0.0785	...		...	2.54	...						
$CsClO_4$				...	17.3	...						
Cs *p*-dimethyl-aminobenzoate					*b*					...	8.18	...
$AgBPh_4$										...	1.21	...
Ag benzoate				7.2×10^{-3}	1.0	4.85						
Ag acetate		0.54		6.8×10^{-4}	0.28	5.3						
$TlBPh_4$	...	(0.020)	...	...	(0.027)	...	...	3.80	...	0.049	11.5	s
TlPi	0.0104 (in W)	10.7 (in W)	s	3.20×10^{-3}	3.22	2.6						
	0.0133	9.12	s									
$TlClO_4$	0.0780	...	s									
TlCl	...	0.667	...									
TlBr	...	0.094	...									
TlBz	...	5.7	...				...	0.104	...			
	...	48.0 (in W)	...									
$TlNO_3$	0.0680	13.5	3.0									

[a] s denotes salt completely dissociated in saturated solution; (s) complete dissociation assumed. [b] Conductivity of saturated solutions determined in presence of *p*-bromophenol (ref 41). [c] Salt solvated in solid phase (see text). [d] M. K. Chantooni, Jr., and I. M. Kolthoff, *J. Amer. Chem. Soc.*, **89**, 1582 (1967).

able, values of λ_0 were calculated from those in AN using the Walden rule and if not available in AN from a compilation of λ_0 in water.[39] In Table II values of the specific conductivity of saturated solutions of various salts in the five solvents are presented. Values of pK^{sp} of salts calculated from the corresponding ionic solubilities are presented in Table III. Whenever the ionic solubility exceeded 10^{-3} M, conductivities of undersaturated solutions were determined at various dilutions, such as potassium chloride in DMF, potassium bromide in M and DMF, sodium chloride and acetate in DMSO, thallous picrate in W, M; and AN, thallous perchlorate in M, thallous tetraphenylborate, and silver nitrate in DMSO. For some salts the total solubility was determined and included in Table II. For the sake of brevity, conductivity data at various dilutions are submitted separately (Table a).[40] Values of Λ_0 calculated from Fuoss and Kraus plots are in reasonable agreement with those from the literature, considering the non-precision nature of the conductance data in this study ($\pm 2\%$). Also in Table II are entered values of pK^{d}_{MA} derived from the Fuoss and Kraus plots. In methanol the solubility of alkali metal benzoates is large.[13] On the other hand, in AN the ionic solubility of alkali metal benzoates and acetates is too small to be measured directly. Hence, pK^{sp} values of these salts were found from the ionic solubility calculated from the conductivity of the saturated solutions in the presence of various concentrations of p-bromophenol (HR)[14] using eq 7, knowing the formation con-

$$f^2[M^+]^2 = K^{sp}_{MA}[1 + K^{f}_{HR\cdot A^-}[HR] + K^{f}_{(HR)_2A^-}[HR]^2] \quad (7)$$

stants of the heteroconjugates $HR\cdot A^-$ and $(HR)_2A^-$. Values of $K^{f}_{HR\cdot A^-}$ and $K^{f}_{(HR)_2A^-}$ are found from the effect of HR on the paH of equimolar mixtures of the acids and their tetraalkylammonium salts.[14] For unsubstituted benzoate, values of $K^{f}_{(HR)_2Bz^-} = 3.7 \times 10^4$ and $K^{f}_{HR\cdot Bz^-} \cong 0$ are calculated from the paH data given in a previous publication.[41] Values of paH in AN of equimolar mixtures of acetic acid, p-bromobenzoic acid with their tetraethylammonium salts, and p-dimethylaminobenzoic acid with its tetrabutylammonium salt in the presence of HR are presented in Table b.[40] A plot of solubility data in AN solutions of HR from which solubility products of sodium acetate, benzoate, potassium p-bromobenzoate and of sodium, potassium, rubidium, and cesium p-dimethylaminobenzoate have been calculated[14] is presented separately (Figure 1).[40] The resulting pK^{sp} values (eq 7) are entered in Table III.

Potentiometric Determinations: pK^{sp} of Silver Tetraphenylborate, Acetate, and Benzoate. Values of $pK^{sp}_{AgBPh_4}$ were found in AN, DMF, and DMSO as previously in M[9] from a_{Ag^+} in saturated solutions of silver tetraphenylborate in the absence and in the presence of sodium tetraphenylborates. Complete dissociation of the latter salt was assumed in DMF and DMSO as was found in AN[19] in solutions <0.01 M; therefore $C_{Na^+} + [Ag^+] = [BPh_4^-]$. Experimental data are given in Table c.[40]

Due to extensive complexation of silver benzoate and acetate in AN the determination of pK^{sp} from potentiometric titration data is involved. However, pK^{sp} of silver salts of weak acids can be determined rather simply in protophobic solvents where complexation occurs from paH and paAg$^+$ measurements in saturated solutions of the silver salt in the presence of the parent acid. Applying this method, values of pK^{sp} of silver acetate equal to 8.7 and 6.8 in AN and M and $pK^{sp}_{AgBz} = 7.0$ in AN were found (Table III). Details will be presented in a subsequent paper. Values of pK^{sp} of various uni-univalent salts obtained in this study in the five solvents are compared in Table III with those from the literature.

Using eq 1 and the tetraphenylborate assumption, the values of $p^M\gamma^S_{ion}$ presented in Table IV were calculated from the solubility products in Table III. As an illustration, $p^M\gamma^S_{Rb^+}$ values were found in the following way: S = W; $p^M\gamma^W_{Rb^+} = {}^W\Delta^M pK^{sp}_{RbPi} - p^M\gamma^W_{Pi^-} = 3.7 - 4.8 - 0.8 = -1.9$, the value of $p^M\gamma^W_{Pi^-}$ having been found from K^{sp} of potassium and silver picrates and $p^M\gamma^W_{K^+}$ and $p^M\gamma^W_{Ag^+}$, respectively. Rubidium and potassium perchlorates yield $p^M\gamma^W_{Rb^+} = 2.5 - 5.4 + 1.0 = -1.9$, and from rubidium tetraphenylborate ${}^M\gamma^W_{Rb^+} = 8.5 - 6.0 - 4.1 = -1.6$. S = AN; from rubidium (and potassium) picrates $p^M\gamma^{AN}_{Rb^+} = 4.6 - 4.8 - 0.5 = -0.7$, from perchlorate $4.6 - 5.4 - 0.2 = -0.6$, from bromide (and silver bromide) $5.6 - 2.7 - 3.6 = -0.7$, and from tetraphenylborate $3.9 - 6.1 + 1.6 = -0.6$. S = DMF; from rubidium (and silver) bromides: $p^M\gamma^{DMF}_{Rb^+} = 3.2 - 2.7 - 4.1 = -3.6$. S = DMSO; $p^M\gamma^{DMSO}_{Rb^+} = p^M\gamma^{AN}_{Rb^+} + p^{AN}\gamma^{DMSO}_{Rb^+}$; from rubidium p-dimethylaminobenzoate (RbA) and NaA, $p^{AN}\gamma^{DMSO}_{Rb^+} = {}^{DMSO}\Delta^{AN}pK^{sp}_{RbA} - {}^{DMSO}\Delta^{AN}pK^{sp}_{NaA} + p^{AN}\gamma^{DMSO}_{Na^+} = 4.1 - 7.7 - (4.7 - 10.0) - 4.7 = -3.0$, $p^M\gamma^{DMSO}_{Na^+}$ being found from K^{sp} of sodium and silver chloride. Thus, $p^M\gamma^{DMSO}_{Rb^+} = -3.0 - 0.7 = -3.7$.

An example of the application of eq 6 in the calculation of $p^M\gamma^S_{H^+}$ (S = AN) follows. Values of pK^{d}_{HPi} in M and AN are 3.7[13] and 11.0,[20] respectively, or ${}^{AN}\Delta^M pK^{d}_{HPi} = 7.3$. From solubility data we find

(39) R. A. Robinson and R. N. Stokes, "Electrolyte Solutions," 2nd ed, Butterworths, Washington, D. C., 1959.

(40) Conductivity data at various dilutions will appear following these pages in the microfilm edition of this volume of the journal. Single copies may be obtained from the Business Operations Office, Books and Journals Division, American Chemical Society, 1155 Sixteenth St., N.W., Washington, D. C. 20036, by referring to code number JPC-72-2024. Remit check or money order for $3.00 for photocopy or $2.00 for microfiche.

(41) I. M. Kolthoff and M. K. Chantooni, Jr., *Anal. Chem.*, **39**, 1080 (1967).

Table III: pK^{sp} of Salts at $\mu = 0$ and at 25°. (Molar Scale, Except Alkali Halides in W, Molal Scale.) Values in Parentheses Are

Salt	W	M	AN	DMF	DMSO
$AsPh_4BPh_4$	(17.3)	9.0[a]	5.6,[c] 5.8[a]	3.9,[a] 3.9[d]	3.6,[a] 4.3[d]
$AsPh_4Pi$	8.8,[a] 8.9[h]	3.9,[a] 4.1[h]	2.6,[a] 2.8[h]		
$AsPh_4I$	5.1[a]	2.3[a]	2.7[a]		
$AsPh_4ClO_4$	8.4,[j] 8.2[b]	5.4,[d,e] 5.0[b]	3.5[d,e]		
$TABBPh_4$	(13.9)[i]	5.13[i]			
TABPi	7.3[i]	1.9[i]			
NaCl		[2.3],[k,cc] [2.1][b]	8.3,[d] [9.0][l] 8.1[u]	5.0,[d,f] 4.9[n]	2.9,[d,f] 2.9[m]
Na *p*-dimethylaminobenzoate			10.0[d]	6.54[d]	4.7[d]
Na benzoate			8.7[d]	5.4[d]	
Na acetate			9.1[d]	6.7[d]	4.8[d]
$KBPh_4$	7.5,[i] 7.5[a]	5.2,[i] 5.1[a]	3.3,[a] 3.2,[e] 3.05[h]		
KPi	3.5,[o] 3.36,[i] 3.4[h]	4.46[i] 4.4[a]	4.7,[a] 4.55,[p] 4.2[i]	[1.0][a]	
KCl	[−0.3],[a] [−0.9][q] / [−0.9][h]	3.0,[a] 2.9[m] / 3.36,[i] 3.2[f]	8.0,[a] [7.2],[d] 7.9[m] / [7.2][h]	5.5,[a] 5.44[n] / 5.5[d,f]	
KBr	[−1.14][m]	2.54,[d,e] 2.4[l] / [3.3][m]	5.7,[d] 5.7[l]	2.9,[d,f] 2.9[a]	
$KClO_4$	1.94,[r] 2.1[e]	4.7,[t] 4.7[b]	4.2[u]		
K *p*-dimethylaminobenzoate			8.26[d]		4.2[d]
K *p*-bromobenzoate		[2.14][d,e]	7.9[d]	4.7[d]	
$RbBPh_4$	8.54[h]	6.05[i]	3.9[h]		
RbPi	3.7,[d] 3.9[o]	4.8[d]	4.6[d]		
RbBr	[−0.9][m]	[3.8],[m] 2.7[f]	[6.1],[m] 5.6[d] 5.44,[h] 5.4[l]	3.16[f]	[2.5][m]

[a] Reference 7; A. Parker and R. Alexander, *J. Amer. Chem. Soc.*, **90**, 3313 (1968). [b] Reference 45, corrected to $\mu = 0$. [c] Reference 19. [d] This work, from conductance of saturated solution. [e] This work, from weighing residue of saturated solution. [f] This work, from potentiometric or conductometric titration of halide in saturated solution. [g] This work, from potentiometric value of a_{Ag^+} in saturated solution. [h] Reference 11, D. H. Berne and O. Popovych, *J. Chem. Eng. Data*, in press. [i] Reference 5 and ref 8, A. J. Dill and O. Popovych, *J. Chem. Eng. Data*, **14**, 240 (1969). [j] K. Loach, *Anal. Chim. Acta*, **47**, 315 (1969). [k] A. Seidell, "Solubility of Inorganic and Organic Compounds," Van Nostrand, New York, N. Y., 1960. [l] T. Pavlopoulos and H. Strehlow, *Z. Phys. Chem.*, **202**, 474 (1954). [m] F. Chiang, Ph.D. Thesis, University of Minnesota, 1967. [n] Reference 44. [o] K. Toei, *Nippon Kawgaku Kwai Shi*, **78**, 1379 (1957). [p] Reference 20. [q] Total solubility (4.81 *M*) from Seidell (footnote *k*) and activity coefficients from R. Bates, B. Staples, and R. Robinson, *Anal. Chem.*, **42**, 867 (1970). [r] W. Guenther, *J. Amer. Chem. Soc.*, **91**, 7619 (1969). [s] C. Deno and H. Berkheimer,

$p^M\gamma^{AN}_{HPi} = -0.7$, while $p^M\gamma^{AN}_{Pi^-} = +0.5$ (Table IV). Thus, $p^M\gamma^{AN}_{H^+} = +6.1$. In order to find $p^{AN}\gamma^{DMF,DMSO}_{H^+}$, we have used data obtained in a study of substituted benzoic acids;[14] $p\gamma_{HA}$ values are to be reported in a subsequent paper.

Estimation of E^0_{Ag} in DMSO. Potentiometric measurements with the hydrogen electrode in mixtures of benzoic or 2,6-dihydroxybenzoic acids and their tetraethylammonium salts were made in DMSO *vs.* silver–0.01 *M* silver nitrate in DMSO as the reference electrode. The salt bridge was composed of 0.01 *M* tetraethylammonium perchlorate in DMSO. Experimental data are submitted in Table d.[40] Also, hydrogen electrode potential data of Kolthoff and Thomas in sulfuric acid–tetraethylammonium bisulfate mixtures in AN[42] have been recalculated, using $pK^d_{H_2SO_4} = 7.8$,[43] $K^d_{Et_4NHSO_4} = 3 \times 10^{-2}$,[43] $K^f_{H_2SO_4\cdot HSO_4^-} = 5 \times 10^3$.[43] Resulting E^0_{Ag} values in DMSO and AN are included in Table I.

Crystalline Solvates of Salts. Criss[44] reports that sodium, potassium, cesium chlorides, and cesium bromide do not form solid solvates in DMF. However, Kentamaa found that potassium chloride is solvated in DMSO as KCl·0.66DMSO, while sodium chloride and potassium bromide are not.[25] We found that potassium, silver, and tetraphenylarsonium tetraphenylborates are unsolvated in M and AN, as are[45] silver chloride and tetraphenylborate in DMF and silver bromide in DMSO. We also find that sodium benzoate, *p*-dimethylaminobenzoate in DMF, AN, *p*-bromobenzoate in DMSO and acetate in AN, DMF, and DMSO are unsolvated, but that sodium *p*-bromobenzoate forms a solvate in DMF. When sodium *p*-dimethylaminobenzoate was shaken with DMSO, the specific conductivity of the saturated solution attained

(42) I. M. Kolthoff and F. G. Thomas, *J. Phys. Chem.*, **69**, 3049 (1965).

(43) I. M. Kolthoff and M. K. Chantooni, Jr., *J. Amer. Chem. Soc.*, **90**, 5961 (1968).

(44) C. M. Criss and E. Luksha, *J. Phys. Chem.*, **72**, 2966 (1968).

(45) R. Alexander, E. Ko, Y. Mac, and A. J. Parker, *J. Amer. Chem. Soc.*, **89**, 3703 (1967).

Calculated Values (Eq 2a); Values in Brackets Are Uncertain

Salt	W	M	AN	DMF	DMSO
$RbClO_4$	2.54,[r] 2.5[t]	5.4[t]	4.6[d]		
Rb *p*-dimethyl-aminobenzoate			7.7[d]		4.13[d]
$CsBPh_4$	8.7,[b] 8.8[h]	6.2[b]	3.6,[b] 3.9[h]		
CsPi	4.1,[o] 4.24,[d] 4.2[b]	5.2,[d] 4.5[b]	4.7,[i] 4.72[u]		
CsCl		[2.6],[b] [2.4][l]	[6.9][l]	5.1[b]	
CsBr	[−0.8][m]	[3.7],[m] 2.8[l]	5.8,[d] [4.6][m]	3.5,[n] 3.7[b]	
$CsClO_4$	2.4[r]	5.0[t]	4.04[d]		
Cs *p*-dimethyl-aminobenzoate			6.94[d]		3.3[d]
$AgBPh_4$	17.2[v]	13.5,[a] 14.4[v]	7.5,[a] 7.7[g]	7.1,[a] 7.5[g]	5.1,[a] 4.75,[g] 4.7[d]
AgPi	2.8[w]	3.4[w]			
AgCl	9.74[z]	13.2,[z] 13.4[a]	13.2,[a] 13.1[v]	14.8[a]	10.6,[a] 10.9,[v] 10.8[z]
AgBr	12.2[z]	15.5,[z] 15.5[a]	13.2,[a] 13.9[v]	15.3[a]	10.8,[a] 11.1[v]
AgI	16.0[z]	18.4,[z] 18.6[a]	14.5[a]	16.1[a]	11.6,[a] 12.5[v]
Ag benzoate	3.7[w]	6.3[w]	7.0[g]		
Ag acetate	2.77[aa]	6.6,[b] 6.8[g]	[7.9],[b] 8.7[g]	10.5[b]	4.9[b]
AgN_3	8.3[b]	11.5[b]	9.9[b]	11.3[b]	6.9[b]
AgCNS	11.95[bb]	14.2[a]	10.3[a]	11.8[a]	7.5[a]
$TlBPh_4$		[9.3],[d] (9.8)	[9.5][d]	4.5[d]	2.9[d,e]
TlPi	4.0,[k,cc] 4.1[d,e]	3.9,[k,cc] 4.1[d,e]	5.5[d,e]		
$TlClO_4$	1.14[dd]	2.9[d,e]	3.6[dd]		
TlCl	3.7[ee]	4.75,[z] 6.5[d]	13.2[dd]	9.7[ff]	6.7,[gg] 6.9,[ff] 6.8,[hh] 7.1[v]
TlBr	5.4,[ii] 5.5[jj]	8.2[d]	13.04[dd]		
Tl benzoate	2.7[d]	4.5[d]			
$TlNO_4$	1.3[dd]	4.2[d,e]	6.9[dd]		
TlCNS	3.8[dd]		8.3[dd]		

J. Org. Chem., **28**, 2143 (1963), who quoted solubility from Seidell;[k] Guggenheim equation used to calculate mean ionic activity coefficients. [l] H. H. Willard and G. F. Smith, *J. Amer. Chem. Soc.*, **45**, 286 (1923). [u] M. K. Chantooni, Jr., and I. M. Kolthoff, *ibid.*, **89**, 1582 (1967). [v] Reference 10. [w] Reference 21. [z] P. Buckley and H. Hartley, *Phil. Mag.*, **8**, 320 (1929). [y] D. Leurs, R. Iwamoto, and J. Kleinberg, *Inorg. Chem.*, **5**, 201 (1966) (cor to $\mu = 0$). [z] N. Rumbaut and H. Peeters, *Bull. Soc. Chim. Belges*, **79**, 45 (1970) (cor to $\mu = 0$). [aa] F. H. MacDougall and L. Topol, *J. Phys. Chem.*, **56**, 1090 (1952). [bb] M. Randall and J. O. Halford, *J. Amer. Chem. Soc.*, **58**, 1121 (1936). [cc] Complete dissociation of electrolyte assumed in saturated solution. [dd] J. F. Coetzee and J. Campion, *J. Amer. Chem. Soc.*, **89**, 2517 (1967). [ee] M. Randall and W. Vietti, *ibid.*, **50**, 1526 (1928). [ff] J. Synott and J. Butler, *Anal. Chem.*, **41**, 1890 (1969). [gg] Reference 47. [hh] D. Cogley and J. Butler, *J. Electrochem. Soc.*, **113**, 1074 (1966) (cor to $\mu = 0$). [ii] F. Ishikawa and Y. Terui, *Bull. Inst. Phys. Chem. Res. Tokyo*, **12**, 755 (1933). [jj] E. Anderson, Jr., Thesis, Washington State College, 1955.

a maximum value of 1.6×10^{-4} ohm^{-1} cm^{-1} within 10 min (Table II), remained at that value for 10 min, and then suddenly decreased to about one half the maximum value within 40 min, yielding a crystalline monosolvate. No significant further change in conductivity of the saturated solution was observed after 2 days. The other alkali metal *p*-dimethylaminobenzoates did not exhibit the above behavior in any of the aprotic solvents, indicating no crystal solvate formation.

Discussion

In general, the agreement between recommended values and those from ref 7 and 11 of $p^M\gamma^S_{C^+}$ in Table IV obtained by using eq 3 and pK^{sp} of various salts was found to be ±0.15. Our values of $pK^{sp}_{AgBPh_4}$ in W and M have been made the basis of a comparison with other data from Parker, *et al.*[7] Values of E^0 and $E_{1/2}$ of all univalent metal ions dealt with in this paper are known in water, but only a few in nonaqueous solvents (Table I). For this reason we compare in Table V $p^W\gamma^S_{C^+}$ obtained from pK^{sp}, E^0, and $E_{1/2}$ data instead of $p^M\gamma^S_{C^+}$. There is excellent agreement between $p^W\gamma^S_{C^+}$ values obtained from pK^{sp} and E^0 data, and as expected, to a lesser extent from $E_{1/2}$ data. All $p^W\gamma^S_{C^+}$ values are based on the tetraphenylborate assumption.

Parker, *et al.*,[7] have presented values of $p^{AN}\gamma^S_{Ag^+}$ based on various assumptions, one being that the ferrocene–ferricinium couple has the same potential, E_{Fc}, in the various solvents (Strehlow), with the probable exception of water. Using methanol as the reference solvent they report the following values of $p^M\gamma^S_{Ag^+}$

S =	W	AN	DMF	DMSO
$p^M\gamma^S_{Ag^+}$	+2.1	−4.0	−2.9	−5.7
	(−1.3)	(−5.1)	(−4.3)	(−7.2)

The values between parentheses refer to our recommended values based on the tetraphenylborate assumption (italics in Table IV). The difference between values based on the two assumptions is, with the exception of water, −1.1, −1.4 and −1.5, with S = AN, DMF, and DMSO, respectively, with an average of

Table IV: Values of $p^{M}\gamma^{S}_{ion}$ Derived from pK^{sp}_{MA} Values Using Tetraphenylborate Assumption; at 25° (Molar Scale). Recommended Values in Italics

Ion	$p^{M}\gamma^{W}_{ion}$	$p^{M}\gamma^{AN}_{ion}$	$p^{M}\gamma^{DMF}_{ion}$	$p^{M}\gamma^{DMSO}_{ion}$
$AsPh_4^+$	*4.1*	*−1.6*[b]	*−2.6* (−2.6)[b]	*−2.4* (−2.7)[b]
TAB^+	*4.2*[a]	*−1.7*[a]		
Na^+	*−1.5*	*0.9*	*−3.1*	*−3.9*
K^+	*−1.8* (−1.9)[a] (−1.7)[b]	*−0.4* (−0.5)[a] (−0.2)[b]	*−3.5* (−3.6)[b]	*−3.9*
Rb^+	*−1.8* (−1.7)[a]	*−0.6* (−0.5)[a]	*−3.6*	*−3.7*
Cs^+	*−1.7* (−1.7)[a] (−1.6)[b]	*−0.8* (−0.5)[a]	*−3.3* (−3.6)[b]	*−3.9*
Ag^+	*−1.3* (−0.9)[a] (−1.2)[d]	*−5.1* (−5.3)[b] (−4.8)[d]	*−4.3* (−4.7)[b] (−3.9)[d]	*−7.2* (−6.6)[b] (−6.9)[d]
Tl^+	*−0.7*	*0.9*	*−2.7*	*−4.3*
H^+	*−1.9* (−1.95)[a]	*6.2*	*−4.4*	*−5.2*
Pi^-	*0.8* (1.05)[a] (0.8)[b]	*0.5* (0.3)[a] (0.4)[b]	(−0.7)[b]	
ClO_4^-	*−1.0*	*−0.2*		
Cl^-	*−2.2* (−2.1)[a] (2.4)[b]	*5.2* (5.1)[b]	*5.9* (6.1)[b]	*4.6* (3.8)[b]
Br^-	*−2.0* (−2.0)[b]	*3.6* (3.0)[b]	*4.1* (4.5)[b]	*2.5* (1.9)[b]
I^-	*−1.2* (−1.3)[b]	*2.1* (1.2)[b]	*2.1* (2.2)[b]	*0.4* (−0.4)[b]
CNS^-	*−1.0* (−0.9)[b]	*1.2* (1.4)[b]	*1.9* (2.3)[b]	*0.5* (−0.1)[b]
N_3^-	*−1.9* (−1.9)[b]	*3.5* (3.7)[b]	4.1 (4.5)[b]	2.6 (2.0)[b]
NO_3^-	*−2.2*	*1.5*		
OAc^-	*−2.8*	*7.0*	*8.6*	*7.5*
Bz^-	*−1.3*	*5.8*	*6.5*	
BPh_4^-	*4.1*[a] (4.1)[c]	*−1.6*[b]	*−2.6* (−2.6)[b]	*−2.4* (−2.7)[b]

[a] Reference 5, $^{M}\gamma^{S}_{TAB^+} = {}^{M}\gamma^{S}_{BPh_4^-}$ assumption. [b] References 7 and 45, $^{M}\gamma^{S}_{AsPh_4^+} = {}^{M}\gamma^{S}_{BPh_4^-}$ assumption. Values of $pK^{sp}_{AgBPh_4}$ in AN, DMF, and DMSO from ref 7 and in W and M from ref 10. [c] Reference 9. [d] Mean values quoted from ref 7 from a variety of assumptions.

Table V: Comparison of Recommended $p^{W}\gamma^{S}_{ion}$ Values with Those from Standard Potentials, E^0_c, Polarographic Half-Wave Potentials, $(E_{1/2})_c$, and Solubility Data Using Tetraphenylborate Assumption. Molar Scale at 25°

Ion	$p^{W}\gamma^{M}_{ion}$	$p^{W}\gamma^{AN}_{ion}$	$p^{W}\gamma^{DMF}_{ion}$	$p^{W}\gamma^{DMSO}_{ion}$
Na^+	1.5[f] (E^0)[a]	2.4,[f] 2.7$(E_{1/2})$[d] 2.8[e]	−1.8,[f] −1.7$(E_{1/2})$[d]	−2.4,[f] −2.1$(E_{1/2})$[d]
Rb^+	1.8,[f] 1.65(E^0)[a]	1.2,[f] 1.2(E^0)[c] 0.9$(E_{1/2})$[d]	−1.8,[f] −1.35$(E_{1/2})$[d]	−1.9,[f] −1.75$(E_{1/2})$[d]
Ag^+	1.3,[f] 1.2(E^0)[a]	−3.8,[f] −3.8(E^0)[a]	−3.0[f]	−5.9[f]
Tl^+	0.7,[f] 0.8(E^0)[a]	1.6,[f] 1.6(E^0)[c] 1.6$(E_{1/2})$[d]	−2.0,[f] −2.4$(E_{1/2})$[d]	−3.6,[f] −4.4(E^0)[c] −3.45$(E_{1/2})$[d]
H^+	1.9,[f] 1.7(E^0)[a] 1.9(E^0)[b]	8.1,[f] 8.1(E^0)[c] 7.8(E^0)[b]	−2.7(E^0)[c] −2.5[f]	−3.3,[f] −3.6(E^0)[c'] −3.8(E^0)[c'']

[a] From $E^0_M - E^0_K$ and $p^{W}\gamma^{S}_{K^+}$. [b] From $E^0_M - E^0_{Rb}$ and $p^{W}\gamma^{S}_{Rb^+}$. [c] From $E^0_M - E^0_{Ag}$ in W and S and $p^{W}\gamma^{S}_{Ag^+}$. [c'] $(E^0_{Ag})_{DMSO}$ value taken from present work. [c''] $(E^0_{Ag})_{DMSO}$ taken from ref 47. [d] From $[(E_{1/2})_M - (E_{1/2})_K]$ in W and S and $p^{W}\gamma^{S}_{K^+}$. [e] From amalgam partition method (A. Dadgar and K. Schug, *J. Phys. Chem.*, **68**, 112 (1964)) and $p^{W}\gamma^{AN}_{K^+}$. [f] Recommended values from solubility data (Table IV).

−1.3 units. It may be concluded that within the experimental error the difference is constant for these protophobic and protophylic aprotic solvents with reference to methanol. However, for $p^{M}\gamma^{W}_{Ag^+}$ (and all other univalent cations) the difference is −3.4. Hence, with water as the reference solvent $p^{W}\gamma^{S}_{Ag^+}$ (S = AN, DMF, and DMSO) the difference between the values based upon the tetraphenylborate and ferrocene assumptions is 3.4 − 1.3 = 2.1 units. On the basis of the ferrocene assumption, Kolthoff and Thomas[42] reported $p^{W}\gamma^{AN}_{Ag^+} = -5.8$ at an ionic strength of zero in satisfactory agreement with Parker's[7] value of −6.1 (ferrocene method). The following values at an ionic strength of 0.1 reported on the basis of the ferrocene assumption and recalculated by us to an ionic strength of zero are $p^{W}\gamma^{DMF}_{H^+} = -4.9$[46] and $p^{W}\gamma^{DMSO}_{H^+} = -5.7$.[47] These values differ by −2.4 and −2.4 units, respectively, from our recommended values (Table IV) based on the tetraphenylborate assumption. For $p^{W}\gamma^{DMSO}_{Tl^+}$ Courtot's[41] value of −5.9 differs by

(46) G. Demange-Guérin, *Talanta*, **17**, 1075 (1970).

(47) J. Courtot-Coupez, M. Le Démézet, A. Laouenan, and C. Madec, *J. Electroanal. Chem.*, **29**, 21 (1970).

−2.3 units from the value in Table IV. For silver this difference is −1.8 units. Evidently there is good agreement between the values based on the ferricinium assumption by Parker, *et al.*, and the French workers. The difference between values of $p^M\gamma^S_{Ag^+}$ (S = AN, DMF, and DMSO) between Parker[7] and Benoit[48] is attributed to instability[7] of the ferricinium ion in methanol (and probably in other solvents; Benoit used the conventional potentiometric method). The constant difference of −2.3 ± 0.1 units between these values obtained on the basis of the two assumptions supports our contention that our recommended values of $p^M\gamma^S_{ion}$ (tetraphenylborate assumption (Table IV)) and $p^W\gamma^S_{ion}$ (Table V) are reliable within about ±0.15 unit.

Demange-Guérin[46] and Courtot[47] compare their values of $p^W\gamma^{DMF}_{H^+} = -4.9$ and $p^W\gamma^{DMSO}_{H^+} = -5.7$ (ferrocene assumption, $\mu = 0$) with values obtained on the basis of the Hammett acidity function of −1.4 and −1.6, respectively. Our values of −2.5 and −3.3, respectively, from the tetraphenylborate assumption are closer to those based on the Hammett function. The agreement is even closer if we base the Hammett acidity function on $\Delta pK^d_{IH^+}$, I being dimethylaminoazobenzene. This would yield $p^W\gamma^{DMSO}_{H^+} = -2.6$.[21] For $p^W\gamma^{AN}_{H^+}$ we find +8.1 (tetraphenylborate assumption) and 6.8 ($\Delta pK^d_{IH^+}$), respectively. Agreement does not indicate that one assumption is closer to the truth than another.

Since the values of $p^W\gamma^S_{ion}$ (S = AN, DMF, and DMSO) based on the tetraphenylborate and ferrocene assumptions, respectively, differ by 2.4 and those of $p^M\gamma^S_{ion}$ (S = AN, DMF, and DMSO) by −1.3 ± 0.2 unit, $p^M\gamma^{DMSO}_{H^+} = -5.2$ (Table IV) would become −6.5 on the basis of the ferrocene assumption. Ritchie[49] found an average difference in pK^d_{HC} of carban acids (HC) between M and DMSO of 5.8. As Ritchie[49] and Streitwieser, *et al.*,[50] state, specific solvent effects and hydrogen bonding of carbanions are minimized as a result of extensive charge delocalization in these highly conjugated ions. Assuming that $^M\gamma^{DMSO}_{HC} = {}^M\gamma^{DMSO}_{C^-}$, we arrive from Ritchie's work at $p^M\gamma^{DMSO}_{H^+} = -5.8$, which is virtually the same as Courtot's value of $p^W\gamma^{DMSO}_{H^+} = -5.7$. This would mean that $p^M\gamma^W_{H^+} \sim 0$, while all chemical evidence indicates that water is a stronger base than methanol with respect to the proton. We agree with Parker, *et al.*,[7] that the tetraphenylborate assumption with reference to water would appear to yield γ values closer to the true value than the ferrocene assumption does. It is of interest to note that Parker's[7] data of $p\gamma_{Ag^+}$ based upon the negligible liquid junction potential assumption are in good agreement with our recommended values (Table IV), except for $p^M\gamma^W_{Ag^+}$.

Popovych[2] has presented a clear discussion of the calculation of values from the simple Born equation (eq 8) and its modifications

$$\Delta G^\circ = \frac{z^2e^2}{2r}\left(1 - \frac{1}{\epsilon}\right) \qquad (8)$$

in which ΔG° is the difference between the electrostatic free energy required to impart charge of ze to an ion (sphere) of radius r *in vacuo* and in a solvent of dielectric constant ϵ. Equation 8 and its modifications consider only electrostatic effects and ignore nonelectrical effects and thus fail to explain, for example, the large difference in γ_i between the two isodielectric solvents AN and DMF. A similar conclusion was arrived at by Choix and Benoit[51] from a comparison of the difference in enthalpy in solvation of ions ΔH_t between the solvents studied and the values of ΔH_t calculated on the basis of the Born equation. There is an indication that the simple Born equation might yield semiquantitative values of $p^{S_1}\gamma^{S_2}_i$ between two solvents like water and methanol, with similar dipole moment and acid–base properties. Using ionic crystal radii (r_c) we find for $^W\gamma^M_i$ ($\epsilon_W = 78.3$, $\epsilon_M = 32.7$): $p^W\gamma^M_{K^+} = 1.6$ (1.5), $p^W\gamma^M_{Na^+} = 1.5$ (0.7), the values between parentheses being recommended values in Table IV. For $p^W\gamma^M_{Cl^-,ClO_4^-,NO_3^-}$ the values are 1.2 (2.2), 1.1 (1.1) and 1.2 (2.2) respectively; admittedly the fair agreement between the calculated and recommended values is fortuitous. The agreement between calculated (eq 8) and recommended values of $p^M\gamma^{AN,DMF,DMSO}_{A^-}$ is poor. For anions with a localized charge (*e.g.*, chloride, carboxylate) the hydrogen bond donating effect in M overshadows by far the simple electrostatic effect in eq 8 or its modifications, as compared in AN, DMF, and DMSO. Considering the solvation of anions it is most interesting to note that $p^W\gamma^{M,AN}_{Pi^-} = -0.8$ and −0.5, respectively, and $p^W\gamma^{DMF}_{Pi^-} = 0.7$. Hence the free energy of solvation of the picrate ion with its delocalized charge is of the same order of magnitude in these solvents, a conclusion which is not affected by the assumption upon which γ_i is based. The small effect of the nature of solvent on $p\gamma_{Pi^-}$ is attributed to dispersion forces[52] which also account for the very small value of the homoconjugation constant $K^f_{H(Pi)_2^-}$ in AN.[20] Also, the solvation of the perchlorate ion appears to be of the same order of magnitude in W, M, and AN. Because of the large solubility of all perchlorates in DMF and DMSO, $p^M\gamma^{DMF,DMSO}_{ClO_4^-}$ could not be determined by the solubility method. As has been emphasized by Parker, we find for the halide and other anions with a localized charge in Table IV that the hydrogen bonding in the amphiprotic solvents W and M makes their solvation much greater in these

(48) R. Benoit, *Inorg. Nucl. Chem. Lett.*, **4**, 723 (1968).

(49) C. D. Ritchie, *J. Amer. Chem. Soc.*, **91**, 6749 (1969).

(50) A. Streitwieser, Jr., W. Hollyhead, A. Pudjaatmaka, P. H. Owens, T. Kruger, P. Rubenstein, R. MacQuarrie, M. Brokan, W. Chu, and H. Kiemeyer, *ibid.*, **93**, 5088 (1971).

(51) O. Choix and R. L. Benoit, *ibid.*, **91**, 6221 (1969).

(52) E. Grunwald E. Price, *ibid.*, **86**, 4517 (1964).

solvents than in the aprotic solvents AN, DMF, and DMSO. The free energy of solvation of halides CNS^- and N_3^- is of the same order of magnitude in AN and DMF, but is somewhat greater in DMSO, $p^{DMF}\gamma^{DMSO}_{Cl^-,Br^-,I^-,N_3^-,CNS^-}$ being of the order of -1.5. As compared to chloride, the order of solvation of these anions is $Cl^- < Br^- \sim N_3^- < I^- \sim CNS^-$. Since the positive parts of the dipoles in AN, DMF, and DMSO are shielded, as inferred from the mobilities of these ions in these solvents,[29] the difference in solvation of these anions must be attributed to the effect of the nonelectric part of the molecules. Benzoate and acetate ions have $p^M\gamma^{AN}_i$ values similar to that of chloride, but are somewhat more solvated in DMF and DMSO than in AN. Undoubtedly this difference is due in part to a nonelectric effect, which is the subject of further study.

In the evaluation of the entropy of transfer ion single ions, $\Delta\Delta S_t$, between M and DMSO use was made of the calorimetrically determined single-ion enthalpies of transfer, $\Delta\Delta H_t$, of halide ions[53] in conjunction with the corresponding free energy of transfer, $2.303RT\ p^M\gamma^{DMSO}_i$ (Table IV). The $\Delta\Delta H_t$ values are based on the $\Delta\Delta H_t(Bu_4N^+) = \Delta\Delta H_t(BBu_4^-)$ assumption which may yield slightly different values of $\Delta\Delta H_t$ from that based on the tetraphenylborate assumption with which the $\Delta\Delta G_t$ values in Table IV are found. Considering that the differences $\Delta\Delta H_t - \Delta\Delta G_t$ are small as compared to $\Delta\Delta H_t$ there is an uncertainty involved in the values of $(\Delta\Delta H_t - \Delta\Delta G_t)/T = \Delta\Delta S_t$. These values are $(6.6 - 6.2)10^3/298 = +1.2$ (-2.4); $(2.3 - 3.4)10^3/298 = -3.7$ (-10.4) and $(-1.2 - 0.54)10^3/298 = -5.9$ (-12.7) eu for chloride, bromide and iodide, respectively. Values in parentheses are from $\Delta\Delta G_t$ data of Parker.[6] With our $\Delta\Delta G_t$ data it appears that $\Delta\Delta S_t$ becomes more negative going from Cl^- to I^-, indicating that the small Cl^- ion exhibits a greater structure-making tendency in M than I^-, the solvation of these ions being slight in DMSO.

In conclusion, it should be emphasized that Grunwald, *et al.*,[4] have presented strong evidence that the tetraphenylborate assumption yields values of γ_i which must be close to the true values. Based on an idealized model of a large ion in which a central charge is surrounded by a sizeable insulating layer, the reasonable assumption that

$$\frac{d(F_{PPh_4^+} + F_{BPh_4^-})}{dZ} = \frac{2dF_{CPh_4}}{dZ} - \frac{Ne^2d/n\epsilon}{2b\epsilon dZ_i}$$

was supported by experimental evidence in 50 wt % dioxane–water mixture (dielectric constant 35.85), where F is the standard partial molar free energy on the mole-fractional scale, Z is the mole fraction of water, and the other symbols have the usual significance.

From proton magnetic resonance studies Coetzee, *et al.*,[54] concluded that varying extent of solvation of $AsPh_4^+$, PPh_4^+, and BPh_4^- occurs in water and to a lesser degree in several aprotic organic solvents. Popovych, *et al.*,[11] also obtained experimental evidence that there is a small difference in $p\gamma$ of triisoamyl-*n*-butylammonium and tetraphenylarsonium ion in water with reference to methanol and acetonitrile.

Acknowledgment. We thank the National Science Foundation for a grant (GP-20605) in support of this work.

(53) R. Fuchs, J. L. Bear, and R. F. Rodewald, *J. Amer. Chem. Soc.*, 91, 5797 (1969).

(54) J. F. Coetzee, J. M. Simon, and R. J. Bertozzi, *Anal. Chem.*, 41, 766 (1969); J. F. Coetzee and W. R. Sharpe, *J. Phys. Chem.*, 75, 3141 (1971).

High Molecular Weight Boron Sulfides. VIII. Vapor Pressures of $B_2S_3(g)$ and $B_4S_6(g)$ over Stoichiometric B_2S_3[1]

by Horng-yih Chen and Paul W. Gilles*

Department of Chemistry, University of Kansas, Lawrence, Kansas 66044 *(Received October 29, 1971)*

Publication costs assisted by the U. S. Atomic Energy Commission

A mass spectrometric study on the congruent vaporization of B_2S_3, with zinc used as a pressure calibrant, resulted in the following vapor pressure equations for $B_2S_3(g)$ and $B_4S_6(g)$. Over solid B_2S_3 (722–840°K): $\log P(\text{atm}, B_2S_3) = -(12.04 \pm 0.13) \times 10^3/T + (10.26 \pm 0.17)$; $\log P(\text{atm}, B_4S_6) = -(13.52 \pm 0.27) \times 10^3/T + (10.62 \pm 0.34)$. Over liquid B_2S_3 (840–939°K): $\log P(\text{atm}, B_2S_3) = -(9.51 \pm 0.37) \times 10^3/T + (7.28 \pm 0.42)$; $\log P(\text{atm}, B_4S_6) = -(9.21 \pm 0.41) \times 10^3/T + (5.44 \pm 0.45)$. The absolute uncertainties in the pressures are much larger than given by these standard deviations because of uncertainties in ionization cross sections. Enthalpies and entropies of vaporization are readily calculated from these equations. The melting point was established as 567 ± 10°, and the enthalpy and entropy of fusion per mole of B_2S_3 as 11.6 ± 1.8 kcal and 13.7 ± 2.1 cal/deg. For the dimerization of B_2S_3, $\Delta H°$(dimerization) = −47.8 ± 1.6 kcal/mol of dimer, and $\Delta S°$(dimerization) = −44.6 ± 2.0 cal/deg mol of dimer. The value of the heat of dimerization suggests that the polymerization proceeds by the formation of a four-membered ring from two B=S units in two B_2S_3 molecules. The remarkable difference in the vaporization behavior of B_2S_3 and B_2O_3 is explained by the absence of the interaction of the boron atom with a fourth sulfur atom in $B_2S_3(s)$.

Introduction

The vapor species and the vaporization behavior of the boron–sulfur system have been studied by groups of investigators. The results of these studies have been reviewed in the authors' previous report.[2] Because of the complexity of the vapor, very few thermodynamic data are available for the vaporization properties of this system. The enthalpy of vaporization of $B_2S_3(g)$ from the decomposition product of $(HBS_2)_3$ has been reported as 35.9 kcal/mol from spectroscopic studies by Greene.[3] The same value was obtained mass spectrometrically by Greene and Gilles[4] for a sample of similar nature. A recent work on the thermal dissociation of $B_2S_3(g)$ at temperatures above 700° was reported by Grinberg, Zhukov, and Koryazhkin.[5] In this report, the sample was obtained by vapor deposition at 550–600° from the product of a direct combination of elementary sulfur and amorphous boron; the experiments were carried out by direct pressure measurement; and a surprisingly high B_2S_3 vapor pressure, >20 mm at 350°, was implied.

Chen and Gilles[2] concluded that the vaporization behavior of a boron sulfide sample depends strongly on the activity of sulfur in the sample: a sample more sulfur-rich than B_2S_3 vaporizes incongruently into $(BS_2)_n(g)$ and $(B_2S_3)_n(g)$; but stoichiometric B_2S_3 vaporizes congruently to give $B_2S_3(g)$ and its polymers. The present work was undertaken to measure the thermodynamic properties of the congruent vaporization of B_2S_3.

The present study was carried out mass spectrometrically with crystalline B_2S_3 and with a mixture of iron sulfide and amorphous boron. As demonstrated previously,[2] these two systems are equivalent as far as the vaporization of B_2S_3 was concerned. With some metallic zinc added for the calibration of the pressure scale, the vapor pressures of $B_2S_3(g)$ and $B_4S_6(g)$ were measured in the temperature range of 722–939°K. The corresponding heats and entropies were calculated according to the second law of thermodynamics. Also obtained were the heat and entropy of dimerization of $B_2S_3(g)$. Changes of second-law slopes were observed at 840°K and were concluded to be associated with the fusion of the sample. Accordingly, the melting point, the heat, and the entropy of fusion were established and are reported.

Experimental Section

Apparatus and Samples. The study was carried out with a single-focusing, 60°, 12-in. sector magnetic mass spectrometer. The instrument and its operation, the devices for temperature control and measurement, and the design of the graphite Knudsen crucible with a 0.25-in. cylindrical orifice were essentially the same as those described by Edwards, Wiedemeier, and Gilles.[6]

(1) Abstracted in part from the Ph.D. Thesis of H. Chen, submitted to University of Kansas, 1969.

(2) H. Chen and P. W. Gilles, *J. Amer. Chem. Soc.*, **92**, 2309 (1970).

(3) F. T. Greene, "The Spectra and Thermodynamics of Some Boron Sulfides and Oxides," Ph.D. Thesis, University of Wisconsin, 1961.

(4) F. T. Greene and P. W. Gilles, *J. Amer. Chem. Soc.*, **86**, 3964 (1964).

(5) J. Kh. Grinberg, E. G. Zhukov, and A. Koryazhkin, *Dokl. Akad. Nauk SSSR*, **184**, 847 (1969).

(6) J. G. Edwards, H. Wiedemeier, and P. W. Gilles, *J. Amer. Chem. Soc.*, **88**, 2935 (1966).

The samples have been previously described.[2] For experiment MS-7, which covered a temperature range of 708–913°K, 0.569 g of FeS and amorphous boron mixture in 3:8 mole ratio were used; for MS-8, about 0.7 g of crystalline B_2S_3 was studied in a temperature range of 713–857°K. The crystalline B_2S_3 did not melt when heated at 520° in a sealed Pyrex tube. Chemical analyses of a portion of the sample, slightly contaminated with graphite, gave the following results: 18.12 ± 0.06 and 80.89 ± 0.24 wt % for boron and sulfur, respectively, corresponding to an atomic ratio S/B = 1.506 ± 0.006.

Procedure. In each experiment, a small amount of metallic zinc of 99.8% purity was added for pressure calibration. In MS-7, intensity data for B–S binary ions were measured after B_2S_3 and ZnS had formed. In MS-8, 8.44 mg of zinc was vaporized to exhaustion in a temperature range of 499–650°K. After the conclusion of the zinc vaporization, indicated by the absence of the mass spectrum of zinc ions, the temperature of the crucible was then raised for the study of B–S systems. The temperature was varied randomly during the measurements. At each temperature, the intensities of all the B–S binary ions not heavier than $B_4S_6^+$ were measured. The signals for the heavier ions were too weak to produce good temperature dependencies. All the intensity data were for 70-eV electrons and had positive shutter effects. For some intense ion peaks, electron multiplier gains were also determined from the ratios of the outputs of the multiplier to the corresponding input currents.

Orifice Parameters. The thickness of the lid of the crucible was measured with a micrometer as 6.22 ± 0.05 mm and was taken as the length of the orifice. A precise measurement of the diameter with a microscope gave a value of 0.402 ± 0.004 mm, corresponding to an area of 0.127 ± 0.002 mm². The ratio of the length to the radius of the orifice was about 32. By interpolation from the values calculated by Freemen and Edwards,[7] the transmission coefficient of the orifice was taken to be 0.076 with better than 2% accuracy.

Ionization Cross Section. The values of ionization cross sections needed for a pressure calculation were obtained from Mann's tabulation.[8] With the values of 2.11 and 4.10 × 10^{-16} cm², respectively, for boron and sulfur atoms and the assumption of additivity, the ionization cross sections 16.52 and 33.40 × 10^{-16} cm² were obtained for B_2S_3 and B_4S_6, respectively. The value for zinc is 3.17 × 10^{-16} cm².

Results

Vapor Pressure of $B_2S_3(g)$ and $B_4S_6(g)$. From the ion intensity data, the vapor pressure P of a given species at temperature T can be calculated according to the equation

$$P = C(I_x^+/f_x\sigma)T \qquad (1)$$

where σ is the ionization cross section of the species; I_x^+ and f_x are, respectively, the ion current and the isotopic abundance of a given isotopic combination; and C is a constant assumed independent of vapor species. For the intensity data from MS-8, the value for the constant C was obtained from the calibration with zinc. For those from MS-7, where a total vaporization of zinc did not take place, the calibration was made from the data in MS-8. In the pressure calculation according to eq 1, the total ionization cross sections were used. This procedure required the inclusion in I_X^+ of the intensities of all the fragment ions arising from a particular species. The ion intensities of B^+, S^+, BS^+, BS_2^+, and $B_2S_2^+$ relative to $B_2S_3^+$ were measured as 0.026, 0.012, 0.023, 0.116, and 0.038. These ions were fragment ions from $B_2S_3^+$, because under the present experimental conditions $B_4S_6(g)$ is much less abundant than $B_2S_3(g)$. Addition of these intensities to that of $B_2S_3^+$ gives a factor of 1.22 to be applied to the measured intensity of $B_2S_3^+$. The ion intensities of BS_3^+, $B_3S_3^+$, $B_2S_4^+$, and $B_3S_4^+$ relative to $B_4S_6^+$ were 0.069 , 0.121, 0.049, and 0.990. A value of 0.30 is estimated to be the extent of fragmentation of $B_4S_6^+$ into $B_2S_3^+$ or smaller ions. Addition of these intensities to that of $B_4S_6^+$ gives a factor of 2.53 to be applied to the measured intensity of $B_4S_6^+$. The uncertainty in these two values of 1.22 and 2.53 is estimated to be about 10%. The weak ion BS_3^+ is assumed to be a fragment, but its intensity is so low that the identity of its parent is of no consequence.

The vapor pressures thus obtained have been tabulated[1] for $B_2S_3(g)$ and $B_4S_6(g)$, and their logarithms are plotted against $1/T$ as shown in Figure 1. The pressures have random uncertainties estimated to be about 8%; absolute uncertainties are much larger because of cross section uncertainties.

An attempt was made to fit these data to equations of three parameters, but the standard deviations were unsatisfactorily large for all the parameters. Instead, two equations of the usual form

$$\log P(\text{atm}) = -10^3A/T + B \qquad (2)$$

were used to represent the vapor pressure data for $B_2S_3(g)$ and another two were used for $B_4S_6(g)$. For both gases, the intersections of the lines fell in the vicinity of 840°K. These breaks were concluded to be associated with melting of the sample. Accordingly, the vapor pressure equations could be separated into those for solid and for liquid samples. The coefficients and their standard deviations are shown in Table I for $B_2S_3(g)$ and $B_4S_6(g)$ as obtained from the least-squares fit.

(7) R. D. Freeman and J. G. Edwards in "The Characterization of High-Temperature Vapors," J. L. Margrave, Ed., Wiley, New York, N. Y., 1967, p 508.

(8) J. B. Mann, *J. Chem. Phys.*, **48**, 1646 (1967).

Table I: Vapor Pressure Equations and $\Delta H°$ and $\Delta S°$ for the Vaporization of Stoichiometric B_2S_3 into $B_2S_3(g)$ and $B_4S_6(g)$. Log P(atm) = $-10^3A/T + B$

Gas	No. of points	A	B	Temp range, °K	$\Delta H°$, kcal/mol	$\Delta S°$, cal/deg mol
B_2S_3	55	12.04 ± 0.13	10.26 ± 0.17	659.6–839.5	55.10 ± 0.60	46.97 ± 0.78
B_4S_6	31	13.52 ± 0.27	10.62 ± 0.34	722.4–835.1	61.9 ± 1.2	48.6 ± 1.6
B_2S_3	27	9.51 ± 0.37	7.28 ± 0.42	841.8–937.7	43.5 ± 1.7	33.3 ± 1.9
B_4S_6	13	9.21 ± 0.41	5.44 ± 0.45	847.6–938.5	42.1 ± 1.9	24.9 ± 2.1

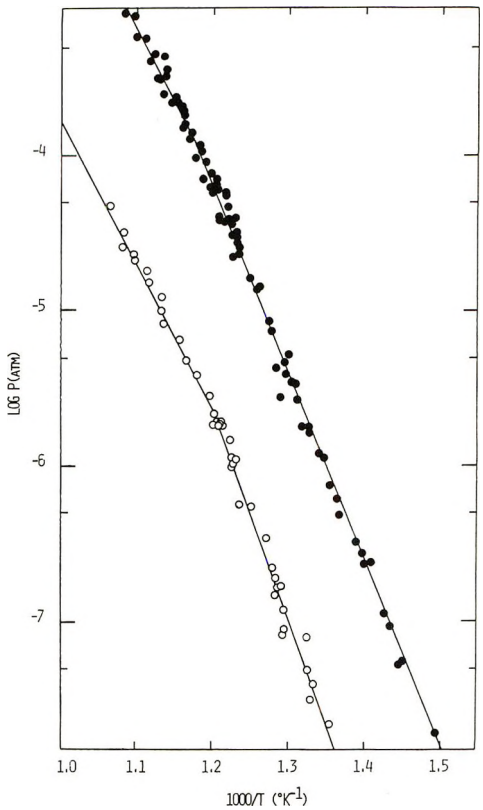

Figure 1. Pressures of $B_4S_6(g)$ (○) and B_2S_3 (g) (●) over B_2S_3.

Thermodynamics of Vaporization. From these coefficients, the enthalpies and the entropies at the temperature of the experiments were calculated and are given in Table I. The uncertainties of the thermodynamic quantities were calculated similarly from the standard deviations of these coefficients. The complexity of the species and the absence of thermal data for solid and liquid precluded a third-law treatment.

Fusion. As previously mentioned, the breaks in the plot of log P *vs.* $1/T$ in Figure 1 indicate fusion. The enthalpy and entropy of fusion obtained from the B_4S_6 equations, 19.7 ± 2.2 and 23.7 ± 2.6, are about twice those obtained from the B_2S_3 equations, 11.6 ± 1.8 and 13.7 ± 2.1, which are taken as more reliable, and this agreement between observed and anticipated doubling renders strong support for the conclusion regarding fusion. Moreover, the present study revealed that the crystalline B_2S_3 did not melt at 520° while Chopin and Hagemuller[9] reported a melting point around 600°. Fusion of the sample was then concluded to be responsible for such breaks. Accordingly, the melting point, 567 ± 10°, of the stoichiometric B_2S_3 was established from the intersections of the two lines. The uncertainty in the melting point was estimated from the difference of the two values obtained from $B_2S_3(g)$ and $B_4S_6(g)$ data, 847 and 833°K, respectively.

Dimerization. The equilibrium constant K of the dimerization process

$$2B_2S_3(g) = B_4S_6(g) \quad (3)$$

can be readily obtained from the vapor pressures of $B_2S_3(g)$ and $B_4S_6(g)$ since

$$K = P_{B4S6}/P^2_{B2S3} \quad (4)$$

From the equations in Table I, the following equations were obtained: log K = (10.56 ± 0.37) × $10^3/T$ − 9.91 ± 0.47, from the solid, and log K = (9.82 ± 0.83 × $10^3/T$ − 9.13 ± 0.95, from the liquid. Average weighted values from the equations are $\Delta H°$ = −47.8 ± 1.6 kcal and $\Delta S°$ = −44.6 ± 2.0 cal/deg mol of the dimer.

Discussion

The heat of vaporization of $B_2S_3(g)$ from the liquid in this study is about 8 kcal/mol higher than the admittedly approximate value reported by Greene, *et al.*,[3,4] even though the temperature in the present experiments was about 150° higher. A B_2S_3 sample prepared from thermal decomposition of thiometaboric acid, $(HBS_2)_3$ such as those used by the previous workers, is amorphous, contains excess sulfur, and vaporizes with a continually changing composition. In comparison with a sulfur-rich sample, a B_2S_3 sample of little or no excess sulfur has a smaller total volatility. The effects of excess sulfur in a B_2S_3 sample have been clearly shown,[2] and they can be explained as a weakening of the binding force by the formation of an S–S bond, which is about 35 kcal/mol weaker than a B–S bond. The very high vapor pressure implied by the work of Grinberg, *et al.*,[5] cannot be explained, unless elemental sulfur vapor was responsible.

(9) F. Chopin and P. Hagenmuller, *C. R. Acad. Sci. Paris*, **255**, 2259 (1962).

The entropy of vaporization for $B_4S_6(g)$ from the liquid is 24.9 cal/deg mol. This value, after correction to the value for the boiling point of B_2S_3, is close to, or slightly smaller than, the Troutou's law value, 22 cal/deg mol, predicted for the entropy of vaporization of a normal liquid at its boiling point. The molten B_2S_3 is therefore best described as a normal liquid of B_4S_6, with a little higher degree of disorder, *i.e.*, some monomer B_2S_3 is present also. Since the liquid is essentially dimer, a high entropy of vaporization to form $B_2S_3(g)$ is expected. The value, 33.3 cal/deg mol, seems in accord with this explanation.

The heat of dimerization of $B_2S_3(g)$, -47.8 kcal/mol, and the heat of dimerization of $HBS_2(g)$ may be compared. The latter has not been reported, but from Greene's result[3] for the heats of reactions for the formation of $HBS_2(g)$ and its dimer, $(HBS_2)_2(g)$, from boron and $H_2S(g)$ at 808°K, the heat of dimerization for $HBS_2(g)$ at this temperature is obtained as -56.2 kcal. The uncertainty of this value could not be obtained but should be at least several kilocalories because of the small number and relatively wide scatter of Greene's data. This value is close to the heat of dimerization of gaseous B_2S_3.

The structure of the gaseous B_2S_3 molecule has been studied by Greene[3] and by Sommer,[10] and both suggested a structure with two B=S units bridged with a sulfur atom. The structure of the dimer, $B_4S_6(g)$, has not been reported. Several possible structures all with boron and sulfur atoms in their respective ordinary valence states can be suggested. The similarity of the heats of dimerization of $HBS_2(g)$ and $B_2S_3(g)$ seems to suggest that both $(HBS_2)_2$ and B_4S_6 are formed in a structurally similar way, *i.e.*, the formation of a four-membered ring at the expense of two B=S units, one from each of the two monomers.

The differences between B_2S_3 and B_2O_3 are striking. They probably have drastically different crystal structures; B_2S_3 melts at 567°, and B_2O_3 at about 455–475°, according to Mackenzie and Claussen;[11] yet the vapor pressure of B_2S_3 at 700°K is about the same as that of B_2O_3 at 1300°K. Fajans and Barber[12] attempted to explain the low melting point and yet low volatility by suggesting a molecular entity of B_4O_6 in the crystalline state and accepting a three-dimensional network of B_2O_3 in the liquid. This explanation was, however, not supported by the experimental evidences by Berger[13] and by Kline, Bray, and Kriz.[14]

We propose here a major difference in the melting processes of B_2S_3 and B_2O_3. In crystalline B_2O_3 the interaction of the boron atom with a fourth oxygen is so strong that the crystal is built up with intertwined spiral network with BO_4 units. When the crystal melts, the process involves only the disordering of the three-dimensional network so that $B_2O_3(l)$ retains much of the three-dimensional structure. Therefore, $B_2O_3(l)$ does not gain the entire freedom associated with normal fusion as evidenced from the low entropy of fusion, 7.3 cal/deg mol. On the other hand, B_2S_3 is proposed to be built up with B_2S_3 units in long chains without interaction between a boron atom and a fourth sulfur atom. The boron atom in the BS_3 unit is very well shielded by the three surrounding sulfur atoms. During melting, the polymeric chains of B_2S_3 break down into smaller fragments, mainly B_4S_6, with a much higher entropy of fusion, 13.7 cal/deg mol of B_2S_3.

Acknowledgments. The authors are pleased to acknowledge the support of the U. S. Atomic Energy Commission under Contract AT(11-1)-1140 with the University of Kansas.

(10) A. Sommer, "Thermodynamics and Spectroscopic Studies of the Vapor Species of the Boron-Oxygen and Boron-Sulfur Systems," Ph.D. Thesis, Ohio State University, 1962.

(11) J. D. Mackenzie and W. F. Claussen, *J. Amer. Ceram. Soc.*, **44**, 79 (1961).

(12) K. Fajans and S. W. Barber, *J. Amer. Chem. Soc.*, **74**, 2761 (1952).

(13) S. V. Berger, *Acta Chem. Scand.*, **7**, 611 (1963).

(14) D. Kline, P. J. Bray, and M. M. Kriz, *J. Chem. Phys.*, **48**, 5277 (1968).

Association of Trifluoroacetic Acid in Vapor and in Organic Solvents

by Sherril D. Christian* and Thomas L. Stevens

University of Oklahoma, Norman, Oklahoma 73069 *(Received September 13, 1971)*

Publication costs borne completely by The Journal of Physical Chemistry

Thermodynamic and infrared spectral results are reported for the monomer and dimer of trifluoroacetic acid (TFA) in vapor and in the solvents cyclohexane, carbon tetrachloride, benzene, and 1,2-dichloroethane. The more reactive solvents interact strongly with the TFA monomer, greatly reducing the energy and free energy of this species with respect to vapor and decreasing the carbonyl- and hydroxyl-stretching frequencies. The dimer, which is thought to be cyclic, is considerably less affected by change of medium; it is less than half as effectively solvated as two separated monomer molecules. A new spectral-partition method is introduced which can be used to study association equilibria in media which are opaque to radiation in spectral regions of interest.

There have been numerous investigations of the association of trifluoroacetic acid (TFA)[1-4] and other fluorinated carboxylic acids.[3,5,6] Most investigators have concluded that TFA associates primarily to the cyclic dimer, at least in the vapor phase and as a solute in nonpolar solvents.[4] However, infrared spectral results for solutions of the perfluorinated aliphatic acids in slightly basic solvents have been interpreted as evidence for the existence of linear dimers and/or higher polymers.[5,7]

Recently, Kirszenbaum, *et al.*,[4] have reexamined the infrared spectra of TFA in various nonpolar and slightly polar solvents. Their spectra (in the ν(OH) and ν(C=O) vibration regions) show no effects which are inconsistent with an assumed monomer–cyclic dimer equilibrium. Although the carbonyl- and hydroxyl-stretching vibrations of the TFA monomer shift progressively toward lower frequencies in the more reactive media, the dimer carbonyl-stretching frequency appears to be practically independent of the solvent.

This paper summarizes spectral and thermodynamic constants obtained for TFA in a range of media and includes a discussion of the effects of nonpolar and slightly polar solvents on physical properties of the TFA monomer and dimer. Spectral results from this laboratory for TFA in vapor, CCl_4, benzene, and 1,2-dichloroethane (DCE) are in essential agreement with those reported by Kirszenbaum, *et al.*[4] Our thermodynamic results provide additional evidence that the more reactive solvents interact strongly with the TFA monomer. However, the observed medium effects on values of energies, free energies, and spectral characteristics of the TFA dimer support the view that the dimer is primarily cyclic in all the media investigated.

Experimental Section

Trifluoroacetic acid (Matheson Coleman and Bell reagent grade) was distilled through a 30-plate bubble-cap column at a reflux ratio of 10:1. Only the middle portion (bp 72°, corrected to 760 Torr) was collected; it was stored in a desiccator over $CaSO_4$. Solvents were purified by distillation, where necessary, and stored over $CaSO_4$ or P_2O_5. All transfers of liquids were performed using closed all-glass systems fitted with Teflon-bore stopcocks; stock solutions of TFA in solvents were kept in vapor contact with $CaSO_4$. Great care was taken to avoid introducing water into spectral cells, either in the process of adding chemical components or during measurements. Complete details of procedures used in storing and transferring components are given in ref 3b.

Infrared spectral measurements were made using a Beckman DK-1A extended-range spectrometer (in the 3500-cm^{-1} region) and a Perkin-Elmer 12C single-beam instrument equipped with a CaF_2 prism (in the 1800-cm^{-1} region). Three types of spectral experiments, requiring different apparatus and procedures, were performed: (1) vapor spectral studies, in which TFA samples at known pressures in the range 0–60 Torr were introduced into a gas cell thermostated at 25.0 ± 0.2°; (2) conventional condensed-phase experiments, in which solutions of TFA at known concentrations in various solvents were transferred into thermostated solution cells; and (3) spectral condensed-phase–vapor-phase partition studies, requiring new techniques and apparatus. Since experiments of types

(1) N. Fuson, M. L. Josien, E. A. Jones, and J. R. Lawson, *J. Chem. Phys.*, **20**, 1627 (1952).

(2) R. E. Kagarise, *ibid.*, **27**, 519 (1957); Naval Research Laboratory Report No. 4955, Aug 8, 1958.

(3) (a) S. D. Christian, Ph.D. Dissertation, Iowa State University, Ames, Iowa, 1956; (b) T. L. Stevens, Ph.D. Dissertation, University of Oklahoma, Norman, Okla., 1968.

(4) M. Kirszenbaum, J. Corset, and M. L. Josien, *J. Phys. Chem.*, **75**, 1327 (1971), and references cited therein.

(5) T. S. S. R. Murty, *ibid.*, **75**, 1330 (1971).

(6) C. C. Costain and G. P. Srivastava, *J. Chem. Phys.*, **35**, 1903 (1961).

(7) T. S. S. R. Murty and K. S. Pitzer, *J. Phys. Chem.*, **73**, 1426 (1969).

1 and 2 resemble those commonly employed in infrared studies, the reader is referred to ref 3b for complete details. However, the spectral-partition method has several novel features which justify our describing the main features of the method here.

Partition methods have been used with success in numerous studies of the activities and association reactions of solute species.[8] In applying partition methods to studies of complex formation, it is necessary to establish equilibrium between an indicator phase (in which the component of interest is maintained at a known activity) and a second phase (the reaction phase) in which the association reaction is presumed to occur. From measurements of the concentration (or some related property) of the associating component in the reaction phase as a function of its activity in the indicator phase, thermodynamic properties of complexes can be inferred. The spectral-partition method as applied here involves measurement of the spectra of TFA in the vapor phase above the reaction phase, which in the present experiments consists of TFA dissolved in organic solvent. Initially, base-line spectra are recorded with the thermostated, evacuated 10-cm cell (Figure 1) mounted in the DK-1A spectrometer; then, TFA vapors from an external reservoir are transferred into the cell under vacuum to give a monomer absorbance (at 3589 cm^{-1}) in the required range (usually 0.2–0.7). After equilibration at 25.0 ± 0.2°, the spectra in the 3600-cm^{-1} region are recorded. Next, a sample of dry solvent is delivered quantitatively through the sintered-glass disk, using a 0.2-ml Roger Gilmont Industries microburet (No. S-1200 A). Equilibrium is reestablished after 10 or 15 min, whereupon the vapor spectra are again recorded. Successive samples are added and spectra measured at intervals of 10–15 min, until a maximum reaction phase volume of not more than 4–5 ml has been reached. (In the 10-cm cylindrical cell, at volumes less than 4 ml, the liquid level lies safely below the beam, and there is little tendency for droplets to accumulate on the cell windows. Apparently, the energy absorbed from the beam maintains a sufficient vertical temperature gradient to prevent condensation of the volatile components on the windows.) From the vapor spectrum the absorbance of the TFA monomer is obtained. Then, by utilizing results of experiments on TFA vapor at known pressures (*vide infra*) it is possible to infer the total molar amount of TFA in the vapor phase. The concentration of TFA in the condensed phase can be calculated from knowledge of the total amount of TFA in the cell, the volume of the cell, the volume of solvent added, and the vapor pressure of the solvent at 25.0°. Slight corrections are made for the reduction in vapor pressure of the solvent caused by the dissolved TFA.

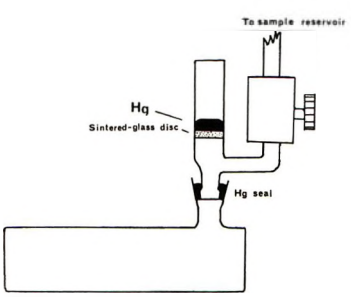

Figure 1. Spectral-partition cell.

Calculations and Results

(*1*) *Vapor-Phase Results.* Measurements were made of the absorbance A of TFA vapor samples at measured total pressures P in a 10.0-cm cell at 25.0°. Assuming the presence of only TFA monomers and dimers, individually obeying the ideal gas law, the total pressure may be expressed as

$$P = P_M + P_D = P_M + K_2 P_M^2 \quad (1)$$

where P_M and P_D are the monomer and dimer partial pressures and K_2 is the association constant for dimerization in reciprocal pressure units. If the absorbance at 3589 cm^{-1} is attributable solely to the monomer, which is assumed to obey Beer's law, P_M may be replaced by $A_M RT/\epsilon_M b$, where A_M is the peak absorbance of the monomer band, ϵ_M is the absorptivity of the monomer, and b is the path length of the cell. Thus, eq 1 becomes

$$P = \frac{A_M RT}{\epsilon_M b} + K_2 \left(\frac{A_M RT}{\epsilon_M b}\right)^2 \quad (2a)$$

or

$$\frac{P}{A_M} = \frac{RT}{\epsilon_M b} + \frac{K_2 (RT)^2}{\epsilon_M^2 b^2} A_M \quad (2b)$$

Figure 2 displays absorbance measurements at 3589 cm^{-1} plotted as P/A_M *vs.* A_M; from least-squares

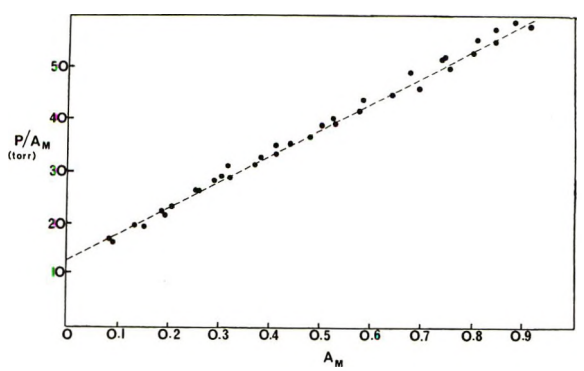

Figure 2. Vapor-phase spectral results for trifluoroacetic acid at 25.0°. Absorbance measured at 3589 cm^{-1}, using a 10-cm cell.

(8) S. D. Christian, A. A. Taha, and B. W. Gash, *Quart. Rev., Chem. Soc.*, **24**, 1 (1970).

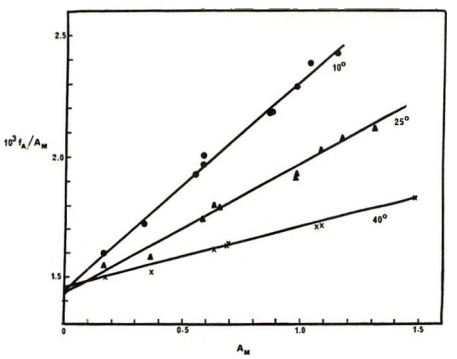

Figure 3. Spectral results for dilute solutions of trifluoroacetic acid in carbon tetrachloride. Absorbance measured in a 5-cm cell at 3508 cm^{-1}; formal concentration in molar units.

analysis of these data in the form of eq 2, it is possible to calculate ϵ_M and K_2. The dashed line in Figure 2 corresponds to the least-squares values $\epsilon_M = 143 \pm 5$ cm^{-1} l. mol^{-1} and $K_2 = 0.30 \pm 0.02$ $Torr^{-1}$ or 5660 $\pm$ 370 l. mol^{-1}. Previously, Ling, *et al.*,[9] reported the value $K_2 = 0.30$ $Torr^{-1}$ for TFA vapor at 25°, based on vapor density and infrared spectral measurements.

(2) *Dilute Solution Measurements for TFA in CCl_4—Hydroxyl-Stretching Region.* In the condensed phase, if it is assumed that the monomer and dimer individually obey Henry's law, the total or formal concentration of dissolved TFA may be expressed as

$$f_A = C_M + 2K_2C_M^2 \tag{3}$$

where C_M is the monomer concentration and K_2 is the dimerization constant in reciprocal concentration units. The band attributed to monomeric TFA in CCl_4 is at 3508 cm^{-1}; assuming that the absorbance at this frequency is linear in monomer concentration, one may write

$$\frac{f_A}{A_M} = \frac{1}{\epsilon_M b} + \frac{2K_2}{(\epsilon_M b)^2} A_M \tag{4}$$

Figure 3 includes data for TFA in CCl_4 at three temperatures, plotted in the form f_A/A_M *vs.* A_M. Least-squares analysis of the data, using eq 4, yields the values of the constants shown in Table I. From the temperature dependence of the K_2 values, the enthalpy change for the dimerization reaction is calculated to be -9.0 ± 0.4 kcal/mol, in good agreement with that reported by Kagarise (-8.85 kcal/mol).[2]

Table I: Dimerization Constants and Monomer Absorptivities

T, °K	K_2, l. mol^{-1}	ϵ_M, cm^{-1} l. mol^{-1}
288	205 ± 8	138 ± 2
298	128 ± 7	139 ± 2
313	58 ± 4	137 ± 2

(3) *Spectral-Partition Results.* In the spectral-partition studies, data are reduced to sets of values of the monomer absorbance in the vapor phase, A_M, and the formal concentration of TFA in the condensed phase, f_A. Since the TFA monomer in solution is assumed to obey Henry's law, its concentration may be equated to $A_M RT/(\epsilon_M K_H b)$, where K_H is the Henry's law constant for the monomer in units of pressure/concentration. Then, the formal pressure equation may be written

$$f_A = \frac{A_M RT}{\epsilon_M K_H b} + 2K_2\left(\frac{A_M RT}{\epsilon_M K_H b}\right)^2 \tag{5a}$$

or

$$f_A/A_M = \frac{RT}{\epsilon_M K_H b} + 2K_2\left(\frac{RT}{\epsilon_M K_H b}\right)^2 A_M \tag{5b}$$

where A_M and ϵ_M are properties of TFA in vapor, and f_A and K_2 pertain to the liquid phase. Figure 4 shows spectral-partition data plotted as f_A/A_M *vs.* A_M for four TFA–solvent systems. The solid lines represent least-squares fits of data in the form of eq 5; Table II summarizes constants inferred from the spectral-partition results. In the case of the benzene solutions, significant departure from linearity is observed at the highest TFA concentrations. Therefore, for this solvent system, least-squares constants were calculated from results for solutions at molarities less than 0.21.

It should be noted that the presence of linear as well as cyclic dimers in the condensed phase would not affect the validity of the K_2 value inferred from spectral-

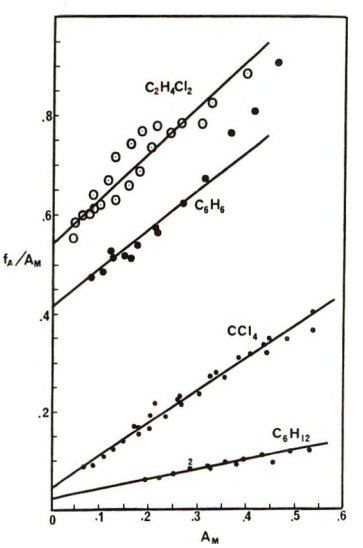

Figure 4. Spectral-partition data for trifluoroacetic acid in four solvents at 25.0°. Absorbance of vapors measured at 3589 cm^{-1} in a 10-cm cell; formal concentrations of trifluoroacetic acid in condensed phases in molar units.

(9) C. Ling, S. D. Christian, H. E. Affsprung, and R. W. Gray, *J. Chem. Soc. A*, 293 (1966); C. Ling and H. E. Affsprung, unpublished work.

Table II: Association Constants and Henry's Law Constants for Trifluoroacetic Acid (TFA) in Several Solvents at 25.0°

System	Concentration range, M	K_2, l. mol^{-1}	K_H, Torr l. mol^{-1}
TFA–cyclohexane	0.01–0.07	192 ± 36	592 ± 110
TFA–CCl_4	0.007–0.23	149 ± 19	275 ± 35
TFA–benzene	0.04–0.21	2.6 ± .9	32.5 ± 3.5
TFA–1,2-dichloroethane	0.02–0.35	1.5 ± .4	23.8 ± 4.2

partition data. The calculated K_2 would represent the sum of the association constants for the two types of dimers, whereas conventional dilute solution studies will yield correct values for K_2 only if the monomer and dimer hydroxyl-stretching bands do not overlap significantly.

(4) *Condensed-Phase Studies of the Carbonyl-Stretching Region.* Spectra in the 1800-cm^{-1} region were obtained for solutions of TFA in cyclohexane, CCl_4, and 1,2-dichloroethane, using a Beckman VLT-2 thermostated cell with AgCl windows. Path lengths used were 0.2 mm for dichloroethane and cyclohexane and 1.0 mm for CCl_4. A typical spectral curve is shown in Figure 5, where absorbance is plotted against frequency for a solution of TFA in dichloroethane at 32.8°. The peak at 1805 cm^{-1} is attributed to monomer and that at 1789 cm^{-1} is ascribed to the dimer. The individual absorbance curves for the monomer and dimer have been inferred using a nonparametric graphical method developed by Stevens for resolving overlapping-band spectra.[3b] Spectral features of the monomer and dimer bands agree generally with those reported by Kirszenbaum, *et al.*,[4] although the dimer frequency in 1,3-dichloroethane was observed at 1789 cm^{-1}, as compared with the value 1782 cm^{-1} given earlier. However, there is more overlap between the monomer and dimer bands in dichloroethane than in the other two solvents, and therefore the dimer band maximum is more difficult to locate.

Measurements of the temperature dependence of the dimer and monomer absorbance at the peak maxima of these species may be used to infer the enthalpy change

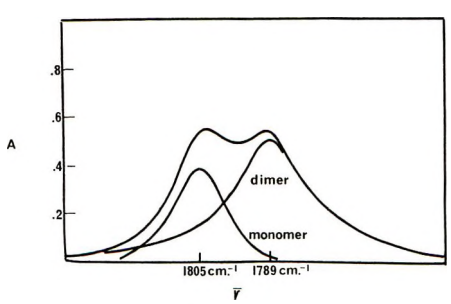

Figure 5. Spectra of the trifluoroacetic acid monomer and dimer in the carbonyl-stretching region.

for the dimerization reaction. The dimerization constant may be related to the dimer and monomer absorbances by the expression

$$K = (A_D/A_M^2)(\epsilon_M^2/\epsilon_D)b \qquad (6)$$

where ϵ_M and ϵ_D are absorptivities of monomer and dimer, respectively, and b is the cell length. Assuming that the ratio ϵ_M^2/ϵ_D is constant with changing temperature, a plot of log A_D/A_M^2 *vs.* $1/T$ should yield a straight line with slope $-\Delta H/2.303R$. Figure 6 shows plots of this type for the three solvent systems; values of ΔH obtained are -11.7 ± 0.6 kcal/mol in cyclohexane, -9.2 ± 0.4 kcal/mol in CCl_4, and -7.0 ± 0.8 kcal/mol in dichloroethane. The ΔH value for CCl_4 agrees well with that determined from the dilute solution measurements (*vide supra*) and with that reported by Kagarise.[2]

Summary of Thermodynamic Results. The spectral results described above provide the basis for deriving thermodynamic constants for the individual steps in the cycles

$$\begin{array}{ccc} 2\text{TFA in vapor} & \rightleftharpoons & (\text{TFA})_2 \text{ in vapor} \\ \downarrow\uparrow & & \downarrow\uparrow \\ 2\text{TFA in solvent} & \rightleftharpoons & (\text{TFA})_2 \text{ in solvent} \end{array}$$

for each of the four solvents investigated. Table III lists the values of Gibbs free energy (ΔG) and internal energy (ΔE) changes for the solvation and reaction steps in these cycles.

Discussion

Qualitatively, the thermodynamic results in Table III show the important influence of the solvent on the energetics of the monomer and the dimer of trifluoro-

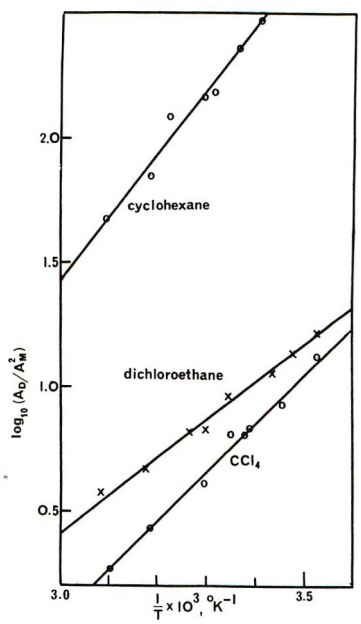

Figure 6. Absorbance ratio measurements for trifluoroacetic acid in several solvents as a function of temperature.

Table III: Energy and Free Energy Changes for Association and Solvation of Trifluoroacetic Acid

Reaction	Medium	$-\Delta G°$, kcal[a]	$-\Delta E°$, kcal[a]
$2TFA = (TFA)_2$	Vapor	5.12 ± 0.04	(13.4)[b]
	Cyclohexane	3.11 ± 0.12	11.7 ± 0.6
	CCl_4	2.97 ± 0.08	9.2 ± 0.4
		(2.88 ± 0.03)[c]	(9.0 ± 0.4)[c]
	Benzene	0.57 ± 0.18	(7.4)[d]
	1,2-Dichloroethane	0.24 ± 0.14	7.0 ± 3.8
TFA(vapor) = TFA(medium)	Cyclohexane	2.04 ± 0.11	2.3 ± 0.4
	CCl_4	2.51 ± 0.07	3.4 ± 0.6
	Benzene	3.76 ± 0.07	5.2 ± 0.6
	1,2-Dichloroethane	3.94 ± 0.12	5.3 ± 0.6
$(TFA)_2$(vapor) = $(TFA)_2$(medium)	Cyclohexane	2.07 ± 0.23	2.9 ± 1.0
	CCl_4	2.83 ± 0.18	2.6 ± 1.4
	Benzene	2.97 ± 0.16	4.4 ± 1.3
	1,2-Dichloroethane	3.00 ± 0.27	4.2 ± 1.5

[a] Standard states are unit molarity, ideal dilute solution states for components in all phases. Internal energies are assumed to be equal to enthalpies for species in condensed phases and to differ from enthalpies by $-RT$ in the gas phase. [b] C. Ling, S. D. Christian, H. E. Affsprung, and R. W. Gray, *J. Chem. Soc. A*, 293 (1966). [c] Dilute-solution studies, this work. [d] Assumed to be the same as ΔE for the reaction $2TFA = (TFA)_2$ in diphenylmethane, reported by W. S. Higazy and A. A. Taha, *J. Phys. Chem.*, **74**, 1982 (1970).

acetic acid. Even the nearly inert solvents considerably reduce the energy and free energy of the individual species. That the monomer is much more strongly solvated than the dimer (per mole of CF_3COOH) is indicated by the marked decrease in the magnitude of the energy of the dimerization reaction in the condensed phases. Changes observed in $\Delta G°$ and $\Delta E°$ (and of course $\Delta S°$) for the reaction $2TFA \rightleftharpoons (TFA)_2$ parallel those noted by Allen, *et al.*,[10] for the dimerization of benzoic acid in several media.

The influence of solvents on the energies and free energies of formation of molecular complexes may be rationalized in terms of a solvation model developed in this laboratory.[8,11] Application of the model requires introduction of the dimensionless parameters

$$\alpha = \frac{\Delta E^{c}_{\underset{v\rightarrow s}{\text{complex}}}}{\Sigma\Delta E^{c}_{\underset{v\rightarrow s}{\text{reactants}}}}$$

and

$$\alpha' = \frac{\Delta G^{c}_{\underset{v\rightarrow s}{\text{complex}}}}{\Sigma\Delta G^{\circ}_{\underset{v\rightarrow s}{\text{reactants}}}}$$

where

$$\Delta E^{\circ}_{\underset{v\rightarrow s}{\text{complex}}} \text{ and } \Delta G^{\circ}_{\underset{v\rightarrow s}{\text{complex}}}$$

represent internal energy and Gibbs free energy changes for transferring the complex from the ideal vapor phase at unit molarity into the unit molarity ideal dilute solution state in solvent S, and

$$\Sigma\Delta E^{\circ}_{\underset{v\rightarrow s}{\text{reactants}}} \text{ and } \Sigma\Delta G^{\circ}_{\underset{v\rightarrow s}{\text{reactants}}}$$

are the sums of the corresponding energy and free energy changes for the monomers which unite to form the complex. In the case of the TFA dimerization reaction

$$\Sigma\Delta E^{\circ}_{\underset{v\rightarrow s}{\text{reactants}}} = 2\Delta E^{\circ}_{\underset{v\rightarrow s}{\text{TFA}}} \text{ and } \Sigma\Delta G^{\circ}_{\underset{v\rightarrow s}{\text{reactants}}} = 2\Delta G^{\circ}_{\underset{v\rightarrow s}{\text{TFA}}}$$

It has been noted that α and α' for a given electron donor–acceptor association reaction (of either the charge-transfer or hydrogen-bonded type) are generally nearly equal to each other and nearly invariant throughout a range of different media. (In several previous communications from this laboratory,[11] the constant α has been used to represent both the energy and the free energy ratio, although the ratios α and α' are not necessarily equivalent. It is probably desirable to use different symbols to designate these two ratios, while recognizing that they are ordinarily nearly equal.) In terms of the parameters α and α' one may write the thermodynamic identities

$$\Delta G°_{v} = \Delta G°_{s} + (1 - \alpha')\Sigma\Delta G^{\circ}_{\underset{v\rightarrow s}{\text{monomers}}} \qquad (7)$$

and

$$\Delta E°_{v} = \Delta E°_{s} + (1 - \alpha)\Sigma\Delta E^{\circ}_{\underset{v\rightarrow s}{\text{monomers}}} \qquad (8)$$

where $\Delta G°_{v}$ and $\Delta G°_{s}$ are the standard free energy changes for the association reaction in the vapor and solvent phases, respectively, and $\Delta E°_{v}$ and $\Delta E°_{s}$ are the corresponding internal energy changes in the two phases; unit molarity ideal dilute solution states are employed throughout. Equations 7 and 8 imply that if α and α' are nearly equal and constant for the TFA dimerization reaction in the media investigated here, plots of

$$-\Delta G°_{s} \textit{ vs. } -2\Delta G^{\circ}_{\underset{v\rightarrow s}{\text{TFA}}} \text{ and } -\Delta E°_{s} \textit{ vs. } -2\Delta E^{\circ}_{\underset{v\rightarrow s}{\text{TFA}}}$$

should be linear and have equal slopes.[8-11] Figure 7 shows data from Table III plotted in these forms; the two solid lines are both drawn with slopes equal to -0.56, corresponding to $\alpha = \alpha' = 0.44$. Thus, the

(10) G. Allen, J. G. Watkinson, and K. H. Webb, *Spectrochim. Acta*, **22**, 807 (1966).

(11) (a) S. D. Christian, J. R. Johnson, H. E. Affsprung, and P. J. Kilpatrick, *J. Phys. Chem.*, **70**, 3376 (1966); (b) J. Grundnes and S. D. Christian, *J. Amer. Chem. Soc.*, **90**, 2239 (1968); (c) S. D. Christian and J. Grundnes, *Acta Chem. Scand.*, **22**, 1702 (1968); (d) J. R. Johnson, P. J. Kilpatrick, S. D. Christian, and H. E. Affsprung, *J. Phys. Chem.*, **72**, 3223 (1968); (e) S. D. Christian, *J. Amer. Chem. Soc.*, **91**, 6514 (1969); (f) S. D. Christian, Office of Saline Water Research and Development Progress Report No. 706, July 1971.

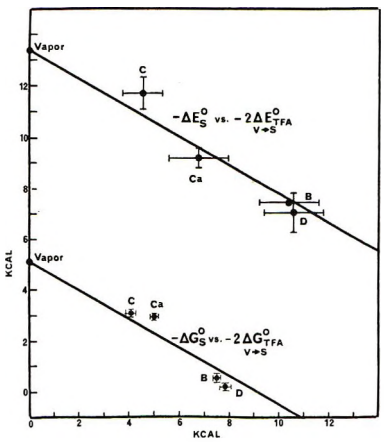

Figure 7. Dependence of the energy and free energy of dimerization of trifluoroacetic acid on transfer energies and free energies of the monomer; solvents cyclohexane (C), carbon tetrachloride (Ca), benzene (B), 1,2-dichloroethane (D).

internal energy and the free energy results conform reasonably well to a solvation model in which the dimer is somewhat less than half as effectively solvated as two separated monomer molecules.

Stevens has developed a quasi-lattice model for predicting α from group interaction energy parameters, tabulated for specific atomic and submolecular groups of molecules participating in complex formation reactions.[3b,11f] Assuming that $(TFA)_2$ is cyclic, he estimates values of α equal to 0.44, 0.59, 0.56, and 0.42, respectively, for the solvents cyclohexane, CCl_4, benzene, and 1,2-dichloroethane. The experimental value of α (0.44) is one of the lowest which has been reported for complex formation reactions. This in itself suggests that the dimer is predominantly cyclic, and the reasonable agreement with values of α estimated from the lattice calculations strengthens the argument that the dimer is cyclic.

The spectral results from this laboratory and those of Kirszenbaum, *et al.*,[4] do not indicate that more than one self-associated form of TFA exists in the solvents investigated. Gradual changes do occur in values of the frequencies and half-widths of the dimer spectral bands and of the thermodynamic properties of the dimer as the medium is varied from vapor to nonpolar solvents to slightly polar solvents. However, these effects are of the sort to be expected even if only a single monomer–dimer association reaction is occurring,[8,10] and there seems to be no reason to assume the presence of an open dimer.

The spectral-partition results for TFA in benzene (see Figure 4) suggest that there may be partial polymerization to species larger than the dimer at TFA concentrations greater than 0.2 M. However, in CCl_4 at concentrations up to 0.2 M we can find no thermodynamic or spectral evidence for higher polymerization. Moreover, the value obtained for K_2 in CCl_4, using the conventional spectral method in the very dilute region ($f_A < 3.5 \times 10^{-3}$ M), agrees well with that obtained with the spectral-partition method at much higher concentrations. This is also an indication that higher polymers and large activity coefficient effects are not important. The present results therefore do not support the observation by Murty and Pitzer[7] that there is a pronounced dilution effect on spectra in the carbonyl stretching region for TFA in CCl_4 in the concentration range 1.3×10^{-3}–3.3×10^{-2} M. Possibly the reported dilution effect may be attributed to the presence of small concentrations of water in the TFA solutions. Water is known to interact strongly with TFA to form hydrogen-bonded complexes in both vapor and solvents, and it is exceedingly difficult to remove the last traces of water from liquid TFA or its solutions in organic solvents.

Acknowledgment. This work was supported by National Science Foundation Grant No. GP-23278.

Aqueous Solution Structure as Determined from Thermodynamic Parameters of Transfer from Water to Heavy Water[1,2]

by D. B. Dahlberg

Department of Chemistry, Cornell University, Ithaca, New York 14850 *(Received January 10, 1972)*

Publication costs assisted by the U. S. Atomic Energy Commission

The free energy and enthalpy of transfer from H_2O to D_2O at 25° have been measured for several ketones and alcohols. Free energy of transfer is near zero for most substances studied. Exceptions to this occur for many cyclic compounds with side groups. Enthalpies of transfer range from −514 cal/mol for 3-pentanol to +70 cal/mol for 3,3-dimethylacetylacetone. These data combined with results from other laboratories have been interpreted in terms of solvent structure-breaking and -making spheres of influence caused by polar and nonpolar groups of the solute and the interactions caused by the overlap of such spheres. Polar groups have been found to be structure breakers, while methylene groups have been found to be structure makers. Overlap of regions of structural influence decreases the capabilities of such groups to alter solvent structure. Ring compounds show unusually small enthalpies of transfer probably due to the inability of water to enter the interior area of the ring. Some ring solutes such as cyclohexanone, xylene, and naphthalene show relatively large free energies of transfer, but most nonelectrolytes show free energies of transfer near zero.

Introduction

For many years the lack of knowledge about water and solution structure has hindered the understanding of the role of the solvent in equilibria and reaction mechanisms for aqueous solutions. In some systems medium effects have been unjustly neglected. For example, the relative acidities of alcohols in aqueous solutions are a popular textbook justification for the belief that alkyl groups are electron donating. However, Brauman and Blair[3] have recently shown that the relative acidities of alcohols in water are reversed as compared to those in the gas phase, and that medium effects are responsible for the altered behavior. The medium effect is also very important in biological systems. Scheraga[4] has stressed the importance of solvation in determining the conformation of proteins. It is of particular interest in that water is the "natural" solvent for proteins and enzymes. Jenks,[5] in discussing the role of hydrophobic interactions in equilibria and reactions in solution, postulated that such effects are the result of attractive van der Waals–London dispersion forces, competing with the strong attraction of water molecules for each other; *i.e.*, "water structure." A detailed quantitative model for such interactions is not yet available owing to the numerous types of rather weak forces adding and competing with each other. It is for this reason that initial studies of water and solution structure have depended heavily on interpretation of thermodynamic parameters. Entropies, enthalpies, and free energies of hydration have been very valuable to such studies, but meaningful interpretation of data requires a gas-phase standard state and thus very accurate values of such quantities as heats of vaporization combined with heats of solution. This is not possible for many relatively nonvolatile solutes. The search for a more easily interpretable solvent had led Krishnan and Friedman[6] to the use of propylene carbonate with some success. Such a solvent was chosen for its high dielectric constant, its lack of hydrogen bonding capabilities, and minimal basic and acidic tendencies. However, it is still quite difficult to correct for different subtle interaction between this solvent and various solutes. In a recent review, Arnett and McKelvey[7] pointed out that if one is willing to accept the assumption that H_2O and D_2O have the same properties, differing only in degree, thermodynamic quantities of transfer can provide a great deal of information about aqueous solution structure without complication of large conformational changes of solutes and extraneous interactions in the standard state. Gurney[8] and Frank and coworkers[9] have presented similar models for the

(1) Work supported by the Atomic Energy Commission.

(2) Send requests for reprints in care of F. A. Long, Department of Chemistry, Cornell University.

(3) J. J. Brauman and L. K. Blair, *J. Amer. Chem. Soc.*, **92**, 5986 (1970).

(4) H. A. Scheraga, *Advan. Phys. Org. Chem.*, **6**, 103 (1968).

(5) W. P. Jenks, "Catalysis in Chemistry and Enzymology," McGraw-Hill, New York, N. Y., 1969.

(6) (a) C. V. Krishnan and H. L. Friedman, *J. Phys. Chem.*, **73**, 1572 (1969); (b) *ibid.*, **73**, 3934 (1969); (c) *ibid.*, **74**, 3900 (1970); (d) *ibid.*, **75**, 3598 (1971).

(7) E. M. Arnett and D. R. McKelvey, "Solute–Solvent Interactions," J. F. Coetzee and C. D. Ritchie, Ed., Marcel Dekker, New York, N. Y., 1969, Chapter 6.

(8) R. W. Gurney, "Ionic Processes in Solution," McGraw-Hill, New York, N. Y., 1953.

(9) (a) H. S. Frank and M. W. Evans, *J. Chem. Phys.*, **13**, 507 (1945); (b) H. S. Frank and W-Y. Wen, *Discuss. Faraday Soc.*, **No. 24**, 133 (1957).

structure of the solvent water around both ions and nonelectrolytes. These models describe spheres of structure-making and -breaking influence caused by various types of solutes. This paper presents new thermodynamic data for transfer of solutes from H_2O and D_2O and attempts to analyze the data in terms of an expanded version of the aforementioned model.

Experimental Section

(*A*) *Materials.* Water was singly distilled, and 99.8% A.R. heavy water was purchased from Mallinckrodt Chemical Works and was used without further purification. Cyclohexane was Fisher Certified spectral grade as were acetone, benzene, toluene, and 2-propanol. Hexane-2,5-dione showed an unusually high uv extinction coefficient, which was not eliminated by distillation. Recrystallization of the diketone at $-60°$ in *n*-pentane yielded pure diketone with a reasonable extinction coefficient of 37.4 in cyclohexane at 275 mμ. All other compounds were distilled to at least a 1° range.

(*B*) *Free Energy of Transfer from H_2O to D_2O.* Slightly soluble solids and liquids were stirred separately with both H_2O and D_2O for at least 48 hr submerged in a 25.00 ± 0.05° thermostated bath. The uv absorbance of a centrifuged sample of the aqueous phase was measured on a Cary 14. The ratio of the absorbance of the water and heavy water phases provided the ratio of solubilities, if it is assumed that extinction coefficients are the same in both media. This assumption was verified for acetone and 2-butanone.

For more soluble materials, a few drops of the solute was stirred for 48 hr at 25.00 ± 0.05° in a flask containing 10 ml of light or heavy water. The uv absorbance of centrifuged samples of all phases was measured. Extinction coefficients were determined in H_2O and cyclohexane for the ketones to check purity and to calculate free energy of transfer from H_2O to cyclohexane. Concentrations of solutes were always less than 10^{-2} *M*. Using cyclohexane as a standard state yielded the free energy of transfer and the degenerate activity coefficients from H_2O to D_2O, as defined by

$$KH^{(D_2O)} \rightleftharpoons KH^{(H_2O)}, \gamma_{KH} \quad (1)$$

$$\gamma = [A_{KH}{}^{(H_2O)}/A_{KH}{}^{(\text{cyclohexane})}]/[A_{KH}{}^{(D_2O)}/A_{KH}{}^{(\text{cyclohexane})}] \quad (2)$$

$$\Delta\bar{G}^\circ{}_{tKH} = RT \ln \gamma_{KH} \quad (3)$$

where *A* is the observed absorbance of the solute KH in the indicated partitioned solvent.

(*C*) *Enthalpies of Transfer.* Enthalpies of transfer from H_2O to D_2O were determined by dilution adiabatic calorimetry exactly as described by Scheraga and coworkers.[10] A typical experiment involves placing about 40 mg of carefully weighed solute and about 3 ml of weighed H_2O in a small cell. After bringing the system to 25°, a window in the cell was broken by an electrically controlled spring, releasing the contents into a larger cell containing about 46 g of weighed D_2O. The temperature was monitored using thermocouples to within $1 \times 10^{-4}°$. Similar measurements were done to determine the heat of dilution in pure H_2O. The heat of exchange of the H_2O and D_2O was determined by Scheraga.[10] The heat change q_t due to the transfer of the solute is given by

$$q_t = q_{mix} - q_{H_2O} - q_{dil} \quad (4)$$

where q_{mix} represents the heat of dilution of the H_2O solution into D_2O, q_{H_2O} is the heat of exchange from mixing an equivalent amount of D_2O, and q_{dil} is the heat of dilution of the H_2O solution into H_2O. Table I shows typical data for acetone. Table II shows the enthalpies of transfer obtained from the experiments

Table I: Illustrative Experimental Data for Acetone at 25° for Determination of Enthalpy of Transfer

Expt no.	Acetone, mg	H_2O, g	D_2O, g	q_{mix}, cal	q_{H_2O}	$-q_{dil}$, cal
1	54.6	2.9882	46.96	4.696	4.841	0.018
2	48.0	2.9892	46.91	4.691	4.843	0.016

Table II: The Enthalpies of Transfer of Various Nonelectrolytes from Dilute H_2O to Dilute D_2O at 25.0°

Compound	$-\Delta\bar{H}^\circ_t$, cal/mol: to 93% D_2O	to 100% D_2O	Average
	Ketones		
Acetone	135	144	160 ± 16
	164	176	
2-Butanone	215	232	232 ± 0
	216	232	
	215 (15°)	233 (15°)	230 (15°)
3-Pentanone	309	331	318 ± 12
	286	306	
3-Hexanone	392	420	419 ± 1
	390	418	
Cyclohexanone	157	168	186 ± 18
	190	203	
Hexane-2,5-dione	8	9	18 ± 10
	26	28	
3,3-Dimethyl-acetylacetone	−66	−70	−70
	Alcohols		
2-Propanol	357	383	384 ± 2[a]
	359	386	
3-Pentanol	485	520	514 ± 6
	475	508	
Cyclohexanol	408	437	449 ± 12
	429	460	

[a] Scheraga and coworkers[10] determined $\Delta\bar{H}^\circ_t = -417 \pm 4$ cal/mol for 2-propanol.

(10) G. C. Kresheck, H. Schneider, and H. A. Scheraga, *J. Phys. Chem.*, 69, 3132 (1965).

performed in this laboratory. Since the final solutions after dilution contain about 7% protium, it is necessary to correct these values to 100% D_2O by dividing the determined molar enthalpy of transfer $\Delta\bar{H}_t°$ values by the final hole fraction deuterium of the solvents. One experiment was performed at 15° to determine the heat capacity of transfer for 2-butanone, which turned out to be near zero.

Results

Enthalpy of Transfer. The molar enthalpies of transfer from H_2O to D_2O were determined in this laboratory for a homologous series of four monoketones plus two diketones, two secondary alcohols, cyclohexanone, and cyclohexanol. From Table II it can be seen that all except 3,3-dimethylacetylacetone have negative enthalpies of transfer. Figure 1 contains these values as well as selected values obtained in other laboratories.[11] Arnett and McKelvey[7] have suggested that since D_2O is believed to be more structured than H_2O, it is more susceptible to structure breaking and structure making, the former being shown by a positive enthalpy of transfer and the latter by a negative enthalpy of transfer. This assignment was based on the fact that certain compounds and ions show structure-making and -breaking qualities in water as measured by other techniques such as enthalpies and entropies of hydration, viscosity, diffusion, and conductivity. All of these methods give a rather consistent picture of the influence of certain types of solutes on water structure and correlate well with the enthalpies of transfer from H_2O to D_2O.

Most of the nonelectrolytes and some of the sodium carboxylate salts are indicated in Figure 1 to be structure makers. In all cases, it is seen that the more carbons in a series of homologs, the more negative the enthalpy of transfer, which is consistent with the proposal that methylene groups are structure makers. Also, it is noted that diketones have a much less negative enthalpy of transfer than do monoketones, indicating that the polar carbonyl groups are structure breakers. It can be seen from Figure 1 that for a constant number of carbons the order of increasing enthalpy of transfer is primary alcohols < amino acids < monoketones < sodium carboxylates < diketones. With the exception of the amino acids, this is the order of increased polarity and number of the functional groups. The unexpected low values for the amino acids are probably due to the three quickly exchangeable protons, which apparently create a more negative enthalpy of transfer. A similar result has been observed from the less accurate results of Krishnan and Friedman[6c] for alkylammonium ions after correcting for the anion transfer. Arnett and McKelvey assumed that if the enthalpy of transfer of the lithium ion is zero, the sodium ion would take on a value of about +160 cal/mol. This would lower the values of the alkyl carboxylate ions by that amount, making all except formate structure makers. This would not change the relative order of increasing enthalpies of transfer.

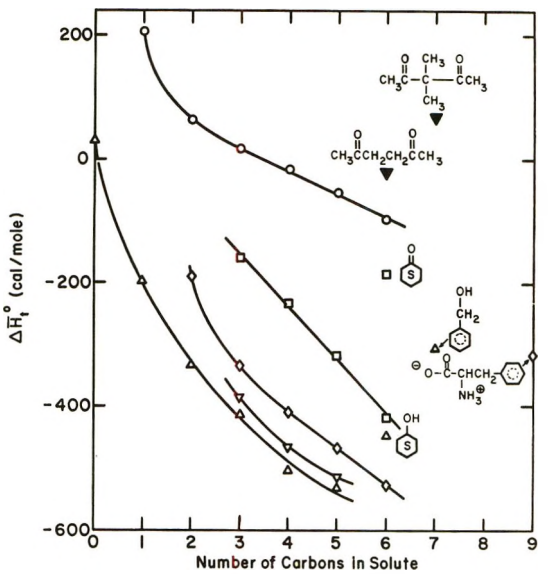

Figure 1. The enthalpy of transfer from light to heavy water *vs.* the number of carbons in the solute molecule: (△) primary alcohols, (▽) secondary alcohols, (◇) amino acids, (□) monoketones, (▼) diketones, (○) sodium salts of carboxylic acids.

It should also be noted that the plot of $\Delta\bar{H}°_t$ *vs.* the number of carbons in the molecule is linear for the monoketones, while it is curved for small alcohols, amino acids, and sodium carboxylates and fairly linear for the longer molecules. Finally, molecules with saturated or aromatic cyclic frameworks show much less negative enthalpies of transfer than linear molecules containing the same number of carbons and the same functional groups.

Free Energy of Transfer. The free energies of transfer from H_2O to D_2O, $\Delta\bar{G}°_t$, as obtained in this laboratory, are listed in Table III. Arnett and McKelvey have summarized a few other values of $\Delta\bar{G}°_t$ for nonelectrolytes and noted that in most cases enthalpies of transfers are five to ten times the free energies of transfer. The ketones studied in this laboratory show zero free energies of transfer within experimental error, except for cyclohexanone. The free energy of transfer is also near zero for benzene, but slightly positive for toluene and much larger for the xylenes and naphthalene. Finally, from the keto–enol equilibrium of 3-methylacetylacetone the value of $\Delta\bar{G}°_t$ for the cyclic enol is approximately 200 cal/mol, while for the keto form $\Delta\bar{G}°_t = 25 \pm 40$ cal/mol.[12]

(11) (a) $\Delta\bar{H}°_t$'s for primary alcohols and amino acids are from ref 10; (b) $\Delta\bar{H}°_t$'s for the sodium salts of carboxylic acids were obtained from H. Snell and J. Greyson, *J. Phys. Chem.*, **74**, 2148 (1970).

(12) D. B. Dahlberg and F. A. Long, to be published.

Table III: The Free Energies of Transfer from H_2O to D_2O at 25.0°

Compound	$\Delta\bar{G}^\circ_t$, cal/mol, mole fraction units
Ketones	
Acetone	0 ± 15
2-Butanone	7 ± 20
3-Pentanone	−18 ± 23
3-Hexanone	0 ± 15
Cyclohexanone	+52 ± 10
Hexane-2,5-dione	0 ± 15
3,3-Dimethylacetylacetone	+41 ± 40
3-Methylacetylacetone (keto)	+25 ± 40
3-Methylacetylacetone (enol)	+200
Aromatic	
Benzene	0 ± 15
Toluene	+25 ± 15
m-Xylene	+45 ± 12
o-Xylene	+84 ± 20
Naphthalene	+108 ± 15
Benzyl alcohol	−9 ± 20
Deuterioquinone[a]	+110
Nitrobenzene[b]	+157
L-Phenylalanine[c]	+127 ± 1

[a] B. Hayes, Thesis, M.I.T., Cambridge, Mass., 1964. [b] H. E. Vermillion, *et al.*, *J. Amer. Chem. Soc.*, **63**, 1346 (1941), determined at 30°. [c] Reference 10.

Discussion

Enthalpy of Transfer. In their recent review Arnett and McKelvey[7] noted that $\Delta\bar{H}^\circ_t \simeq T\Delta\bar{S}^\circ_t$ due to the extremely small values of $\Delta\bar{G}^\circ_t$ for such compounds as methyl halides, small alkanes, and amino acids. This relationship was also observed for most nonelectrolytes studied in this labotatory, as seen from Table III. This is a special case of the "Vaslow–Doherty compensation" phenomenon as reviewed by Lumry and Rajender.[13] When $\Delta\bar{H}^\circ_t$ is plotted against $\Delta\bar{S}^\circ_t$ for some equilibrium process of closely related compounds, a straight line is obtained, which has a slope of the order of 300°K and a relatively small intercept which is a measure of $\Delta\bar{G}^\circ_t$. Although this phenomenon is not unique to water solutions, it is believed to be related to the structural changes of the solvent. Lumry and Rajender have suggested that water acts as a "volume buffer" to counteract the changes of volume associated with certain structural changes of the solute and solvation shells. At least it is obvious that the binding of water by any mechanism, shown by a negative $\Delta\bar{H}^\circ_t$, also restricts the degrees of freedom of that water, shown by a negative $\Delta\bar{S}^\circ_t$. Thus the enthalpies of transfer, which measure the energetics of solvent–solute and solute–solute interactions, are linearly related to the entropies of transfer, which is a measure of the order–disorder caused by such interactions. This allows at least qualitative discussion of solution structure in terms of enthalpies of transfer, when entropies of transfer are not available.

The Gurney[8] and Frank and Wen[9b] models for the structure of the aqueous solvent near ionic solutes suggest that there is a region of highly structured water surrounding the ion owing to the strong attractive forces between the ion and polar water. However, farther away from the ion the electrostatic forces are no longer strong enough to structure the water, but may be strong enough to break up some of the normal bulk water structure. Very far from the ion, the bulk solvent contains the normal unperturbed water structure. The observed entropy change is the sum of the changes for the two regions, *i.e.*, ion structured, ion broken as compared with bulk water. For large ions, the charge is more diffuse and the region of highly structured water near the ion is smaller. Also, water is held away from the center of the charge by the physical size of the ion. This leads to a net structure-breaking quality to most large ions. A similar picture can be applied to charged groups or even polar groups, explaining the structure-breaking influence seen here. The mechanism for the structure-making influence of a methylene group is not understood, but the effect has been observed many times.[7,9a]

Gurney[8] has considered the problem of very concentrated solutions where various solute molecules or ions are forced so close together that their regions of structure-making or -breaking influence overlap. This should cause an overlap of effects with much duplication; *i.e.*, the structure-breaking or -making effects would be reduced owing to the fact that in the regions of overlap of influence the structure effect of one molecule or ion makes no added contribution, since the region has already been structured or destructured by another ion or molecule. This would lead to a decrease in the absolute value of the molar entropy and enthalpy of transfer with increased solute concentration for both structure makers and structure breakers.

Arnett and coworkers[14] have observed this effect in the decrease of the molar enthalpy of solution of benzene as the concentration of the benzene or tetrabutylammonium bromide (both structure makers) is increased. Snell and Greyson[11b] have observed the same trend in the molar enthalpies of transfer from H_2O to D_2O of sodium salts of aliphatic acids as their concentrations increased. Those with positive enthalpies of transfer, structure breakers, yielded less positive values with increasing concentration, while those with negative enthalpies of transfer, structure makers, yielded less negative values with increasing concentration.

Another example of the significance of overlap of spheres of influence was provided by Wetlaufer, *et al.*,[15] who discovered that urea, a structure breaker, de-

(13) R. Lumry and S. Rajender, *Biopolymers*, **9**, 1125 (1970).

(14) E. M. Arnett, M. Ho, and L. L. Schaleger, *J. Amer. Chem. Soc.*, **92**, 7039 (1970).

(15) D. B. Wetlaufer, S. K. Malik, L. Stoller, and R. I. Coffin, *ibid.*, **86**, 509 (1964).

creased the evolution of heat from dissolving several structure-making hydrocarbon gases in water. This seems to demonstrate that when a sphere of structure-breaking influence is overlapped with a sphere of structure-making influence, the result is at least partial cancellation of structure-making and -breaking effects.

The concept of overlapping spheres of influence is applicable to molecules containing varying numbers of both polar and nonpolar groups, in that the structure breakers and makers are held closely together by chemical bonds. This idea was presented in a speculative way as early as 1957 by Everett,[16] but he did not analyze the specific nature of the solvent structure near various types of groups. The following is an analysis of the $\Delta\bar{H}^\circ_t$ data obtained in this and other laboratories in terms of the model of overlapping spheres of influence.

Examination of Figure 1 shows that the structure-making effect of the methylene groups is dominant and is fairly constant per methylene group for any given series of homologs, except when there are only one or two carbons in the molecule, which are near part of the polar head group. Here the overlap of the structure-making and -breaking spheres of influence cause a greatly reduced structure-making effect as seen by the upswing in the lines for shorter molecules. This effect is also apparent when comparing secondary alcohols with their primary isomers. Here the polar hydroxyl group is near three carbons, while for primary alcohols, it is near only two carbons. The influence seems to taper off quickly somewhere near the carbon α to the head group.

For the four monoketones the plot of $\Delta\bar{H}^\circ_t$ *vs.* the number of carbons in the solute molecules is linear because the polar group is always centrally located as in the secondary alcohols. Acetone has a $\Delta\bar{H}^\circ_t = -160$ cal/mol, while hexane-2,5-dione has a $\Delta\bar{H}^\circ_t = -18$ cal/mol. If the diketone is looked upon as two acetones connected together, an enthalpy of transfer of -320 cal/mol would be expected. The diketone has a $\Delta\bar{H}^\circ_t \sim 300$ cal/mol higher than expected, and that of 3,3-dimethylacetylacetone is even higher. This suggests that the structure-making influence of the central carbons is greatly reduced by their overlap with each other in hexane-2,5-dione and that such overlap is enhanced even more by branching as in 3,3-dimethylacetylacetone.

Also of interest are the much less negative enthalpies of transfers of cyclic compounds. Both cyclohexanol and cyclohexanone are of the order of 200 cal/mol higher in $\Delta\bar{H}^\circ_t$ than their linear counterparts and values for benzyl alcohol and phenylalanine are about 270 cal/mol higher than expected values for their linear counterparts. A reasonable explanation is that there is no space for water in the interior of the ring and thus there is a great loss in water-structuring capability per methylene group. Aromaticity seems to further reduce the structure-making influence of the methylene groups, which is in line with the higher solubilities of aromatic compounds compared to saturated hydrocarbons. A final example of extreme overlap is observed for enthalpies of transfer for tetraalkylammonium salts.[6] Even after correcting for the anion, the values are surprisingly high and the slope is very small (approximately 20 cal/mol per methylene group). The compact spherical geometry apparently greatly reduces the number of methylenes exposed to the water.

Attempts to make such a model quantitative are hampered by several problems. First, the so-called "spheres of structure influence" are probably neither spherical nor do they have a definite radius. Their shape and range of influence would depend on the shape and polarity of the functional groups in question as well as the distance from the group. Also, there is no reason to believe that the mechanism of the structure-making influence of methylene groups is the same as the mechanism of structure-breaking influence of polar groups. Almost all solutes studied so far contain both polar and hydrophobic groups in close proximity, so there is no way of assigning values for the structure influence of either type alone. Finally, for the compounds studied so far, the overlap effects of polar groups seem to be so short ranged as to affect only atoms one or two places removed. However, further study in this field would be greatly rewarding, because it would provide valuable information on the influence of water structure on the configuration of such molecules as proteins in water, as well as the interactions between molecules while involved in transition states of a reaction.

Free Energies of Transfer. As stated earlier, the free energies of transfer from H_2O to D_2O are near zero for most nonelectrolytes. However, some solutes do show significant free energies of transfer. It is apparent from the data of simple salts obtained by Salomaa and Aalto[17] that anions are characterized by positive $\Delta\bar{G}^\circ_t$ values, while those of cations are close to zero. They suggest that the difference arises because of a deuterium isotope effect for the H bonding to the anions which is not present in aqueous solutions of cations. One would then expect to see the same effect with ketones, which are good H-bond recipients. However, the ketones show zero free energies of transfer. Reuben[18] saw no difference in the oxygen-17 nmr chemical shifts of acetone in H_2O and D_2O, indicating that there is no difference between the strengths of the H bond and D bond to the carbonyl. This may not be the case for the much stronger H bonds to anions. A large positive value of $\Delta\bar{G}^\circ_t$ also occurs with some nonelectrolytes. Scheraga and coworkers[10] pointed out that the $\Delta\bar{G}^\circ_t$ for

(16) D. H. Everett, *Discuss. Faraday Soc.*, No. 24, 220 (1957).
(17) P. Salomaa and V. Aalto, *Acta Chem. Scand.*, 20, 2035 (1966).
(18) J. Reuben, *J. Amer. Chem. Soc.*, 91, 5725 (1969).

L-phenylanine was +127 cal/mol, while values for amino acids not containing rings ranged from −28 cal/mol for glycine to +13 cal/mol for DL-norleucine. Deuterioquinone[19] and nitrobenzene[20] show unusually high $\Delta\bar{G}^\circ_t$ of +100 and ±157 cal/mol, respectively. The ring alone is not the cause of such a high $\Delta\bar{G}^\circ_t$, as demonstrated by the near-zero values for benzene and benzyl alcohol; however, the addition of certain side chains often causes significantly larger increases in $\Delta\bar{G}^\circ_t$, as shown by toluene, the xylenes, naphthalene, and cyclohexanone. The importance of shape is seen from the keto–enol isomer equilibrium of 3-methylacetylacetone,[12] where the keto form acts as most ketones, while the enol, which with its intramolecular H-bonded ring structure looks very much like trimethylbenzene, shows a very high $\Delta\bar{G}^\circ_t$. Even quite subtle differences like *o*- and *m*-xylene cause relatively substantial changes in $\Delta\bar{G}^\circ_t$.

With only limited data it is difficult to interpret these results in terms of water structure. The low solubility of alkyl-substituted cyclohexanones and of benzene prevents the study of $\Delta\bar{H}^\circ_t$ for these compounds. Franks, *et al.*,[21] have, however, studied the heats of hydration $\Delta\bar{H}^\circ_h$ of several cyclic ether derivatives in H_2O. They noted that little net change in total interactions occurs when the tetrahydrofuran ring is enlarged. They also concluded that the addition of a $-CH_2OH$ group causes $\Delta\bar{H}^\circ_h$ to be markedly more exothermic. It appeared to them that side groups of cyclic compounds determine the $\Delta\bar{H}^\circ_h$ value, which was only slightly modified by the ring. This agrees with the observation made here that the $\Delta\bar{H}^\circ_t$ is affected very little by methylene groups involved in a ring structure. Clemmentt and coworkers[22] studied cyclic ethers in H_2O by nmr and diffusion techniques and concluded that such ring compounds in water-rich mixtures are closely enveloped by water molecules but do not interact strongly with them. Whether or not this "envelope" is different from the structure-making region of linear alkyl groups and how sensitive this structure is to the shape of the solute, as well as size, remain to be seen. The fact that for anions and a few nonelectrolytes, especially rings with branches, the enthalpies of transfer are not completely compensated for by the entropies of transfer indicates that special solvent–solute and solute–solute interactions occur with these solutes, which are not present with simple cations and most nonelectrolytes. The lack of understanding of the nature of these interactions and the resulting nonzero free energies of transfer stand in the way of truly understanding medium effects on equilibria and kinetics in aqueous solutions.

Acknowledgment. I am indebted to Professor H. A. Scheraga for the use of his adiabatic dilution calorimeter. I also wish to thank Mr. B. Lentz for many helpful discussions. Special gratitude is expressed to F. A. Long for the use of his laboratory facilities and for many helpful discussions.

(19) B. Hayes, Thesis, M.I.T., Cambridge, Mass., 1964.

(20) H. E. Vermillion, *et al.*, *J. Amer. Chem. Soc.*, **63**, 1346 (1941), determined at 30°.

(21) F. Franks, M. A. S. Quickenden, D. S. Reid, and B. Watson, *Trans. Faraday Soc.*, **66**, 582 (1970).

(22) C. J. Clemmentt, *et al.*, *J. Chem. Soc. A*, 455 (1969).

Dissipative Structures and Diffusion in Ternary Systems[1]

by V. Vitagliano,* A. Zagari, R. Sartorio, and M. Corcione

Istituto Chimico, Università di Napoli, Naples, Italy *(Received November 8, 1971)*

Publication costs borne completely by The Journal of Physical Chemistry

Gravitational instability generally arises within free diffusion boundaries when more than two components are involved in the diffusion process. As a consequence ascending and descending convective motions appear which destroy the initial boundary. A special case of gravitational instability has been found which *stabilizes* the diffusion boundary, for the system chloroform–water–acetic acid. An anomalous bimodal boundary can be observed and the diffusion speed seems to be two to three orders of magnitude lower than expected. This irreversible process has been classified as a special case of "dissipative process." Some evidence has been found of the existence of oscillatory processes within the anomalous diffusion boundary.

It has been observed that free diffusion in ternary or more complex systems may develop gravitationally unstable boundaries that make experimental measurements on such systems rather difficult.

Any appreciable difference between the mobilities of two components of the ternary system makes the diffu-

(1) This research has been carried on with the financial support of the Italian C.N.R.

Table I: Data for the Diffusion Runs on the Ternary System Acetic Acid–Chloroform–Water[a]

Run	$\bar{c}$ AcH	$\bar{c}$ $CHCl_3$	$\bar{c}$ H_2O	Δc AcH	Δc $CHCl_3$	Δc H_2O	$d\uparrow$	$d\downarrow$	R	D_a, $cm^2\ sec^{-1}$	
1	7.958	6.382	1.595	−0.065	0.000	0.300	1.2677	1.2693			A
2	7.923	6.382	1.595	−0.275	0.101	0.500	1.2624	1.2686	4.952	6.0×10^{-5}	B
3	7.925	6.382	1.595	−0.475	0.200	0.750	1.2621	1.2709	3.748	4.5×10^{-5}	B
4	7.927	6.382	1.595	−0.480	0.200	0.750	1.2624	1.2709	3.745	4.4×10^{-5}	B
5	7.920	6.381	1.595	−0.347	0.150	0.500	1.2631	1.2692	3.333	3.0×10^{-5}	B
6	7.925	6.382	1.595	−0.347	0.200	0.250	1.2627	1.2703	1.248	2.366×10^{-5}	C
7	7.930	6.382	1.595	−0.416	0.240	0.290	1.2635	1.2703	1.209	2.372×10^{-5}	C
8	7.950	6.382	1.599	−0.350	0.240	0.002	1.2643	1.2719	0.008	1.400×10^{-5}	C
9	7.935	6.381	1.598	−0.359	0.300	−0.244	1.2622	1.2721	−0.814	0.824×10^{-5}	C
10	7.974	6.382	1.595	−0.183	0.200	−0.440	1.2670	1.2719	−2.197	32×10^{-7}	B
11	7.914	6.389	1.597	−0.035	0.101	−0.400	1.2655	1.2683	−3.969	7.0×10^{-7}	B
12	7.952	6.389	1.597	−0.036	0.101	−0.400	1.2678	1.2705	−3.967	6.9×10^{-7}	B
13	7.944	6.382	1.595	−0.082	0.140	−0.600	1.2672	1.2681	−4.286	5.8×10^{-7}	B
14	7.947	6.281	1.595	0.027	0.104	−0.653	1.2667	1.2690	−6.245	0.6×10^{-7}	B
15	7.924	6.382	1.595	0.081	0.136	−1.020	1.2652	1.2679	−7.500	0.5×10^{-7}	B

[a] $\bar{c}$, average concentration in moles per liter; Δc, concentration difference ($C_{\text{lower solution}} - C_{\text{upper solution}}$); $d\uparrow\downarrow$, upper and lower solutions density; R, $\Delta c_{H_2O}/\Delta c_{CHCl_3}$ ratio; D_a, apparent diffusion coefficient (reduced area/maximum height) ratio; A, unstable boundary; B, Schlieren optics registered runs; C, Gouy interferometric technique registered runs.

sion path curved on the composition diagram[2] so that layers may develop within the diffusion boundary with densities higher than that of the bottom solution or lower than that of the top solution. As a consequence the appearance of convective motions contributes to a fast destruction of the boundary.

This phenomenon is well known,[3] and it has recently been discussed from a theoretical point of view.[4,5]

We would like to discuss here a case where the gravitational instability is not sufficient to destroy the diffusing boundary. On the contrary it acts as a stabilizing agent on the boundary so that diffusion seems to proceed at a rate two orders of magnitude slower than expected. We suggest that this "anomalous diffusion" might be classified as a special case of dissipative process.[6,7]

Experimental Section

Materials. Doubly distilled water was used. Freshly distilled acetic acid, reagent grade (C. Erba, Milan), was used. The chloroform, reagent grade (C. Erba, Milan), was shaken with bidistilled water (ratio 1:2) several times to eliminate ethyl alcohol. It was then kept on anhydrous calcium chloride for a few hours. Finally it was passed through a basic alumina column to eliminate the last alcohol traces and was used immediately for diffusion runs. The purity was controlled by gas chromatography.

Solutions. Each solution for the diffusion runs was made by weighing all components in a 250-ml bottle. The third component (acetic acid) was added in a thermostatic bath (25 ± 0.02°). In this way it was possible to roughly estimate the solutions' densities (Table I). No correction for the weighing under vacuum was made.

Diffusion Runs. We took a set of free diffusion experiments on the ternary system acetic acid–chloroform–water at 25 ± 0.02° and constant average concentration: $CHCl_3$, 6.382 mol/l.; H_2O, 1.595 mol/l., varying the concentration differences of the three components between the upper and lower solutions.[8]

Two experimental techniques were used: the Gouy interferometry[9,10] and the Philpot Schlieren optics.[11–13] A single channel cell[10] was used with a Teflon–glass stopcock which avoided lubrication problems. The initial boundary was made by means of the siphoning technique[9,10] at the level of the diffusiometer optical axis.

It must be remembered that the experimental result is an "apparent diffusion coefficient." Dealing with a ternary system we obtain in fact a value called reduced area/maximum height ratio

$$D_a = \frac{(\Delta n)^2}{4\pi t(\mathrm{d}n/\mathrm{d}z)_{\max}^2} \qquad (1)$$

(2) Y. Oishi, *J. Chem. Phys.*, **43**, 1611 (1965).

(3) M. Brakke, *Arch. Biochem. Biophys.*, **55**, 175 (1955).

(4) R. P. Wendt, *J. Phys. Chem.*, **66**, 1740 (1962).

(5) W. K. Sartory, *Biopolymers*, **7**, 251 (1969).

(6) I. Prigogine, "Fast Reactions and Primary Processes in Chemical Kinetics," S. Claesson, Ed., Interscience, New York, N. Y., 1967, p 371.

(7) I. Prigogine, "Introduction to Thermodynamics of Irreversible Processes," 2nd ed, Interscience, New York, N. Y., 1961.

(8) This average composition is far enough from the phase separation compositions so that no phase separation has ever occurred during the diffusion runs.

(9) L. J. Gosting, E. H. Hanson, G. Kegeles, and M. S. Morris, *Rev. Sci. Instrum.*, **20**, 209 (1949).

(10) V. Vitagliano, "Introduzione allo Studio della Diffusione nei Liquidi," Fondazione Beneduce, Ed., Tip. D'Agostino, Napoli, 1959.

(11) M. Bier, "Electrophoresis," Academic Press, New York, N. Y., 1959, p 145.

(12) J. S. Philpot, *Nature*, **141**, 283 (1938).

(13) H. Svensson, *Kolloid Z.*, **87**, 181 (1939).

where Δn is the total refractive index difference between upper and lower solution, dn/dz is the refractive index gradient along the diffusion coordinate z, and t is the time measured from the initial infinitely sharp boundary. D_a is a direct measure of the spreading velocity of the diffusion boundary, it corresponds to the diffusion coefficient only in the case of a two-component system.[14]

The accuracy of the Gouy technique (± 0.1–0.3%) is, of course, much higher than that of the Schlieren optics; however, it can be used only with diffusing boundaries which do not deviate much from a Gaussian shape. On the other hand, the Schlieren technique can be used with any boundary shape and allows one to visualize this shape. We were forced to apply this technique in most of our measurements, as will become clear later.

All significant data of the diffusion runs are collected in Table I where the "boundary spreading velocity constants," D_a, are given as a function of the ratio $R = (\Delta C_{H_2O}/\Delta C_{CHCl_3})$ between the water and chloroform concentration differences. Negative R's indicate a higher water concentration in the upper solution.

Discussion

As can be seen in Table I, the apparent diffusion coefficient, D_a, decreases with decreasing R.

The Gouy technique can be applied only in a narrow R range around zero (runs 6 to 9); for R values higher than 1.5 the Gouy fringes become anomalous and the progress of the diffusion must be followed with the Schlieren optics. At $R > 5$–6 the boundary becomes unstable, and it destroys itself very rapidly at the beginning of the run.

For runs 2 to 5 and 10, D_a was computed by means of eq 1 by measuring the areas and the maximum heights of the Schlieren patterns, these patterns being essentially symmetric see (Figure 1B). The D_a's accuracy is about 7–10%; the order of magnitude of 10^{-5} cm^2 sec^{-1} was found, as expected for mixtures of not particularly viscous liquids ($\eta \cong 0.01$ P).

For negative R values a peculiar refractive index gradient distribution can be observed inside the diffusion cell (see the Schlieren patterns of Figure 1A and Figure 6, and the graph of Figure 5E). Two very sharp boundaries seem to develop from the original one, set at $z = 0$. These boundaries move very slowly upward and downward, respectively.

The solution concentration is not constant between them, as can be realized from the fact that the dn/dz is not zero.

The peculiar shape of the diffusion boundary suggests that the mixing process might go on through a diffusion process within the boundary and through some kind of convective layering at the upper and lower limits of the boundary. This layering hinders the regular diffusion spreading of the boundary.

The D_a's cannot be obtained, in this case, by using eq 1 since neither the area under the refractive index gradient curves nor the maximum of these curves have the meaning of the corresponding terms of eq 1.

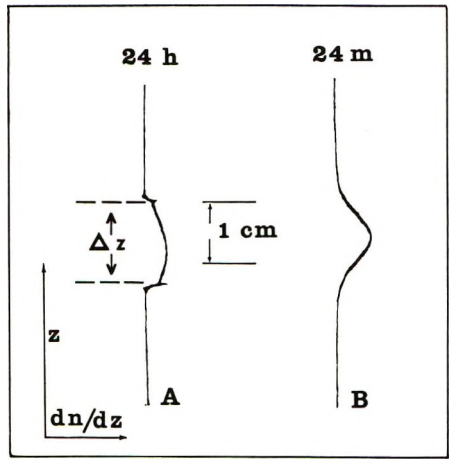

Figure 1. Comparison of anomalous and normal diffusion Schlieren patterns: A, run 14; B, run 3.

In the case of a binary system, where the diffusion boundary takes a Gaussian shape, D_a can also be obtained by the following expression

$$D_a = \frac{(\Delta z)^2}{8t} \qquad (2)$$

where Δz is the width of the dn/dz curve at its inflection points.[15] D_a corresponds in this case to the diffusion coefficient of the binary system.

We thought it reasonable to use eq 2 to evaluate the "spreading velocity constants" for the anomalous boundaries observed at negative R values. We put Δz equal to the width of the diffusing region between the upper and lower sharp layering levels, as shown in Figure 1A.[16]

The D_a coefficients computed by using eq 2 with the time values corrected for the nonzero width of the initial boundary[17] reach, for runs 10 to 15, extremely small values, two to three orders of magnitude lower than those measured at positive R values.

By visual inspection of this anomalous diffusion process, the initial boundary seems to remain sharp and narrow for hours or days giving the erroneous impression that there is no tendency of the matter to diffuse.

(14) In this paper we are discussing a particular case of boundary spreading behavior for a ternary system; we are only dealing with D_a data and not with actual diffusion coefficients.

(15) H. Neurath, *Chem. Rev.*, **30**, 357 (1942).

(16) We realize that this choice is somewhat arbitrary; it has just the meaning of assuming that, in our case, the borders of the diffusion region correspond to the inflection points of a Gaussian diffusing layer. Of course we are not interested in obtaining very accurate numerical D_a values since the observed effects involve two to three orders of magnitude in the D_a values.

(17) The time correction Δt is obtained by plotting the experimental D_a values *vs.* $1/t_s$, where t_s is the time measured from the starting of the run: $(D_a)_{exptl} = D_a + D_a\Delta t(1/t_s)$. By using $t = t_s + \Delta t$ in eq 1 and 2, constant D_a values should be obtained as a function of time.[9,10]

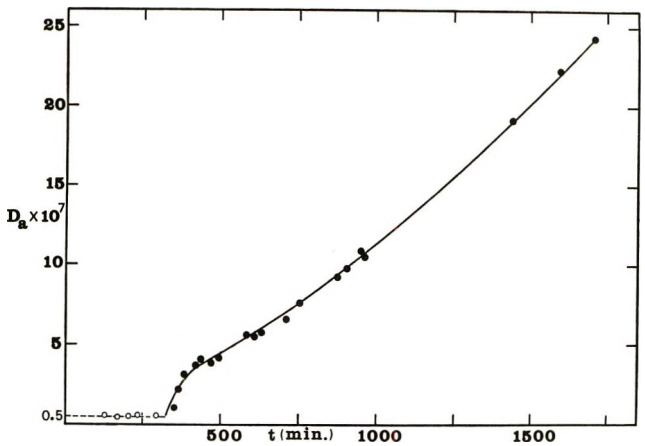

Figure 2. Apparent diffusion coefficient (or boundary spreading velocity), D_a (cm^2 sec^{-1}), evaluated from each Schlieren photogram as a function of corrected time for run 15 (time correction for noninfinite sharpness of the initial boundary Δt = 70 min[17]).

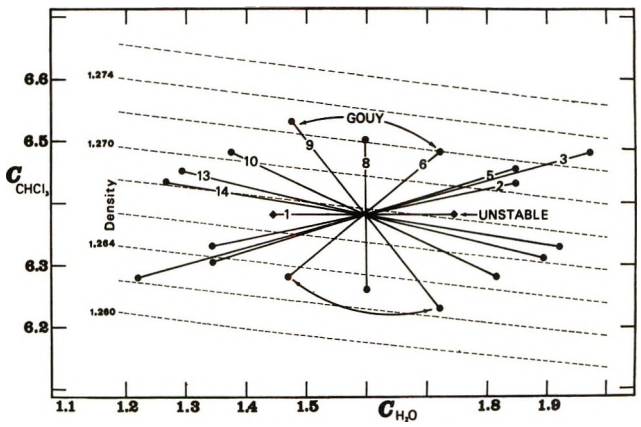

Figure 3. Densities of the ternary system as a function of water and chloroform concentrations, in moles per liter, and compositions of upper and bottom solutions for most of the runs (the numbers in the figure correspond to the run numbers given in Table I).

By following the boundary spreading in time during an anomalous diffusion process, it has been found that the D_a coefficient remains constant for a period of a few hours; after this initial period the D_a value keeps increasing regularly with time, and it does not reach any limiting value during the run.

This behavior can be seen in the graph of Figure 2 where the D_a data computed from the Schlieren patterns of run 15 has been reported as a function of time; the D_a values given in Table I always correspond to the initial time values.

We have no explanations for this peculiar behavior of the D_a's *vs.* time; it might be due to a weakening of the strength of the layering mechanism related to the continuous concentration changes in the upper and lower solutions. Anyhow it must be pointed out that the D_a values always remain very small until the end of the run.

To discuss the mechanism of this anomalous diffusion let us see with the aid of a graph how a diffusion path is curved on the composition diagram.[2]

In Figure 3 we report the composition of the upper and lower solutions for most of our runs; the ternary system density graphs[18,19] are also given as a function of water and chloroform concentrations.

A linear diffusion path would mean that the composition of all solutions within the boundary would lie along the straight line connecting the upper and lower solution compositions, as shown in the figure for all runs. Regular diffusion boundaries develop between solutions whose compositions are set along the maximum density gradient; runs 6 to 9 fulfill this requirement and can be followed by the Gouy technique. Solutions with compositions set along the isodensity curves develop unstable or anomalous boundaries.

We have computed the concentration distribution within the boundary for some model system using the expressions proposed by Oishi.[2] In Figure 1 we report the concentration path for run 1 and run 14 assuming the following values for the intrinsic diffusion coefficients to be used in eq 29 of Oishi's paper:[2] $D_1 = 1 \times 10^{-5}$, $D_2 = 6 \times 10^{-5}$, $D_3 = 10 \times 10^{-5}$ cm^2 sec^{-1}, where indices 1, 2, and 3 are given to chloroform, water, and acetic acid.[20,21]

The concentration paths of Figure 4 explain why runs taken with total concentration differences set at low angle with the isodensity curves develop gravitationally unstable boundaries.

If the water concentration difference has the same sign as that of chloroform ($R > 0$) such as for run 1, the lower boundary layers have densities lower than the upper layers and, possibly, even lower than the upper solution. The upper boundary layers have densities higher than the lower ones, and, eventually, even higher than the bottom solution.

(18) The density curves of Figure 3 have been drawn by graphical interpolation of literature data.[19] The absolute values of the densities can be trusted only to the third decimal figure, but the relative values of these densities in the diagram are sufficiently correct for our purposes.

(19) A. N. Campbell, E. M. Kartzmark, and J. M. T. H. Gieskes, *Can. J. Chem.*, **41**, 407 (1963).

(20) The diffusion paths of Figure 4 mean that chloroform can partly diffuse against its own concentration gradient. This happens because D_1 is quite low and $D_3 > D_2$ (see Oishi's paper, part IIID, p 1619. Actually we do not have any direct evidence for setting $D_3 > D_2$ in the ternary system. (The chosen values are arbitrary and they may be only a guess at the order of magnitude of possible actual values.) Anyhow we can point out that the limiting diffusion coefficient of water in acetic acid[21] is lower than the limiting diffusion coefficient of undissociated acetic acid in water. We also measured the diffusion coefficients of the binary system chloroform–acetic acid and found that going from concentrated chloroform solutions to concentrated acetic acid solutions the diffusion coefficient decreases; finally, addition of water to the chloroform–acetic acid system decreases the measured value of D_a. These facts and the experimental evidence that the concentration paths of runs 10 to 15 are similar to that computed on the model system shown in Figure 4 are in favor of the inequality $D_3 > D_2$.

(21) V. Vitagliano and P. A. Lyons, *J. Amer. Chem. Soc.*, **78**, 4538 (1956).

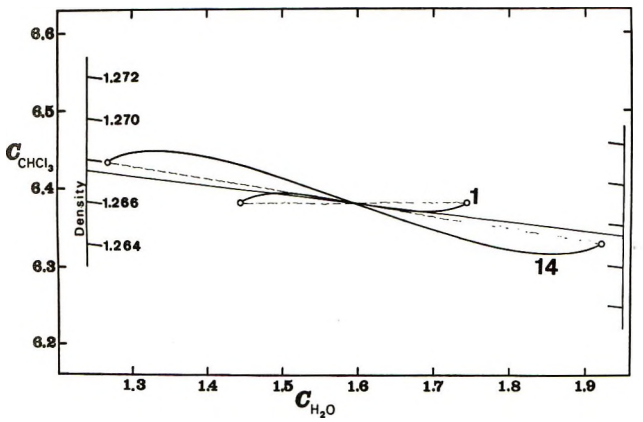

Figure 4. Concentration profiles for run 1 and run 14 computed according to Oishi's[2] eq 29, by using the following arbitrary values for the intrinsic diffusion coefficients: chloroform, $D_1 = 1 \times 10^{-5}$ cm² sec⁻¹; water, $D_2 = 6 \times 10^{-5}$; acetic acid, $D_3 = 10 \times 10^{-5}$.

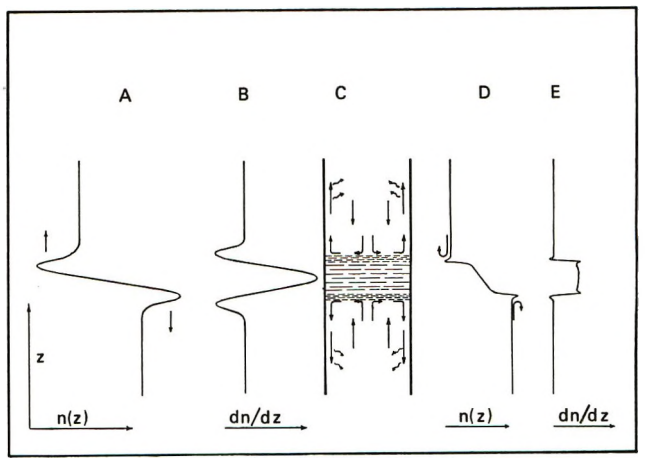

Figure 5. Refractive index and refractive index gradient profiles along the diffusion coordinate, z, within the diffusion cell: A and B, unperturbed case with evident gravitational instability; D and E, anomalous diffusion case; C, diffusion cell and a picture of the mechanism of stabilization of anomalous boundaries.

(Gravitational instability is not a sufficient condition for a growth of boundary perturbations. We have direct experimental evidence of stable boundaries with reverse density distribution, which give stable Schlieren patterns similar to that drawn in Figure 5B. We have obtained them, for instance, in some ternary diffusion experiments with polyelectrolytes in in aqueous solution.)

Such a situation favors circular convective motions within the boundary and the growth of ascending or descending liquid currents that rapidly destroy the initial boundary. This is the case observed in run 1. If the water concentration difference is opposite to that of chloroform ($R < 0$), the upper boundary layers have densities lower than that of the top solution and the lower boundary layers have densities higher than that of the bottom solution. In this case convection mixing within the boundary is avoided; however, it would be expected that ascending and descending motions of the fluid would destroy the initial boundary in this case too.[20,21]

It is quite strange indeed to observe that going from run 10 to 15 there is an apparent progressive overstabilization of the diffusing boundary. However, if we admit that the cell walls favor the growth of gravitational instability perturbations along them, we must not expect irregular convective motions starting from the boundary but a rather regular laminar ascending and descending motion of the fluid along the cell walls, as shown in Figure 5C. In the meantime fresh upper and bottom solutions reach the boundary at the center of the cell channel.

This kind of circular convective motion contributes to the sharpening of the upper and lower layers of the boundary, as shown in Figure 5C, and prevents its destruction; actually the overall mixing process must proceed at a higher rate than in the case of simple diffusive motions.

Figure 5 (D and E) shows the shape of the refractive index and that of the refractive index gradient to be expected within the cell.[22] The shape of the Schlieren patterns obtained in our runs 11 to 15 is very similar to that shown in Figure 5E (see Figure 1A and Figure 6).

We have also repeated run 15 adding a trace amount of rodamine alternatively to the upper and lower solution and following the mixing process by using a uv Wood source. The initial boundary was made (a) inside the diffusion cell (2.5 × 0.3 cm² cross section) and (b) in a cylindrical cell (3-cm diameter).

In case a the motion of the fluorescent dye confirmed the suggested layering mechanism. In case b thin ascending (or descending) fluorescent threads started from different points of the boundary. The threads were discontinuous both in time and position; no more than two or three threads could be seen simultaneously.

This fact suggests the possibility of some influence of the cell shape on the layering mechanism, even though the boundary remains stable for a long time in both cases.

The growth of ordered structures (dissipative structures) due to the coupling of gravitational and thermal forces is already known in hydrodynamics.[23,24] These structures are stabilized by the high rate of dissipation of free energy during the proceeding of an irreversible process.[7]

Recently a peculiar layering process resulting from combined saline and temperature gradients has been discussed by Turner and Stommel[25] and by Turner.[26]

(22) Owing to the small concentration differences within the cell, the refractive index is generally assumed to be directly proportional to density or concentration. Density and refractive index data for our system support this assumption.[19]

(23) H. Bénard, *Ann. Chim. Phys.*, **23**, 62 (1901).

(24) S. Chandrasekhar, "Hydrodynamic and Hydromagnetic Stability," Oxford University Press, London, 1961.

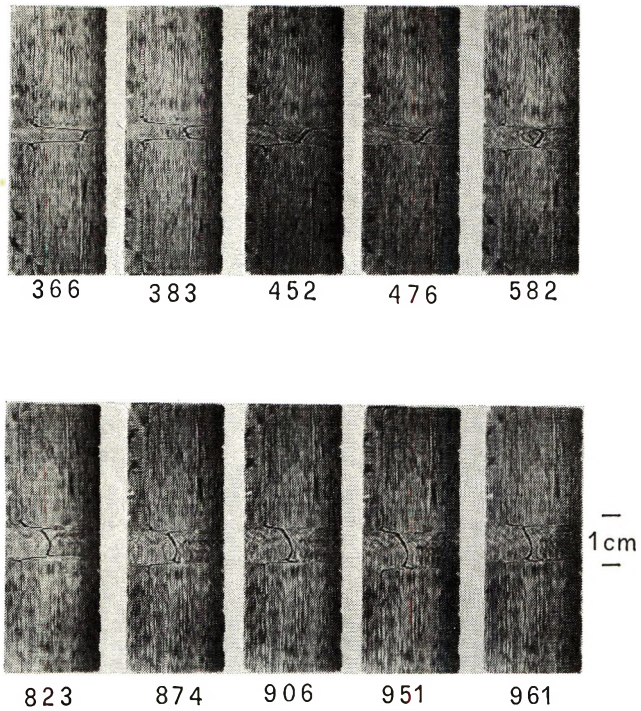

Figure 6. Set of Schlieren pictures taken at different times (in minutes) of run 15. The existence of a periodic sharpening on one side of the boundary can be seen.

When a linear, stable salt gradient is heated uniformly and at a steady rate from below, a convective stirring of the solution is promoted which builds up a series of layers separating solutions at different density and composition.

The mechanism of this layering process ressembles in somes aspect our anomalous diffusion process, even though turbulence plays a much more important role in Turner's experiments than in ours. In both cases, however, fluxes are present with definite different rates: in Turner's experiment the heat flow is much faster than the diffusion flow; in our case one of the components has a diffusivity much lower than the others.

Our anomalous diffusion process seems to be the first case of a dissipative structure built up by the coupling of only gravitational and diffusion forces.

Finally, we would like to point out the possibility of oscillatory effects on the growth of density perturbations which promote our anomalous diffusion process. We had some evidence during our runs of effects that could be interpreted in such a way. The sharpness of the upper and lower boundary layers is not constant, but it increases and decreases regularly during most of the running time. This effect is shown in Figure 6 where we report a set of Schlieren patterns taken at different times. It can easily be seen that the sharp peaks at the upper and lower sides of the boundary appear and disappear on time. We have not observed any very striking effect during our runs, but we think that by conveniently changing the running conditions it might be possible to develop an anomalous boundary showing considerable periodic fluctuations.

Acknowledgment. The authors wish to thank Dr. H. Schönert of the Rhein-Westf. Techn. Hochschüle, Aachen, for his critical reading of the paper and useful suggestions.

(25) J. S. Turner and H. Stommel, *Proc. Nat. Acad. Sci. U. S.*, **52**, 49 (1964).

(26) J. S. Turner, *J. Fluid Mech.*, **33**, 183 (1968).

COMMUNICATIONS TO THE EDITOR

Detection and Identification of Gas Phase Free Radicals by Electron Spin Resonance Spin Trapping[1]

Publication costs assisted by Environmental Protection Agency Air Pollution Control Office

Sir: A technique for the detection and identification of short-lived neutral free radicals has recently been developed which depends on the esr detection of nitroxyl addition products of radicals to nitroso or nitrone compounds.[2] Most applications of this technique have been made in liquid solutions using 2-nitroso-2-methylpropane, nitrosobenzene, or phenyl *N-tert*-butylnitrone as a trap for the radicals[3]

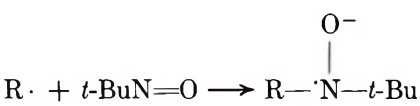

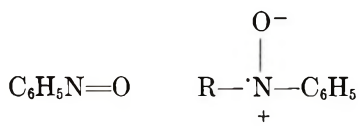

or

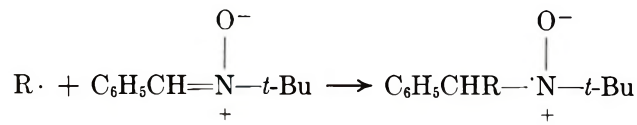

spin trap spin adduct

The nitrogen and proton hyperfine splittings of the spin adducts are diagnostic parameters for the identification of the radical detected.

Phenyl *N-tert*-butylnitrone (PBN) also traps gas phase free radicals. Thus if powdered PBN is confined in a tube in an esr cavity during exposure to a flow of nitrogen containing free radicals a spectrum of three doublets typical of a PBN spin adduct is recorded. Since the line widths of the spectra thus obtained are relatively broad, the samples are disssolved in a solvent such as benzene and the solution spectra characteristic of the appropriate spin adducts are used for analysis. In this manner methyl, ethyl, and perfluoroethyl radicals have been detected from photolysis of acetone, tetraethyllead, and perfluoroazaethane, respectively, in a nitrogen stream at room temperature and at atmospheric pressure.[5] Although initial attempts to detect gas phase radicals by this method at below atmospheric pressures met with failure, we now have found that at pressures below 10 Torr the nitroxides produced by the reaction of the gas-phase radicals with PBN are completely removed from the surface of PBN by volatilization and can be collected in a liquid nitrogen trap downstream. If a solvent is consequently distilled into the trap a solution esr spectrum typical of the PBN spin adduct can be obtained. We thus want to report on a method for detecting gas-phase free radicals at pressures as low as 0.1 Torr which takes advantage of the fast addition reaction of radicals to PBN and the high volatility of the nitroxide spin adducts produced.

The radical trapping apparatus presently being used is shown in Figure 1. It is a detachable part of a typical vacuum system (10^{-6} Torr). The gases under investigation are introduced into the photolysis cell through a needle valve from storage bulbs attached upstream from the cell. A 0.005–5-Torr McLeod gauge attached between the needle valve and the cell is used to measure the pressure of the gases in the photolysis cell. Irradiation is either from the top with a low-pressure mercury lamp (Fischer Mineralight Model R-51 with a 6-bar cold quartz tube) or from an end with a high-pressure mercury lamp (GE 100-W mercury "Spot Light" No. PSP44-4 with Pyrex cover). The gases pass from the photolysis cell directly into coiled 8-mm tubing coated with powdered PBN and out to the pumps through a liquid nitrogen trap constructed from an esr tube. In a typical experiment approximately 0.4 g of finely powdered dry PBN is placed into the front portion of the spiral tube and by suitable movements of the apparatus it is allowed to coat about 7 cm of the walls with a thin layer of powdered crystals. The apparatus is assembled on the vacuum line, with care taken to avoid introducing any PBN powder into the photolysis cell or irradiated region. Usually the edge of the photolysis cell is 1–2 cm from the first powdered PBN. The spiral construction minimizes dispersion of powdered PBN if quick gas surges are created during vacuum line manipulations.

(1) This work is supported by the Environmental Protection Agency Air Pollution Control Office, Public Health Service, Grant AP 01096.

(2) For reviews of this technique, see E. G. Janzen, *Accounts Chem. Res.*, **4**, 31 (1971); C. Lagercrantz, *J. Phys. Chem.*, **75**, 3466 (1971); M. J. Perkins, *Chem. Soc. Spec. Publ.*, **No. 24**, 97 (1970).

(3) These compounds and the radical addition products have been called spin traps and spin adducts to facilitate discussion of these reactions.[4]

(4) E. G. Janzen and B. J. Blackburn, *J. Amer. Chem. Soc.*, **91**, 4481 (1969).

(5) E. G. Janzen and J. L. Gerlock, *Nature*, **222**, 867 (1969).

Table I: Hyperfine Splittings of Methyl and Ethyl Spin Adducts $C_6H_5CH(R)N(O\cdot)C(CH_3)_3$[a]

Radical source	R	Pressure[b]	Time[c]		a^N [d]	a_β^H [d]	a^N,[d] "unknown triplet"
Azomethane	$\cdot CH_3$	0.15	2.0		14.69 ± 0.09	3.57 ± 0.09	None
Azomethane	$\cdot CH_3$	0.20	2.0		14.66 ± 0.11	3.61 ± 0.12	15.11 ± 0.10
Azomethane[e]	$\cdot CH_3$	0.20	2.0		14.60 ± 0.22	3.58 ± 0.14	
Azomethane[f]	$\cdot CH_3$	0.15–0.20	2.0		14.58 ± 0.15	3.55 ± 0.12	
				Av	14.63 ± 0.04	3.58 ± 0.02	
Acetone	$\cdot CH_3$	0.10–0.15	4.5		14.80 ± 0.11	3.56 ± 0.10	
Acetone	$\cdot CH_3$	0.5–0.6	1.0		15.00 ± 0.13	3.43 ± 0.06	15.33 ± 0.08
Acetone	$\cdot CH_3$	1.0	1.5		14.69 ± 0.45	3.33 ± 0.19	
Acetone	$\cdot CH_3$	10	1.0		14.81 ± 0.25	3.56 ± 0.18	
				Av	14.82 ± 0.08	3.47 ± 0.09	
3-Pentanone	$\cdot CH_2CH_3$	0.10–0.15	2.0		14.32 ± 0.10	3.22 ± 0.13	
3-Pentanone	$\cdot CH_2CH_3$	0.20–0.25	1.0		14.32 ± 0.16	3.20 ± 0.14	
Tetraethyllead[g]	$\cdot CH_2CH_3$	0.1–0.5	4.0		14.40 ± 0.16	3.30 ± 0.09	
Diethyl mercury	$\cdot CH_2CH_3$	0.1	1.0		14.33 ± 0.15	3.22 ± 0.15	
				Av	14.34 ± 0.03	3.26 ± 0.04	

[a] In gauss in benzene at room temperature. [b] In Torr; entries which give a range in pressure were experiments where the pressure changed during the photolysis period. [c] Photolysis period (hr) during which radicals were collected. [d] Errors stated in each entry are standard deviations from the average spacing measured; errors given with the average splitting constant are the average of the deviations from the average stated. [e] PBN applied to spiral walls by evaporating PBN–pentane solution. [f] PBN applied to back downstream half of spiral tubing only. [g] Lead mirror accumulated on photolysis cell walls.

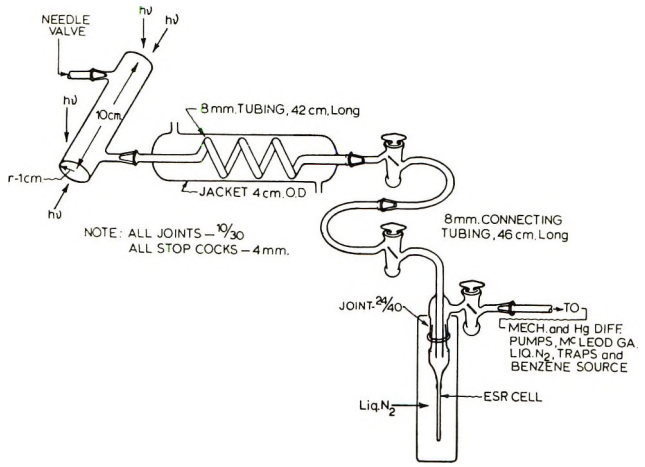

Figure 1. Apparatus for detection of gas-phase free radicals at low pressures.

Azomethane photolysis has been used to develop the technique. Thus in a typical experiment azomethane is pumped through the apparatus at 0.1–0.2 Torr pressure during continuous irradiation at $\lambda > 300$ nm for 2 hr. No visible condensate other than a small amount of PBN collects in the cold trap. After the system is closed off, a small amount of benzene is distilled into the trap and allowed to warm to room temperature. The esr cell is placed in an esr cavity and the spectrum is recorded at room temperature. In this case a typical nitroxide liquid solution spectrum is obtained which can be shown by comparison to known spectra[4,5] to be the methyl spin adduct of PBN (Figure 2)

$$CH_3N{=}NCH_3 \xrightarrow{h\nu} 2CH_3\cdot + N_2$$

$$CH_3\cdot + PBN \longrightarrow C_6H_5CH(CH_3)N(O\cdot)C(CH_3)_3$$

The spectra thus obtained are usually "stable" for many hours at room temperature.

Based on azomethane experiments, the method of applying the PBN powder to the spiral tube does not appear to be crucial. About the same esr signal intensity is obtained by using the method described above or by evaporating off the solvent from a PBN–pentane solution. As expected, locating the powder well back into the second half of the spiral decreases the yield

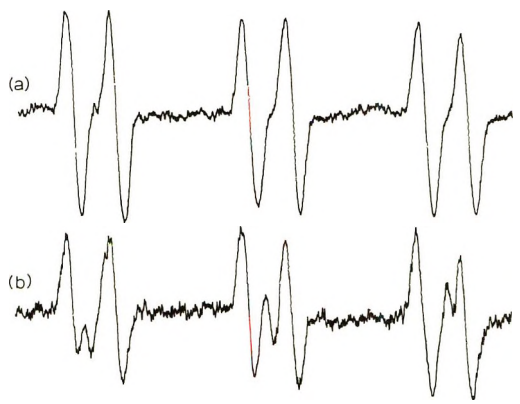

Figure 2. Esr spectra of the methyl spin adduct ($C_6H_5CH(CH_3)N(O\cdot)C(CH_3)_3$) obtained from a 2-hr photolysis of azomethane at 0.20 Torr. Bottom spectrum shows the overlapping triplet due to a nitroxide of unknown structure produced in an experiment where PBN received some light (see text).

of nitroxide considerably (5–10×). The fraction of radicals trapped in a typical azomethane photolysis, as obtained by comparing the esr signal intensity of the nitroxide with the extent of azomethane decomposition,[6] was approximately 0.1% in one experiment. In this experiment the concentration of the nitroxide collected was approximately $1 \times 10^{-5} M$.

In some trials with other systems the amount of nitroxide isolated was close to the sensitivity limit of the esr spectrometer and identification of the spin adduct was difficult. However, the conditions for radical detection are not considered to be optimum. Improvements in sensitivity are expected by using (1) smaller volumes of diluent solvent, (2) spectrum accumulation techniques (CAT), (3) a more intense light source, (4) a cell with better flow characteristics, (5) a more reactive spin trap, and (6) a shorter path length between the reaction zone and the spin trap. The latter appears to be the most difficult factor to change because PBN itself is very sensitive to light in the solid phase (but not in solution) producing a volatile nitroxide of unknown structure. This nitroxide gives a three-line spectrum with a 15 G spacing (Table I, Figure 2b). This signal appears in many spectra obtained under normal conditions where it is presumed that a small amount of PBN has been unintentionally photolyzed. Production of this nitroxide can be avoided by good experimental techniques (see Figure 2a).

The nitrogen and β-hydrogen hyperfine splittings of the methyl spin adduct and the "unknown triplet" (where detected) obtained in typical experiments are shown in Table I. The errors given are the standard deviation from the average of the measured spacings and are mainly due to the poor reproducibility of the Fieldial scanning unit in our Varian 4502 epr spectrometer. However, in utilizing spin-trapping techniques for the identification of detected radicals both in solution and in the gas phase it is more important to obtain authentic spectra for comparison than to base the interpretation of results on previously reported splitting constants. It is also clear from experience with many spectra that the line widths and line shapes of spectra of different spin adducts differ considerably and can be used as diagnostic parameters for identification. Thus, although the methyl and ethyl spin adducts have approximately the same line width of 1.1–1.4 G (thought to be due mainly to unresolved γ-hydrogen splitting of the methyl group), the latter always appears to have a more "slender" line shape than the former.

Photolysis of acetone gave spectra of the methyl spin adduct which were superimposable with the spectrum shown in Figure 1a. The reproducibility of the measured spacings appears to be somewhat poorer in these spectra than in those obtained from azomethane (see Table I). This may be due to a small contribution from the acetyl spin adduct which should be detectable under favorable conditions. Experiments designed to improve the detectability of the acetyl radical are in progress.

The ethyl spin adduct was detected with no difficulty from the photolysis of 3-pentanone (diethyl ketone). The spectrum is the same as produced from the photolysis of tetraethyllead or diethyl mercury in the gas phase (see Table I). Perfluoroalkyl radicals have been detected from gas-phase photolysis of perfluoroalkyl iodides and ketones. These results will be reported in the future.

(6) Standard potassium ferrioxalate actinometric techniques were used.

DEPARTMENT OF CHEMISTRY
THE UNIVERSITY OF GEORGIA
ATHENS, GEORGIA 30601

EDWARD G. JANZEN*
IRENE G. LOPP

RECEIVED JANUARY 28, 1972

Equilibrium Studies by Electron Spin Resonance. II. The Nitrobenzene "Free" Ion–Ion Pair Equilibrium

Publication costs borne completely by The Journal of Physical Chemistry

Sir: We wish to report the thermodynamic parameters controlling the equilibrium between the nitrobenzene ($PhNO_2$) "free" anion radical (α) and the ion pair (β) in hexamethylphosphoramide (HMPA)

$$\beta \rightleftharpoons \alpha \qquad (1)$$

These two species have been observed simultaneously in solution at room temperature and the equilibrium constants have recently been reported for the systems $PhNO_2$–HMPA–Li, $PhNO_2$–HMPA–Na, and $PhNO_2$–HMPA–K.[1]

The esr spectrum of the loose and tight ion pairs of the napthalene anion radical have been observed simultaneously in solution by Chang and Johnson.[2] Both were in the fast exchange region with the neutral molecule. Two different ion pairs of the cyclooctatetraene anion radical have also been observed in dimethoxyethane[3] and in liquid ammonia.[4] To our knowledge, this is the first report of thermodynamic parameters controlling the equilibrium between two simultaneously observed anion radical ion pairs.

(1) G. R. Stevenson, L. Echegoyen, and L. R. Lizardi, *J. Phys. Chem.*, **76**, 1439 (1972).

(2) R. Chang and C. S. Johnson, Jr., *J. Amer. Chem. Soc.*, **88**, 2338 (1966).

(3) H. L. Strauss, T. J. Katz, and G. K. Fraenkel, *ibid.*, **85**, 2360 (1963).

(4) F. J. Smetowski and G. R. Stevenson, *J. Phys. Chem.*, **73**, 340 (1969).

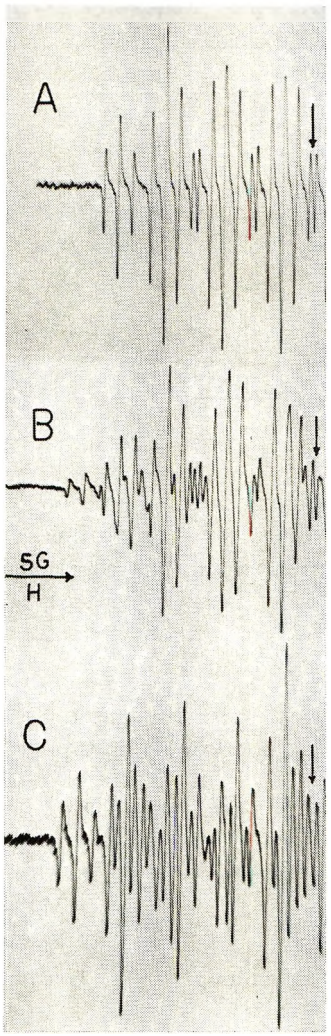

Figure 1. Esr spectra of the $PhNO_2$–HMPA–Li system as a function of temperature. Only the high-field halves of the spectra are shown: A, 0°, "free" ion; B, 25°, "free" ion and ion pair simultaneously; C, 80°, ion pair.

Dramatic spectral changes are observed when these solutions are studied under variable temperature conditions, as shown in Figure 1. For the system $PhNO_2$–HMPA–Li only the esr spectrum of the "free" anion radical is observed at 0°, above 80° only the ion pair is observed, and at intermediate temperatures both species are observed simultaneously. The nitrogen hyperfine coupling constant, A_n, for the "free" anion radical is insensitive to temperature changes with a value of 8.48 G while for the ion pair A_n varies from 10.85 to 11.16 G between 10 and 80°, respectively. At the intermediate temperatures, relative esr line intensities for the two species enable the calculation of the equilibrium constants for eq 1. A simple van't Hoff plot of ln K *vs.* $1/RT$ yields a straight line with a slope, $-\Delta H°$, of 8.3 kcal/mol (Figure 2).

For the system $PhNO_2$–HMPA–Na, only the "free" anion radical is observed at 0° while above 80° only the ion pair is apparent. Unlike the Li reduction, metal splitting from the Na nuclei is observed at all

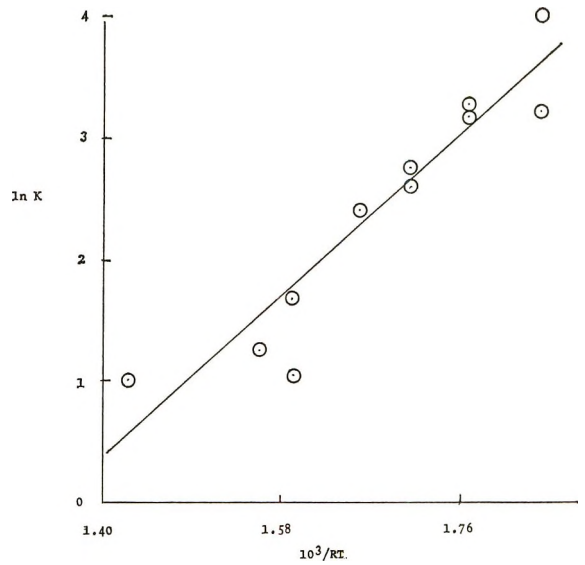

Figure 2. Plot of ln K *vs.* $10^3/RT$ for the system $PhNO_2$–HMPA–Li.

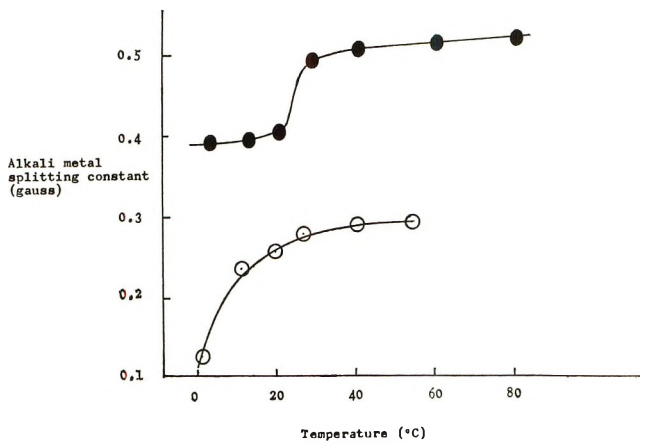

Figure 3. Temperature dependence of the alkali metal splittings for the ion pair radicals in HMPA: ○, potassium splitting; ●, sodium splitting.

temperatures for the ion pair (Figure 3). Owing to the large amount of overlap between the "free" ion and ion pair spectra, the equilibrium constants could only be measured accurately over a narrow temperature range. The plot of ln K *vs.* $1/RT$ yields a $\Delta H°$ value of -7.2 kcal/mol (Figure 4).

When nitrobenzene is reduced with potassium in HMPA, the ion pair and "free" ion are observed simultaneously over the entire temperature range of 0–80°. The equilibrium constant is practically insensitive to temperature variations indicating that $\Delta H°$ is very small. The thermodynamic parameters and coupling constants for all three systems are shown in Table I.

The large negative values of $\Delta H°$ and $\Delta S°$ for the Li and Na systems suggest that the solvation changes associated with the structure of the ion pair and "free" ion require drastic reorganization of the solvation struc-

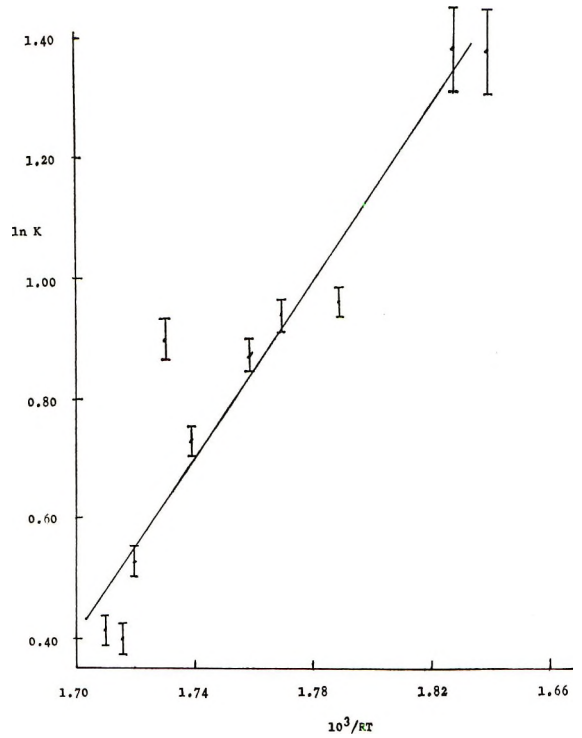

Figure 4. Plot of ln K *vs.* $10^3/RT$ for the system $PhNO_2$–HMPA–Na. The error in K is greater at the lower temperatures owing to the weak esr signal for the ion pair.

ture. In particular, the large negative values of $\Delta H°$ and $\Delta S°$ (Table I) indicate more solvent ordering for the "free" ion than the ion pair.[5] This is in good agreement with the fact that HMPA is a powerful cation solvating agent.[6] In contrast, Hirota and coworkers[7] have shown that the $\Delta H°$ and $\Delta S°$ variations from contact to solvent-separated ion pairs of metal ketyls are small. This supports our conclusion that α is essentially free of ion pairing. Stevenson and Concepción[8] have shown that for the cyclooctatetraene–HMPA–metal

Table I: Thermodynamic Data and Nitrogen Coupling Constants

System	$\Delta H°$, kcal mol^{-1}	$\Delta S°$, cal deg^{-1} mol^{-1}	$A_n(\alpha)$	$A_n(\beta)^a$
$PhNO_2$HMPA–Li	-8.3 ± 0.8	-23 ± 2	8.48 ± 0.02	10.85 ± 0.05
$PhNO_2$HMPA–Na	-7.2 ± 1	-24 ± 2	8.48 ± 0.02	10.9 ± 0.1
$PhNO_2$HMPA–K	>-5	>-15	8.49 ± 0.02	9.80 ± 0.06

[a] At 25°.

systems, potassium exhibits more ion pairing than Li or Na as is evident from the entropies controlling the disproportionation equilibrium constants. The higher value for $\Delta S°$ for the $PhNO_2$–HMPA–K system indicates again that potassium is not solvated as strongly in HMPA as are Li^+ and Na^+.

Acknowledgment. Dr. Stevenson is very grateful for a Research Corporation Grant supporting this work.

(5) N. Hirota, *J. Phys. Chem.*, **71**, 127 (1967).
(6) H. Normant, *Angew. Chem. Int. Ed. Engl.*, **6**, 1046 (1967).
(7) K. S. Chen, S. W. Mao, K. Nakamura, and N. Hirota, *J. Amer. Chem. Soc.*, **93**, 6004 (1971).
(8) G. R. Stevenson and G. Concepción, *J. Phys. Chem.*, in press.

DEPARTMENT OF CHEMISTRY
University of Puerto Rico
Río Piedras, Puerto Rico
GERALD R. STEVENSON*
LUIS ECHEGOYEN

DEPARTMENT OF RESEARCH AND DEVELOPMENT
ECONOMIC DEVELOPMENT ADMINISTRATION
SAN JUAN, PUERTO RICO
LUIS R. LIZARDI

RECEIVED MARCH 29, 1972

Here is the ideal way to obtain the ***most reliable reference data available today!*** *All you need is a subscription to the new*

JOURNAL OF PHYSICAL AND CHEMICAL REFERENCE DATA

published by the American Chemical Society and the American Institute of Physics for the National Bureau of Standards.

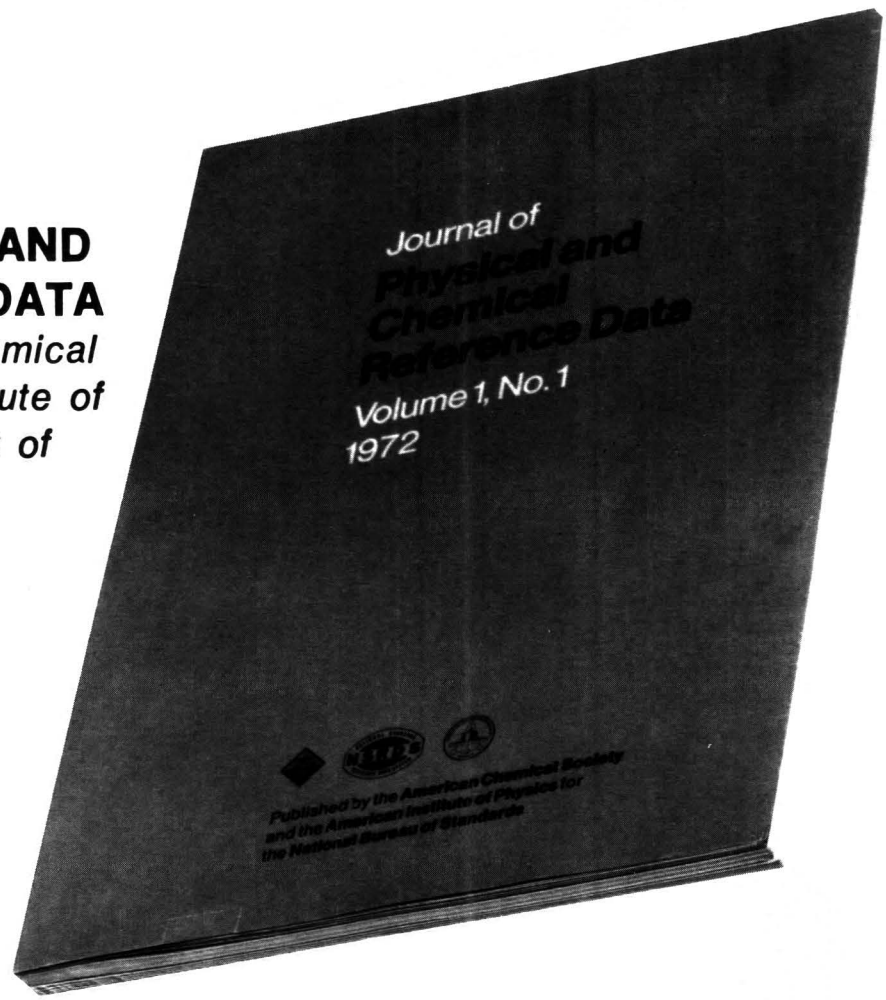

The *Journal of Physical and Chemical Reference Data* fills an important gap in the literature of the physical sciences. Its subject matter is the quantitative numerical data of physics and chemistry. As the new publication vehicle of the National Standard Reference Data System, the *Journal* will contain carefully evaluated data, with recommended values and uncertainty limits chosen by experts in each field. Critical commentary on methods of measurement and sources of error, as well as full references to the original literature, will be an integral part of each compilation.

Examples of some of the critical compilations scheduled for publication in the four issues of Volume I (1972) include:

- Tables of Molecular Vibrational Frequencies, Part 5, T. Shimanouchi
- Gaseous Diffusion Coefficients, by T. R. Marrero and E. A. Mason
- The Spectrum of Molecular Oxygen, by P. Krupenie
- Thermal Conductivity of the Elements, by C. Y. Ho, R. W. Powell and P. E. Liley
- Selected Values of Critical Supersaturation for Nucleation of Liquids from the Vapor, by G. M. Pound
- Gas Phase Reaction Kinetics of the Hydroxyl Radical, by W. E. Wilson, Jr.
- Selected Values of Heats of Combustion and Heats of Formation of Organic Compounds Containing the Elements CHNOPS, by E. S. Domalski
- Microwave Spectra of Molecules of Astrophysical Interest: Formaldehyde, Formamide, Thio-Formaldehyde, by D. R. Johnson, F. J. Lovas and W. H. Kirchhoff

Future compilations are expected to cover areas such as the following:

Band gaps in semiconductors
Nuclear moments
Atomic energy levels and transition probabilities
Diffusion in metals
Electron swarm data
Elastic constants of metals
Surface tension of liquids
Properties of molten salts
Activity coefficients of electrolytes
Equation of state of atmospheric gases
Ionization and appearance potentials

The *Journal of Physical and Chemical Reference Data* is intended to be a definitive source of reliable data on physical and chemical properties. Just fill in the order form at the bottom of this page to receive this invaluable reference source.

JOURNAL OF PHYSICAL AND CHEMICAL REFERENCE DATA
AMERICAN CHEMICAL SOCIETY
1155 Sixteenth Street, N.W.
Washington, D.C. 20036

Yes, I would like to receive the JOURNAL OF PHYSICAL AND CHEMICAL REFERENCE DATA at the one-year rate checked below:

	U.S.	Canada	PUAS	Other Countries
AIP and ACS members	$20.00	$20.00	$23.00	$23.00
Nonmembers	$60.00	$60.00	$63.00	$63.00

Bill me ☐ Bill company ☐ Payment enclosed ☐

Name _____

Street _____ Home ☐ Business ☐

City _____ State _____ Zip _____

JP 72

There when you need them...

are the annual 700 pages of data published quarterly in the

Journal of Chemical & Engineering Data

This American Chemical Society journal is especially valuable in light of today's new instrumentation.

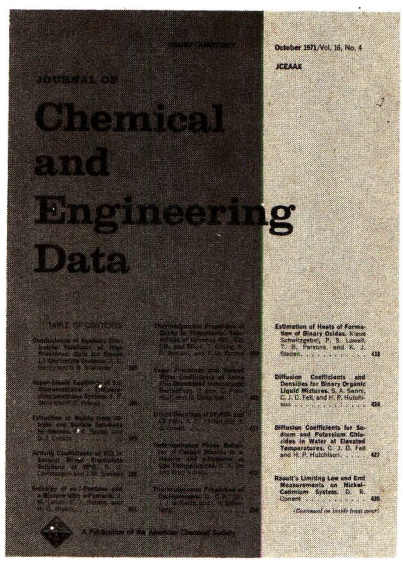

You'll find *four* clearly defined areas in JC & ED. They are:

☐ Experimental data relating to pure compounds of mixtures covering a range of states.

☐ Manuscripts based on published experimental information, which make tangible contributions through the reorganization or systematic presentation of such data . . . or which set forth a well documented method of prediction of properties as a function of state.

☐ Experimental data which aid in the identification or utilization of new organic or inorganic compounds.

☐ Papers relating primarily to newly developed or novel synthesis of organic compounds and their properties.

Sending for a subscription to the JOURNAL OF CHEMICAL & ENGINEERING DATA is so much easier than searching for data deposited in archives. Just fill in and return the form below. We'll do the rest.

American Chemical Society / 1155 Sixteenth Street, N.W., Washington, D.C. 20036

Please enter my subscription to **The Journal of Chemical & Engineering Data** at the rates checked below.

ACS Members: ☐ U.S. $15.00 ☐ Canada, PUAS $18.00 ☐ Other Nations $18.50

Nonmembers: ☐ U.S. $45.00 ☐ Canada, PUAS $48.00 ☐ Other Nations $48.50

☐ Bill me ☐ Bill employer ☐ Payment enclosed (Payable to American Chemical Society)

Name _____ Title _____

Employer _____

Address: ☐ Home ☐ Business _____

City _____ State/Country _____ Zip _____

Nature of employer's business? ☐ Manufacturing or processing ☐ Academic ☐ Government ☐ Other _____ (Please indicate)

Note: Subscriptions at ACS Member Rates are for personal use only.

☐ I am an ACS member ☐ I am not an ACS member

Payment must be made in U.S. currency, by international money order, UNESCO coupons, U.S. bank draft; or order through your book dealer.

T3A